COASTAL GEOLOGY OF THE

GERLACHE STRAIT,

ANTARCTICA

By

ANN MARIE DREWRY

Bachelor of Science in Geology

Oklahoma State University

Stillwater, OK

2006

Submitted to the Faculty of the
Graduate College of the
Oklahoma State University
in partial fulfillment of
the requirements for
the Degree of
MASTER OF SCIENCE
May, 2009

COASTAL GEOLOGY OF THE

GERLACHE STRAIT,

ANTARCTICA

Thesis Approved:

Dr. Alexander Simms

Thesis Adviser

Dr. Regina Kalchgruber-DeWitt

Dr. Jim Puckette

Dr. Anna Cruse

Dr. A. Gordon Emslie

Dean of the Graduate College

ACKNOWLEDGMENTS

The author would like to thank the National Science Foundation (NSF) Grant #OPP0724929 awarded to Dr. Alex Simms and Dr. Regina Kalchgruber-DeWitt without this grant the opportunity to study such an interesting environment would not have been possible. Furthermore, I would like to thank Dr. John Anderson (Rice University) and Dr. Bernard Hallet (University of Washington) for the discussions related to this topic, without those, the idea for this study would not have been considered.

I would also like to my advisor Dr. Alex Simms for not only the opportunity to be part of such an experience, but for encouraging me, inspiring me, and teaching me throughout the entire process. I would also like to thank him for the countless hours of revisions which without would not have made this thesis possible. I would like to thank Dr. Regina Kalchgruber-DeWitt for her time, energy, and patience throughout the time we spent working together. Without her I am not sure I could have made it through all those days in the dark lab, thanks Ginni! To Procopious "Peter" Kouremenous, my shipmate and friend thanks for all your help in the field, lab, and always being willing to answer any question of mine. Without you, the experience would not have been bearable. To Dr. Puckette, I don't know where to begin! Thanks for all your help, not only on this project but throughout my career at OSU, because of you I know I will be a better geologist.

I would also like to express my gratitude to Chris Denker from Raytheon Polar Services, Alison Cook from the British Antarctic Survey, and the students from Rice University who also helped in the field. Chris thanks again for always being willing to help in anyway to get data while we were in the field and for keeping us safe on those sometimes questionable zodiac rides. To Alison Cook, thanks again for working tirelessly to find aerial photos in the Gerlache Strait, which without would not have made this thesis what it is.

Finally, I would like to thank my parents Wayne and Rebecca Drewry for teaching me from the beginning that a great education was important, for all the support throughout my many years in school, and for always believing in me. To my brother Jeremy Drewry I would like to thank you for all your love and support throughout the years. Lastly, to my better half, Charles Baker, you are my Rock, and without you none of this would have been possible.

TABLE OF CONTENTS

Chapter Page

Chapter Page

LIST OF TABLES

Table Page

LIST OF FIGURES

Figure Page

Figure Page

Figure Page

Figure Page

Figure Page

Figure Page

Figure Page

Figure Page

CHAPTER I

INTRODUCTION

Purpose

While searching for raised marine features in the Gerlache Strait small arc-shaped ridges in the intertidal zone were observed. As their origin was not completely clear, they were given the temporary name of "conspicuous ridges at sea-level" (CRASL). CRASLs are prevalent in the Gerlache Strait. The purpose of this study is to map these ridges and determine how they form. My hypothesis is these features are recessional moraines. If they represent recessional moraines these features could indicate that deglaciation of this area began not thirty to forty years ago as presently thought (Cook et al., 2005), but instead predates anthropogenic climate change.

This study will also provide fundamental sedimentary characteristics of three common depositional settings observed in Polar Regions: 1) talus slopes, 2) moraines, and 3) beaches. Currently, little data is available on the basic sedimentology of these depositional environments in polar and subpolar settings. The characterization conducted for this project includes grain size, angularity, sphericity and petrologic diversity of the deposits.

Study Area

The Gerlache Strait (64^{o} 30'S, 62^{o} 20'W) is located on the northwest side of the Antarctic Peninsula (Fig. 1) and separates the Palmer Archipelago from the Danco Coast (Figs. 1 and 2).

The Gerlache Strait is oriented northeast to southwest and averages 40 km in width and 120 km in length; it opens to the continental shelf on both ends and by the Schollaert Channel on the western side (Evans et al., 2004). The strait narrows to the southwest, eventually terminating in the west-trending Bismarck Strait (Scott, 1965). The Gerlache Strait is approximately 300 m deep in the southwest and deepens to 1200 m in the northeast. In areas where tributary bays and fjords feed into the Gerlache Strait, water depths increase to 500 m (Evans et al., 2004).

The geography of the study area is described as rugged and heavily fjorded with distinctive coastlines due to the sharp contacts between ice cliffs and bedrock. The only rock exposures are steep cliff faces, zones of tidal swash, off-shore rocks, and local areas of bedrock exposed by seasonal ablation (Scott, 1965).

Hypothesis

This study will test the hypothesis that CRASLs form as a result of recessional moraines being reworked into beach deposits. Their origin is important in order to gain an understanding of their significance and relationship to the climate history of the region.

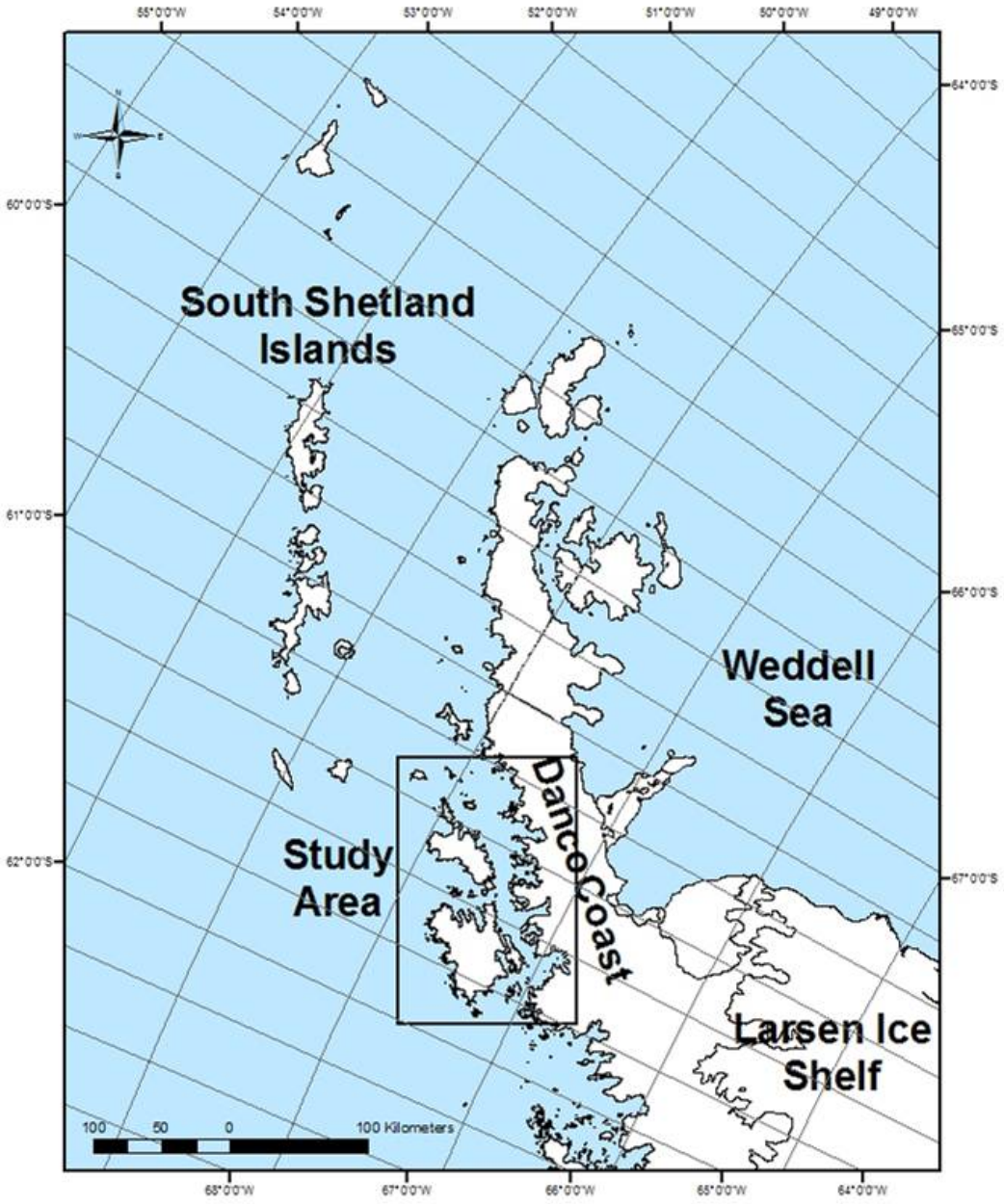

Figure 1 – Map of Antarctic Peninsula showing the location of the study area.

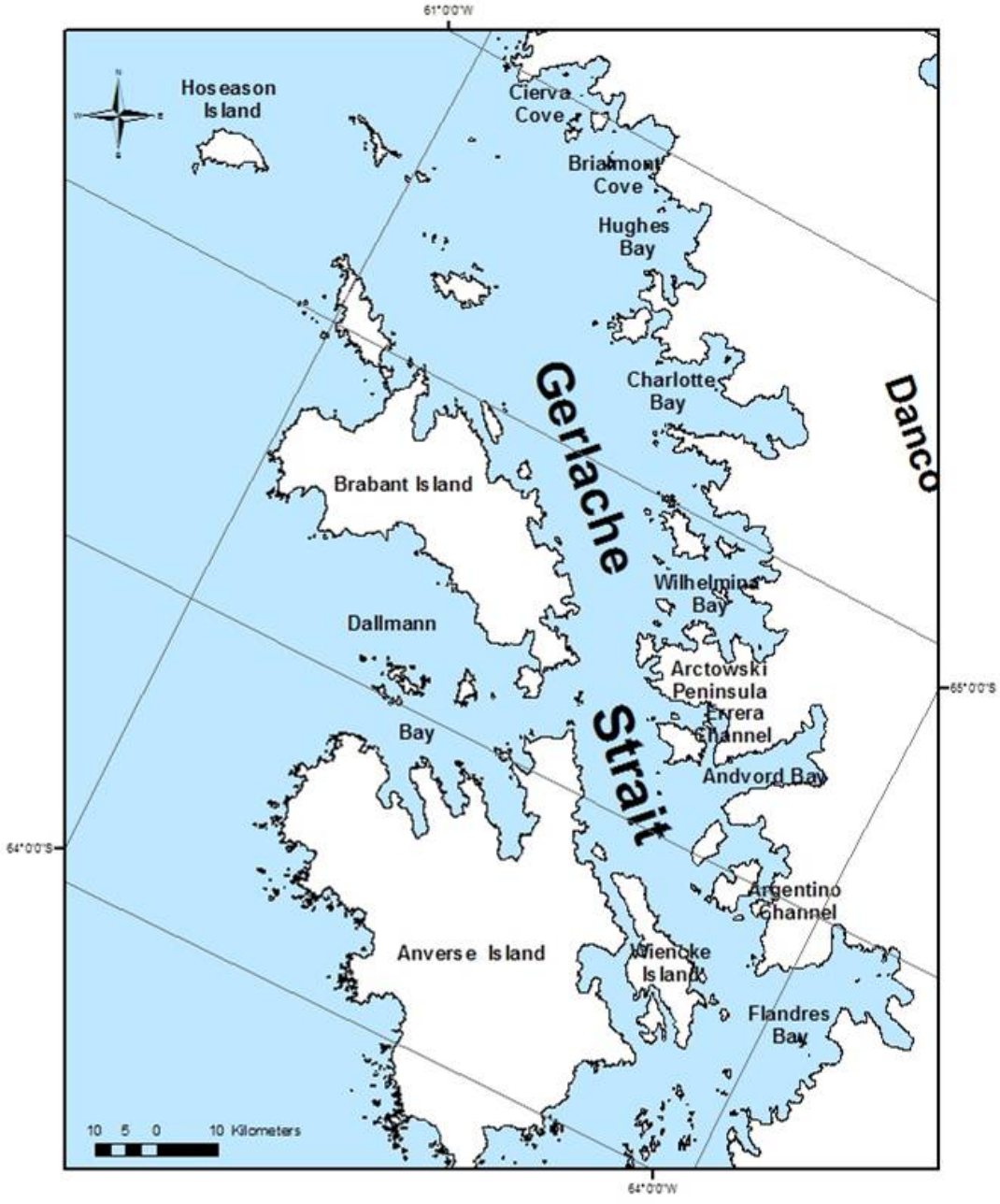

Figure 2 – Detailed location map of study area in Gerlache Strait. See Figure 1 for generalized location.

Throughout the 20th century, British, Chilean, and Argentinean explorers built structures on many parts of the ice-free coastline. If these CRASLs were once recessional moraines that have undergone reworking into arc-shaped ridges and/or spits, they could indicate recent (100s of years) deglaciation of the Gerlache Strait, possibly in response to an exit from the Little Ice Age (LIA). If the structures are built on these features then they must predate their construction. Therefore, deglaciation within the area had to occur prior to the building of the structures. Furthermore, if the structures were built in the 1940s or 1950s, then the glaciers would have had to been retreating by that time and thus, were well into retreat by the 1970's and 1980s.

Three possible hypotheses for the formation of the CRASLs were tested in this study: 1) spit-model, 2) recessional moraine-model, and 3) pro-talus rampart-model (Fig. 3). In order to test each of these hypotheses, I determined the sedimentary characteristics of modern beaches, moraines, and talus slopes and compared those to the sedimentary characteristics of a CRASL. In addition, I mapped over 350 CRASLs to determine if their location, orientation, or distribution provided clues to their origin. I also attempted to place constraints on the sea-level history of the area to provide additional information on the processes operating in the formation of the CRASLs.

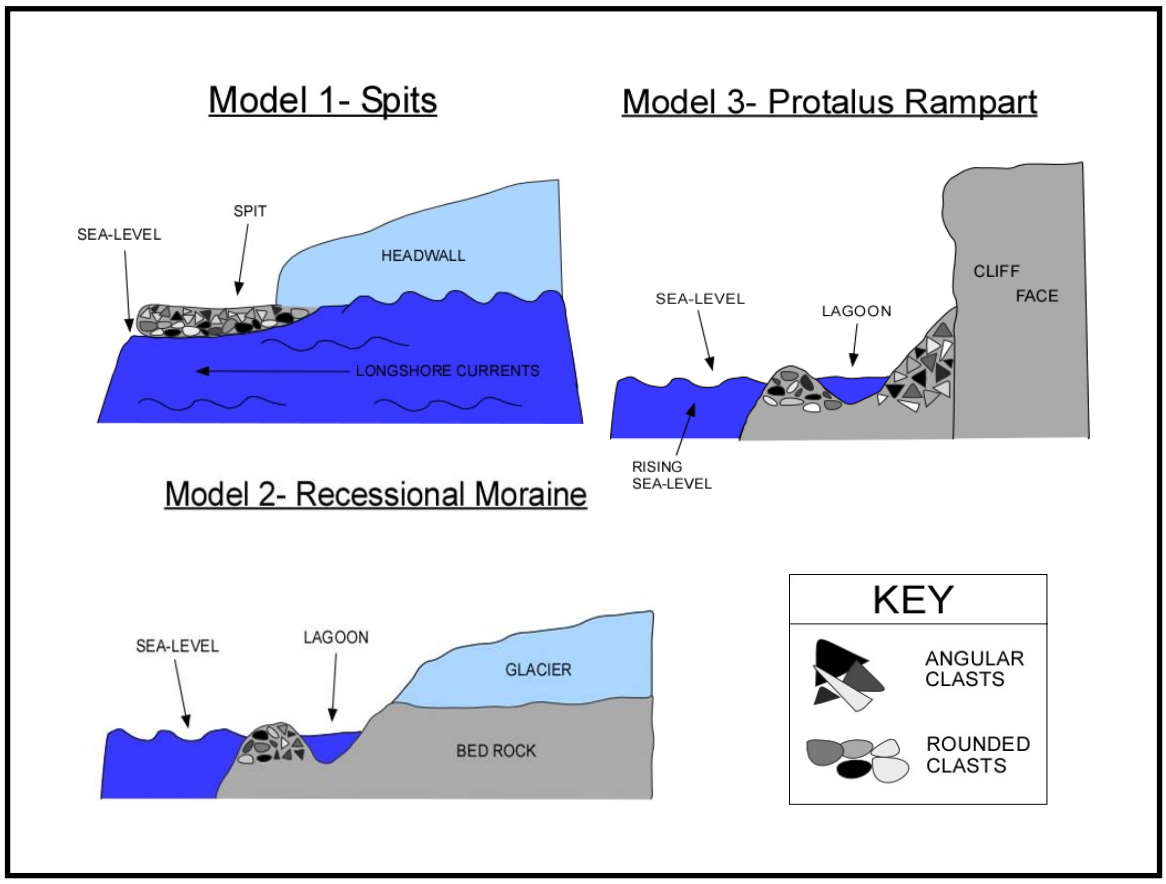

Figure 3 – Models for CRASL formation: Model 1) Spit - wave action erodes transports and rounds the clasts; Model 2) Recessional Moraine – sediment is deposited as the glacier retreats. Clasts on the seaward side are eroded due to wave action and clasts on the landward side are not affected by waves; Model 3) Pro-talus Rampart – sediments transported to sea-level due to rockfalls onto previous ice aprons. Upon melting of the ice apron a ridge is left in front of a talus slope. Clasts on the seaward side are eroded due to wave action and clasts on the landward side are not affected by waves.

CHAPTER II

BACKGROUND

Tectonic History

Like the East Antarctic craton and West Antarctica, during the Cambrian (550-500 m.y.a.) the Antarctic Peninsula was part of Gondwana. Unlike the East Antarctica craton, West Antarctica, including the Antarctic Peninsula, is composed of twelve micro-continental fragments that are thought to have been located between South America, East Antarctica, and New Zealand during the Cambrian (Fig. 4; Willan, 2003).

When Gondwana began to fragment and separate during the mid-Jurassic (165 m.y.a), the East Antarctic craton, West Antarctica and the Antarctic Peninsula began to rotate and move south toward the pole. The Antarctic Peninsula eventually collided with West Antarctica and the East Antarctic craton creating the present continent of Antarctica.

The Antarctic Peninsula is composed of well-developed accretionary, fore-arc, magmatic-arc, and back-arc sequences (Willan, 2003). Recent work indicates that the peninsula consists of at least two terranes that collided in the mid-Cretaceous: the Eastern Domain, which consists of Gondwanian rocks, and the Central Domain, which consists of magmatic-arc rocks (Triassic to mid-Cretaceous).

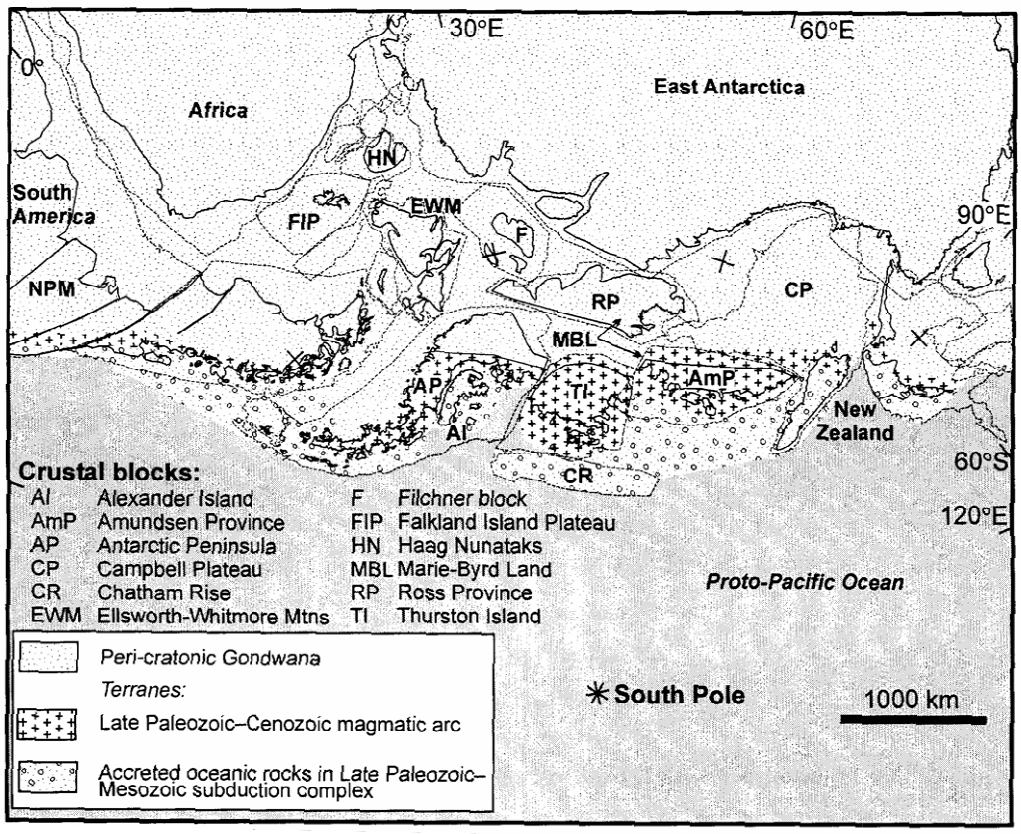

Figure 4 – Map showing the 12 microcontinents that composed Gondwana (Figure from Willan, 2003).

Regional Geology

The Palmer Archipelago and Danco Coast of the Antarctic Peninsula, which surround the Gerlache Strait, are primarily composed of Mesozoic and early Cenozoic plutonic and volcanic rocks. The Antarctic Peninsula consists of igneous complexes, metamorphic sediments and three thick (5 to 10 km) and laterally extensive sedimentary units: the Trinity Peninsula Group (TPG), the LeMay Group (LMG), and the Latady Formation (LF). Only one of the sedimentary units is present in the Gerlache Strait, the TPG (Fig. 5; Vaughan and Storey, 2000).

The Gerlache Strait can be divided into four major tectonic blocks, A-D (Fig. 6), by two systems of Tertiary faults, a longitudinal-and a transversal-fault system (Fig. 6; Birkenmajer, 1998). The Neumayer Fault and Fournier Fault, two longitudinal faults, trend SW-NE in the area. The Neumayer Fault, a strike-slip right-lateral fault, runs from the Peltier Channel to the northern portion of the Neumayer Channel (Fig. 6; Birkenmajer, 1998). According to Birkenmajer (1998), the Neumayer Fault probably continues as the Gerlache Strait Fault. The Fournier Fault, possibly a strike-slip fault, runs subparallel to the Gerlache Strait (Birkenmajer, 1998). According to Birkenmajer (1998), several additional E-W to SE-NW transverse faults can be observed on Brabant, Wiencke, and Anvers Island, as well as, in the Schollaert Channel. These transverse faults are also strike-slip faults (Alarcón et al., 1976).

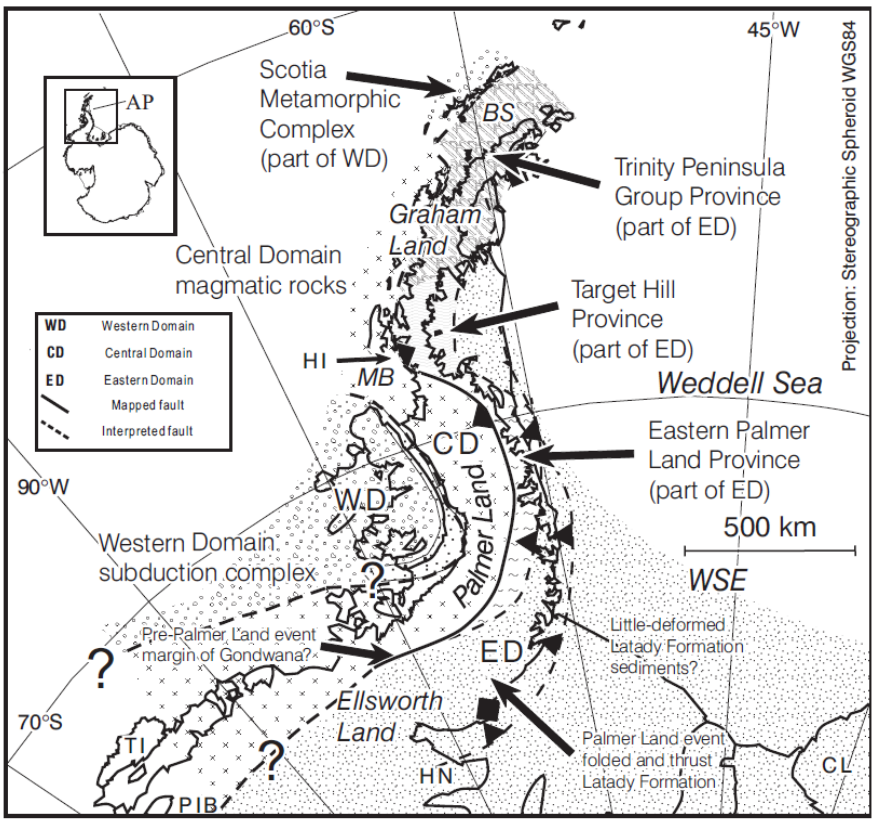

Figure 5 – Map of Antarctic Peninsula (AP) indicating known and inferred extents of provinces and different domains: Western (WD), Central (CD), and Eastern (ED). Notice that the only sedimentary group present in the Gerlache Strait area is the TPG. Abbreviations: Bransfield Strait (BS), Coats Land (CL), Haag Nunataks (HN), Marguerite Bay (MB), Pine Island Bay area (PIB), and Weddell Sea (WSE) (Figure from Vaughan and Storey, 2000).

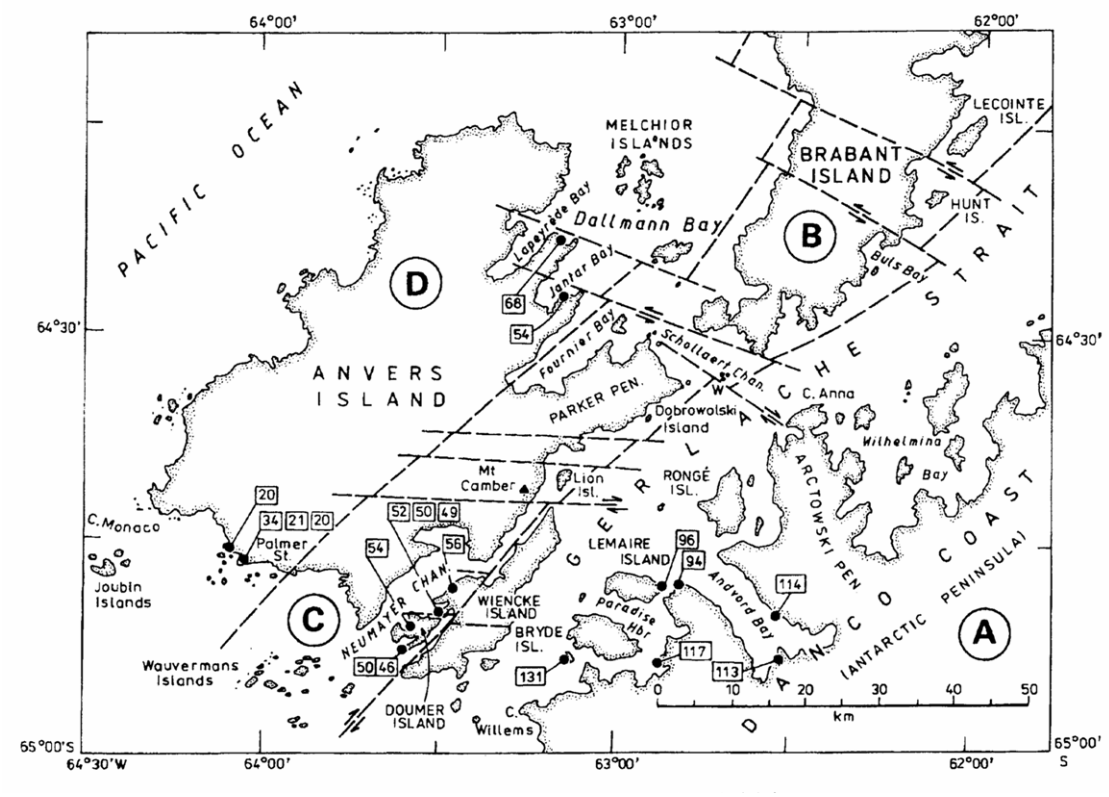

Figure 6 – Map of tectonic units in Gerlache Strait. A- Danco Coast; B- Brabant Island; C- Neumayer Block; D- Anvers-Melchoir Islands Block. Strike-slip faults are indicated by dashed lines (Figure from Birkenmajer, 1998).

Danco Coast

On the Danco Coast Block (Block A; Fig. 6), four major rock groups have been distinguished: Trinity Peninsula Group (TPG), Antarctic Peninsula Volcanic Group (APVG), and the two Andean Intrusive Suites (AIS-1 and AIS-2; Birkenmajer, 1998).

The TPG is mostly composed of unfossilierous marine turbidite sequences that vary in thickness from 5-1000 km (Birkenmajer, 1998; Willan, 2003). These metasediments account for the majority of rocks that crop out in the Gerlache Strait. Although the U-Pb provenance ages on clasts and detrital zircons are poorly constrained between 398-310 Ma, the deformation of the sediments is widely associated with accretion and arc magmatism during the Gondwanian Orogeny (Trinity phase) close to the Triassic/Jurassic boundary (Birkenmajer, 1998; Willan, 2003). Furthermore, the TPG group is thought to have been eroded sometime in the Jurassic prior to the Early Cretaceous (Birkenmajer, 1998).

The TPG can be further broken down into three formations: the View Point (VPF), Legoupil (LgF), and Hope Bay (HBF) formations. According to Willan (2003) the VPF consists of "*polymict boulder conglomerates interbedded with massive or thin-bedded cleaved mudstones, and amalgamated turbiditic sandstones*." Willan (2003) also states that the LgF is characterized by "*fine-grained sandstones, laterally impersistent cleaved mudstones, thin bedded sandstone-mudstone, minor pebbly mudstones, and a slide block of deltaic facies*." Furthermore, Willan (2003) states HPF consists of "*relatively underformed, amalgamated, thick lithic sandstones, mudstones, and thin interbedded siltstones and mudstones*."

The APVG extrusive rocks, thought to be lower Cretaceous in age, unconformably overly sediments from the TPG (Birkenmajer, 1998). Basaltic and andesitic lavas primarily make up the APVG; however tuffs and agglomerates with subordinate rhyodacite volcanics are present (Birkenmajer, 1998). According to Birkenmajer (1998), this group is approximately 2000 m thick and in some areas of the Gerlache Strait more than 1000 m can be seen in outcrop (Birkenmajer, 1995). During the Tertiary these rocks were folded and faulted along with the TPG sediments (Birkenmajer, 1998).

The Andean Intrusive Suite is divided into two phases: an older, Lower – Upper Cretaceous (Berriasian-Cenomanian) phase and a younger, phase that was emplaced sometime during the Late Cretaceous/Tertiary (Birkenmajer, 1998). The older phase (AIS-1) consists of granite to gabbro medium-scale plutons and sills that intruded both the TPG and APVG rocks (Birkenmajer, 1998). The younger phase (AIS-2) consists mostly of dykes that have both minor melanocratic and leucocratic hypabyssal intrusions (Birkenmajer, 1998).

Brabant Island

On the Brabant Island Block (Block B; Fig. 6), four rock units have been identified. However their ages and succession have not yet been determined (Birkenmajer, 1998). According to Birkenmajer (1998) the first unit is composed of 2000 m of "*altered stratiform basaltic-andesitic lavas and volcaniclastics*" that correlate to the APVG lavas of the Danco Coast. Ringe (1991) described them as "*Cretaceous or older purple tuffs and agglomerates…subhorizontally bedded lavas and tuffs,*" and

"*grey-green volcanic agglomerate*." The next unit identified was the granodiorite sill that intrudes the APVG in the area (Birkenmajer, 1998), which correlates to the older phase (AIS-1) on the Danco Coast (Birkenmajer, 1998).

Several melanocratic and leucocratic hypabyssal dykes are present on Brabant and Lecointe Island (Birkenmajer, 1998). These dykes, which cut into the APVG, correlate to the younger AIS phase (AIS-2; Birkenmajer, 1998). According to Ringe (1991), several basaltic dykes on Brabant Island (SE coast) characterize three phases of cross-cutting. Furthermore, K-Ar dating of one of these dykes indicated an Early Eocene (52$\pm$ 2 Ma) age (Ringe, 1991).

The last unit identified was described by Birkenmajer (1998) as "*brown-grey basaltic lavas of small thickness*", which unconformably overlay the APVG rocks. Birkenmajer (1998) suggests that these rocks correlate to the most recent magmatic activity referred to by Alarcón et al. (1976) as "*formación Bahía Bouquet,*" which when radiometrically dated yielded Late Tertiary-Pleistocene ages.

Neumajer Channel

The Neumajer Channel Block (Block C; Fig. 6), which is separated from the other blocks by the Neumajer and Fournier Fault, contains three groups of rocks (Birkenmajer, 1998). The first group, which forms the base of the sequence, is a plutonic rock of granitic to a granodioritic composition (Birkenmajer, 1998). Although these rocks correlate to the AIS rock of the Danco Coast, Birkenmajer (1998) points out that these rocks are much to young to correlate to the AIS-1 phase because of their younger radiometric ages (56-46 Ma, Late Paleocene-Early Eocene).

The second group of rocks observed on the Neumajer Channel block are systems of dykes that cross-cut the plutonic rocks (Birkenmajer, 1998). Birkenmajer (1998) described the third group of rocks as "*a thick complex of basaltic to trachyandestitic lava flows and cross-bedded tuffs*." This group is thought to be correlative to the "*formación Bahía Bouquet*" of Alarcón et al. (1976) by Birkenmajer (1998).

Anvers-Melchoir Islands

The Anvers-Melchoir Islands Block (Block D; Fig. 6) includes the NW part of Anvers Island, its subsidiary islands, and the Melchoir Islands (Birkenmajer, 1998). Although the succession of rock groups on this block are not well understood, three rock groups are present (Birkenmajer, 1998). These include: the APVG volcanic; granite, diorite and tonalite plutons; and two main groups of dykes.

According to Birkenmajer (1998) rocks from the APVG were observed at Palmer Station (Cape Monaco), Bonnier Point, and Quinton Point. Plutons consisting of granite, diorite, and tonalite were also observed in the Anvers Island area. Birkenmajer (1998) suggests that these rocks correlate to the AIS groups, and that the three different compositions actually represent three eruptive phases within this group. The first phase, which was observed at Dallman Bay (Parada et al., 1992), was dated at 68-54 Ma (Maastrichtian-Late Paleocene; Birkenmajer, 1998). The second phase, observed near Palmer Station (Fleming, 1979), dated around 34 Ma (Eocene/Oligocene boundary) and the third, also observed near Palmer Station, dated approximately 21-20 Ma (Early Miocene; Birkenmajer, 1998).

According to Hooper (1966), two groups of dykes were observed on Anvers Island and its offshore islands. The older of the two groups was described by Birkenmajer (1998) as containing "*dominant hornblende-bearing basic dykes, often hornfelsed by Andean intrusions (thus pre-dating the AIS)*" and "*rhyolitic dykes*." Birkenmajer (1998) described the younger group as "*propylitized pyroxene-bearing dykes*" that have intruded into the Cape Monaco granite and therefore are Tertiary in age.

Glacial History

Glaciation in East Antarctica is thought to have begun during the Eocene or Oligocene. The glaciation was initiated by decreasing atmospheric CO_2 concentrations and the opening of the Southern Ocean; eventually spreading to West Antarctica and the Antarctic Peninsula region (DeConto and Pollard, 2003; Florindo et al., 2003).

The tributary bays, and fjords throughout the Antarctic Peninsula were shaped by the Antarctic Peninsula Ice Sheet (APIS). During the Last Glacial Maximum (LGM), 20,000 yr BP – 18,000 yr BP, the APIS was grounded on the continental shelf (Bentley and Anderson, 1998; Anderson et al., 2002; Evans et al., 2004; Heroy and Anderson, 2005). Reconstructions of the maximum extent of grounded ice during the LGM have been determined using glacial geology and geomorphology data (Heroy and Anderson, 2005; Fig. 7).

Heroy and Anderson (2005) suggested that the continental shelf could be divided into two zones based on its geology: 1) the outer shelf characterized by the "*offlapping sedimentary wedges*", and 2) the inner shelf, characterized by igneous and metamorphic bedrock (Heroy and Anderson, 2005).

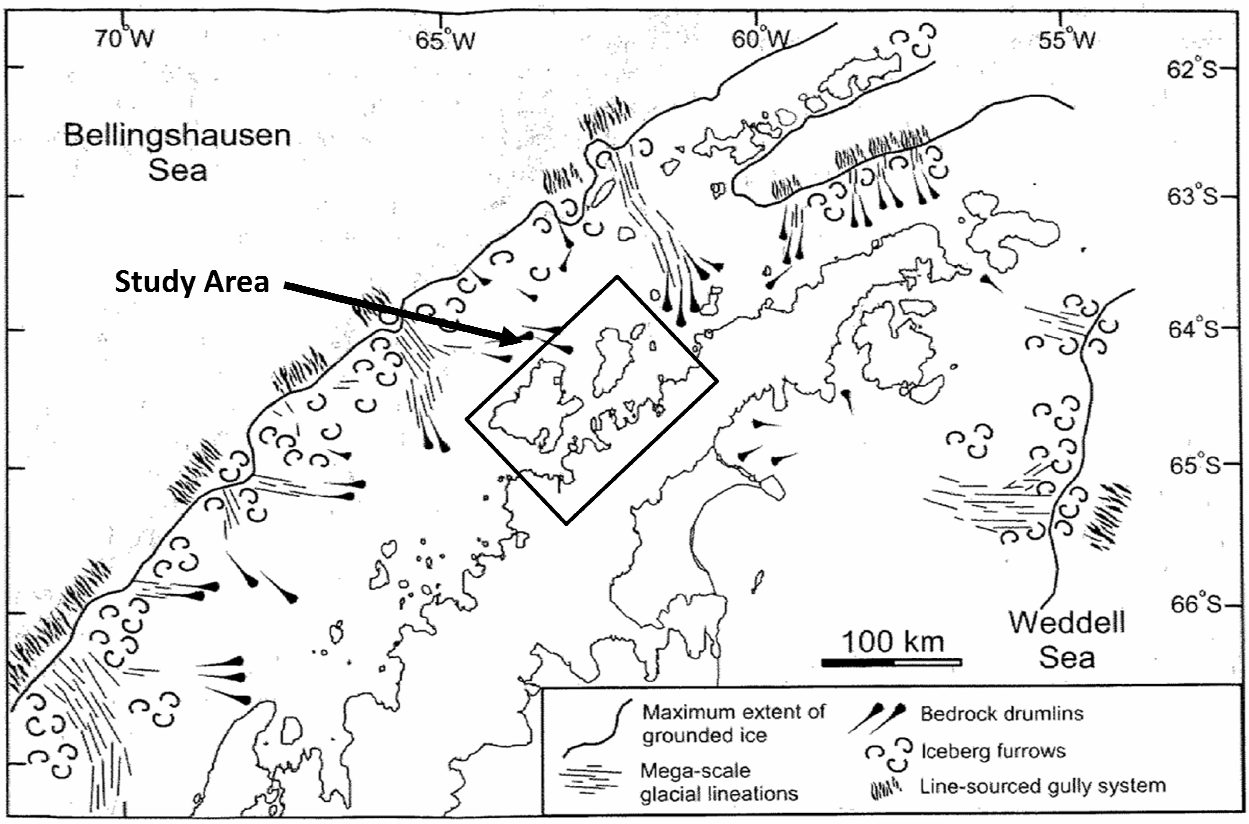

Figure 7 – Reconstruction of grounding line at LGM and geomorphic features identified on the continental shelf (Figure from Heroy and Anderson, 2005).

A piston core was taken from a glaciomarine unit in the Bransfield Basin by Heroy and Anderson (2005). A carbonate sample from this unit yielded a radiocarbon age of 17,340 cal yr B.P. indicating that the ice was already in retreat prior to this time (Heroy and Anderson, 2005). Radiocarbon dates from glacial-marine sediments near Anvers Island suggest the APIS retreated from the area sometime between 13,000 yr BP (corrected reservoir effect of 1230 yr; Domack et al., 2001) and 11,000 ^{14}C yr BP (corrected reservoir effect of 1500 yr; Pudsey et al., 1994). Cores taken from the central part of the Gerlache Strait suggest the glacial-marine sedimentation commenced sometime after 8,000 ^{14}C yr BP (uncorrected; Harden et al., 1992). According to Heroy and Anderson (2005) glacial retreat on the outer shelf began about 18,500 cal yr B.P. and on the inner shelf around 13,000 cal yr B.P. The APIS continued to retreat into the Holocene (Anderson et al., 2002).

Today the APIS averages ~500 m thick (Denton et al., 1991) and is grounded primarily above sea level (Heroy and Anderson, 2005). However, over most of the area outlet glaciers and local ice aprons still terminate at the ocean.

Geomorphic Features

Talus Deposits

Talus deposits are rock fragments that have broken off a rock face, fallen, and accumulated at the base of a cliff (Fig. 8). Although not exclusive to subpolar and polar regions they are common in areas of high relief. Talus deposits are the result of frost shattering on ice-free rock faces (Behre, 1933). The deposits usually are characterized by their cone or apron shapes (Easterbrook, 1999). Bryan (1934) states that "*if blocks fall*

Figure 8 – Talus slope in the Errera Channel. Photo taken during the *Nathaniel B. Palmer* 0307 Cruise, April 2007.

from a cliff to form such a heap, the larger will roll farther than the smaller and the heap will be graded upward from coarse to fine." Talus deposits are very angular due to the lack of transport or lack of erosional processes. Usually the slope of the deposits is determined by the grain-size with maximum slopes of 36.5° (Behre, 1933).

Pro-talus Rampart Deposits

Ono and Watanabe (1986) defined pro-talus ramparts as "*ridge-like accumulations of coarse angular blocks which develop along the lower margin of perennial or semi-perennial snow patches existing below the free face*." First mentioned in the literature by Behre (1933) as nivation ridges, the features were renamed by Bryan (1934) as pro-talus ramparts.

Originally, pro-talus rampart deposits were thought to have formed by sediments that had detached from a free face and fallen onto perennial snow banks. After skating down the snow face, the sediments, which consist of coarse frost shattered blocks, accumulate at the bottom (Tricart and Cailleux, 1962; French 1976). Sekine (1973) provided a detailed summary of this model for the formation of a pro-talus rampart (Fig. 9). According to Easterbrook (1999), the snowbanks that transport the rock debris beyond the base of the slope are seasonal. When the depression behind the rampart is filled with sediment, it is possible for the pro-talus rampart to blend into the talus slope as a benchlike extension (Fig. 10 and Fig. 11). Like talus deposits, pro-talus ramparts are also fed by frost shattering on an ice-free cliff face. The clasts are very angular due to the short transport distances.

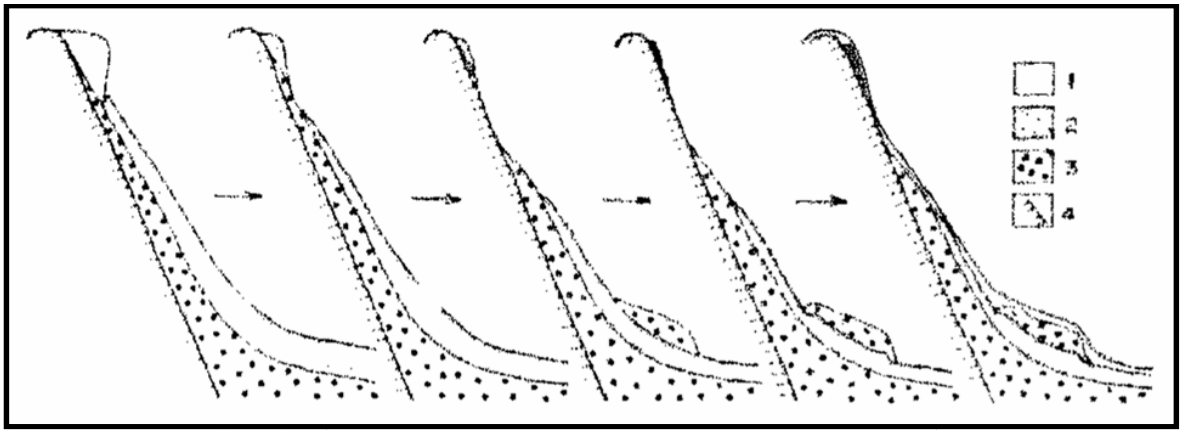

Figure 9 – Formation of a pro-talus rampart. 1) new snow, 2) snow patch, 3) debris, 4) bed rock (Figure from Sekine, 1973).

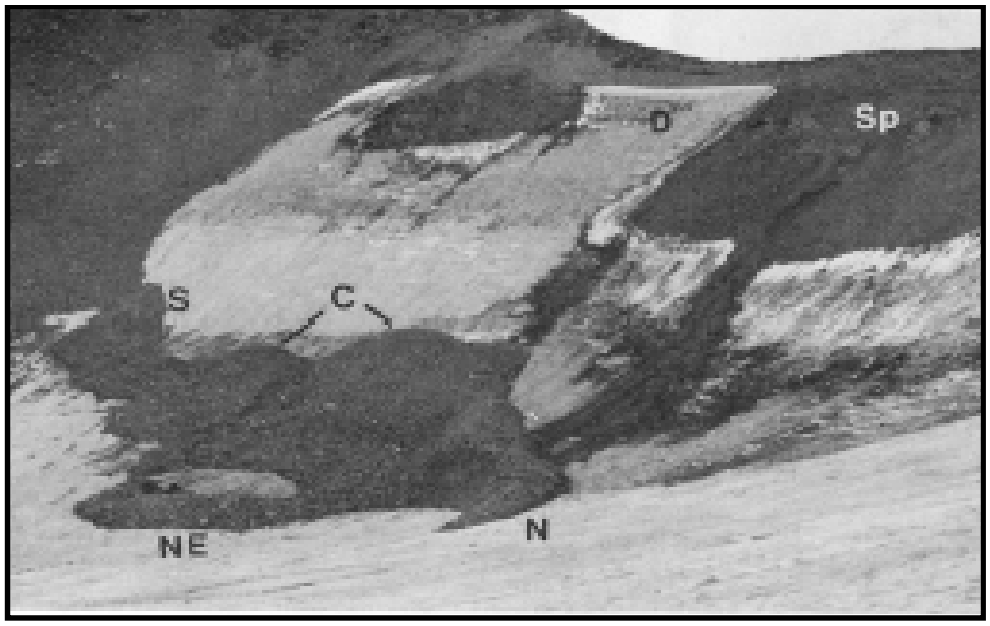

Figure 10 – Sections of a pro-talus rampart and alpine debris. Showing: C) central rampart, S) southern branch, NE) northeastern branch, D) depression on the cirque wall, Sp) snow patch covered with debris (Figure from Ono and Watanabe, 1986).

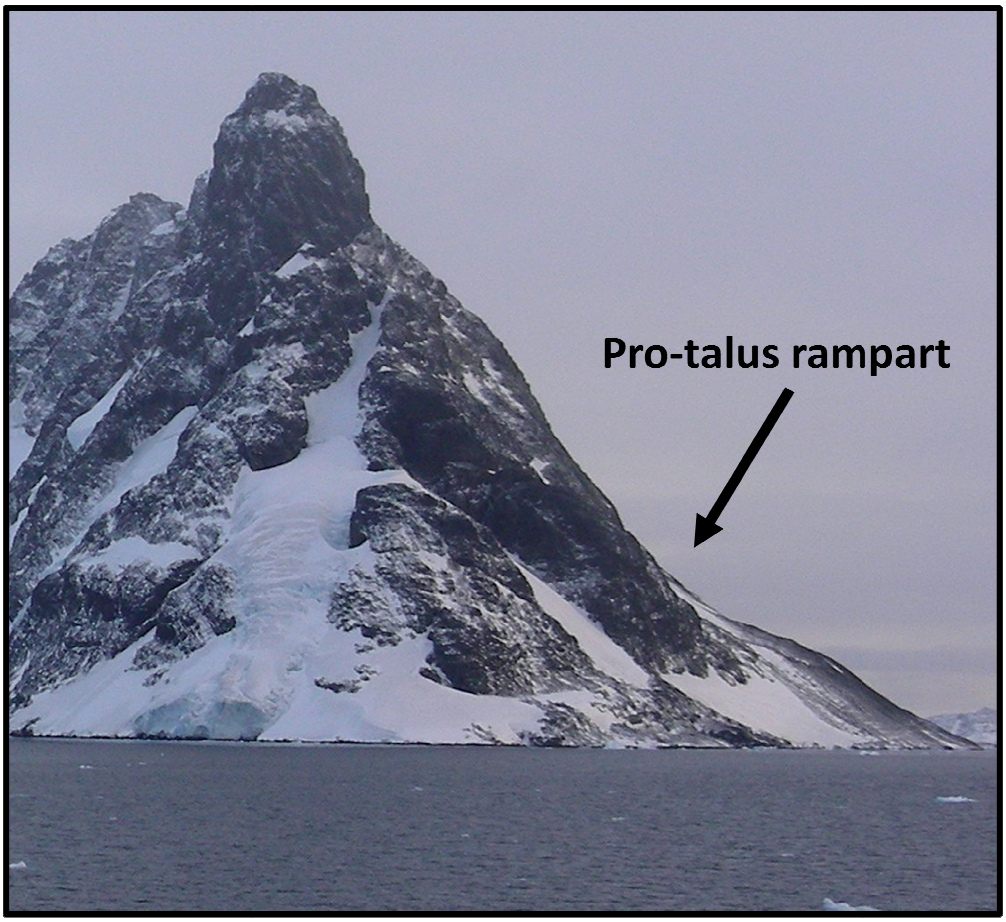

Figure 11 – Pro-talus rampart observed in Antarctica. Photo taken in April 2007.

Moraines

End moraines that form during consecutive retreats and stillstands of glacial margins are known as recessional moraines. Like other moraines, they contain clasts of varying sizes known as till (Plummer and McGeary, 1996). The majority of fragments within till are angular but can range in shape depending on their erosional history (Plummer and McGeary, 1996). The overall geometric shape of moraines is usually curvilinear (Easterbrook, 1999; Fig. 12). Moraines built by valley glaciers are typically crescent-shaped or horseshoe-shaped (Plummer and McGeary, 1996).

Beaches

Plummer and McGeary (1996) define a beach as "*a strip of sediment (usually sand or gravel) that extends from the low-water line inland to a cliff or a zone of permanent vegetation*." Although most beaches would fall into this category some, such as beaches in polar regions, may not completely (Fig. 13).

Polar beaches are distinguished from nonpolar beaches, by features such as: 1) resting on ice, 2) being pitted, 3) containing ridges and mounds due to ice push or deposition of stranded ice, 4) presence of beach ridges that terminate unexpectedly due to the ice when the ridges were formed, 5) ice-rafted fragments, 6) poorly rounded sediments, 7) frost cracks, mounds, stone circles, polygons, and solifluction deposits, 8) striations caused by sea ice and icebergs, 9) beach ridges with erosional gaps due to meltwater streams, 10) beaches with ice-contact features and glaciomarine deposits, 11) ventifacts, 12) cold-water fossils, and 13) presence of soft parts of marine organisms (Nichols, 1961).

Figure 12 – Moraine deposit in the Errera Channel. Photo taken during the *Nathaniel B. Palmer* 0307 Cruise, April 2007.

Figure 13 – Neko Harbour beach in Andvord Bay. Photo taken during the *Nathaniel B. Palmer* 0307 Cruise, April 2007.

Spits

A spit is defined as "*a fingerlike ridge of sediment that extends out into open water*" (Plummer and McGeary, 1996). Meistrell (1966) defines a spit as "*a ridge on the surface of the platform, partially emergent above mean sea level*" and is dependent on the platform as to how it develops.

Sand and or sediment that is transported parallel to the shore by longshore drift supplies the ridges with material (Plummer and McGeary, 1996). Therefore, the sediments within spits are typically similar to beach deposits found in the area. In the case of polar regions this means they are poorly rounded.

Optically Stimulated Luminescence

Optically Stimulated Luminescence (OSL) is a dosimetry-based technique used to date Quaternary sediments (Forman et al., 2000). It measures a time-stored luminescence signal by controlled exposure to light in the laboratory and is reset by exposure to sunlight prior to deposition (Forman et al., 2000). Therefore, sediments that have received exposure to light prior to deposition are considered prime sample candidates.

Sediments in abundant quartz and feldspar grains are needed for luminescence dating. These silicate minerals are ideal because they contain crystal defects and chemical impurities. Defects act as prospective sites for electron storage and source for luminescence signals (Wagner, 1998). However, in principle, other minerals can also be used (Lian and Roberts, 2006).

When the minerals are exposed to ionizing radiation, in the form of alpha (α), beta (β), and gamma (γ) rays, free electrons are generated. Ionizing radiation comes from the

natural decay of radioactive elements (uranium, thorium, and potassium) in the minerals and the immediate surrounding material or from cosmic rays (Lian and Roberts, 2006). The free electrons become trapped in the lattice-defects and are stored. Many of these electrons become trapped in "deep" traps (1.6-1.8 eV), which are theoretically stable for up to $> 10^6$ years and therefore act as long-term radiation dosimeters (Forman et al., 2000).

Exposure to light will release the trapped electrons, which recombine with the ions. The light emitted during this process is called *luminescence*. The luminescence signal increases with a longer exposure to environmental radiation, referred to as *natural radiation dose (ND)*. Therefore, the only limitation to OSL dating is prematurely exposing the sample to light. If this can be done in a controlled environment where the luminescence signal can be measured the *natural dose* can be obtained. Furthermore, if the concentration of radioactive isotopes in the surrounding material is measured, the *natural dose rate* can be calculated, thus giving an age (t; Eq. 1). The age indicates the elapsed time since the sample was last exposed to sunlight.

$$t = ND/NDR \qquad \text{(Eq. 1)}$$

It is important to find sediments that have not been exposed to sunlight since the event one is interested in dating. Sand sized sediments, which are typically used in OSL dating, can be transported easily by erosional processes especially in the harsh Antarctic environment. When the grains are transported they are again exposed to sunlight, releasing the trapped electrons. Therefore, larger clast sizes are necessary to ensure that

the samples were not transported and reset. The coarsest sediments within beaches are generally deposited in the intertidal zone. Cobbles located in the intertidal zone are of interest because they were last turned over while in the swash zone. Within the high-relief area of the Antarctic Peninsula, most beaches are composed of cobbles. Therefore, cobbles in the Antarctic Peninsula are promising for OSL dating because of their size and prominence in beach environments (P. Kouremenos; per. comm., 2008).

In areas glaciated during the LGM, elevated or raised beaches along coastlines are common due to isostatic rebound. Isostatic rebound occurs when the ice is removed from the land and the land moves to maintain equilibrium prompting the land to rebound. Consequently, beaches that form at sea-level become elevated or raised due to removal of ice (Figs. 14 and 15). Ideally, more than one raised beach ridge is preserved in an area to record a history of isostatic rebound.

Raised beaches are good indicators of sea-level changes and have a history of use to construct sea-level curves in Antarctica (Hall and Denton, 1999; Hall et al., 2004; Baroni and Hall, 2004, and Bentley et al., 2005). However, existing sea-level curves rely on radiocarbon dating. Radiocarbon dating presents two problems: 1) the uncertainty of the radiocarbon reservoir in Antarctica and 2) the scarcity of radiocarbon material in Antarctica. Furthermore, dateable organic material at sea level is even less likely and its relationship to sea level is questionable. When dating cobbles from raised beaches using OSL, one avoids the uncertainty of a radiocarbon reservoir. Additionally, the relationship of raised beach cobbles' to paleo sea levels is more precise. Thus, if cobbles can be OSL dated from several raised beaches in an area then a sea level curve for that area can be constructed.

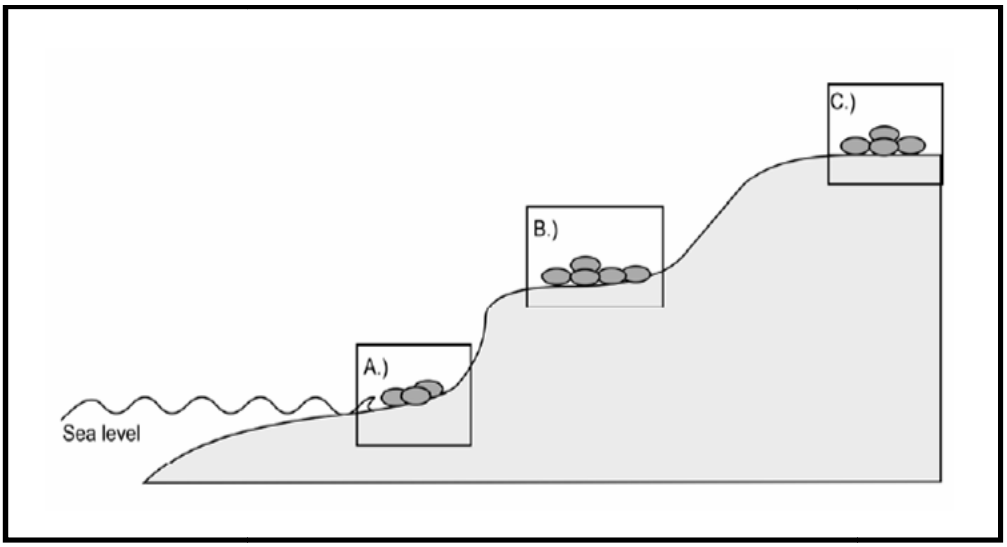

Figure 14 - Schematic of raised beaches. A, B, C represent cobbles on different raised beaches.

Figure 15 - Raised beaches in the South Shetland Islands April, 2007.

CHAPTER III

METHODOLOGY

Sedimentary Characterization

To test my hypotheses that CRASLs form from recessional moraines that are reworked in to beach deposits, samples were collected from modern talus slopes, moraines, beaches, and a CRASL in the Gerlache Strait. This was done in order to determine the basic sedimentological characteristics of each deposit and compare the sedimentology of modern environments to that of a CRASL. The sedimentary characteristics examined included grain size, roundness, sphericity, and petrology. Sampling was also important in constructing a facies model for a CRASL.

Samples were taken from the Gerlache Strait at eight different localities: Palmer Station (-64°7.000'S,-64°0.000'W), Norsel Island (-64°45.646'S, -64°05.118'W), Humble Island (-64°45.923'S, -64°05.074'W), Limitrophe Island (-64°47.814'S, -64°00.631W), Torgerson Island (-64°46.301'S, -64°04.515'W) (Fig. 16 and Fig. 17), Damoy Point (-64°49.000'S, -63°31.000'W) (Fig. 16 and Fig. 18), the Errera Channel (-64°45.500'S, -62°40.000'W), and Neko Harbor (-64°50.591'S,-62°31.653'W) (Fig. 16 and Fig. 19).

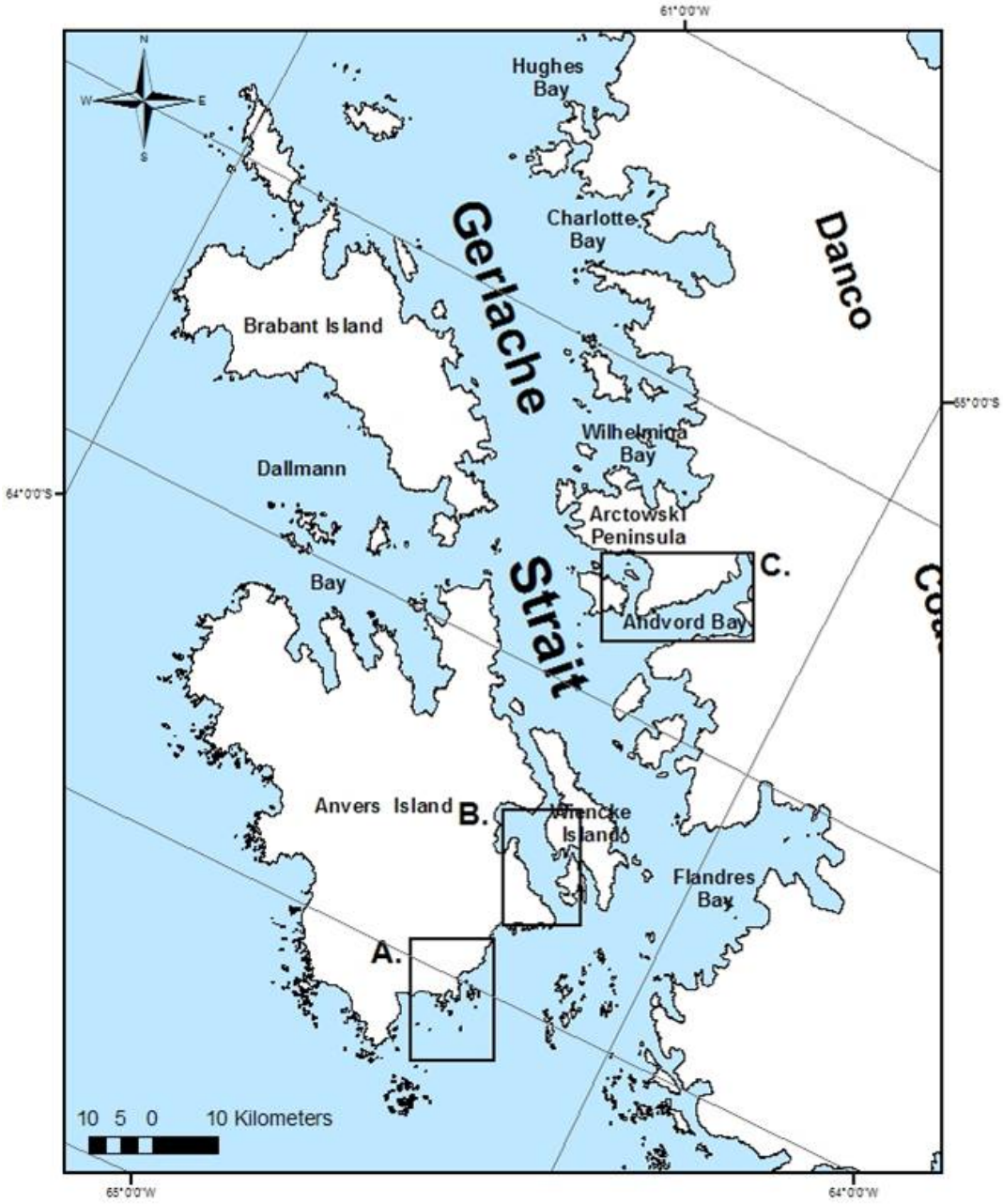

Figure 16 – Map indicating three main sampling areas along the Gerlache Strait.

A.

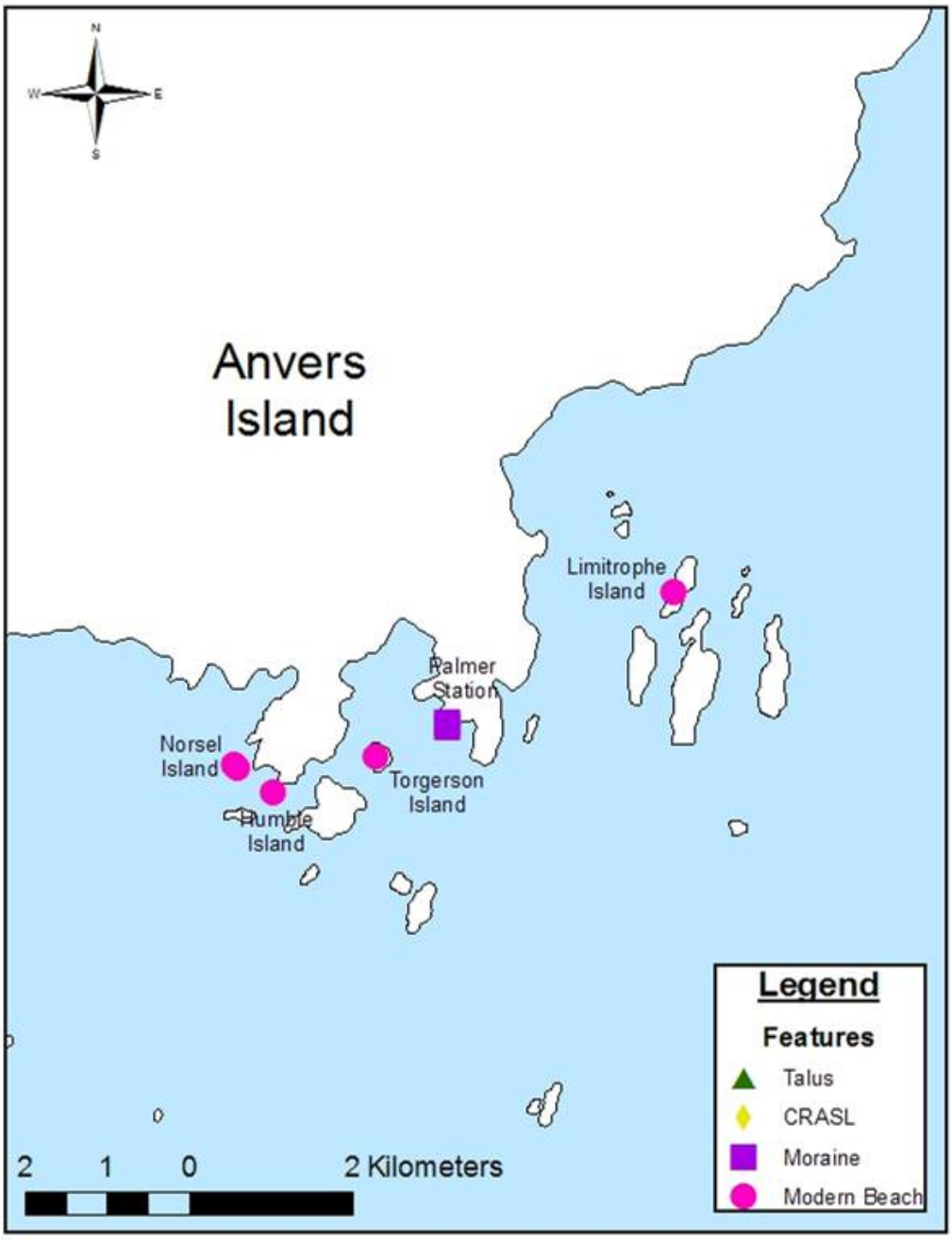

Figure 17 – Location map of sample sites on the southern tip of Anvers Island, near Palmer Station.

B.

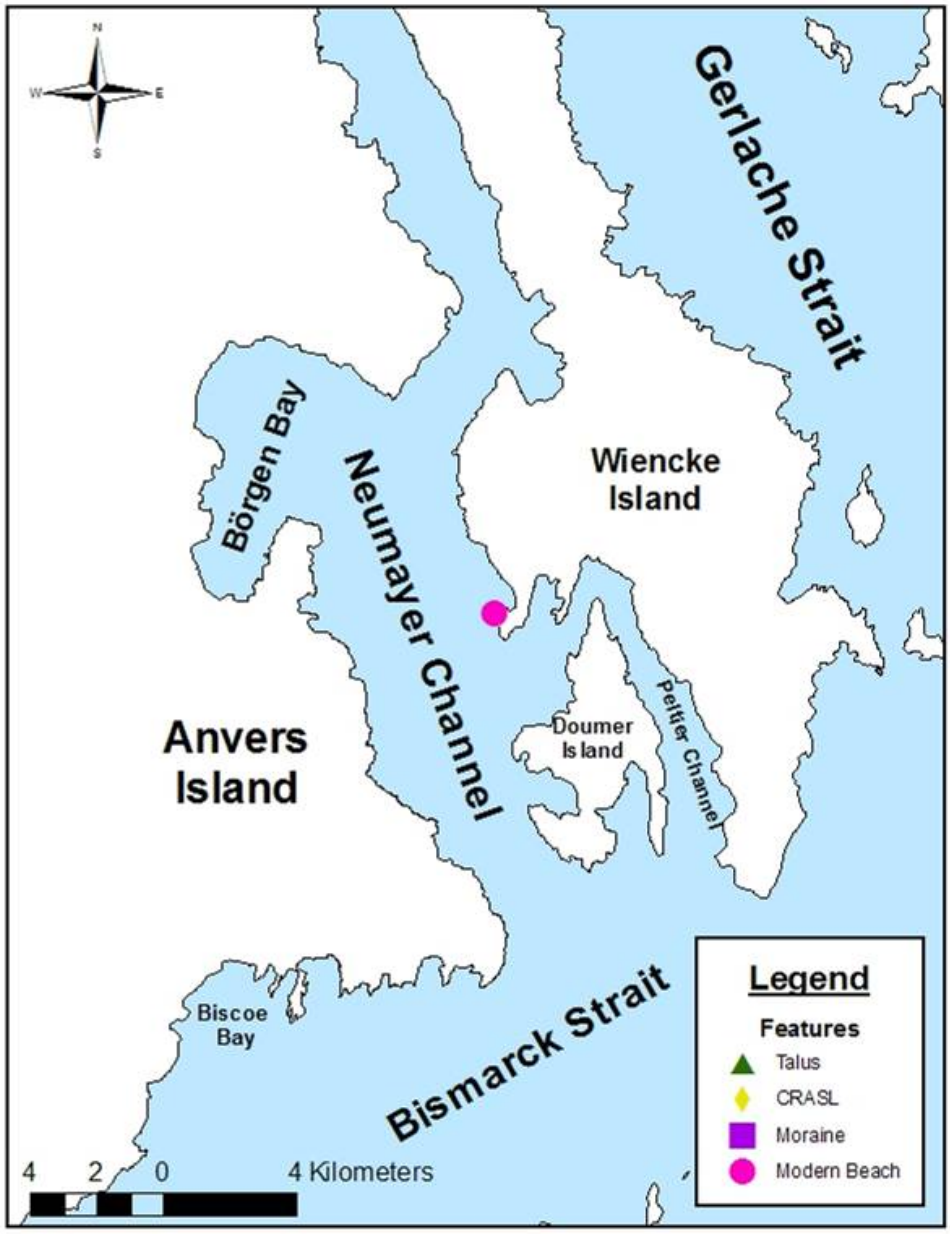

Figure 18 – Location map of sample site on Wiencke Island.

C.

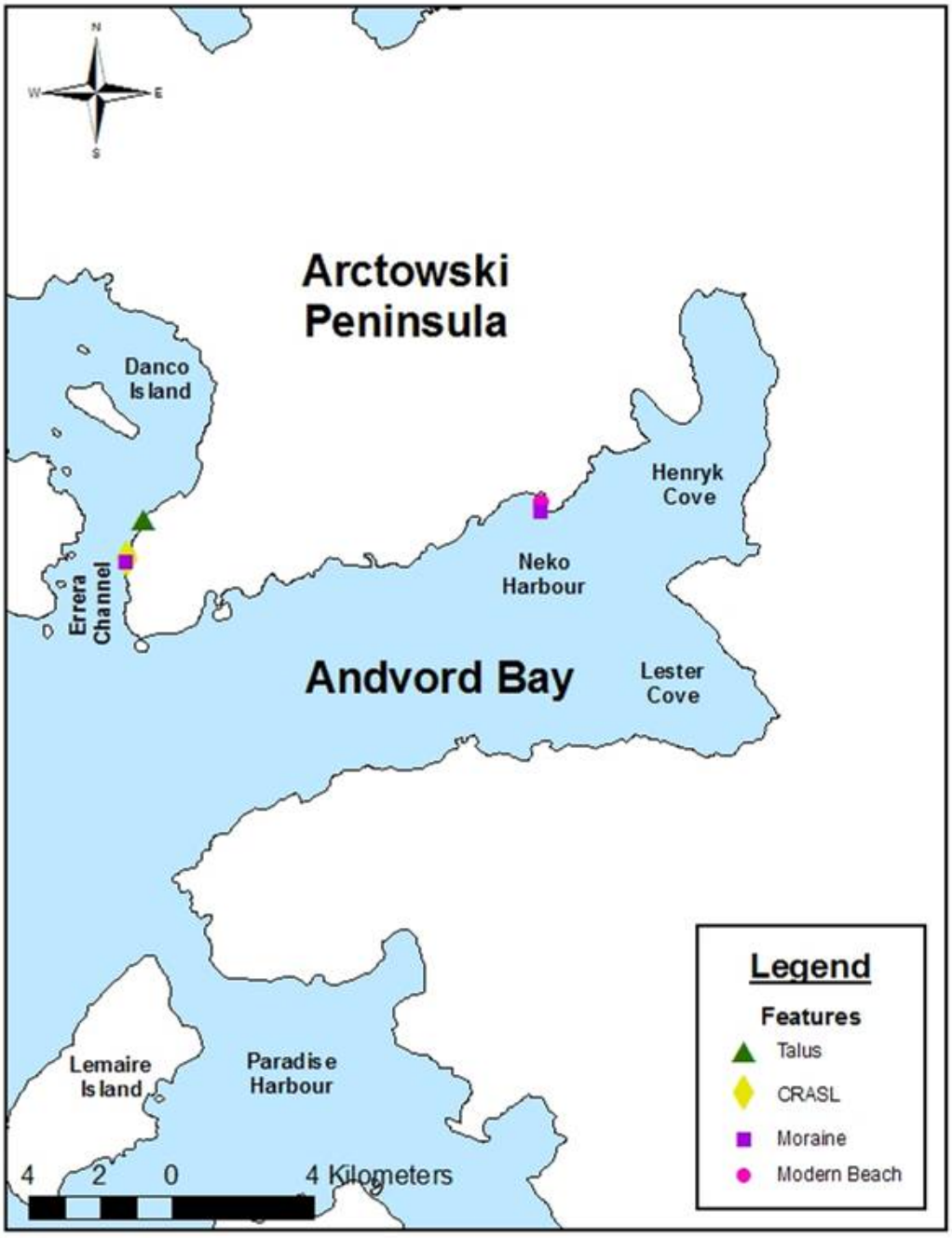

Figure 19 – Location map of sample sites off the Arctowski Peninsula.

Field Work

GPS

A Garmin GPS was used to record latitude and longitude coordinates of each field site. At Damoy Point, a Trimble GPS was used to construct a topographic profile through a series of raised beaches and to provide a more accurate measurement of elevation for the position of sample for OSL analysis. Once the location was recorded, one or two surface samples were obtained from each geomorphologic feature. The CRASL was sampled once each from the lower and higher portion of the seaward side and from the landward side.

Texture Sampling

In locations where time permitted, angularity and sphericity was measured (Table 1). At each site, 100 or more clasts were classified using the American Stratigraphic (AMSTRAT) angularity card for angularity measurements. At Torgerson Island, where sphericity results were also obtained, a ruler was used to measure the short (a), intermediate (b), and long (c) axes of each clast. Pictures documenting an example of each angularity type (well rounded, rounded, sub-rounded, sub-angular, and angular) were taken for every locality (Appendix A, pg 211). Surface samples were stored in plastic bags and labeled for lab analysis.

TABLE 1. TYPES OF FEATURES SAMPLED AT LOCALITIES

Location	Feature	Angularity	Sphericity
Errera Channel	Talus slope	X	N.A.*
	CRASL	X	N.A.*
	Moraine	X	N.A.*
Palmer Station	Moraine	N.A.*	N.A.*
Norsel Island	Beach	X	N.A.*
Humble Island	Beach	X	N.A.*
Limitrophe Island	Beach	X	N.A.*
Torgerson Island	Beach	X	X
Neko Harbour	Beach	X	N.A.*
	Moraine	X	N.A.*
Damoy Point	Beach	N.A.*	N.A.*
	OSL	N.A.*	N.A.*

*N.A. – not available.

OSL Sampling

In order to assure the cobbles obtained for OSL analysis faithfully recorded paleo-sea level and were not reworked by other processes such as freeze-thaw, frost sorting, ice-berg pushup, or glacial activity, it was essential to locate cobbles in boulder pavements or imbricated within beach deposits. Boulder pavements are characterized by flat, tightly packed mosaics of ice-smoothed and striated boulders and only form in polar intertidal and lacustrine areas (Fig. 20; Hansom, 1983). Imbricated beaches are those whose sediments are oriented in the same direction due to wave action. The disturbance of a boulder pavement or an imbricated beach suggests that other processes have been

Figure 20 – Boulder pavement observed in Antarctica. Photo taken in April 2007.

reworking the deposits since deposition, and the deposits OSL age no longer records an accurate time of paleo sea level. Thus, these samples should be avoided.

As OSL analysis works best on quartz grains, it was essential to locate quartz-bearing cobbles within the appropriate boulder pavement or imbricated beach deposits. Once located, a cobble was first labeled and marked to identify the upright side of the cobble. Its location was then recorded and a photo taken to record its *in situ* state. It was then sampled under a special tarp to ensure no light exposure and placed in a black, plastic bag in order to transport it back to the lab. In addition, samples from the surrounding sediment were also collected in the same manner to calculate the dose rate.

Lab Work

Processing procedures shown in Figure 21, and described in detail below.

Grain Size

First, the samples were dried and weighed in 1000-mL glass beakers (Fig. 21). Once the samples were dry, they were sieved using a Ro-Tap Sieve Model RX-29-16. The Standard Screen Scale screen sizes used during sieving were: 50 mm, 25 mm, 16 mm, 8 mm, 5.6 mm, 4.75 mm, 4.00 mm, 3.35 mm, 2.80 mm, 2.36 mm, 1.7 mm, 500 μm, 250 μm, 125 μm, 63 μm, and 38 μm. Anything smaller than 38 μm was captured in the bottom plate. All eighteen samples were sieved for two minutes and visually inspected to assure samples were completely broken down. The samples from each Standard Screen size were then weighed in 150-mL plastic beakers, transferred to plastic bags and labeled.

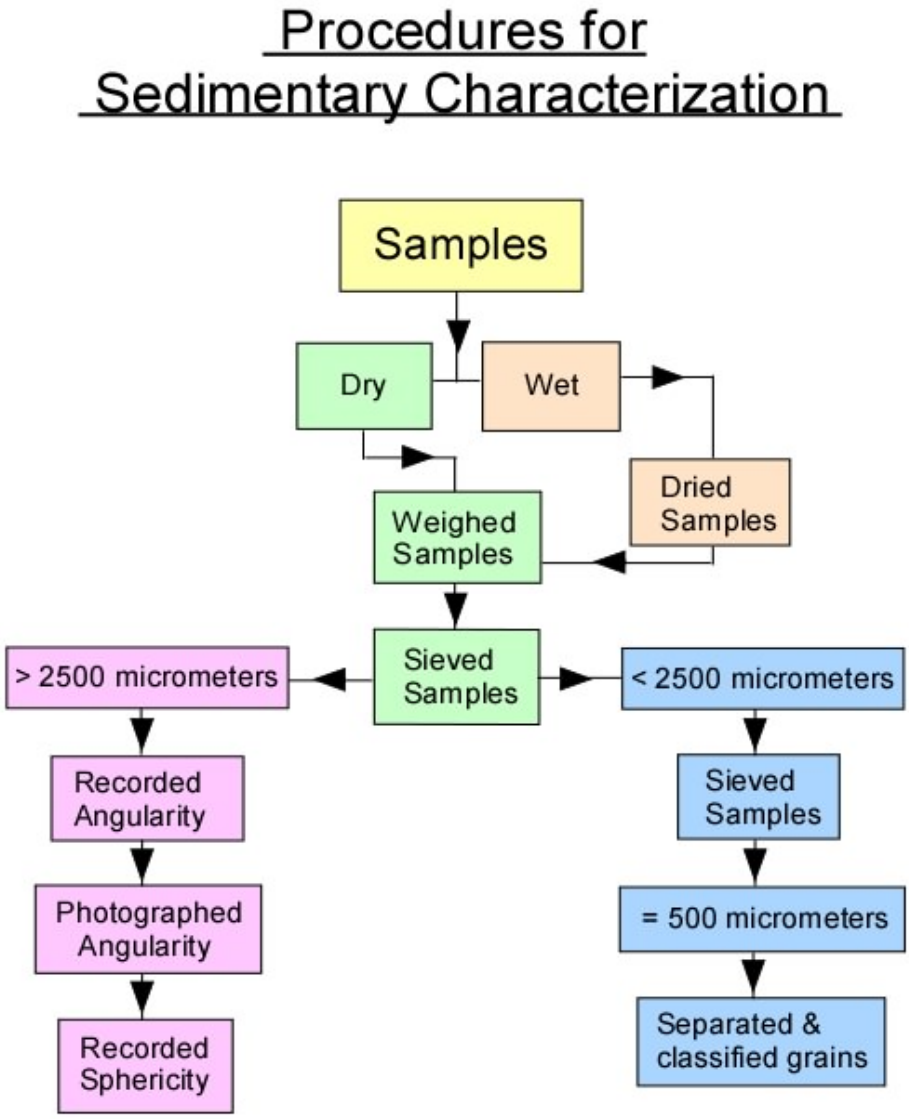

Figure 21 – Procedures used for sedimentary characterization sample preparation.

After sieving, the graphic mean (M_Z, Eq.2), inclusive graphic standard deviation (σ_i, Eq. 3), and inclusive graphic skewness (SK_i, Eq. 4) were calculated using the following formulas originally from Krumbein (1938) and modified by Folk and Ward (1957):

$$M_Z = \frac{\Phi_{16} + \Phi_{50} + \Phi_{84}}{3} \qquad \text{(Eq. 2)}$$

$$\sigma_i = \frac{\Phi_{84} - \Phi_{16}}{4} + \frac{\Phi_{95} - \Phi_5}{6.6} \qquad \text{(Eq. 3)}$$

$$SK_i = \frac{(\Phi_{84} + \Phi_{16} - 2\,\Phi_{50})}{2(\Phi_{84} - \Phi_{16})} + \frac{(\Phi_{95} + \Phi_5 - 2\,\Phi_{50})}{2(\Phi_{95} - \Phi_5)} \qquad \text{(Eq. 4)}$$

The sieving results were graphed on a phi (Φ) scale and the cumulative weights were found for each of the following percentages: 95%, 84%, 50%, 16%, and 5%. However, the percentages did not always fall within the sieving subdivisions. In those cases an extrapolation of the grain-size data from the cumulative graph was made using a linear approximation (Eq. 5).

$$y = mx + b \qquad \text{(Eq. 5)}$$

The x and y values of the closest data points on the plotted cumulative weight (%) vs. phi graph were used to solve for m (Eq. 6).

$$\frac{y_2 - y_1}{x_2 - x_1} = m \qquad \text{(Eq. 6)}$$

The calculated value of 'm' was used with y_1 and x_1 to solve for 'b' using Equation (5). Once the appropriate percentages were calculated, these values were used in Equations (2), (3), and (4). Calculated values for M_Z, σ_i, and SK_i were then compared to the categories for standard deviation (Table 2) and skewness (Table 3) proposed by Folk (1974).

TABLE 2. STANDARD DEVIATION CLASSIFICATIONS (Folk, 1974)

Phi sizes (Φ)	Classification
< 0.35	Very well sorted
0.35 – 0.50	Well sorted
0.50 – 0.71	Moderately well sorted
0.71 – 1.00	Moderately sorted
1.00 – 2.00	Poorly sorted
2.00 – 4.00	Very poorly sorted
> 4.00	Extremely poorly sorted

TABLE 3. SKEWNESS CLASSIFICATIONS (Folk, 1974)

Values	Classification
> +0.30	Strongly fine skewed
+0.30 - +0.10	Fine skewed
+0.10 - -0.10	Near symmetrical
-0.10 - -0.30	Coarse skewed
< -0.30	Strongly coarse skewed

Angularity

Angularity was determined from a minimum of one hundred clasts while in the field. Angularity counts were also performed on all clasts larger than 16 mm obtained from surface samples brought back to the lab. Angularity was only compared among clasts of similar grain sizes. Clasts were divided into three sieve sizes (50 mm, 25 mm, and 16 mm) and angularity was also determined by comparing the clasts to an AMSTRAT angularity chart. The clasts were then classified accordingly as: angular, sub-angular, sub-rounded, rounded, or well rounded. After angularity classification, pictures documenting an example of each roundness type were taken for every locality.

In order to analyze the samples, all of the results recorded for each geomorphic locality were combined. A sum of all of the individual categories (angular, sub-angular, well rounded, etc.) for each locality (talus deposit, CRASL, moraine, modern beach) was calculated. Once summed, the results were then normalized using the following equation (7).

$$\frac{\text{Category Sum}}{\text{Total Locality Sum}} \qquad \text{(Eq. 7)}$$

Sphericity

Due to time constraints, sphericity measurements in the field were made at only one locality, Torgerson Island. However, sphericity measurements from surface samples collected at each site were made in the lab.

Sphericity was measured for each clast in the 50 mm, 25 mm, and 16 mm Standard Sieve Screen sizes by measuring the short (a-axis), intermediate (b-axis), and long (c-axis) axes using a ruler. The sphericity of each clast was calculated using equations (8) and (9), where the short axis was represented by D_s, the intermediate axis represented by D_i, and the long axis represented by D_L.

$$D_i/D_L \quad \text{(Eq. 8)}$$

$$D_s/D_i \quad \text{(Eq. 9)}$$

The results were then graphed using D_s/D_i vs. D_i/D_L for each of the clasts in each grain-size fraction by locality. Finally, the graphs were compared to the classification of shapes, (oblate, equant, bladed, or prolate; Fig. 22), following the Zingg (1935) classification.

Petrology

In order to avoid any bias of mineral occurrence by grain size, petrology was only compared between the same grain-size fraction from each deposit. The Standard Sieve Screen size of 500 μm was selected for the grain counts because it contained the largest number of grains from the largest number of samples. However, three of the eighteen samples did not contain clasts of that grain size. Fifteen samples that did contain 500 μm grains were: Neko Harbor (NK01, NK02, NK03), Norsel Island (NI02, NI02), Limitrophe Island (LI01), Damoy Point (PLMB), Errera Channel Talus (ECT01), Errera Channel CRASL (ECC01, ECC02), Neko Harbor Moraine (NKM, NKHM), Errera

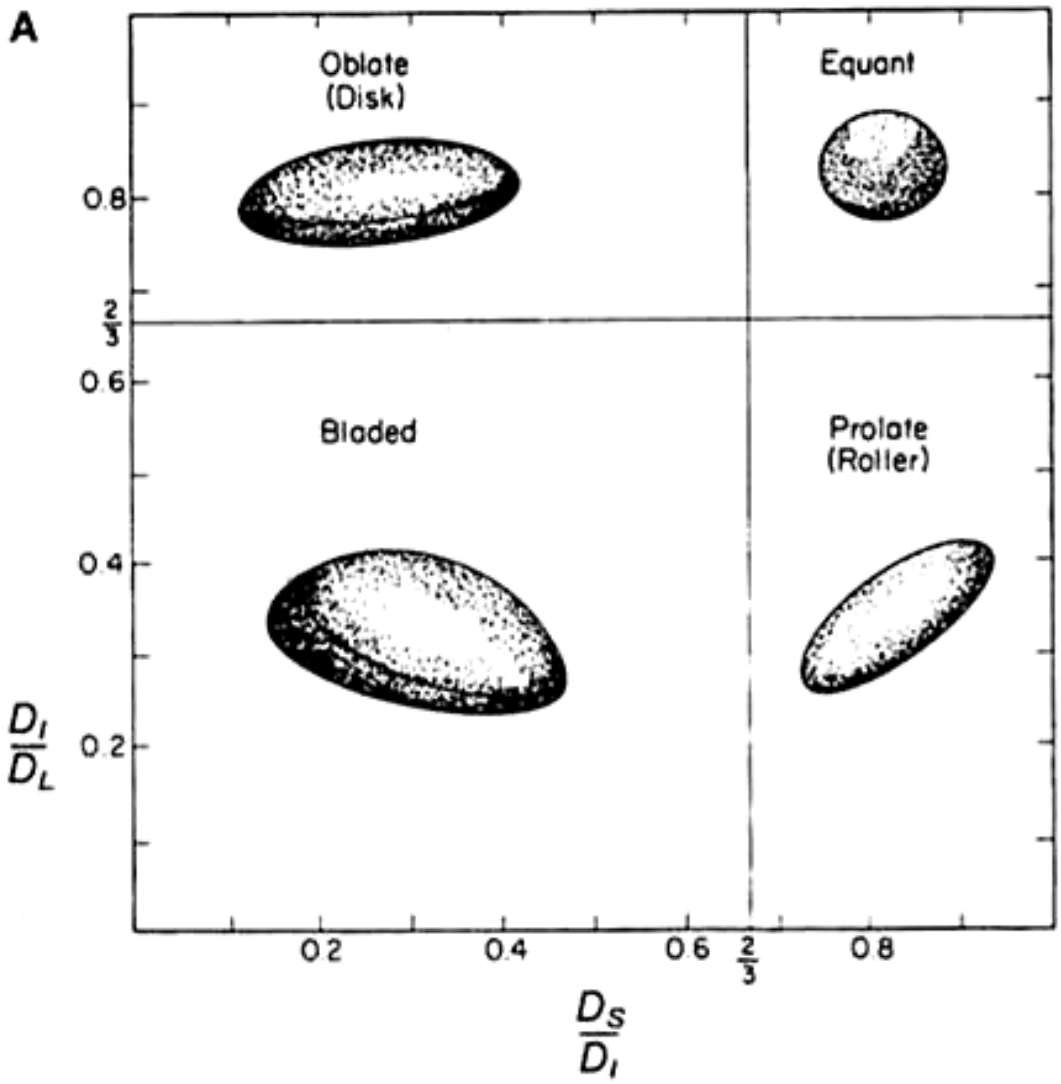

Figure 22 – Shape classification of pebbles from Boggs (1995) modified by Blatt, et al., (1980) after Zingg (1935).

Channel Moraine (ECM01), and Palmer's Station Moraine (PSM, PLMF). Humble Island (HI01), Torgerson Island (TI01) and Errera Channel CRASL (ECC03) did not have samples in that grain size.

In order to secure a random sampling of grains the grains were split two to four times, depending on the amount of sample, using an Ottoman grain splitter. Upon isolating the appropriate grains, they were transferred to a numbered picking plate and counted using a binocular microscope. The *RANDBETWEEN* (1, 141) function in Excel was used to generate random numbers corresponding to the cells on a numbered plate used to pick grains. When either all or 300 grains had been counted, each sample was classified according to color and luster. Approximately 300 grains of each grain type were isolated in order to verify their mineralogy using X-Ray Diffraction (XRD).

Once all fifteen samples were picked and separated, grains representing each mineral type were crushed into a fine powder using a mortar and pestle. The powder was then transferred into sampling plates and placed into the PW 1830 (XRD) machine for XRD analysis. Each sample was x-rayed using the X-Pert Data Collector software for approximately twenty-three minutes. Analysis of the sampling was completed using the X-Pert High Score software.

Maps

Distribution and orientation maps of the CRASLs throughout the Gerlache Strait were created to determine the different processes creating the features. With the aid of the 1980s DEEP FREEZE cruise video and photos taken from the *Nathaniel B Palmer* (NBP) 0703 cruise, the distribution and orientation of these features were mapped using

ArcGIS. Maps indicating the location of samples and anthropogenic structures were also created.

Chronology

Three methods were used to try to constrain the chronology of the CRASLs: relative age relationships between CRASLs and anthropogenic structures (huts and beacons), aerial photos, and reference to regional relative sea levels using OSL dating of raised beaches.

Age of the Huts

The British, Chilean, and Argentinean governments built many small structures (huts and beacons) throughout the Gerlache Strait (Table 4). With the help of the British Antarctica Survey (BAS), Chilean National Antarctic Program (COMNAP), and Argentinian National Antarctic Program (COMNAP) the age of each structure was determined.

Aerial Photos

Aerial photographs taken at Arctowski Peninsula, Argentino Channel, Danco Island, Errera Channel, Paradise Harbor, and Willems Point between December 1956-February 1957 were obtained from the BAS. The similarities and differences between the aerial photos, the 1980s DEEP FREEZE cruise videos, and photos taken from the NBP 0703 cruise were examined in order to identify changes in the Gerlache Strait over the last fifty years.

TABLE 4. STRUCTURE LOCATIONS AND TYPES

Location	Structure Type	Lat. (°S)	Long. (°W)
Arctowski Peninsula	Hut	-64°39’30”	-62°35’
Danco Island	Hut	-64°43’45”	-62°37’
Paradise Harbour (Waterboat Pt.)	Hut	-64°49’30”	-62°52’30”
Arctowski Peninsula (Neko Harbour)	Hut	-64°51’15”	-62°32’30”
Argentino Channel (near Mascias Cove)	Hut	-64°55’30”	-62°59’
Argentino Channel (near Skontorp Cove)	Hut w/beacon	-64°54’	-62°53’
Melchoir Islands	Hut w/beacon	-64°19’30”	-62°55’
Arctowski Peninsula (near cape Anna)	Beacon	-64°35’30”	-62°27’
Arctowski Peninsula (between Spigot Peak and hut)	Beacon	-64°38’30”	-62°34’45’’
Ronge Island (near Ketley Point)	Beacon	-64°43’	-62°47’
Duthiers Point (Danco Coast)	Beacon	-64°48’30”	-62°50’
Lemaire Island (near Molina Pt.)	Beacon	-64°48’45”	-62°52’15”
West of Wienke Island (small island)	Beacon	-64°48’45”	-63°31’31”
Damoy Point	Beacon	-64°48’45”	-63°30’45”
Doumer Island	Beacon	-64°49’50”	-63°34’45”
Argentino Channel (near Oscar Cove)	Beacon	-64°54’45”	-62°56’
Argentino Channel (Dallmayer Peak arm of Peninsula)	Beacon	-64°52’30”	-62°50’30”
Lemaire Island	Not defined	-64°49’30”	-62°57’30”
Weincke Island	Not defined	-64°49’10”	-63°31’
Weincke Island	Not defined	-64°48’50”	-63°31’30”
Gauthiers Pt.	Not defined	-64°50’	-63°35’
Argentine Island (near Skua Island)	Not defined	-65°14’45”	-64°16’30”

OSL Samples

Sample Preparation

Exposure to light prior to Optically Stimulated Luminescence (OSL) measurements will destroy the signal. Therefore, all OSL procedures were conducted in a dark room using only red light. The goal of the sample preparation was to isolate quartz grains from the underside surface of the cobbles for OSL measurements. First, each sample was cut in half using a large Hillquist saw. The top portion of the sawed cobbles were set aside for *Natural Dose Rate* (NDR) measurements, and the bottom half was cut into 2.54 cm x 2.54 cm cubes to prepare for *natural radiation dose* (ND) sampling (Fig. 23). The outer 1-mm surface of the cubes was isolated using a Buehler IsoMet 1000 precision sectioning saw. The cuttings were then dried in an oven for 8 – 24 hrs. So they could be crushed and sieved without the loss of sample. Next, the cuttings were crushed using a mortar and pestle. After all of the samples had been crushed, they were sieved using the following screen sizes: 200 μm, 150 μm, 90 μm, and the bottom plate. Sediments that were captured in the 200 μm and 90 μm screens as well as the bottom plate were transferred to vials and stored. The sediments captured in the 150 μm screen were chemically treated and density separated, to isolate the quartz grains.

Quartz was isolated by first removing carbonate using hydrochloric acid (HCl, 3.75%). HCl was added until the sediments were submerged. When effervescence stopped, the samples were rinsed three times with distilled water. Next, hydrogen peroxide (H_2O_2, 27-29%) was added in order to oxidize all of the organic material. Like the HCL, H_2O_2 was added until the sediments were submerged, and the reaction was considered to be complete once effervescence had ceased.

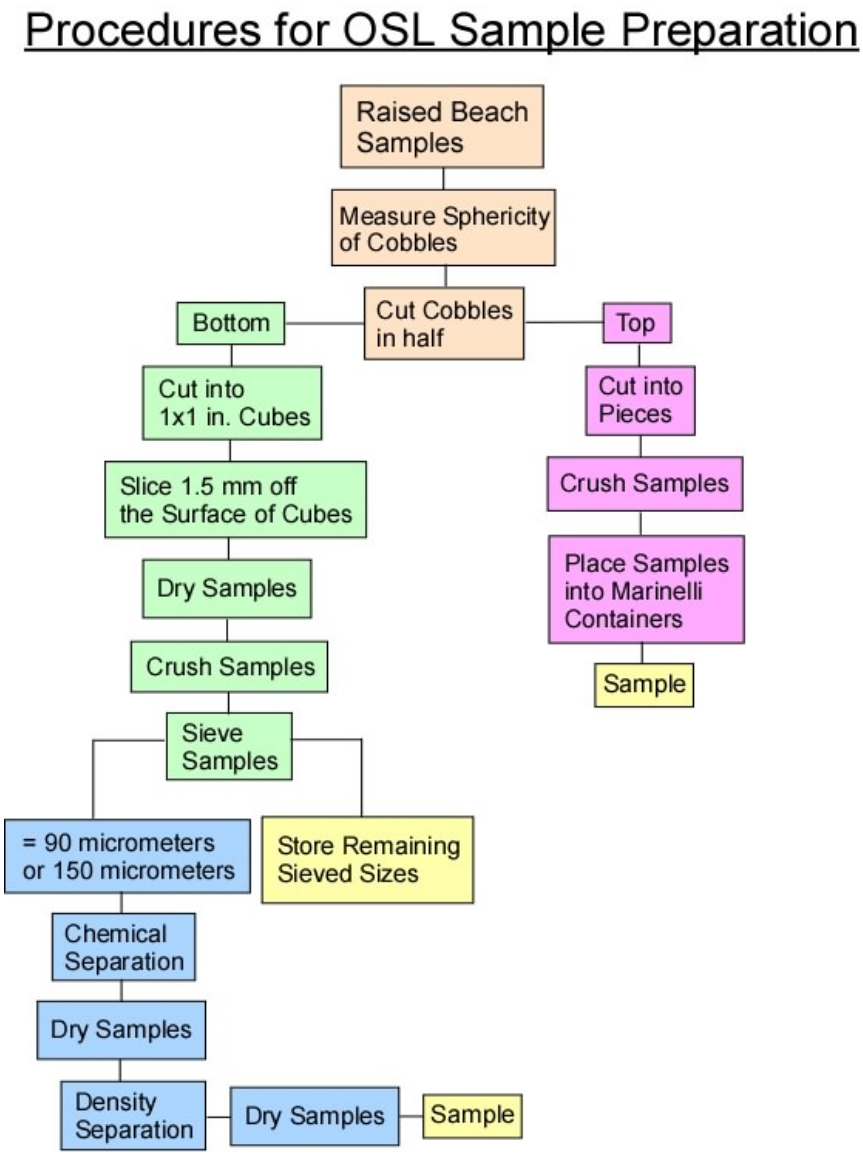

Figure 23 – Procedures used in sample preparation for the OSL cobbles and surrounding sediments.

Following the addition of H_2O_2, the samples were again rinsed three times with distilled water. Hydrofluoric acid (HF, 48%) was added to the beakers until the sediments were submerged, in order to remove the 20 μm shell of quartz that was affected by alpha radiation. All four samples (PL01, PL02, PL03 and PL04) reacted very violently with the HF. This was thought to be caused by the abundance of magnesium (Mg) and calcium (Ca) present in the samples. After 40 minutes, the samples were rinsed three times with distilled water and another 100 mL of HCl was added to dissolve fluoride precipitates that might have formed during the HF reaction. Last, the samples were rinsed three times with distilled water and placed in an oven to dry overnight.

The primary purpose of the density separation is to ensure the isolation of quartz grains. During the chemical treatment process many but not all minerals are dissolved. Those that are left, include heavy minerals and feldspar which need to be separated from the quartz grains. Lithium polytungstate (LST), which has a density of 2.85g/cm^3, is used as a base liquid to produce a fluid with a density required to separate quartz minerals. The two densities needed in this experiment were 2.62g/cm^3 and 2.75g/cm^3.

The 2.75g/cm^3 liquid was used first in the density separation. 50 mL -100 mL of the liquid were added to glass separatory funnels. The sample was added and minerals >2.75g/cm^3 were allowed time to settle. Once it became apparent that all of the heavy minerals had separated to the bottom, the liquid containing the heavy minerals filtered was drained into a flask containing a funnel with filter paper and discarded. Next, the lighter minerals, including quartz and feldspar, that remained were also drained and filtered. These samples were rinsed ten times with distilled water and placed into an oven to dry overnight.

Distilled water was added to the 2.75g/cm^3 liquid to make the 2.62g/cm^3 liquid for the second density separation. Again, 50 mL-100 mL of liquid was added to glass separatory funnels. The dried residual grains from the first density separation were added to the liquid to separate the feldspar grains. This time the quartz grains sank and the feldspar grains floated. After approximately one hour the grains were filtered into a flask. Both the quartz and feldspar grains were transferred into beakers, rinsed ten times with distilled water, and dried overnight in the oven. The feldspars were stored in the event that insufficient quartz grains were isolated.

The top half of each cobble was cut into pieces to measure the concentration of uranium, thorium, and potassium using gamma spectrometry. Once the pieces were approximately 1.5 cm in diameter, they were crushed in a rock crusher. The crushed samples were weighed and transferred into Marinelli containers. The lids were sealed using masking tape to reduce the loss of radon, which is essential for gamma spectrometry measurements. Dr. Art Lucas determined the radioactive nuclide concentrations and calculated the NDR, or decay rate.

Basic Principles

The OSL signal of a sample is measured by stimulating the sample with light of a single wavelength and detecting the emitted luminescence in another wavelength. As the natural signals vary between grains, the luminescence signals must be correlated to the dose. To do this, samples are irradiated with a known dose and the signal is measured a second time (Murray and Wintle, 2000). The two signals are then compared and the dose

calculated. This forms the basis of any single-aliquot regenerative-dose (SAR) protocol (Murray and Wintle, 2000).

Equipment

The Risø TL/OSL-DA-15 luminescence reader used for OSL measurements can measure up to 48 samples that can individually be heated, irradiated, and optically stimulated by blue or infrared light sources (Bøtter-Jensen et al., 2003; OSL Hardware Manual, 2008). Measurements are carried out under nitrogen atmosphere and a light detection system consisted of a photomultiplier tube and detection filters are used to measure the emitted luminescence (OSL Hardware Manual, 2008).

The Risø TL/OSL reader consists of two main units: a) the Reader and b) the Controller (OSL Hardware Manual, 2008). Two programs are used to run the systems: the SEQUENCE EDITOR, used to write measurements sequences, and the CONTROL Program, used to carry out tests on the equipment.

SAR Procedures

The single-aliquot regenerative-dose (SAR) protocol was used as a measurement procedure (Murray and Wintle, 2000; Wintle and Murray, 2006). A dose value is obtained from a single subsample ("aliquot") by measuring the natural luminescence signal and the signals after regenerative-dose exposures. According to Murray and Wintle (2000), the primary assumption of the SAR protocol is that "*it is possible to measure a signal after each dose and stimulation cycle, which acts as a surrogate measurement of the sensitivity applicable to the prior measurement cycle.*" Thus

"*allowing the sensitivity changes to be corrected…in both the natural and regenerated signals*" (Murray and Wintle, 2000). Table 5 outlines the SAR procedure used for the dating measurements based on the generalized SAR protocol (after Murray and Wintle, 2002, 2003).

TABLE 5. GENERALIZED SAR PROTOCOL

Step	Treatment	Observed	Comments
1	Give dose[a], D_i	__	Dose varies with each cycle, see Table 6
1.5*	Stimulate IR for 100s at 60°C	__	*Only for the last cycle of the aliquot
2	Preheat[b] (x°C for 10s)	__	Preheat temperature x is determined by plateau test
3	Stimulate blue for 100s at 125°C	L_i[c]	
4	Give test dose, D_T	__	D_T is 15-20% of the natural dose, estimated value is obtained by initial dose test
5	Heat[b] (x°C)	__	Preheat temperature x is determined by plateau test
6	Stimulate blue for 100s at 125°C	T_i[c]	
7	Stimulate blue for 40s at x+40°C	__	Preheat temperature x is determined by plateau test

[a]For the natural sample, $i = 0$ and D_O is the natural dose.
[b]Aliquot cooled to < 60°C after heating.
[c]L_i and T_i are derived from the stimulation curve, typically the first 1-2s of initial OSL signal, minus a background estimated from the last part of the stimulation curve.

In Step 1 the aliquot is irradiated with a dose, during which process electrons are trapped in the defects. The purpose for preheating the aliquot in Steps 2 and 5 is to remove any unwanted and thermally unstable signals that may be present (Murray and

Wintle, 2000). The preheat temperature has to be determined with the plateau test. For Steps 3, 6 and 7 the samples are stimulated by blue diodes for 100 s in order to measure the most light sensitive part of the signal. In Step 4, a fixed test dose is given in order to determine the capacity of the traps. This test dose should amount to 15-20% of the natural dose of the sample and is determined with an initial dose test. The signal induced by this test dose is obtained in Step 6 and is used to monitor any changes in the luminescence sensitivity. Steps 1-7 are referred to as a cycle, and are repeated 9 times for each aliquot. The irradiation dose in Step 1 changes in each cycle (Table 6). Step 1.5 (Table 5) is introduced in the last cycle only in order to determine the feldspar contamination present in samples.

The first cycle (named cycle C_0) measures the natural signal induced by natural radiation. Therefore the sample is not irradiated. During cycles C_1, C_2, C_3, and C_4 the aliquot is exposed to regeneration doses and the "dose response" is measured. The purpose of the initial "Dose" test is to obtain values for D_1-D_4 that best describe the range of Natural Dose signals. However, in some instances five or six regeneration doses may be necessary. The last 4 cycles test the "reliability" of an aliquot: cycles 6 and 7 test the accuracy with which a known dose can be measured. Cycle 8 determines if any signal is present that was not caused by radiation exposure, and cycle 9 is used to detect a possible feldspar contamination in the sample. Steps 1-7 are the only commands necessary for the first eight cycles. However, on the ninth cycle Run 1.5 has to be added between Run 1 and 2. A complete measurement sequence consists of nine cycles for each of the twenty-four aliquots in a sample carrousel.

Preliminary Tests

Before the samples grains could be transferred into aliquot cups, the cups were prepared for the sample using Rusch Silkospray. This was done by placing a cover tray

TABLE 6. VARIOUS CYCLES & THEIR MEANINGS

Cycles	Cycle Abbreviation	Meaning
Cycle 1	C_0	D_0 = 0 Natural Dose
Cycle 2	C_1	D_1 < Dose
Cycle 3	C_2	D_2 < Dose
Cycle 4	C_3	D_3 > Dose
Cycle 5	C_4	D_4 > Dose
Cycle 6	C_5	D_5 = Expected Dose
Cycle 7	C_6	$D_6 = D_1$
Cycle 8	C_7	$D_7 = D_0$ Whole cycle w/o Irradiation
Cycle 9	C_8	$D_8 = D_4$ Irradiate w/ IRSL

over the tray holder, holding the aliquot cups, and only allowing the flat portion of the cups to be exposed. Once the cover tray was secured the Rusch Silkospray was sprayed across the aliquot cups leaving a sticky film to secure the sample grains. The cover tray was then removed and twenty to fifty grains were added to the cups. The cups were then placed into the Risø carrousel and loaded into the machine.

Before the *natural radiation dose* (ND) sampling of the OSL samples could begin, an initial "Dose" test and temperature test, also known as a plateau test, had to be performed.

Initial "Dose" Test

The initial "Dose" test was necessary in order to roughly estimate the Natural Dose ranges of the samples and to determine the test dose for the SAR procedure. The test indicates if the sample is "bright" and yields a high light intensity or if it is "dark" and yields only low signals even for high-dose exposures. The initial "Dose" test required three aliquots from each of the samples (PL01, PL02, PL03, and PL04). Using the Risø Sequence Editor (RSE) software a protocol was created to establish a method for the Risø TL/OSL-DA-15 machine to measure these samples.

The procedure required 1-2 hours of machine time. The Risø Sequence Editor software graphed the Signal vs. Time, the so-called OSL curve, while the samples were being measured. An example of an OSL curve can be seen in Figure 24. The signal decays over time until the background signal is reached.

After the measurement of the natural signal, the same aliquot was irradiated with a known dose and the signal was measured again. The signal is proportional to the dose, so that an estimate for the natural dose could be determined from the ratio of the two signals and the known dose. This estimate of the natural dose was used to select "Doses" for the plateau test. Once the results from the initial "Dose" test were calculated, work on the plateau test began.

Plateau Test

The plateau test is necessary to determine the preheat temperature needed for the sampling protocol. If the preheat temperature is too low, thermally unstable signals will not be removed; while a temperature that is too high will reduce the OSL signal. The

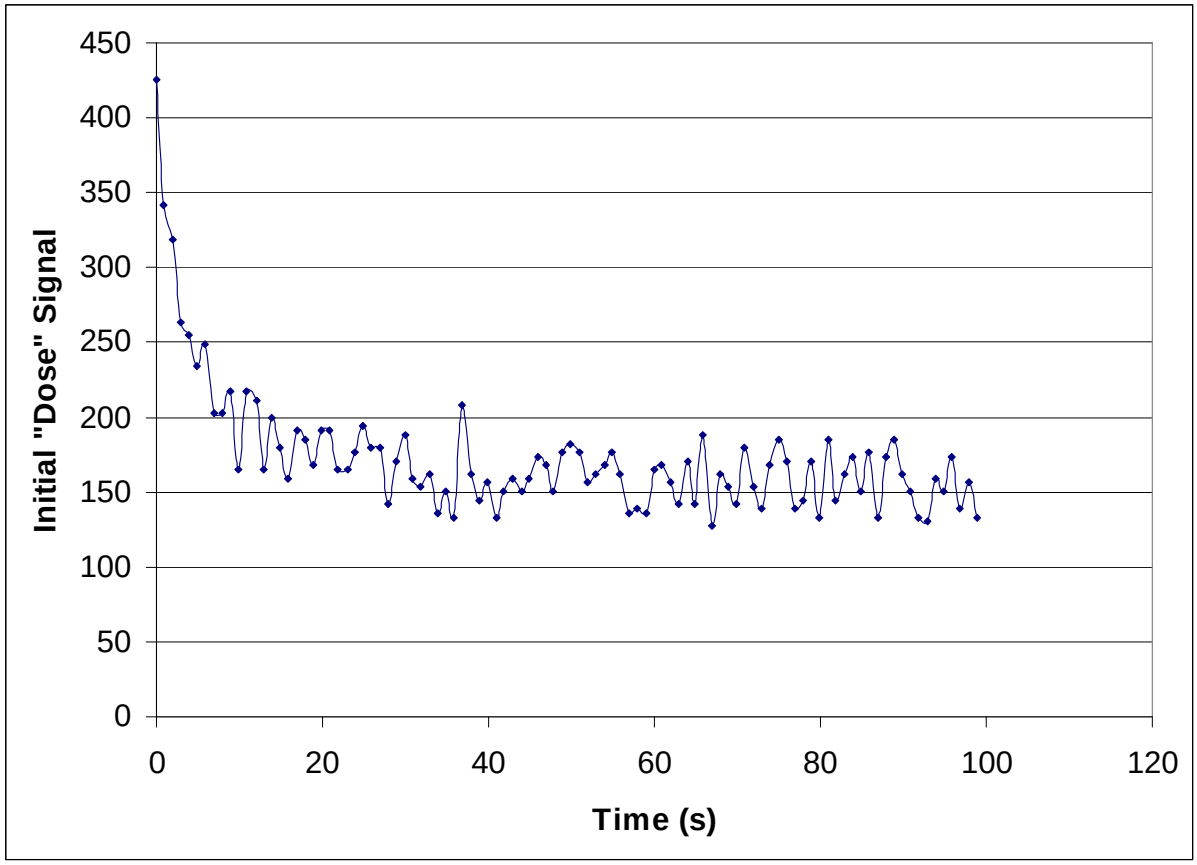

Figure 24 – Graph indicating the initial “Dose” signal plotted against time (s).

plateau test usually shows that the dose varies with the preheat temperature and the temperature range in which the dose is constant, the so-called plateau. The preheat temperature used in the sample protocol is chosen to be in the plateau.

Using the results from the initial "Dose" test, a sequence was written where the preheat temperature was varied from 160°C - 260°C by 20°C every 3rd aliquot position, in order to determine the temperature at which the sample's dose was constant. The plateau test was only performed on sample PL02 because it contained the most grains after sample preparation. Twenty-four aliquots were prepared using the methods stated above (Table 5) for the plateau test: one for every other position available on the sample carrousel. The initial "Dose" test performed on sample PL02 resulted in an estimate for the natural dose corresponding to 60 s irradiation time. Based on this result, the following doses (D) were selected (Table 7).

TABLE 7. DOSES FOR PLATEAU TEST

Cycles	Test Dose (s)
Cycle 1	$D_0 = 0$
Cycle 2	$D_1 = 50$
Cycle 3	$D_2 = 55$
Cycle 4	$D_3 = 70$
Cycle 5	$D_4 = 80$
Cycle 6	$D_5 = 60$
Cycle 7	$D_6 = 50$
Cycle 8	$D_7 = 0$
Cycle 9	$D_8 = 80$

Using the RSE software a cycle was written for the plateau test (Table 8). As explained above, Step 1.5 is only added between Step 1 and 2 during cycle 9 with D_8 = 80 s.

Once analyzed (see Analysis procedures, p. 77), five graphs were made to determine the plateau and to choose a temperature for the Sequence Tests. They were: Natural Dose vs. Temperature (Fig. 25), Dose Recovery vs. Temperature resulting from cycle 6 (Fig. 26), Recycling Ratio vs. Temperature (cycle 7, Fig. 27), Recuperation vs. Temperature (cycle 8, Fig. 28), and the IR (Feldspar Test) vs. Temperature (cycle 9, Fig. 29).

As sample PL02 had no plateau and the other tests did not show a clear advantage of any temperature, 200°C was chosen because it was close to the temperature used for OSL samples dated in the South Shetland Islands (Kouremenous, per. comm., 2008). Therefore, 200°C was used in order to modify the cycles and replace the unknown preheat temperature (Table 5).

TABLE 8. PROCEDURE FOR PLATEAU TEST

Step #	Command	Comments
1	Give dose, D_i	The irradiation time changes with each cycle (Table 7)
1.5*	*IR stimulation for at 60°C	*Only for the last cycle of the aliquot
2	Preheat for 10s under nitrogen atmosphere	Start at 160°C and increase temperature by 20°C every 3rd aliquot
3	Blue stimulation for 100s at 125°C	N.A.#
4	Irradiate the samples for 12s	Time determined by initial dose test
5	Repeat command for Step 2	N.A.#
6	Repeat command for Step 3	N.A.#
7	Blue stimulation at preheat temp. + 40°C	N.A.#

#N.A. = not available.

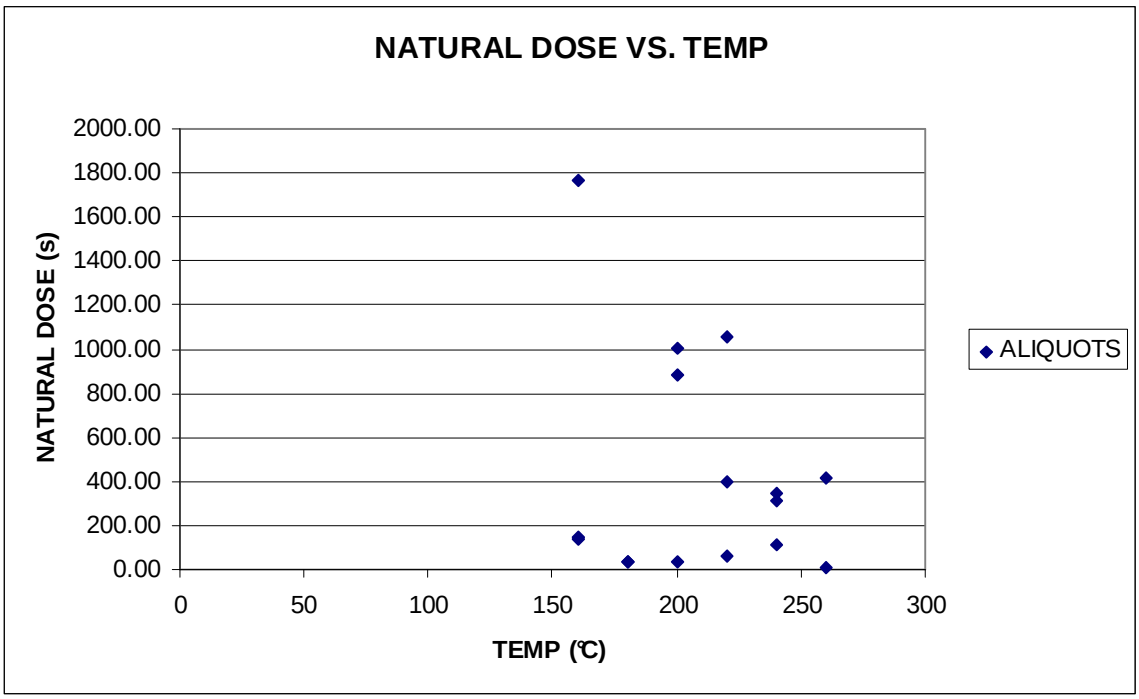

Figure 25 – Irradiation time corresponding to the Natural Dose results plotted against preheat temperature (°C).

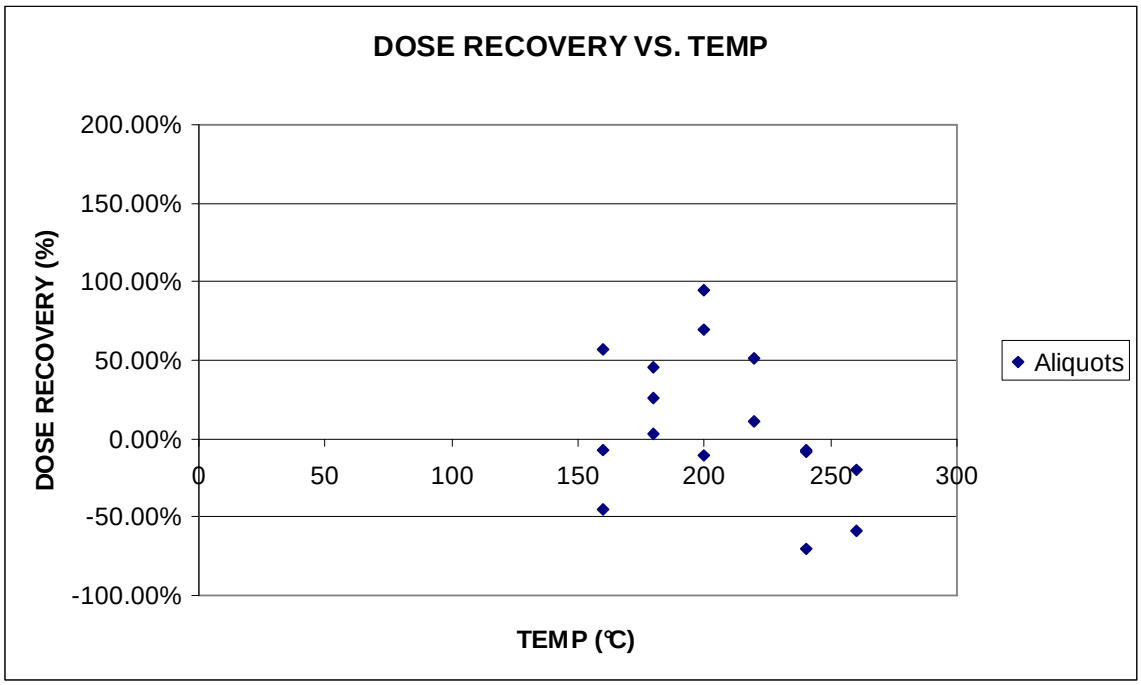

Figure 26 – Dose Recovery results plotted against preheat temperature (°C).

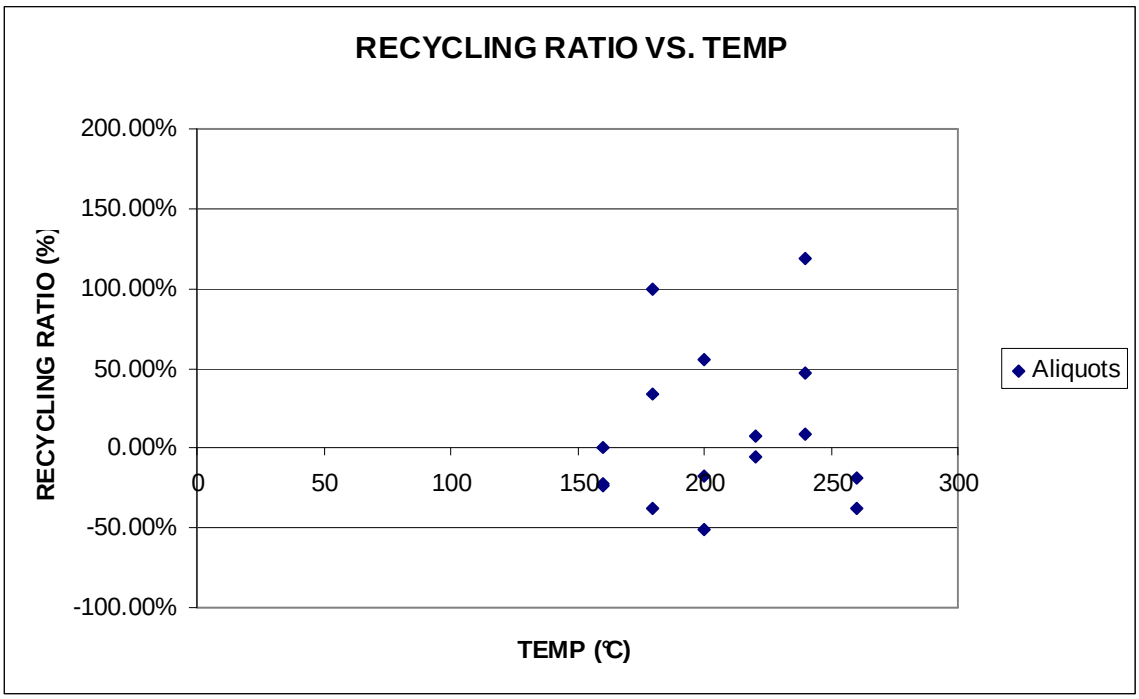

Figure 27 – Recycling ratio results plotted against preheat temperature (°C).

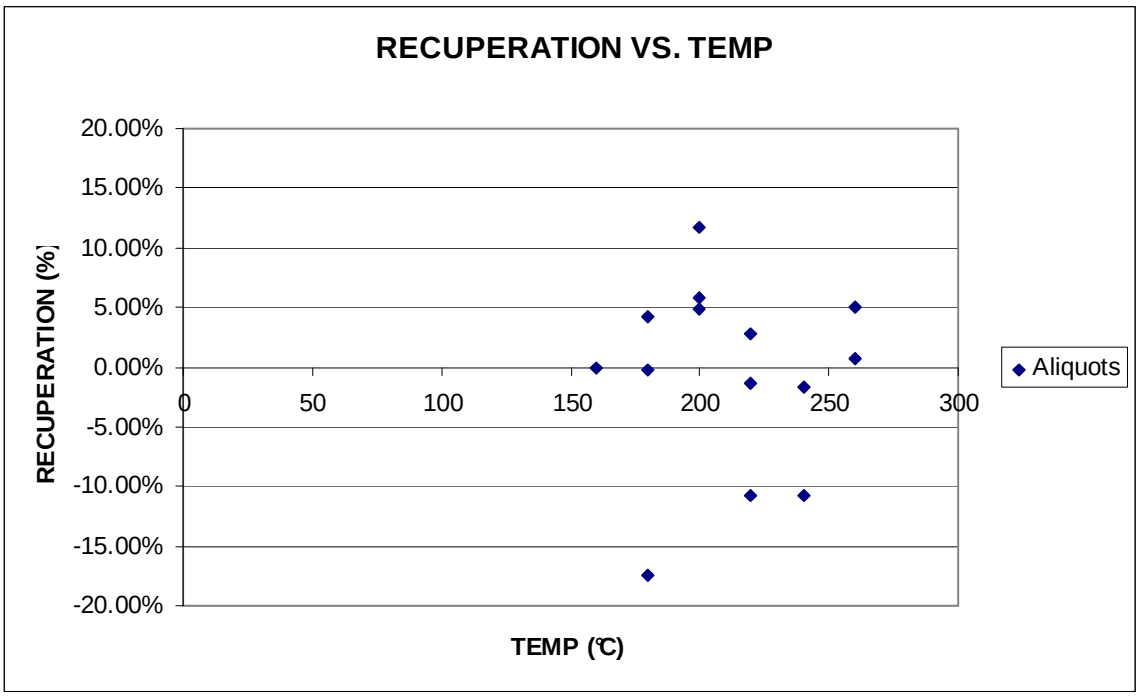

Figure 28 – Recuperation results plotted against preheat temperature (°C).

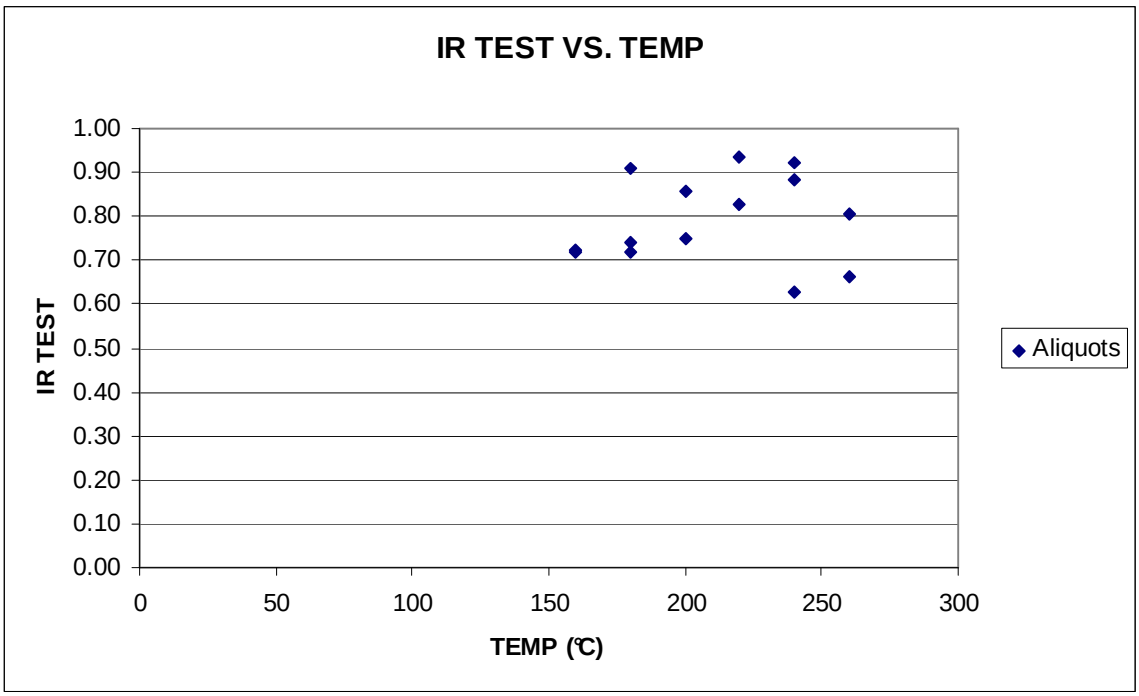

Figure 29 – IR (Feldspar) results plotted against preheat temperature (°C).

Dating Measurements

Using the results from the plateau test a temperature of 200°C was selected to preheat the samples (see Step 2, Table 9). Nine new doses were also selected to cover a larger range (Table 10) of natural doses indicated by the plateau test (Fig. 25).

TABLE 9. PROCEDURE FOR PL02 – TEST 1

Step #	Command	Comments
1	Give dose, D_i	The irradiation time changes with each cycle (Table 10)
1.5*	*IR stimulation for 100s at 60°C	*Only for the last cycle of the aliquot
2	Preheat for 10s at 200°C	N.A.[#]
3	Blue stimulation for 100s at 125°C	N.A.[#]
4	Irradiate for 12s	N.A.[#]
5	Repeat command for Step 2	N.A.[#]
6	Repeat command for Step 3	N.A.[#]
7	Blue stimulation for 40s at 200°C	N.A.[#]

[#]N.A. = not available.

TABLE 10. DOSES FOR PL02-TEST 1

Cycle	Dose (s)
Cycle 1	$D_0 = 0$
Cycle 2	$D_1 = 400$
Cycle 3	$D_2 = 500$
Cycle 4	$D_3 = 600$
Cycle 5	$D_4 = 700$
Cycle 6	$D_5 = 550$
Cycle 7	$D_6 = 400$
Cycle 8	$D_7 = 0$
Cycle9	$D_8 = 700$

Twenty-four aliquots containing grains from PL02 were prepared and placed into the Risø machine. A sequence was written using the cycle commands from Table 9 and the selected doses from Table 10.

A malfunction occurred during the first measurement and prevented completion of the test. However, the usable data suggested that three changes were needed for the measurement procedure. First, doses D_1-D_4 did not cover the whole dose range observed. The analysis also concluded that the samples had relatively low signals, some of which could not be distinguished from the background, even after irradiation with the high doses listed in Table 10. Therefore a new measurement procedure was created. Instead of writing a complete sequence and sampling twenty-four aliquots at a time, the sampling procedure was split into a two-step procedure. The first step would be to measure the aliquots and to determine if a Natural Dose signal could be detected. Upon detection of a Natural Dose signal a regular SAR sequence would be written to proceed with the measurements (2^{nd} Step). Consequently, by only measuring the Natural Dose signals of the samples no irradiation of the samples was necessary and the sample carrousel could be filled with twice as many aliquots.

For PL02 TEST 2, two steps were performed. First, a tray of forty-eight aliquot disks were prepared and placed into the Risø tray. The OSL signal was measured by stimulating each aliquot with blue LED's for 100 s at 125°C.

After approximately two hours of run time and data analysis (See Analysis, Step 1), the aliquots with a natural dose signal were kept and the remaining aliquots were discarded.

The second portion of the sampling procedure required that the aliquots showing a Natural Dose signal to be measured using a sequence similar to the one listed in Table 9. To allow for the great spread of natural doses observed, 3 cycles with additional regeneration doses were added (Table 11, cycle 5a-c)

TABLE 11. DOSES FOR PL02-TEST 2

Cycle	Dose (s)
Cycle 1	$D_0 = 0$
Cycle 2	$D_1 = 25$
Cycle 3	$D_2 = 50$
Cycle 4	$D_3 = 100$
Cycle 5	$D_4 = 200$
Cycle 5a	$D_{4a} = 400$
Cycle 5b	$D_{4b} = 550$
Cycle 5c	$D_{4c} = 700$
Cycle 6	$D_5 = 50$
Cycle 7	$D_6 = 200$
Cycle 8	$D_7 = 0$
Cycle 9	$D_8 = 200$

The machine took forty-eight hours to measure the samples. Once the measurement was completed the results were analyzed and recorded (See Analysis Step 2). It was concluded that the Test Dose signals, which are used to correct for any sensitivity changes, were too small to be usable. Instead of correcting for any sensitivity changes they introduced a very large additional statistical error. Thus, the test dose was removed. The doses were again modified to better reflect the range of Natural Dose signals present in the PL02 sample.

For PL02 TEST 3, forty-eight aliquots were again loaded into the sample carrousel and their natural signals were measured by stimulating each aliquot with blue

LEDs for 100 s at 125°C. After two hours the samples were analyzed and the aliquots with a natural signal were kept and the remaining aliquots were discarded.

The second portion of the measurement required the aliquots with a natural dose signal to be measured. Doses were the same as in Table 11, but without cycles 5b and 5c based on the results of PL02 TEST 2.

The new measurement procedure did not include the test dose correction Steps 4-6 (Table 12).

TABLE 12. COMMANDS FOR PL02 – TEST 3

Step #	Command	Comments
1	Give dose, D_i	N.A.[#]
1.5*	*IR stimulation for 100s at 60°C	*Only for the last cycle of the aliquot
2	Preheat for 10s at 200°C	N.A.[#]
3	Blue stimulation for 100s at 125°C	N.A.[#]
7	Blue stimulation for 40s at 240°C	N.A.[#]

[#]N.A. = not available.

The sequence ran for approximately thirty hours. The data was then converted (Appendix B, p. 212), imported into Excel, combined with the natural dose signal results measured in Step 1 of the measurement procedures and analyzed.

The two-step measurement procedure used in the 3rd TEST of PL02 (Table 12) was applied to the rest of the PL02 aliquots. Table 13 lists the samples that were tested for a natural dose signal (Step 1).

Nineteen trays of forty-eight aliquots and one tray of forty-seven aliquots (959 total aliquots) were measured to determine their natural dose.

TABLE 13. SUMMARY OF ALIQUOTS TESTED FOR NATURAL DOSE SIGNALS

Sample Name	Test #	#A*	#GA$	Comments
PL02 (080723A, Seq)	Test # 1	48	0	Aborted Sampling due to machine complication
PL02 (080724A, Seq)	Test # 2	48	15	
PL02 (080728A, Seq)	Test # 3	48	14	
PL02 (080730A, Seq)	Test # 4A	48	10	
PL02 (080730B, Seq)	Test # 4B	48	4	
PL02 (080730C, Seq)	Test # 4C	48	4	
PL02 (080730D, Seq)	Test # 4D	48	3	
PL02 (080730E, Seq)	Test # 4E	48	8	
PL02 (080730F, Seq)	Test # 4F	48	2	
PL02 (080730G, Seq)	Test # 4G	48	0	
PL02 (080731H, Seq)	Test # 4H	47	6	
PL02 (080731I, Seq)	Test # 4I	48	0	
PL02 (080731J, Seq)	Test # 4J	48	5	
PL02 (080731K, Seq)	Test # 4K	48	0	
PL02 (080731L, Seq)	Test # 4L	48	3	
PL02 (080807A, Seq)	Test # 5A	48	8	
PL02 (080807B, Seq)	Test # 5B	48	7	
PL02 (080807C, Seq)	Test # 5C	48	6	
PL02 (080807D, Seq)	Test # 5D	48	4	
PL02 (080807E, Seq)	Test # 5F	48	6	
PL02 (080807F, Seq)	Test # 5G	48	8	
TOTAL		**959**	**113**	N.A.#

*#A –Represents the number of Aliquots tested for a Natural Dose signal.
$#GA- Represents the number of Good Aliquots (those that had a Natural Dose signal).
#N.A. = not available.

A total of 1055 aliquots were prepared and measured during the initial “Dose” test, Plateau test and above stated tests (Table 13).

Based on the wide range of natural doses from the PL02 samples it was deemed unnecessary, to continue OSL work on samples: PL01, PL03, and PL04.

Analysis

Once the measurements of the OSL samples were completed the data was viewed in the Risø Analyst software and converted into a text document to be analyzed in Microsoft Excel. The natural dose signal results from Step 1 of the procedures were combined with the data from Step 2 of the procedures and analyzed using Microsoft Excel.

Step 1 Analysis

In order to determine whether or not an aliquot had a natural dose signal the following series of calculations were performed with data obtained in Step 1. First the background (B), which is a measure of the signal during the last 10 s of light exposure (Integral 2), had to be determined. This was calculated by using

$$B = \frac{\text{Integral 2}}{5} \qquad \text{(Eq. 10)}$$

with a background error (BE) of

$$BE = \sqrt{}\,(\text{Integral 2}/5) \qquad \text{(Eq. 11)}$$

By taking a measurement of the first 2s of light exposure (Integral 1), and subtracting B from it, a Signal (S) for each aliquot was calculated (Eq. 12):

$$S = \text{Integral 1} - \text{Background} \qquad \text{(Eq. 12)}$$

Likewise, the Signal Error (SE) was calculated using Equation (13).

$$SE = \sqrt{(\text{Integral } 1 + (BE)^2)} \qquad \text{(Eq. 13)}$$

Finally, Equation (14) was used to determine if an aliquot had a statistically significant natural dose signal.

$$S - (SE * 4)) \qquad \text{(Eq. 14)}$$

If Equation (14) yielded a positive number, then the aliquot had a signal that was significantly larger than the signal error, and the aliquot was used for the dating measurement. However, if Equation (14) yielded a negative number the aliquot was discarded.

Step 2 Analysis

Once the aliquots with a statistically significant natural dose signal completed Step 2 of the OSL process, which is the dating measurement. The resulting luminescence data was combined with the data from Step 1 and equations 10 – 14 were used for each OSL signal. Each aliquot had ten signals and signal errors associated with it, one for each dose in the sequence. Using the natural dose as a reference, a graph was created by plotting the dose vs. signal, which is the dose response (Fig. 30). The four closest dose values to the natural dose were graphed against their corresponding signal and signal error. Once the graph was created, the *Slope, Slope Error, Y-intercept, and Y-intercept*

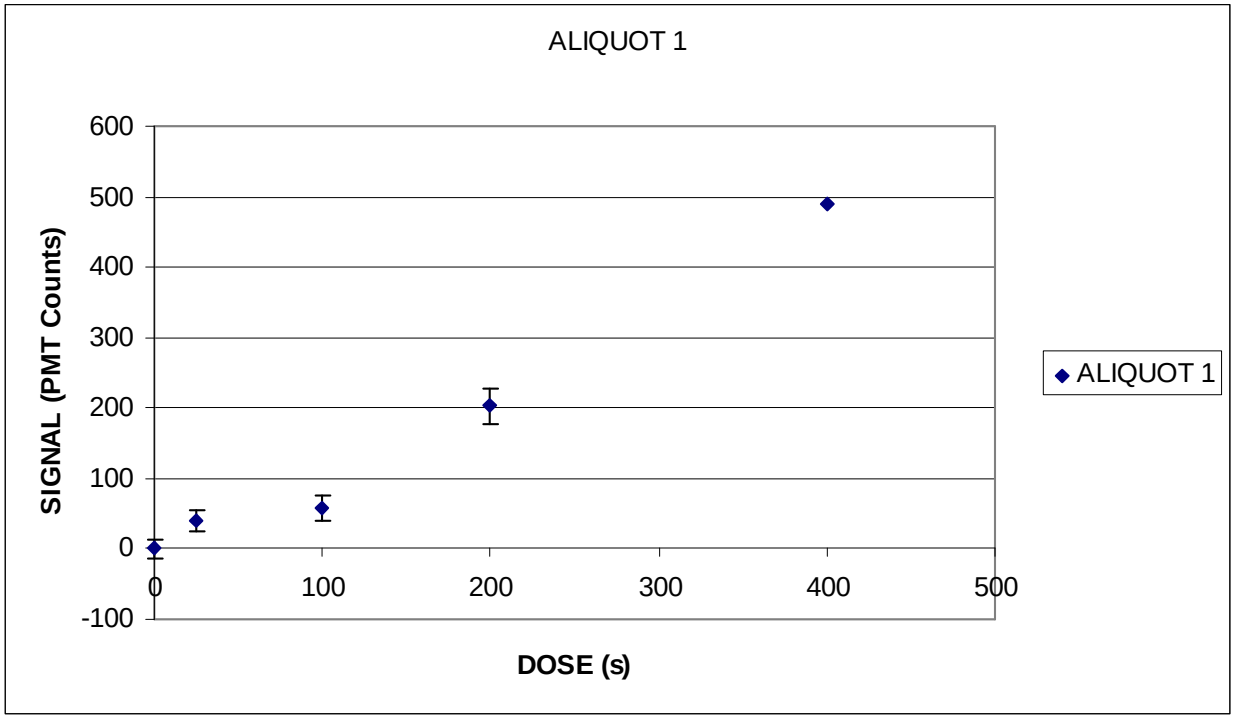

Figure 30 – Example of a Dose vs. Signal graph, or dose response. Note: 1(s) = 0.1 (Gy).

Error values were calculated using the function *LINEST* in Excel. A Dose and Dose Error were calculated for each aliquot, using Equations (15) and (16).

$$\text{Dose} = \frac{(\text{Signal} - \text{Y-intercept})}{\text{Slope}} \qquad \text{(Eq. 15)}$$

$$\text{Dose Error} = \frac{\sqrt{((\text{Signal Error})^2 + (\text{Y-intercept Error})^2 + ((\text{Dose}*\text{Slope Error})^2))}}{\text{Slope}} \qquad \text{(Eq. 16)}$$

Likewise, the Dose for D_5 in the sequence was calculated using equation (17).

$$D_5 \text{ Dose} = \frac{(D_5 \text{ Signal} - \text{Y-intercept})}{\text{Slope}} \qquad \text{(Eq. 17)}$$

Once the dose, dose error, and D_5 dose were calculated for every aliquot, four final calculations were made: dose recovery (Equation 18), recycling ratio (Equation 19), recuperation (Equation 20), and the IR (Feldspar Test, Equation 21).

$$\text{Dose Recovery} = \frac{(D_5 \text{ Dose} - 50)}{50} * 100 \qquad \text{(Eq. 18)}$$

$$\text{Recycling Ratio} = \frac{(D_6 \text{ Signal} - D_1 \text{ Signal})}{D_1 \text{ Signal}} * 100 \qquad \text{(Eq. 19)}$$

$$\text{Recuperation} = (D_7 \text{ Signal} / D_0 \text{ Signal}) * 100 \qquad \text{(Eq. 20)}$$

$$\text{IR (Feldspar Test)} = (D_8 \text{ Signal} / D_4 \text{ Signal}) \qquad \text{(Eq. 21)}$$

The dose recovery test is used to determine if the dose was measured correctly. The recycling ratio test is use to determine if the same dose results in the same signal, this test is similar to the dose recovery test. In some cases preheating or other steps may lead to a signal that is not caused by a dose. The purpose of the recuperation test is to ensure that the signal was caused by a dose; i.e., that no signal is present without irradiation. The IR Feldspar contamination test is used to determine if feldspar is present in the sample, since only feldspar is stimulated by infrared light. During the IR Feldspar test, the sample is given twice the same dose, however only one is stimulated with IR before the OSL. If the two signals are equal no feldspar contamination was present. If the signals are different then feldspars were present.

Depending on the results from these four calculations an aliquot either "passed" or "failed" the four tests. If all of the calculations fell within a set of parameters for the four tests, the aliquot was said to have "passed". If, one calculation fell outside of those parameters, the aliquot failed and was unusable for the final calculation to calculate the actual dose of the sample. The parameters used for these four tests were those of Murray and Wintle (2000) and are listed in Table 14.

TABLE 14. ALIQUOT TESTS

Tests	Requirements
Dose recovery	$\leq$ 20% if possible; $\leq$ 10% ideal
Recycling Ratio	$\leq \pm$ 20% if possible; $\leq \pm$ 10% ideal
Recuperation	$\leq \pm$ 5%
IR (Feldspar test)	$\geq$ 0.9

CHAPTER IV

RESULTS

Sedimentary Characterization

Samples were collected at 8 different localities: Palmer Station, Norsel Island, Humble Island, Limitrophe Island, Torgerson Island, Damoy Point, the Errera Channel, and Neko Harbor (Figs. 16 – 19). A total of 17 samples were collected from these 8 localities: 1 talus sample (Fig. 31), 4 moraine samples (Fig. 32), 9 beach samples (Fig. 33), and 3 CRASL samples (Fig. 34).

Grain Size

The graphic mean (M_Z), inclusive graphic standard deviation (σ_i), and inclusive graphic skewness (SK_i) were calculated for each sample and graphed in Figures 35 – 37. A comparison of the standard deviation to the graphic mean indicates that the grain size for the CRASL sediments were more similar to the beach deposits gathered from Damoy Point, Torgerson Island, Humble Island, and Limitrophe Island, and less similar to the talus, moraine, and other beach deposits sampled (Fig. 35). Plotting the standard deviation against the skewness also indicates that the grain size for the CRASLs sediments are more similar to the beach deposits gathered from Norsel Island, Torgerson Island, Humble Island, and Limitrophe Island than the talus, moraine, and other beach deposits (Fig. 36).

Figure 31 – Errera Channel talus slope.

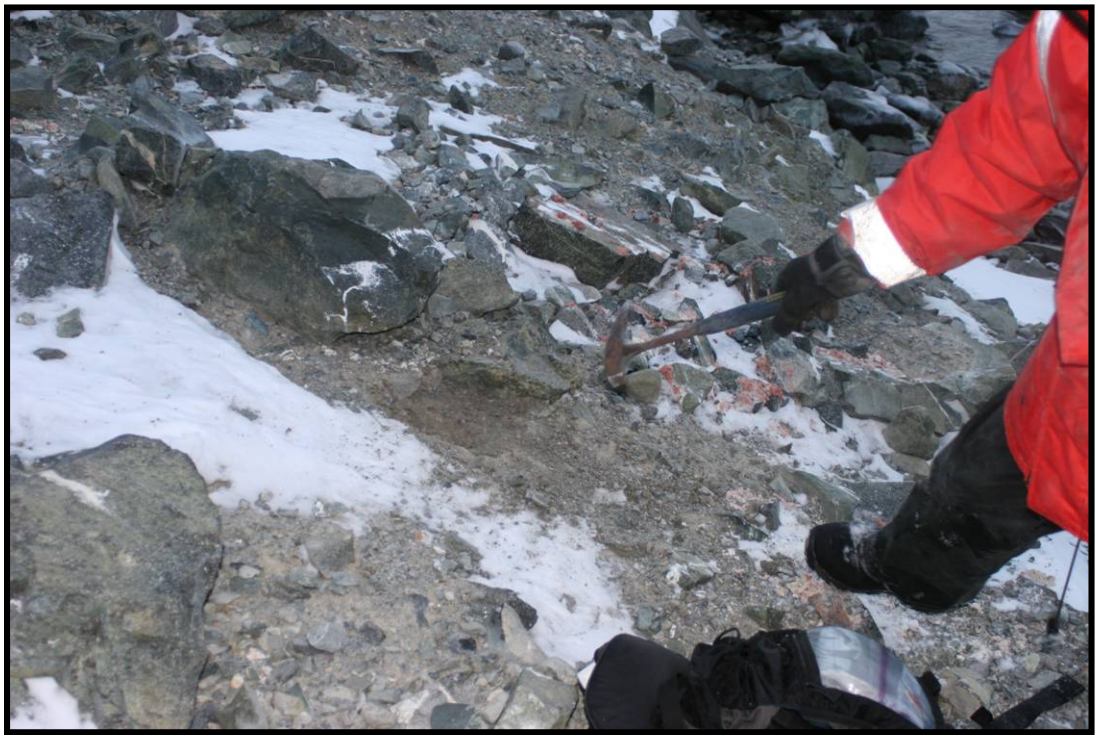

Figure 32 – Errera Channel Moraine.

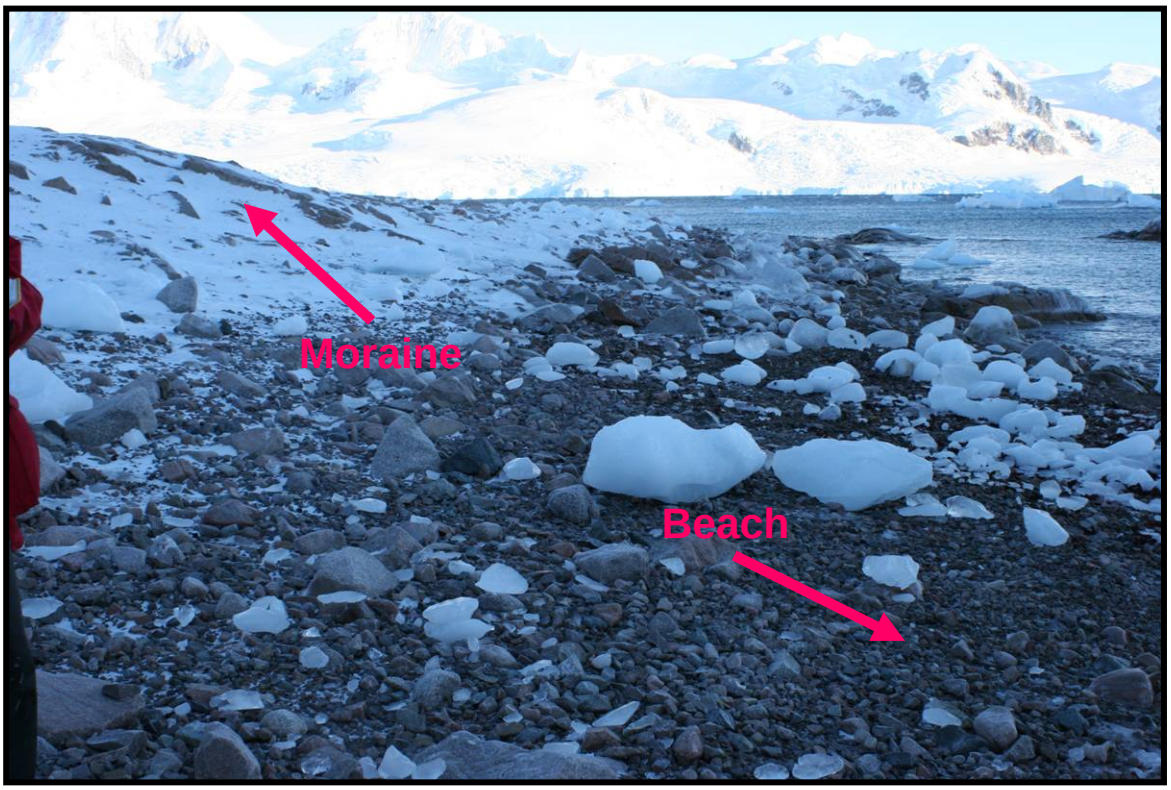

Figure 33 – Neko Harbour in Andvord Bay, sample site of modern beach and moraine deposit.

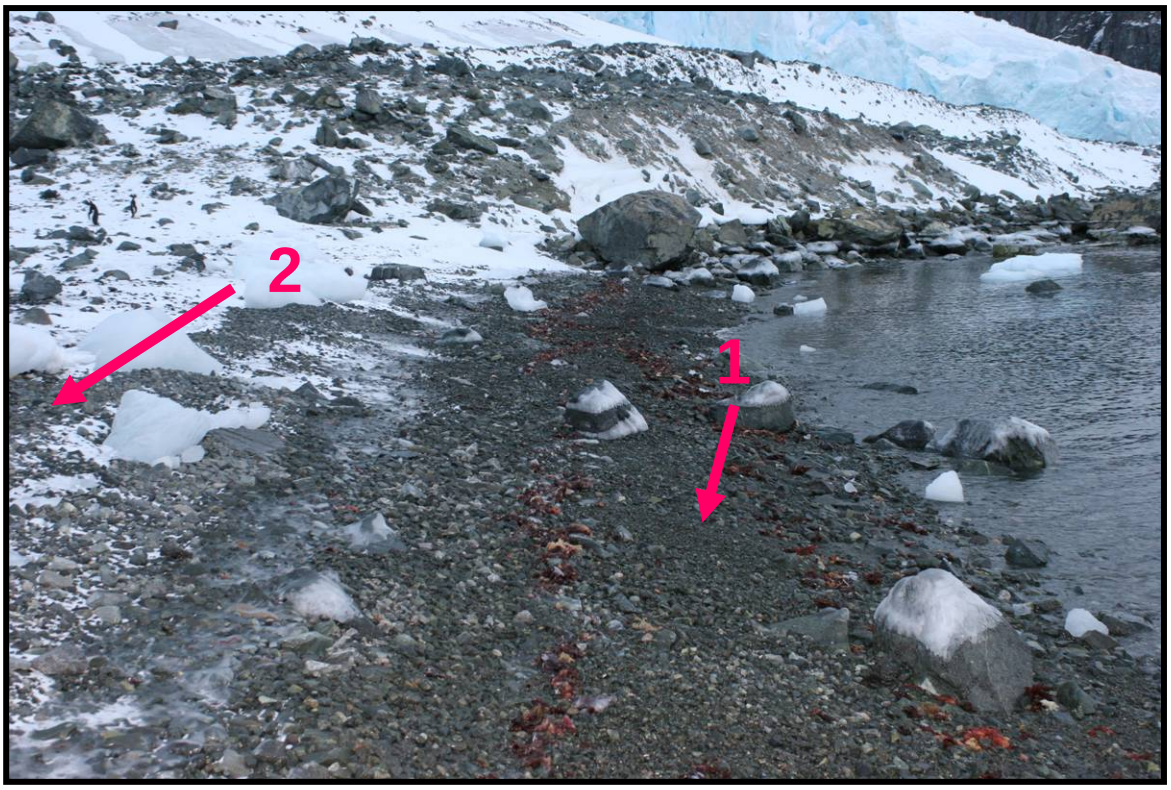

Figure 34 – Errera Channel CRASL, sample site of CRASL deposits. 1) Lower front, 2) Upper front, 3) On back side of features (Not Pictured).

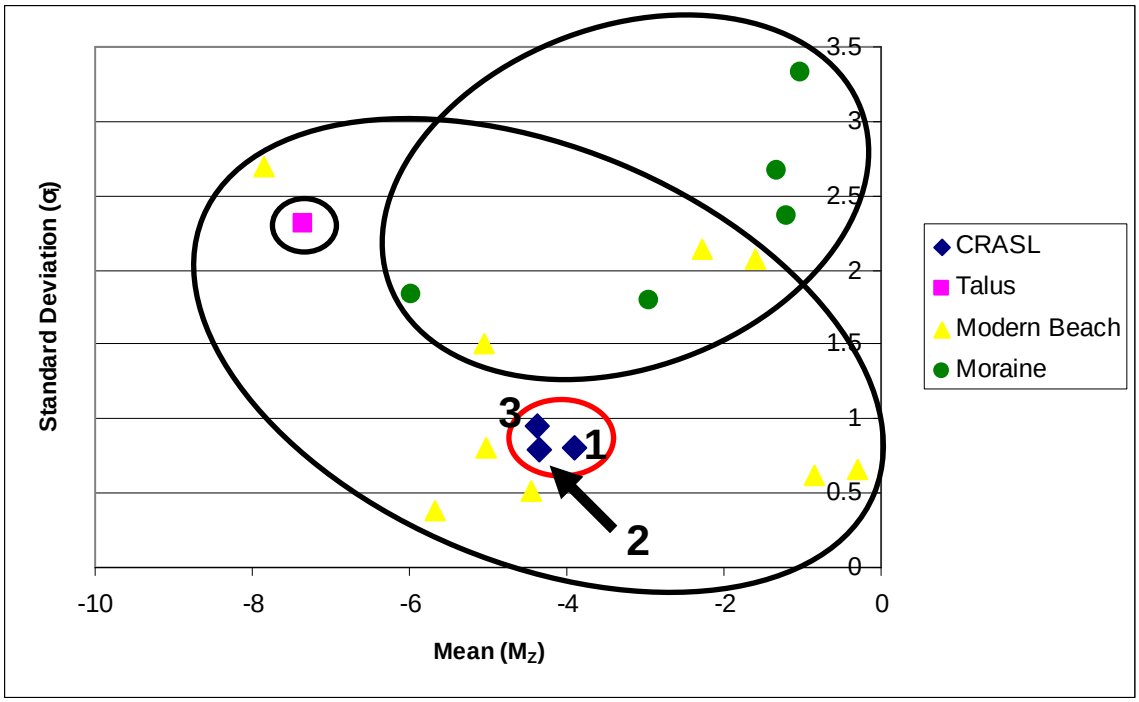

Figure 35 – Standard deviation vs. graphic mean in phi units. Geomorphic positions where samples were taken on the CRASL 1) Lower Front portion of the CRASL, 2) Upper Front portion of the CRASL, and 3) Back of the CRASL (Figure 34).

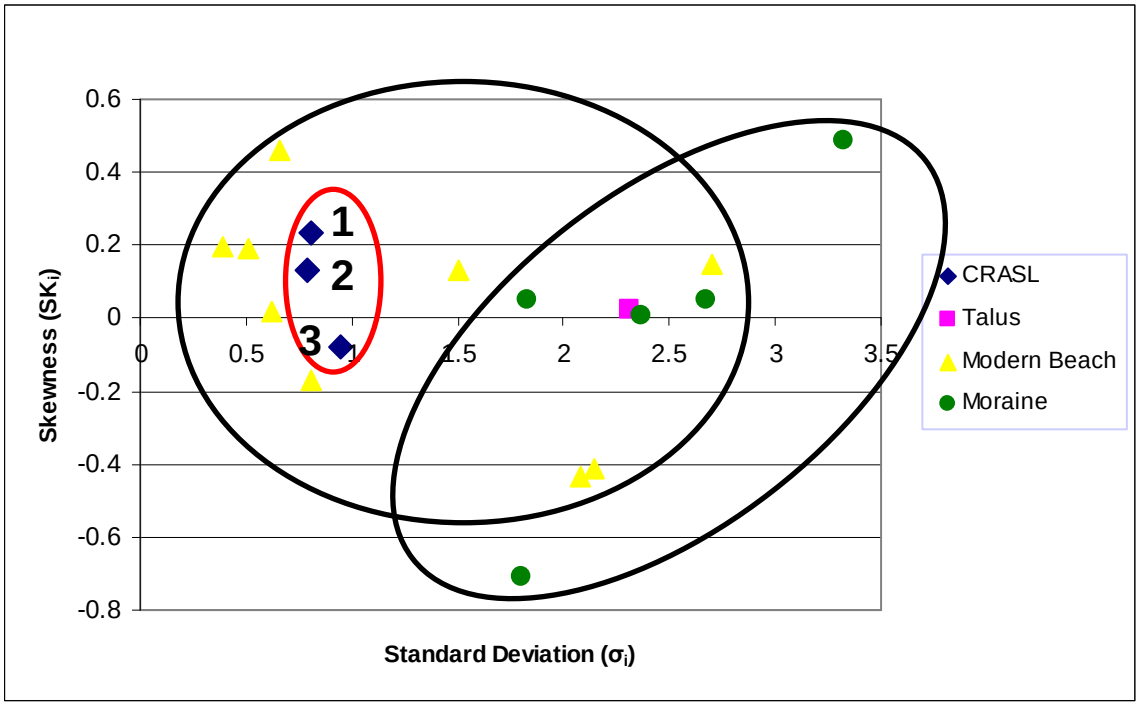

Figure 36 – Skewness vs. standard deviation in phi units. Geomorphic positions for CRASL samples are as in Figure 34.

Finally, when skewness was graphed against graphic mean the results indicate that the CRASL is more similar to the beach samples from Damoy Point, Torgerson Island, Humble Island, and Limtrophe Island than the talus, moraine, and other beach deposits (Fig. 37).

The graphic mean (M_Z), inclusive graphic standard deviation (σ_i), and inclusive graphic skewness (SK_i) for each geomorphic feature (talus deposit, moraine, beach, CRASL) was averaged. The average for each of the geomorphic features was classified using the Wentworth size classes (Boggs, 1995) and standard deviation and skewness proposed by Folk (1974; Table 2 and 3). The graphic mean for the CRASL, beach, and moraine sediments falls within the pebble size fraction, and the CRASL sediments were moderately sorted and finely skewed (Table 15).

The averaged graphic mean (M_Z), inclusive graphic standard deviation (σ_i), and inclusive graphic skewness (SK_i) for each geomorphic feature combined with the results of the graphs (Figs. 35-37) indicate that the grain size of the CRASLs are more closely related to those of the beaches, especially those beaches on Torgerson Island, Humble Island, and Limitrophe Island near the southern tip of Anvers Island than the other sediments.

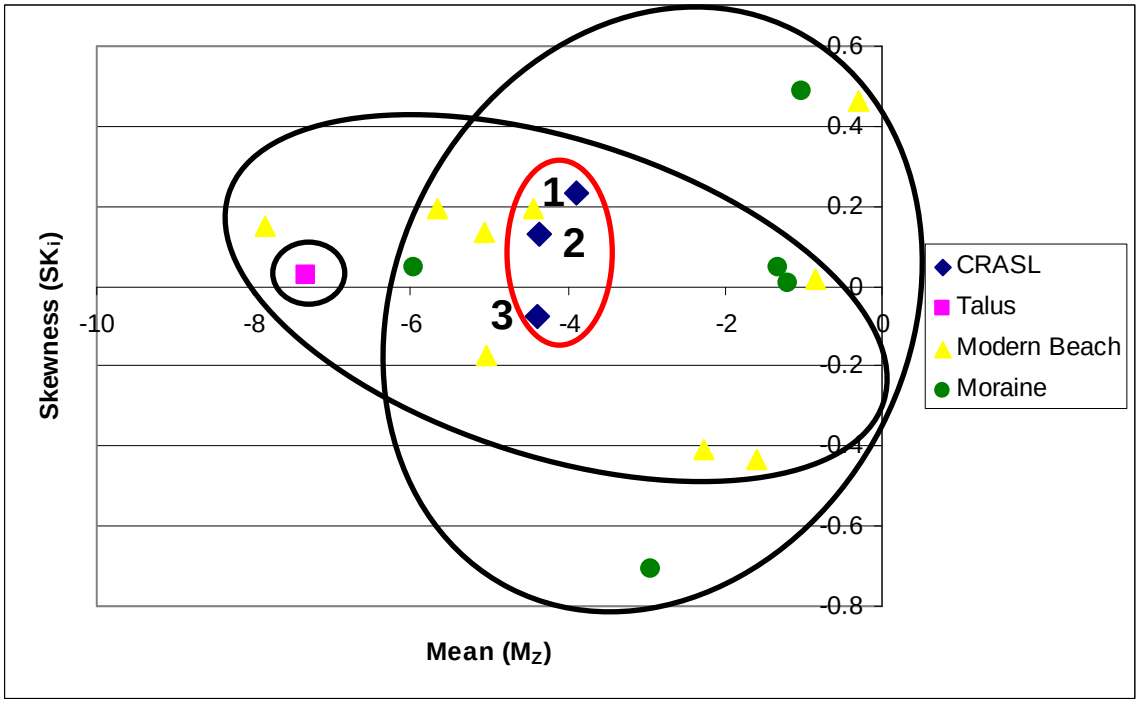

Figure 37 – Skewness vs. graphic mean in phi units. Geomorphic positions for CRASL samples are as in Figure 34.

TABLE 15. GRAIN SIZE RESULTS

Features	M_z*	σ_i#	SK_i@
Talus	-7.34 (Cobble)	2.31 (Very poorly sorted)	0.03 (Near symmetrical)
Moraine	-2.49 (Pebble)	2.40 (Very poorly sorted)	-0.02 (Near symmetrical)
Beach	-3.68 (Pebble)	1.21 (Poorly sorted)	0.01 (Near symmetrical)
CRASLs	-4.21 (Pebble)	0.85 (Moderately sorted)	0.10 (Fine skewed)

Note – results compared to the (Folk, 1974) classification of grains.
*M_z – Graphic mean
#σ_i – Inclusive standard deviation
@SK_i – Inclusive graphic skewness

Angularity

Normalized angularity values are shown in Table 16. The angularity results suggest that the CRASL is more closely related to beach and moraine deposits, rather than the talus slope deposits. The CRASL histogram appears to be a combination of the beach and moraine histograms (Fig. 38).

TABLE 16. ANGULARITY RESULTS

Features	Angular	Subangular	Subrounded	Rounded	Well Rounded	Total # of Clasts
Talus	93%	7%	0%	0%	0%	135
Moraine	57%	27%	7%	8%	0%	260
Beach	11%	30%	36%	23%	1%	715
CRASLs	23%	50%	23%	4%	0%	332

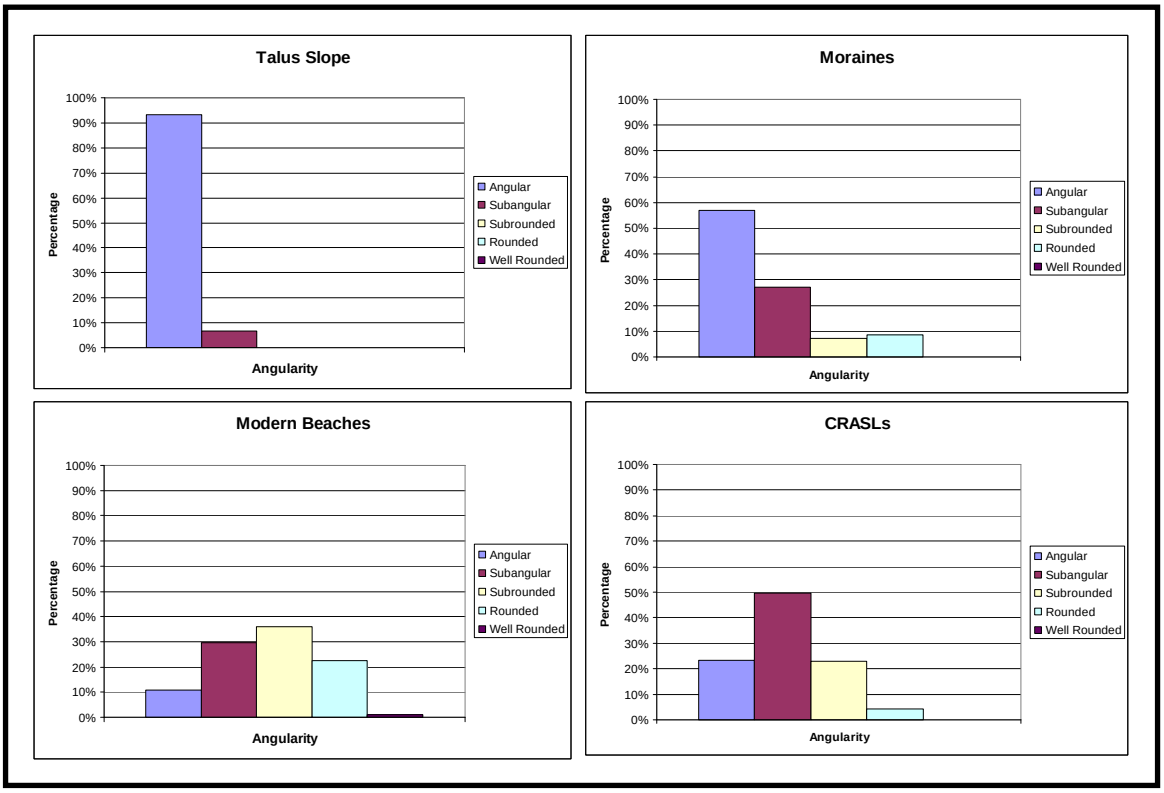

Figure 38 – Angularity results of talus-slope deposits, moraine deposits, beach deposits, and CRASL deposits.

Sphericity

The sphericity of the pebbles were compared to the classification of shapes (oblate, equant, bladed, or prolate) in Table 17. Deposits from the talus slope, beach, moraine, and CRASL are dominated by oblate clasts. No dominant populations within the sphericity measurements can be found. Therefore, sphericity provides no assistance in environmental interpretations (Fig. 39).

TABLE 17. SPHERICITY RESULTS

Features	Oblate	Bladed	Equant	Prolate (roller)	Total # of Clasts
Talus	43%	31%	17%	9%	35
Moraine	33%	15%	29%	23%	52
Beach	48%	20%	15%	17%	471
CRASLs	49%	12%	28%	11%	232

Petrology

The petrology samples were separated into mineral/rock-fragment grain types based on color and luster and counted. The results are shown in Table 18. Four different grain types were found within the talus deposits. Nine different grain types were found within the moraine deposits. Eleven different grain types were found with the beach deposits, and six different grain types were found within the CRASL deposits. Based on the grain counts, the CRASL sediments have more of a petrologic diversity than the talus slope deposits, but less than the moraine and beach deposits.

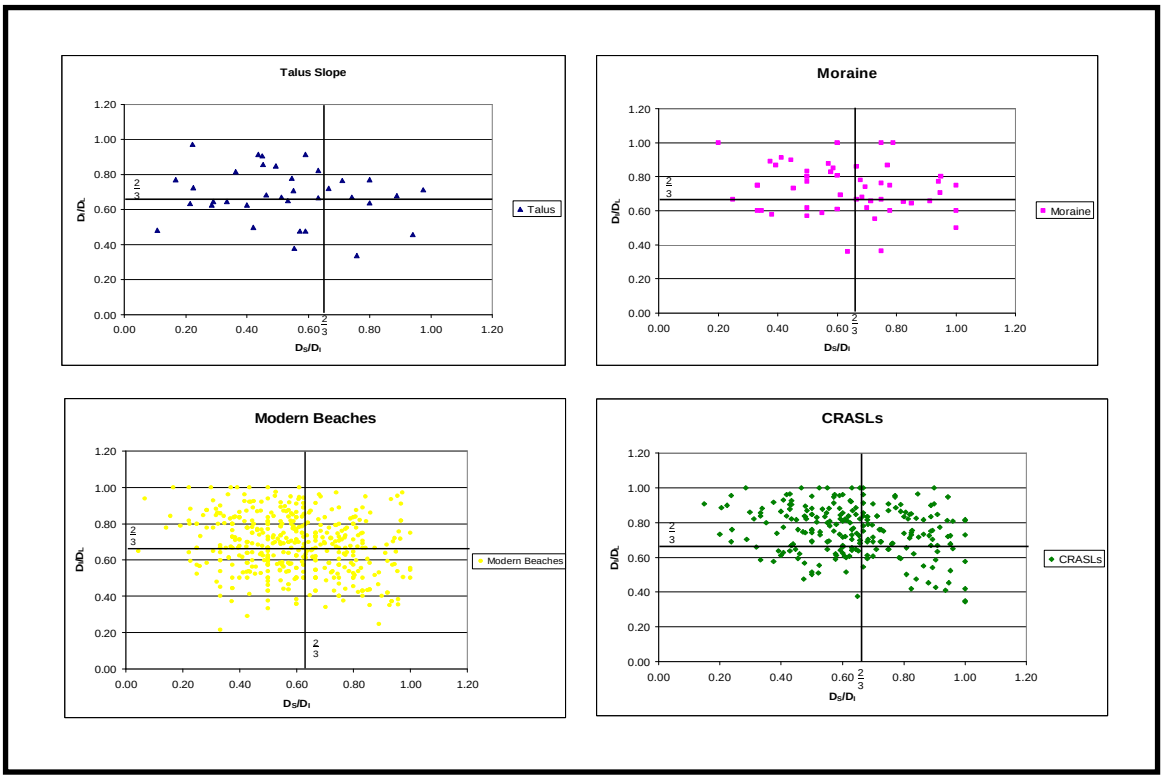

Figure 39 – Sphericity results for the talus slope deposits, moraine deposits, beach deposits, and CRASL deposits.

TABLE 18. GRAIN COUNT RESULTS

Groups	NK 01	NK 02	NK 03	NI 01	NI 02	LI 01	PL MB	ECT 01	ECC 01	ECC 02	NKM	NK HM	ECM 01	PSM	PL MF	Total
DG*	25	6	18	76	88	42	47	150	51	42	10	19	99	15	43	731
P*	48	46	49	5	8						54	53				263
LP*	51	71	58				4				64	55	9			312
W*	22	13	5	5	3	55	43	52	3	4	22	24	18	32	37	338
LG*	27	27	10	114	121	87	80	95	55	28	19	22	48	46	32	811
C*	79	84	104	23	10	79	58	3	5	8	91	92		138	81	855
PG*	44	47	31				8				36	26	15	12	11	230
DB*		5	13													18
B*	4	1	2	77	70	37	46		22	27	4	9	111	57	61	528
PR*			10													10
BR*									2							2
BG*							14									14
QSG*															35	35
Total	300	300	300	300	300	300	300	300	138	109	300	300	300	300	300	4147

Note: – Samples HI01, TI01, and ECC03 were not represent because they did not have any grains at the sample size.
*DG – Dark Green
*P – Pink
*LP – Light Pink
*W – White
*LG – Light Green
*C – Clear
*PG – Pinkish Green
*DB – Dark Black
*B – Black
*PR – Purple
*BR – Brown
*BG – Brownish Green
*QSG – Tan powdery grains

The number of grain categories plotted against the largest category (%) for each sample (Fig. 40). Based on grain types, CRASL deposits are more closely related to the moraine and beach deposits than the talus slope deposit.

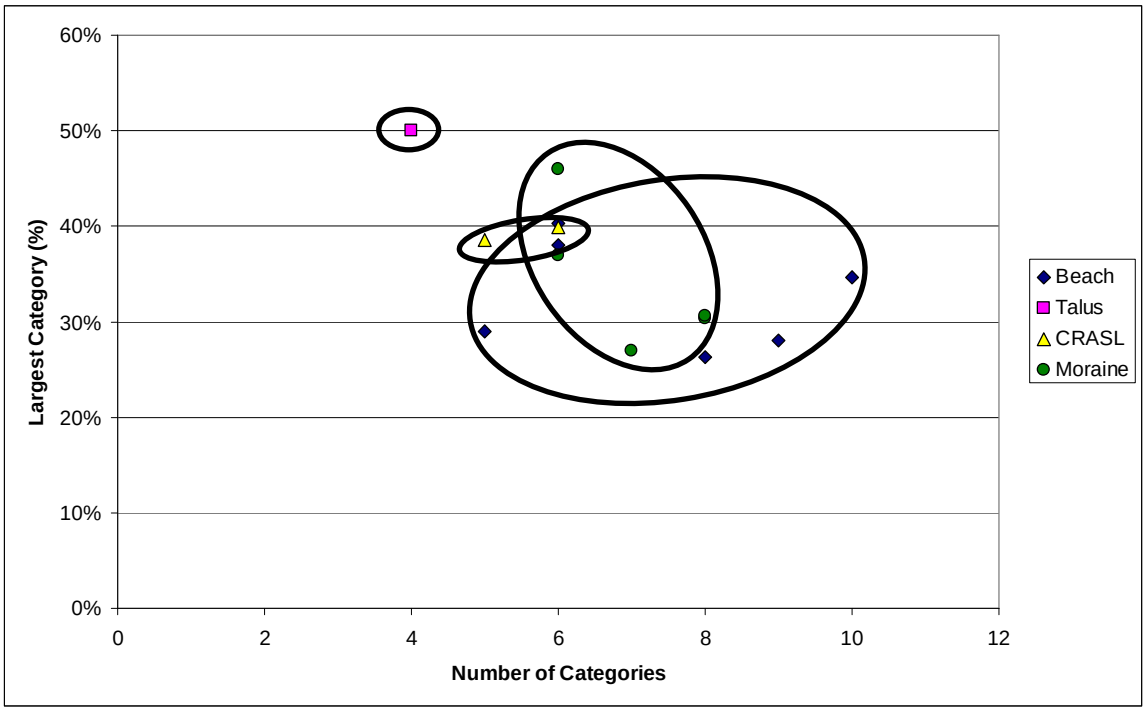

Figure 40 – Number of grain types plotted against the greatest category (%). Black circles indicate populations. The red circle indicates the best trend for the CRASL deposits.

In order to determine the mineralogy of each grain type, XRD analysis was conducted (Table 19). Five different minerals were found in the talus slope deposits; thirty-three different minerals were found in the beach deposits, and thirty-one different minerals were found in the moraine deposits. XRD results indicate that the grains are not individual minerals, but an assemblage of several minerals (Table 20). There was not enough material from the CRASL samples to conduct XRD analysis. Therefore, no relationships could be determined between the CRASL deposit and the other geomorphic features based on the XRD results alone.

Maps

To determine the different processes creating CRASLs, distribution and orientation maps of the CRASLs throughout the Gerlache Strait were constructed. With the 1980s DEEP FREEZE videos and photos taken from the NBP 0703 2007 cruise the distribution, orientation, and shape of the CRASLs were mapped using ArcGIS.

After analyzing the videos and photos, 367 CRASLs were identified in the Gerlache Strait (Fig. 41). Of those, 319 were observed in the 1980s DEEP FREEZE video (Fig. 42) and 45 were observed during the NBP 0703 2007 cruise (Fig. 43). Three areas contained CRASLs observed in both the video and the 2007 cruise (Fig. 44). A moraine was also identified near the Argentinean Base, in the Argentino Channel (Fig. 44).

TABLE 19. XRD RESULTS

Minerals	NK 01	NK 02	NK 03	NI 01	NI 02	LI 01	PL MB	ECT 01	NKM	NK HM	ECM 01	PSM	PL MF
Actinolite						X						X	X
Albite	X	X	X	X	X	X	X	X	X	X	X	X	X
Allanite							X	X					
Anapaite												X	X
Andesine				X	X								
Anorite							X						
Anorthite						X	X	X	X	X		X	X
Anorthoclase				X	X		X						
Anthralin							X						
Augite							X	X					
Baghdadite												X	X
Berlinite												X	X
Biotite				X	X							X	X
Chalcosiderite							X						
Cholorite-Serpentine	X	X	X										
Claudetite												X	X
Clinochlore	X	X	X	X	X				X	X	X	X	X
Cordierite							X						
Corundophilite				X	X								
Cristobolite												X	X
Dickite (Kaolinite)	X	X	X				X				X		
Enstatite												X	X
Epidote				X	X	X	X				X		
Gold	X	X	X										
Labradorite				X	X		X						
Laumonitite											X		
Magnesiohornblende				X	X	X						X	X
Merlinoite											X		
Mica						X							
Microcline	X	X	X	X	X	X	X		X	X	X	X	X
Monetite						X							
Muscovite	X	X	X	X	X		X		X	X	X		
Nepheline potassian											X		
Nimite				X	X								
Orthoclase	X	X	X	X	X		X		X	X	X	X	X
Paraumbite									X	X			
Phlogopite						X							
Piementite				X	X								
Plagioclase							X					X	X
Prehnite											X		
Quartz	X	X	X	X	X	X	X	X	X	X	X	X	X
Richetite						X							
Sanidine									X	X			
Stolzite												X	X
Stottite												X	X
Sylvanite											X		
Triphylite									X	X			
Vermiculite	X	X	X			X			X	X			
Volborthite									X	X			
Wodginite							X						

Note: X indicates that that mineral was observed in the samples.
Note: Samples HI01, TI01, ECC01, ECC02, and ECC03 were not represented because they did not have grains at sample size.

TABLE 20. COMMON MINERALS FOUND IN GRAIN TYPES

Grain type groups	Minerals
DG (dark green)	Albite, Chlorite-Serpentine, Orthoclase, Quartz, Augite, Vermiculite, Phlogopite, Allanite, Anthralin, Clinochlore, Epidote, Muscovite, Actinolite, Anorthite, Nepheline
P (pink)	Quartz, Albite, Orthoclase, Muscovite, Microcline
LP (light pink)	Albite, Orthoclase, Muscovite, Quartz, Microcline, Anorthoclase, Triphylite, Sylvanite, Laumontite
W (white)	Quartz, Albite, Orthoclase, Muscovite, Microcline, Anorthite, Enstatite, Epidote, Prehnite, Laumontite
LG (light green)	Quartz, Albite, Orthoclase, Allanite, Epidote, Vermiculite, Muscovite, Piemontite, Anorthoclase, Actinolite, Anorthite
C (clear)	Quartz, Albite, Muscovite, Microcline, Anorthoclase, Anorthite, Muscovite, Cristobolite
PG (pinkish green)	Quartz, Labradorite, Anorthoclase, Albite, Orthoclase, Gold, Plagioclase, Muscovite
DB (dark black)	Quartz, Albite, Chlorite-Serpentine, Muscovite
B (black)	Magnesiohornblende, Anorthite, Phlogopite, Albite, Actinolite, Qtz, Labradorite, Cordierite, Dickite, Chalcosiderite, Qtz, Albite, Vermiculite, Biotite, Muscovite, Clinochlore, Orthoclase
PR (purple)	Quartz, Albite, Orthoclase, Dickite, Microcline
BR (brown)	Quartz, Albite, Biotite, Phlogopite
BG (brownish green)	Anorite
QSG (tan powdery grains)*	Berlinite, Stolzite, Claudetite, Baghdadite

*QSG – the sample measured in the XRD was a bad sample.

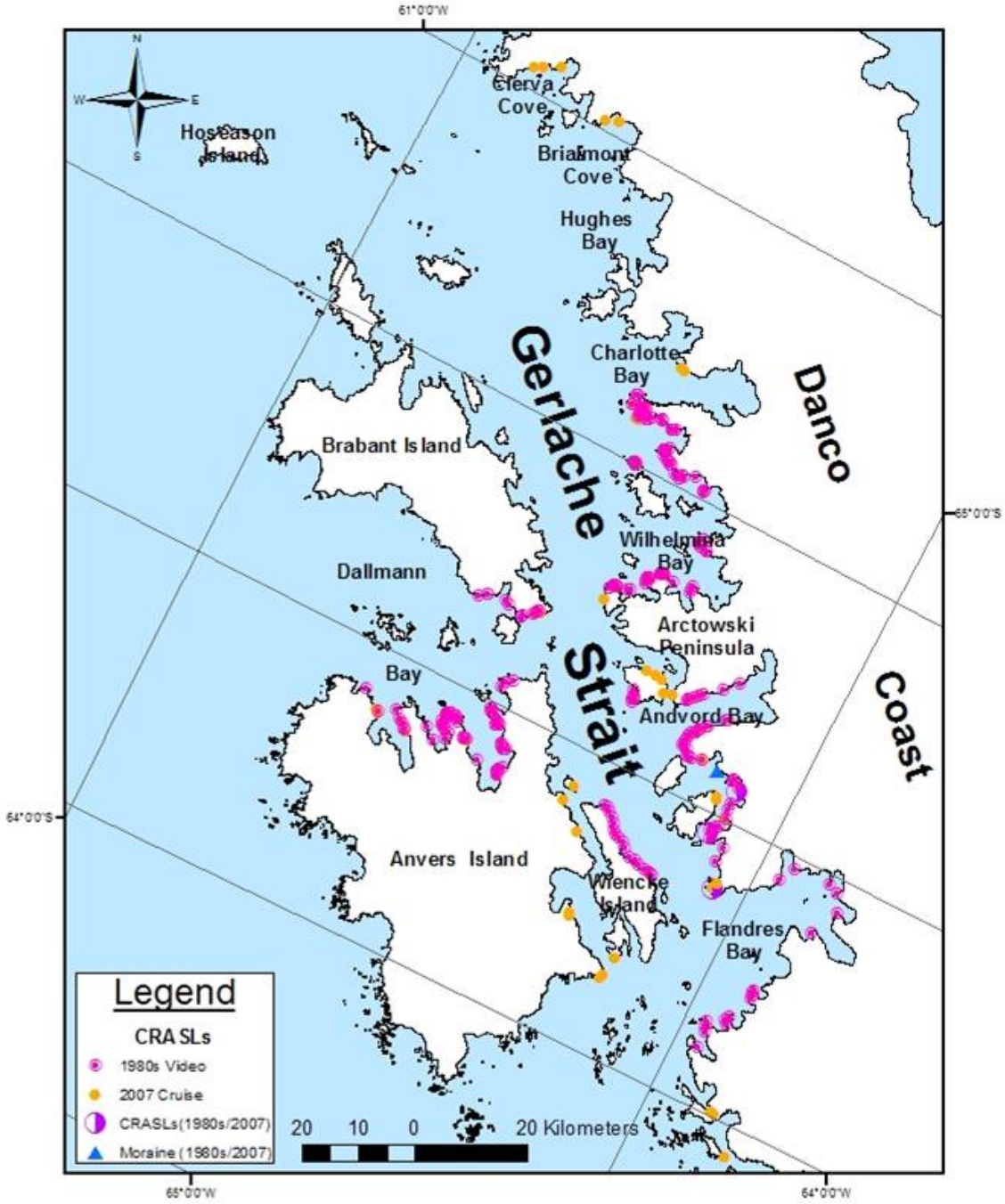

Figure 41 – Distribution map of CRASLs observed in the 1980s DEEP FREEZE video and the NBP 0703 cruise.

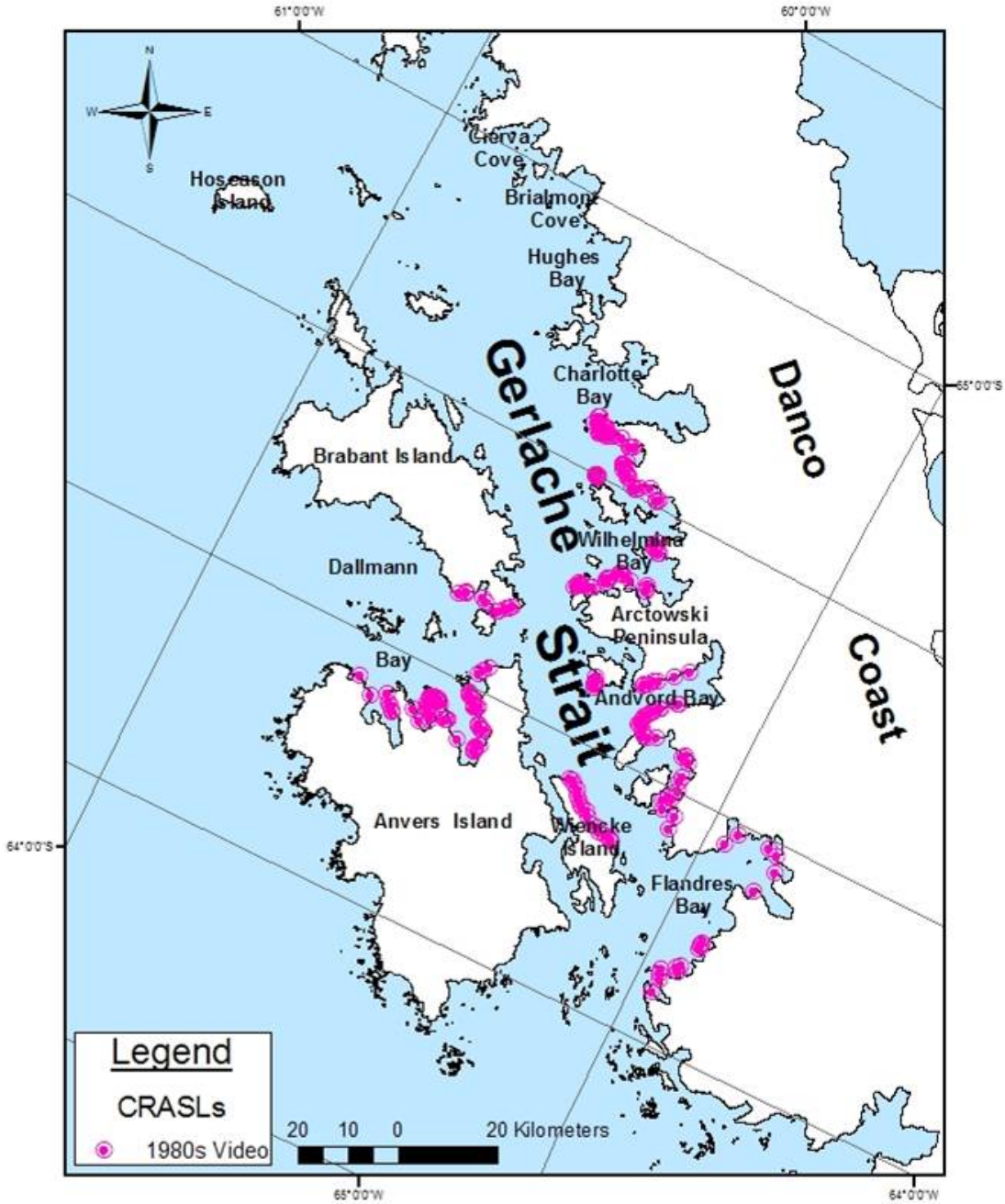

Figure 42 – Distribution of CRASLs observed from the 1980s DEEP FREEZE video.

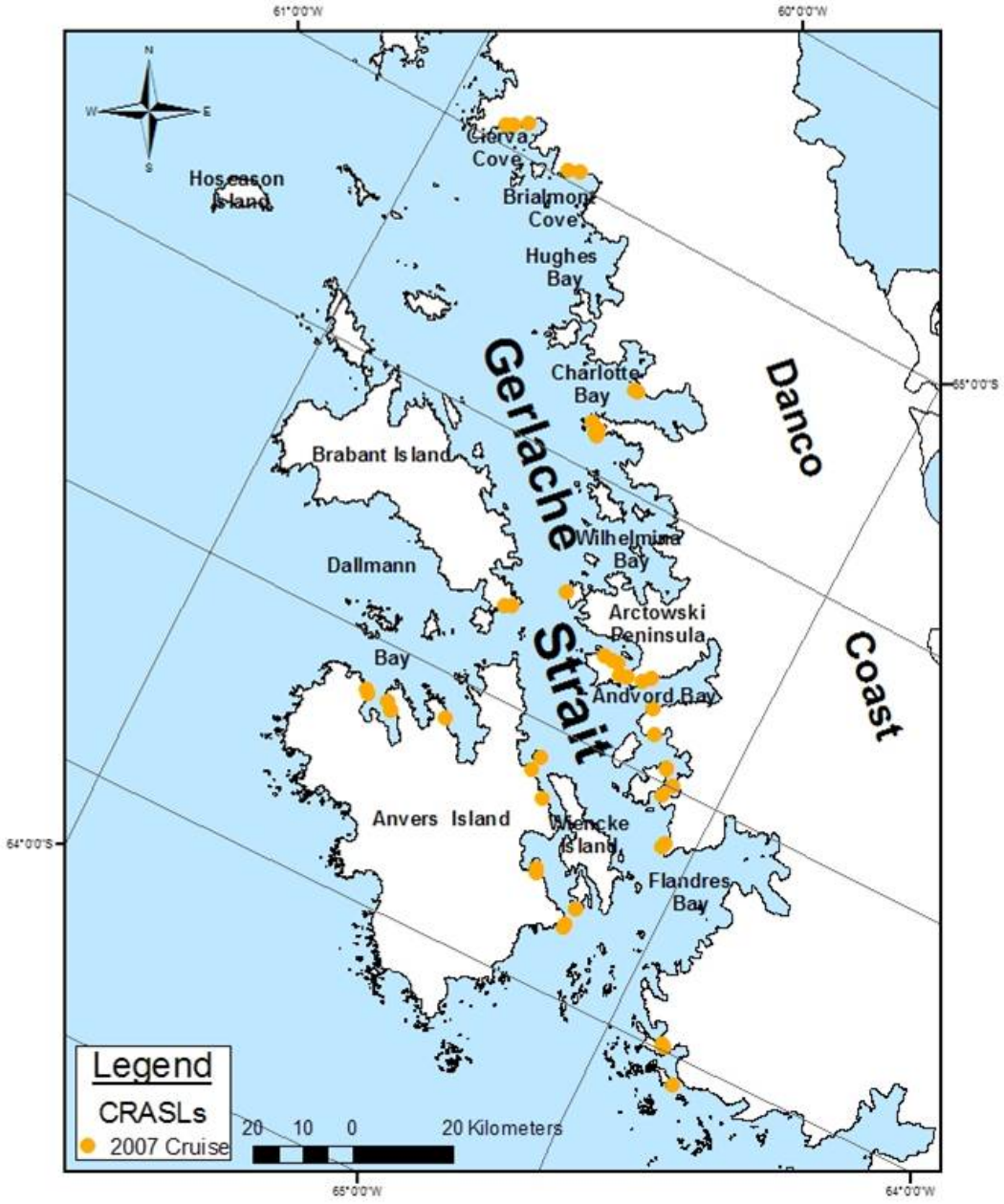

Figure 43 – Distribution of CRASLs observed during the NBP 0703 cruise.

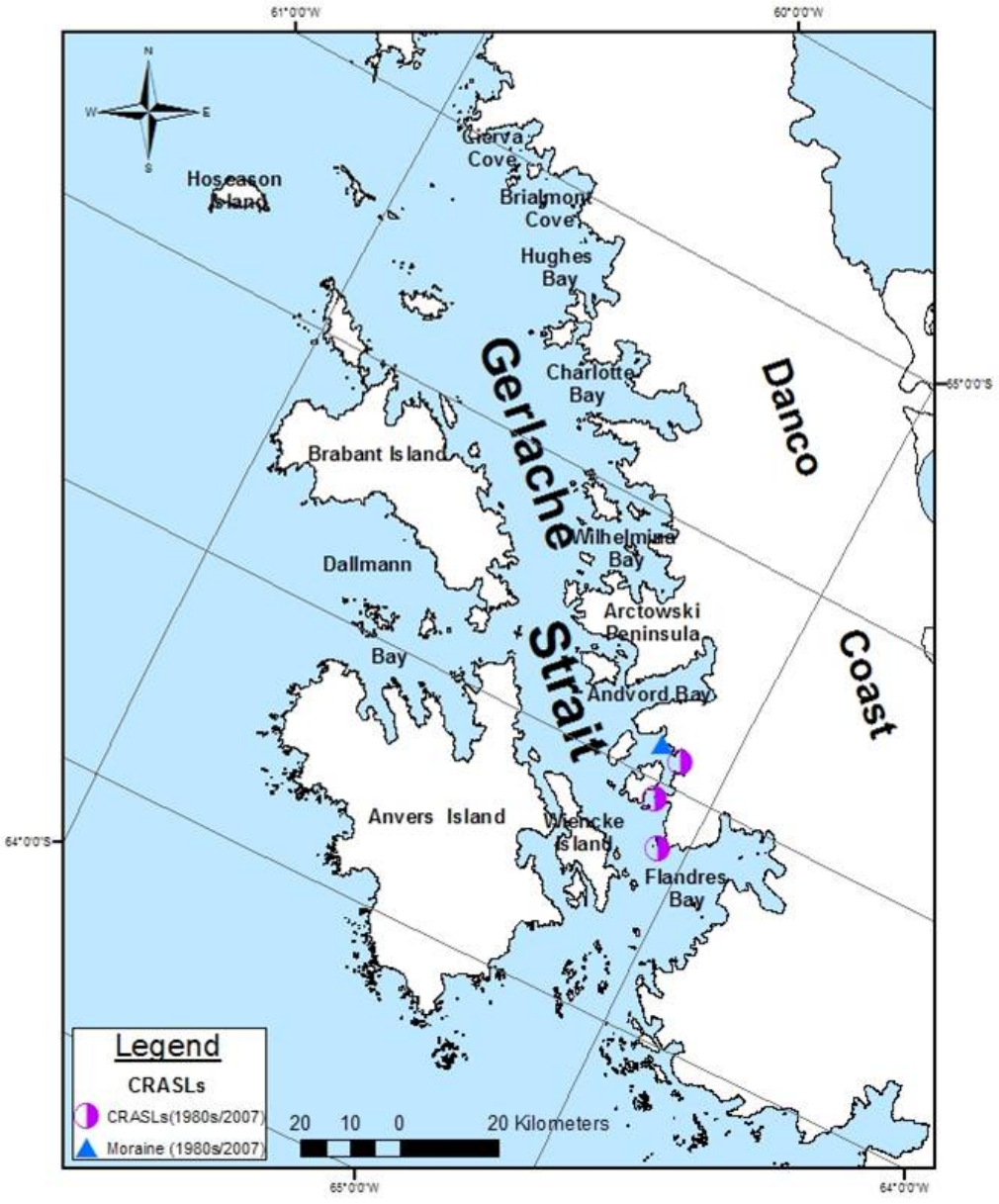

Figure 44 – Distribution of CRASLs observed in both the 1980s DEEP FREEZE cruise and the NBP 0703 2007 cruise.

The 367 identified CRASLs were grouped according to their orientation. Twelve different classification names were assigned (Table 21), and then simplified into four broad groups: Detached, Connected, Left, and Right. Of the 367 CRASLs, 138 were classified as Detached, 80 as Connected, 79 as Left, and 70 as Right. Due to the small size of the CRASLs in relation to the resolution of the maps, the maps were simplified by illustrating trends. For example, if 5 CRASLs were connected to the left side of a cove it was indicated by one large left facing arrow. This further simplification resulted in: 84 Detached, 49 Connected, 43 Left, and 41 Right CRASLs.

TABLE 21. TYPES OF CRASLS IDENTIFIED

Classification	Description	# Classified
Detached (A)	Detached and in front of the coastline	116
Detached (A) Behind	Detached and in front of the coastline, but behind another CRASL	22
Detached (L)	Detached from coastline, but more on the left side of the cove	27
Detached (L) Behind	Detached from coastline, more on the left side of the cove, but behind another CRASL	2
Detached (R)	Detached from coastline, but more on the right side of the cove	14
Detached (R) Behind	Detached from coastline, more on the right side of the cove, but behind another CRASL	3
Left	Attached to the coastline on the left side of the cove	46
Left Behind	Attached to the coastline on the left side of the cove, but behind another CRASL	4
Linked	Runs the whole length of the cove	77
Linked Behind	Runs the whole length of the cove, but behind another CRASL	3
Right	Attached to the coastline on the right side of the cove	44
Right Behind	Attached to the coastline on the right side of the cove, but behind another CRASL	9

The data in Table 21 suggests that the prominent type of CRASL in the Gerlache Strait is the Detached CRASL; followed by the Connected, and Left and Right types (Figs 45 – 57).

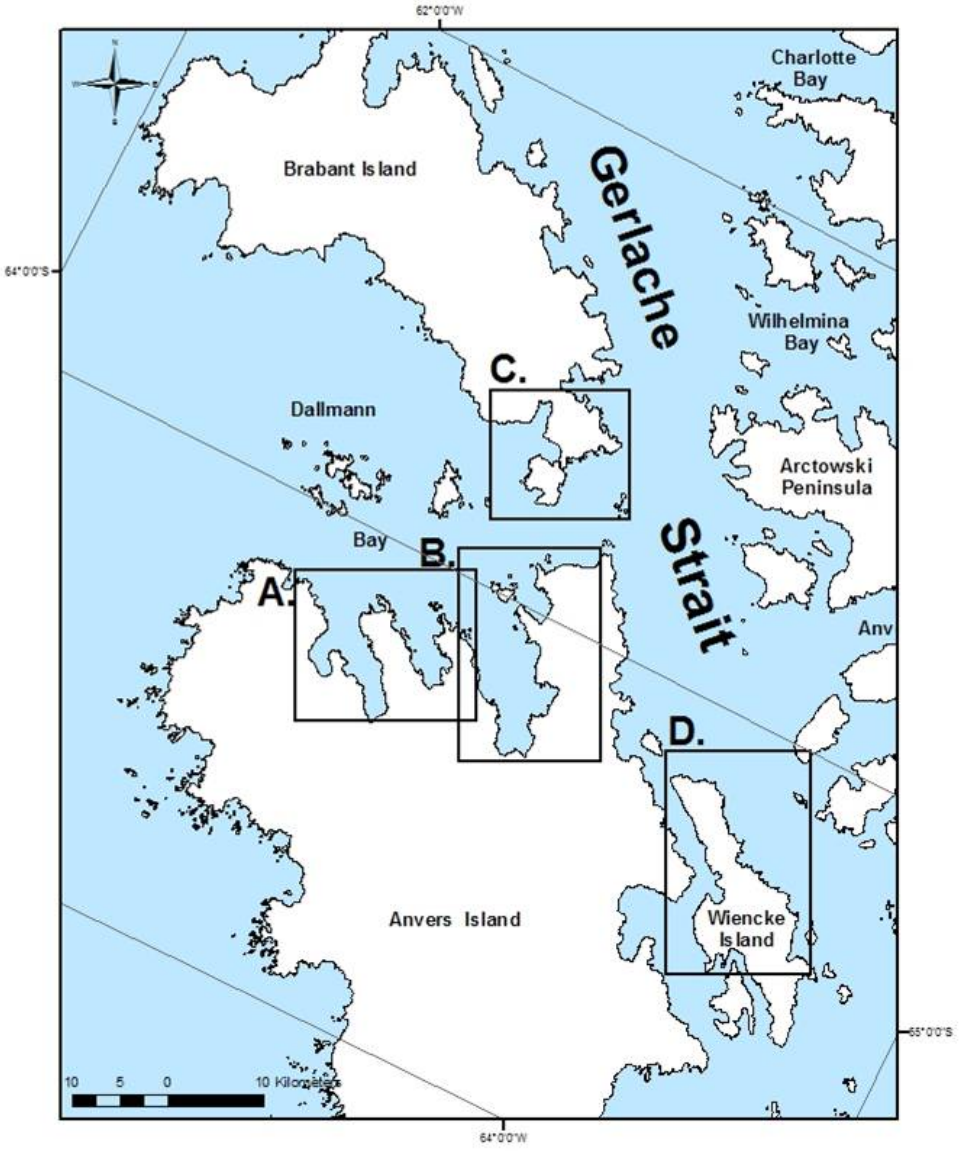

Figure 45 – Location of orientation and shape maps.

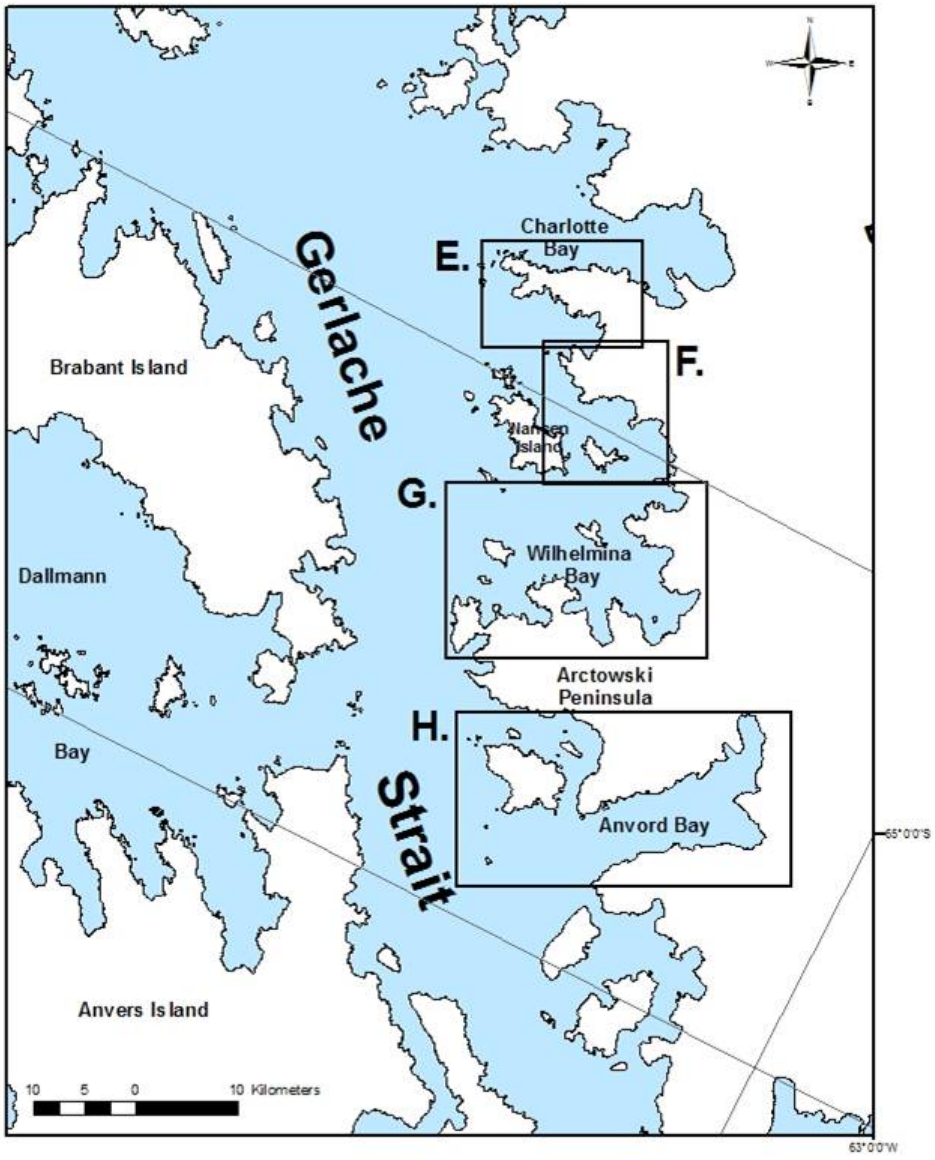

Figure 46 – Location of orientation and shape maps.

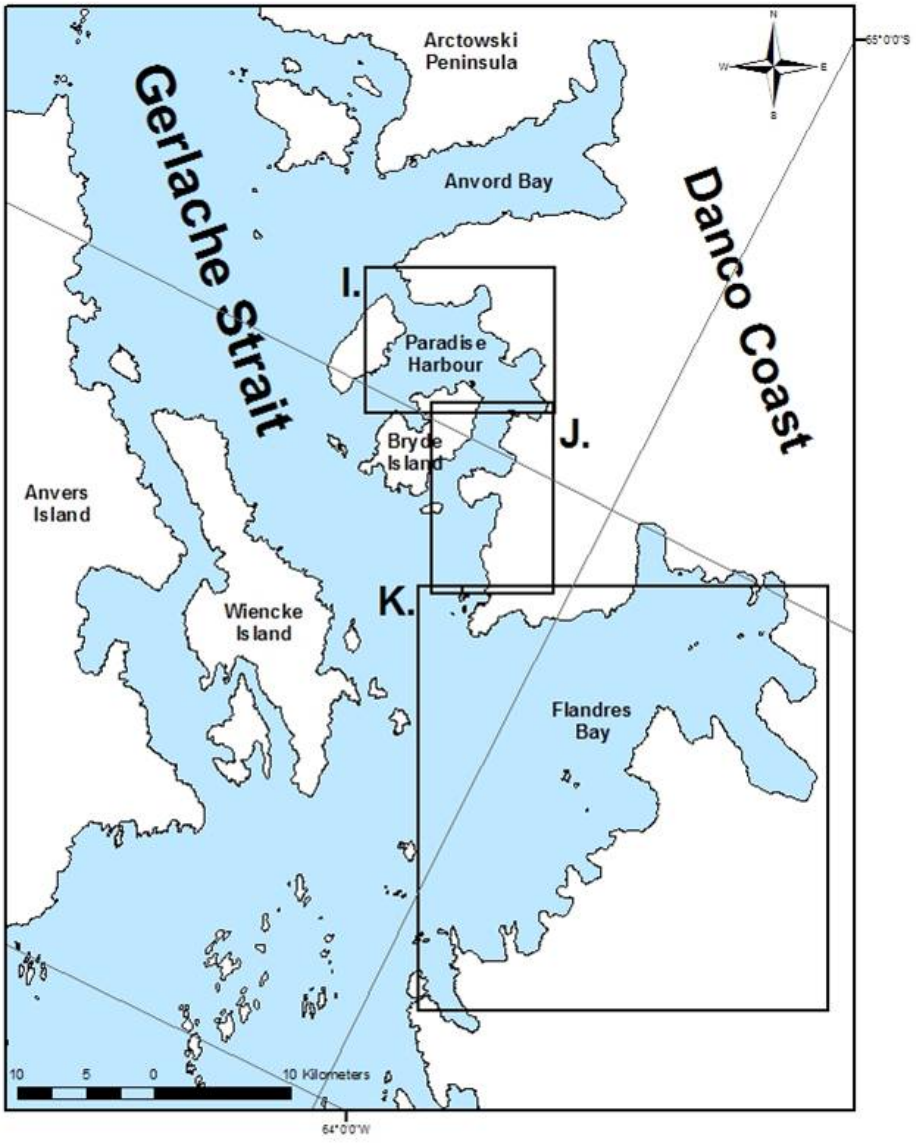

Figure 47 – Location of orientation and shape maps.

A.

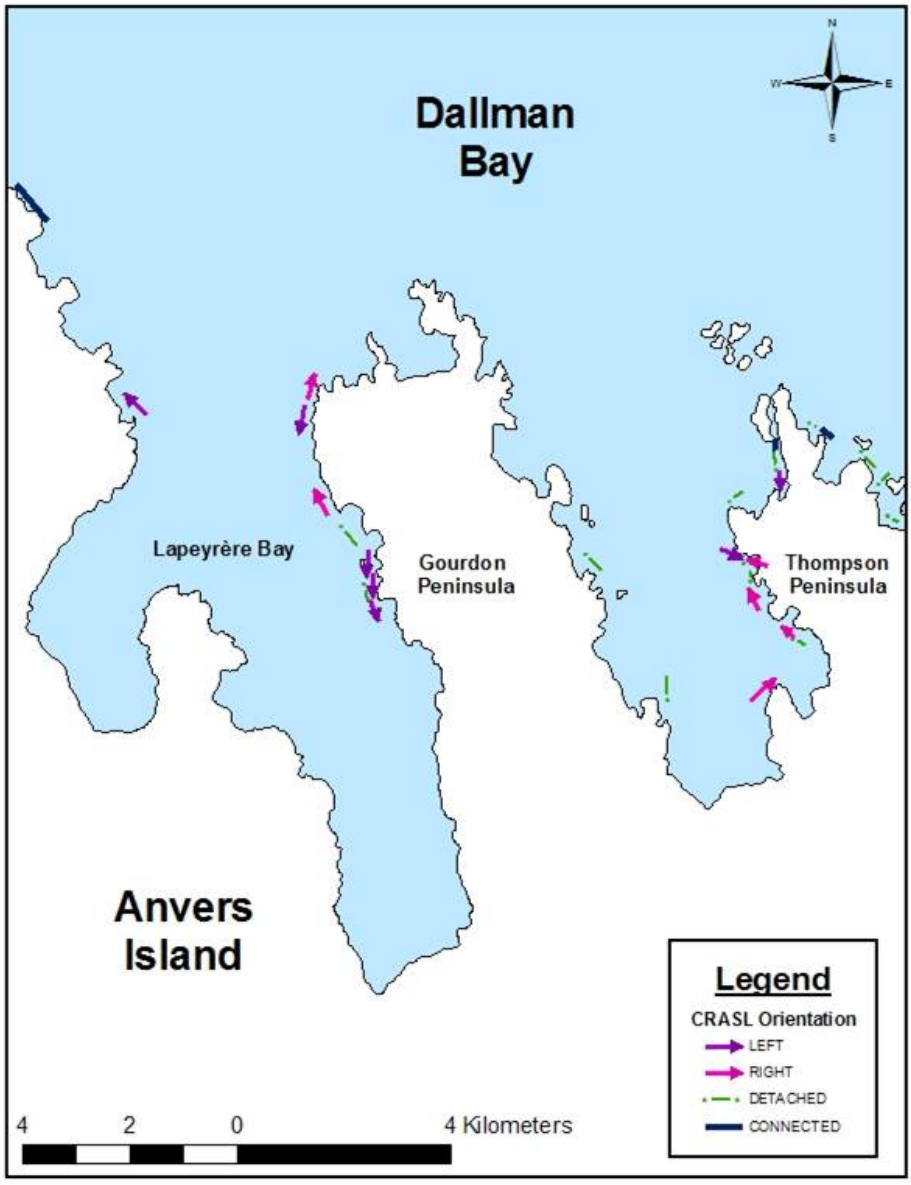

Figure 48 – Orientation map of CRASLs near Gourdon Peninsula, Anvers Island. See Figure 51 for map location.

B.

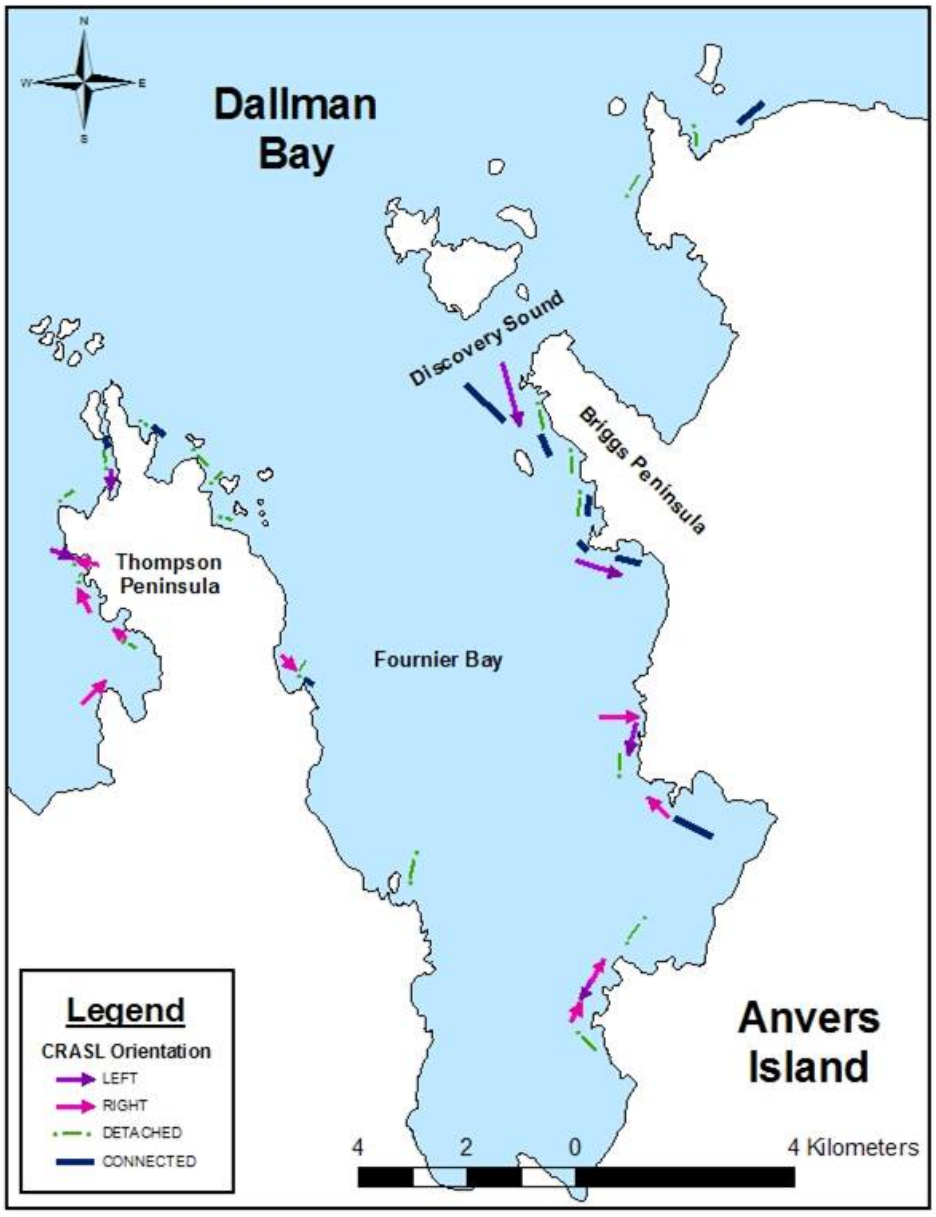

Figure 49 – Orientation map CRASLs located along Fournier Bay, Anvers Island. See Figure 51 for map location.

C.

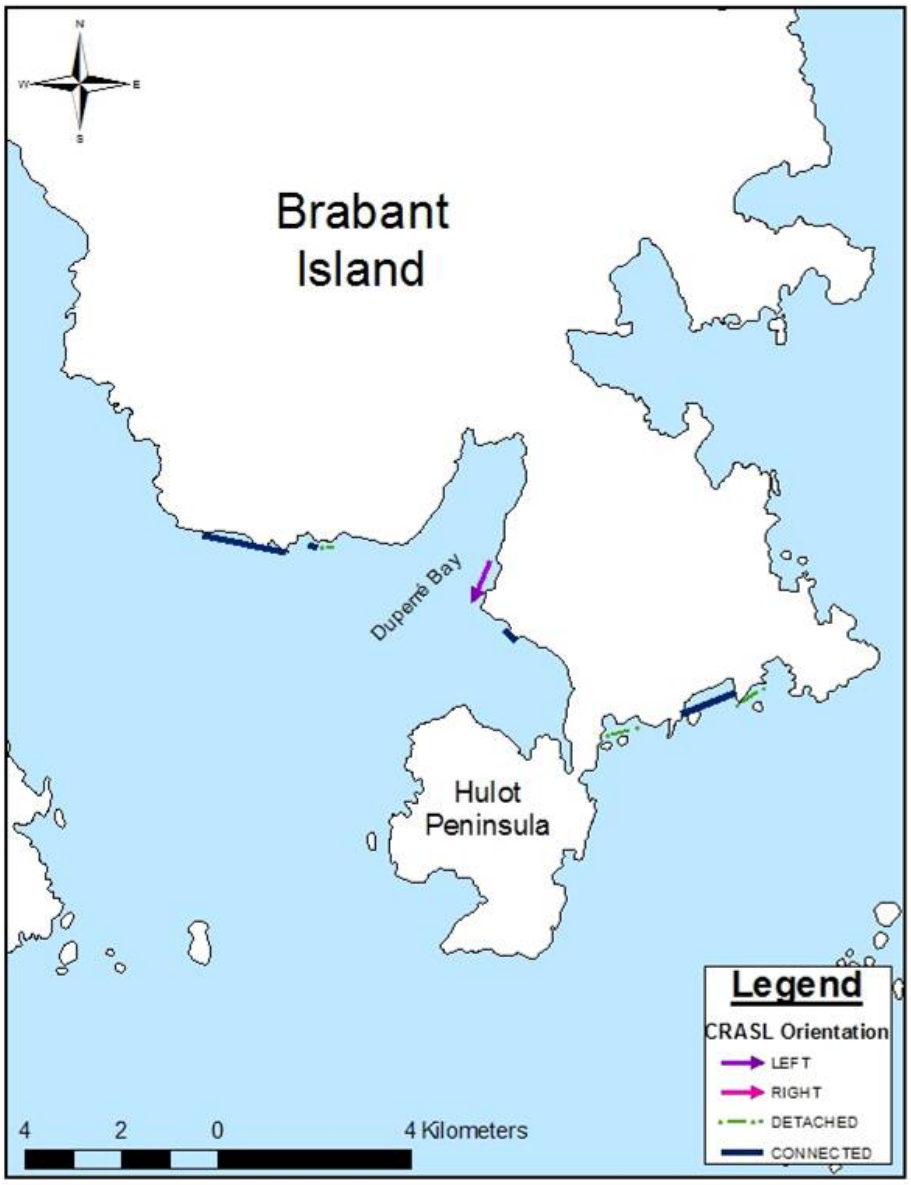

Figure 50 – Orientation map of CRASLs located on Brabant Island. See Figure 51 for map location.

D.

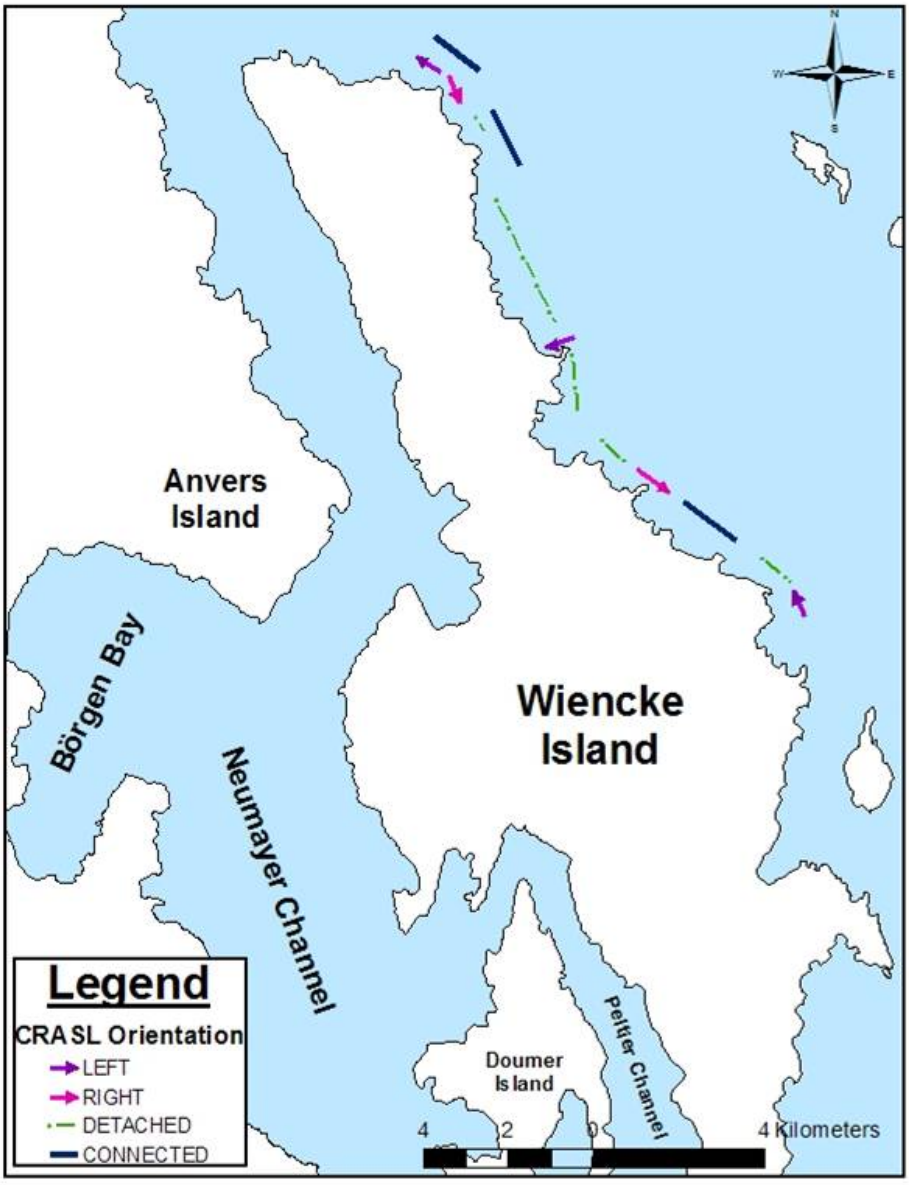

Figure 51 – Orientation map of CRASLs along the shoreline of Wiencke Island. See Figure 51 for map location.

E.

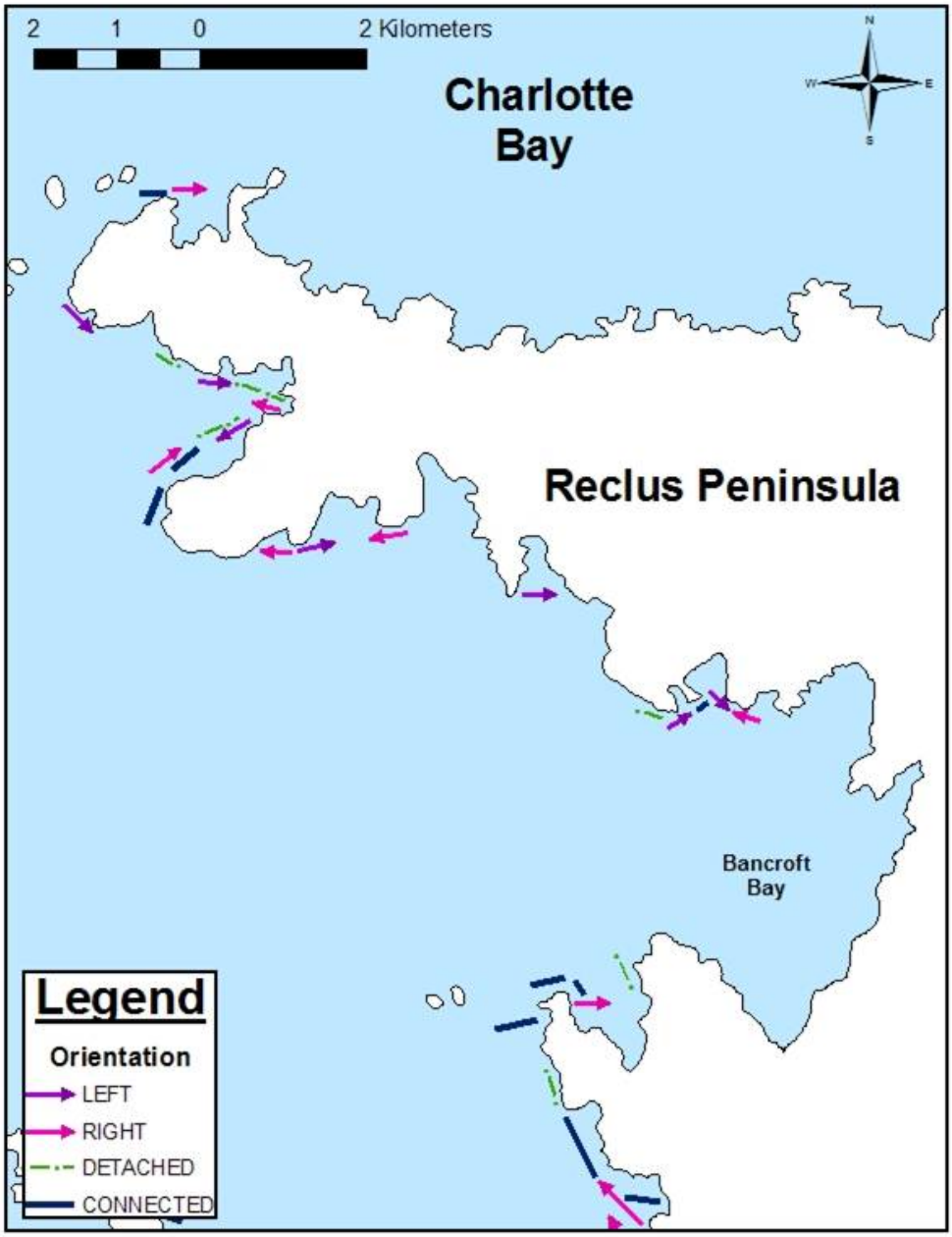

Figure 52 – Orientation map of CRASLs along the Reclus Peninsula. See Figure 52 for map location.

F.

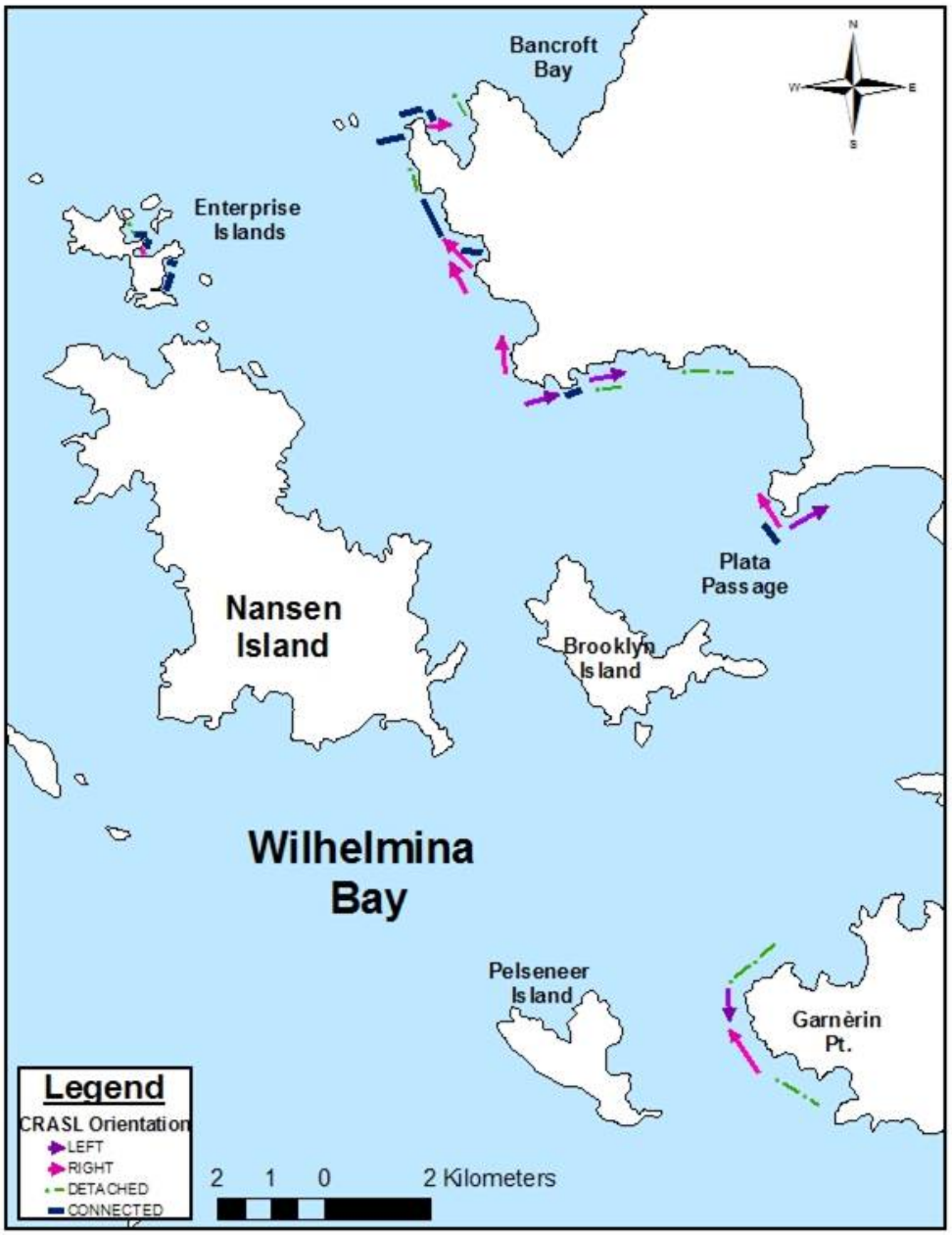

Figure 53 – Orientation map of CRASLs located along Plata Passage. See Figure 52 for map location.

G.

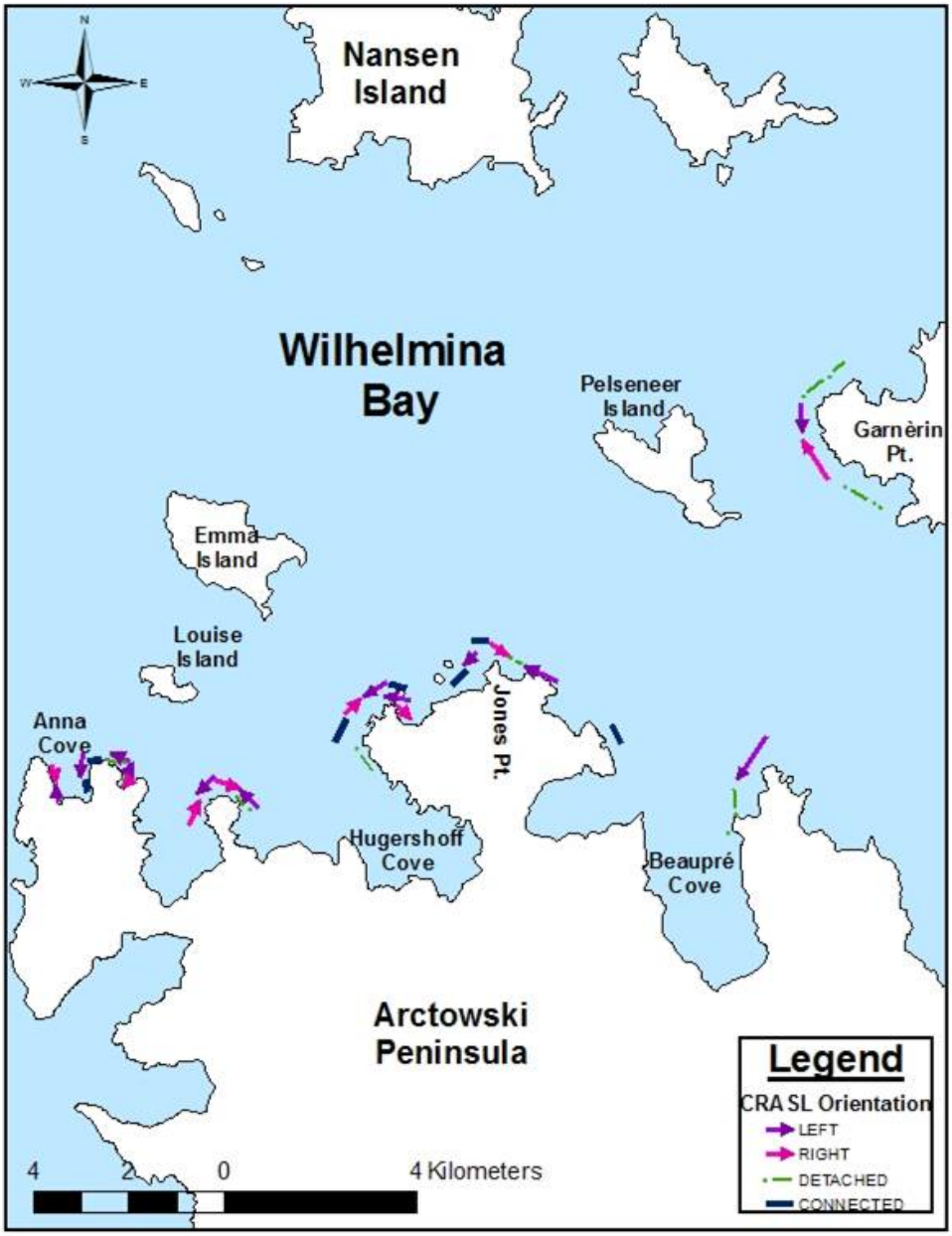

Figure 54 – Orientation map of CRASLs for Wilhelmina Bay. See Figure 52 for map location.

H.

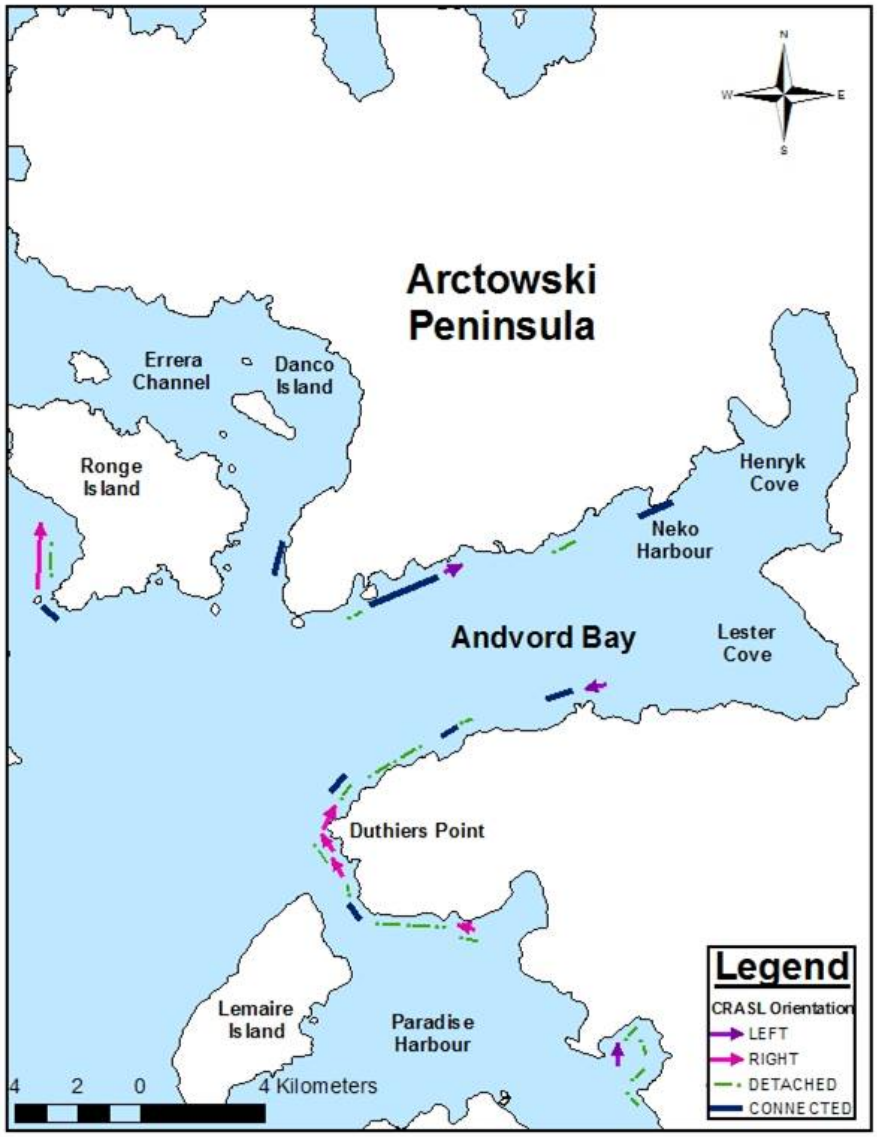

Figure 55 – Orientation map of CRASLs for Andvord Bay. See Figure 52 for map location.

I. & J.

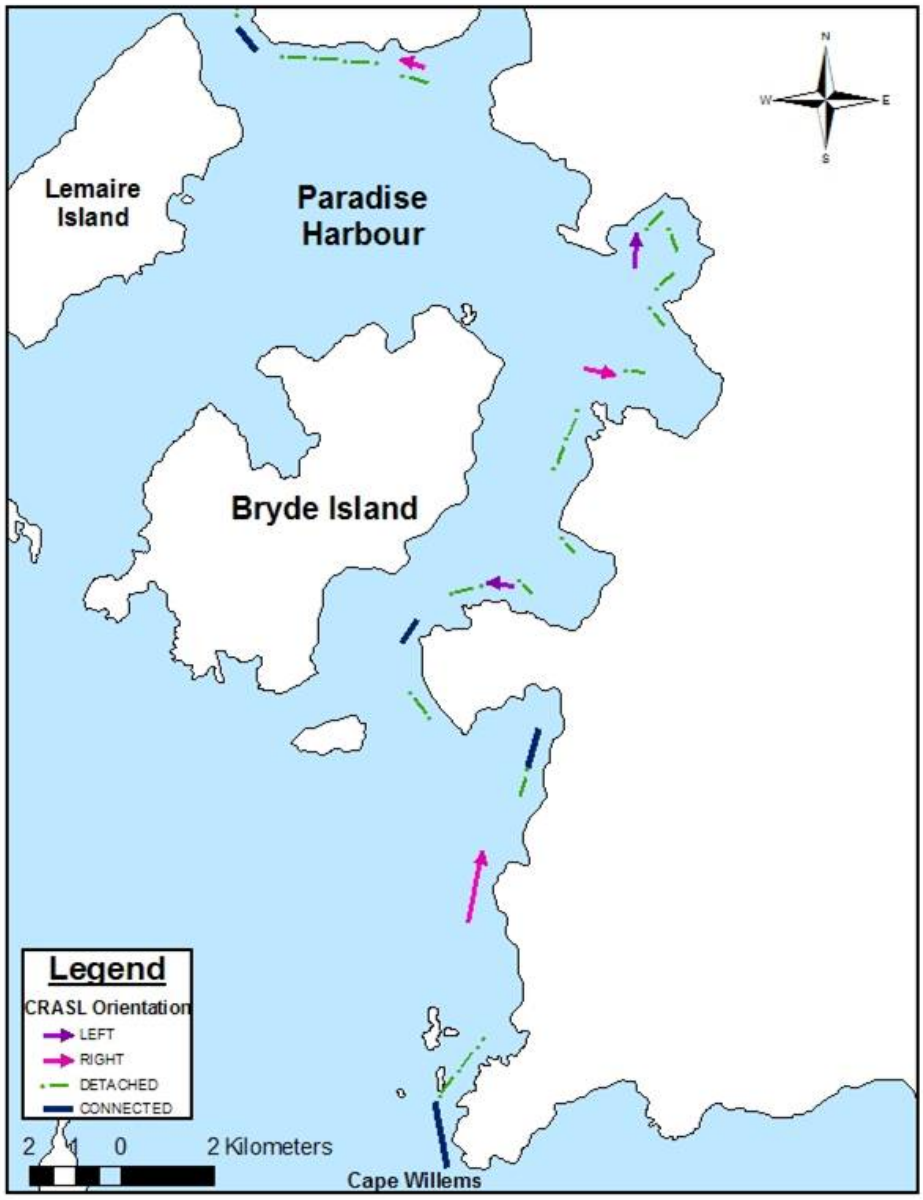

Figure 56 – Orientation map of CRASLs for Argentino Channel. See Figure 53 for map location.

K.

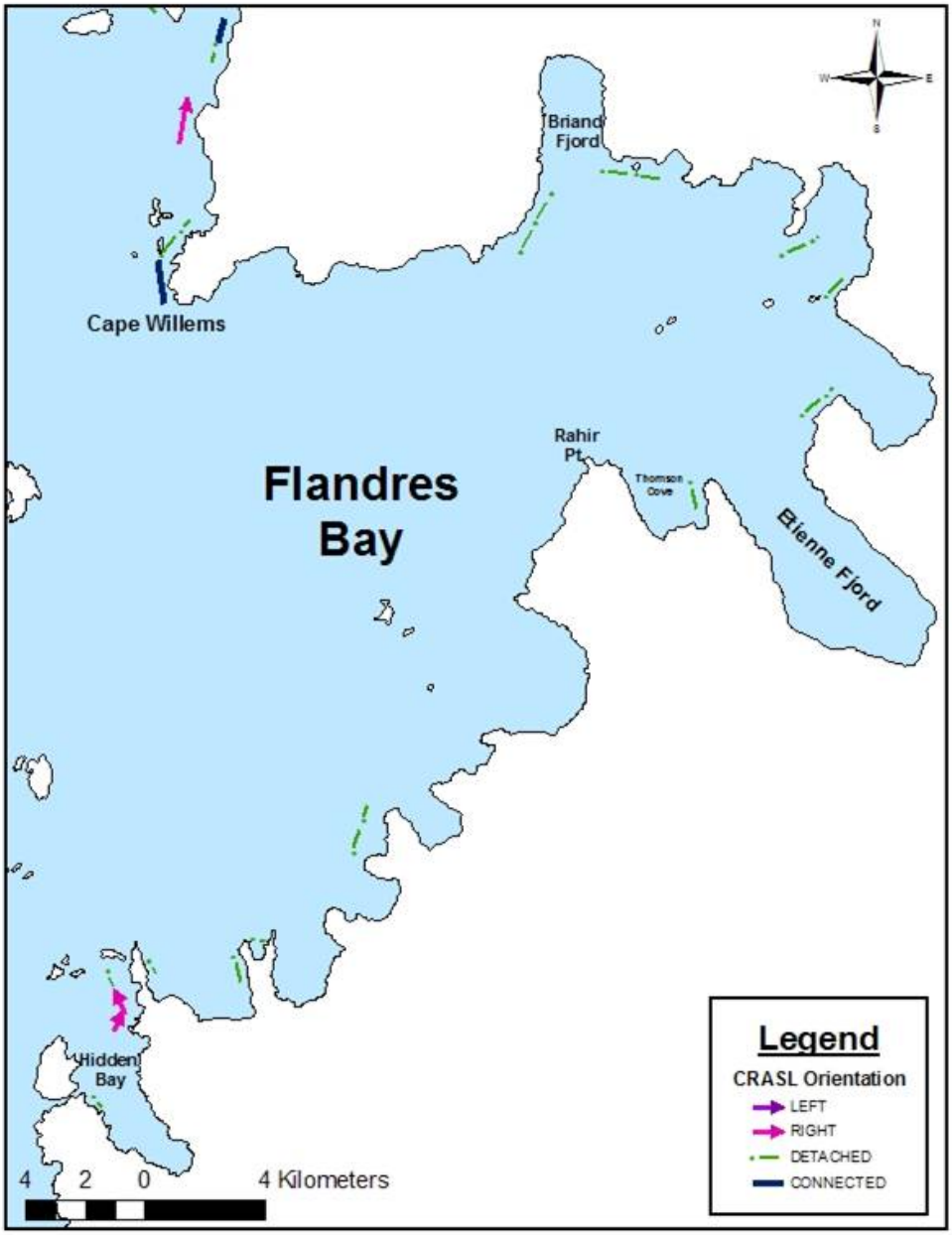

Figure 57 – Orientation map of CRASLs for Flandres Bay. See Figure 53 for map location.

The shape of all CRASLs was also determined and classified into four different groups based on their orientation with respect to the coastline: concave, convex, parallel, and perpendicular. Of the 367 CRASLs, 113 were concave, 18 convex, 218 parallel to the coastline, and 18 perpendicular to the coastline (Figs. 45 - 47, and Figs. 58 – 68).

These results combined with the orientation of the CRASLs suggest that the most common type of CRASL is one that is detached and parallel to the coastline. Furthermore, based on the orientation maps the CRASLs appear to have a random rather than ordered orientation, supporting the hypothesis that they were created by moraines. The random orientation is apparent at both the regional as well as local fjord scale.

Chronology

Three methods were used to place constraints on the age of the CRASLs: relative ages of the structures (huts and beacons), aerial photos in combination with the distribution and orientation maps, and comparison with a constructed sea-level record via OSL dating of raised beaches.

Age of Huts

Throughout the 20th century the British, Chileans, and Argentineans established many small stations (huts and beacons) throughout the Gerlache Strait (Fig. 69). According to the BAS, the purpose for having a strong British presence in Antarctica was to discourage access to anchorages by enemy ships and ultimately reinforce Britain's

A.

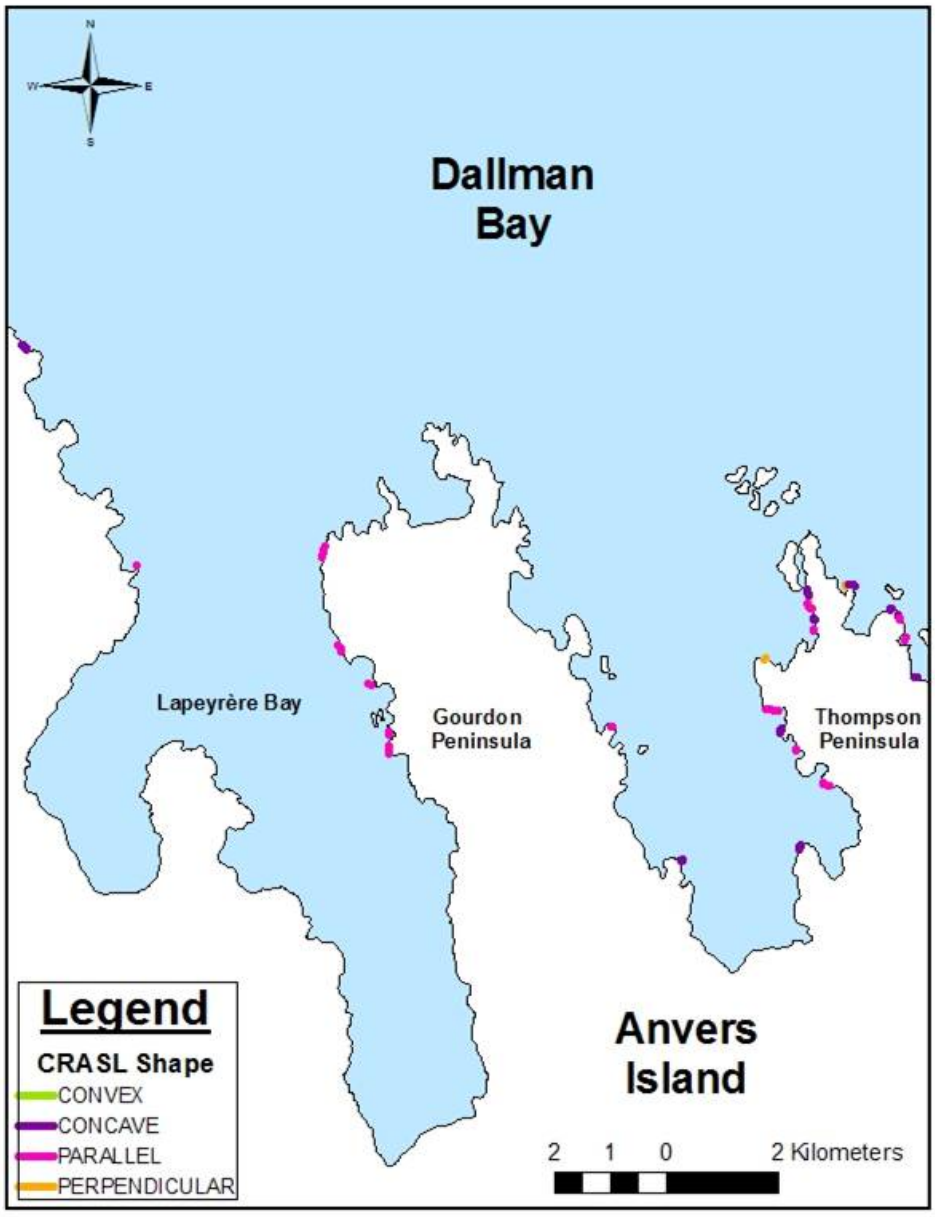

Figure 58 – Map showing the shape of CRASLs for Gourdon Peninsula, Anvers Island. See Figure 51 for map location.

B.

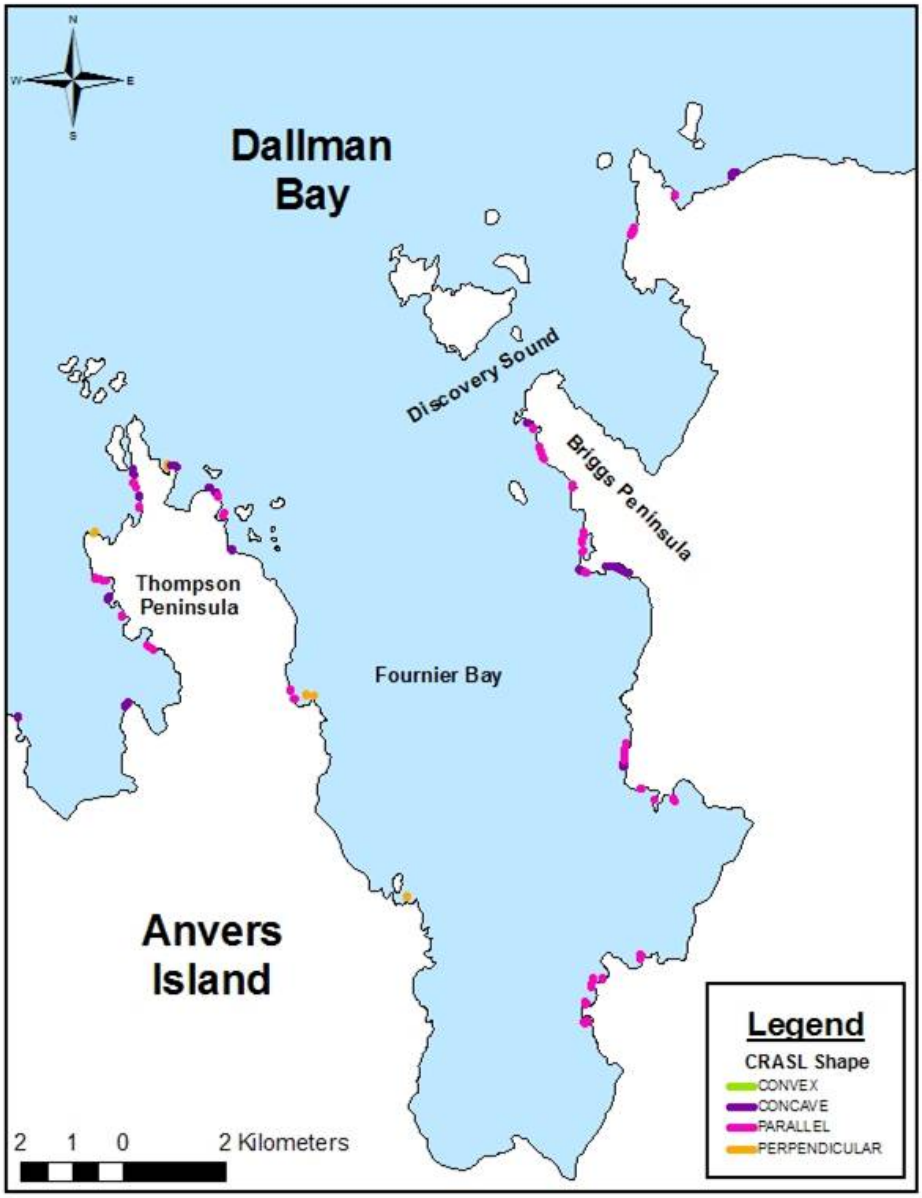

Figure 59 – Map showing the shape of CRASLs for Thompson Peninsula, Anvers Island. See Figure 51 for map location.

C.

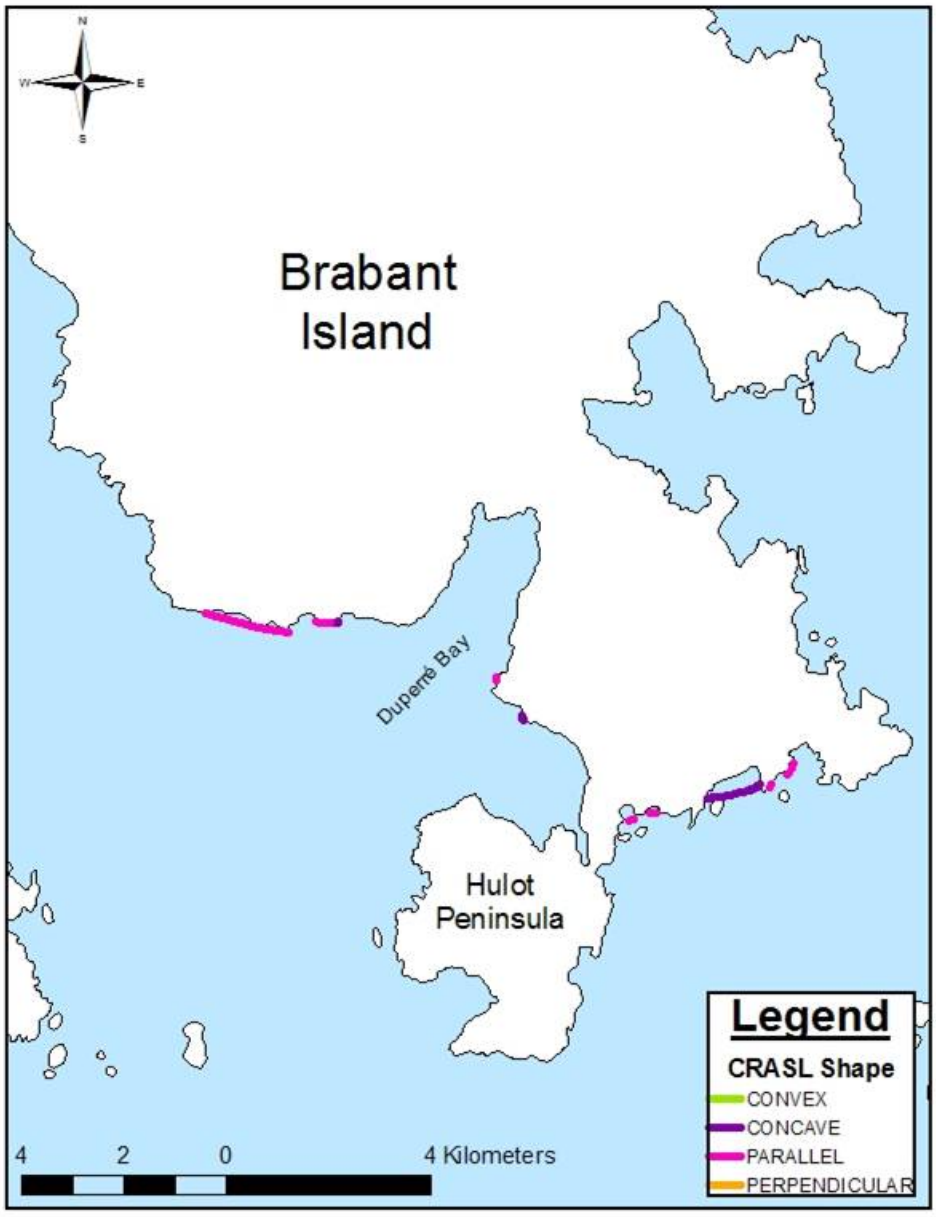

Figure 60 – Map showing the shape of CRASLs for Brabant, Island. See Figure 51 for map location.

D.

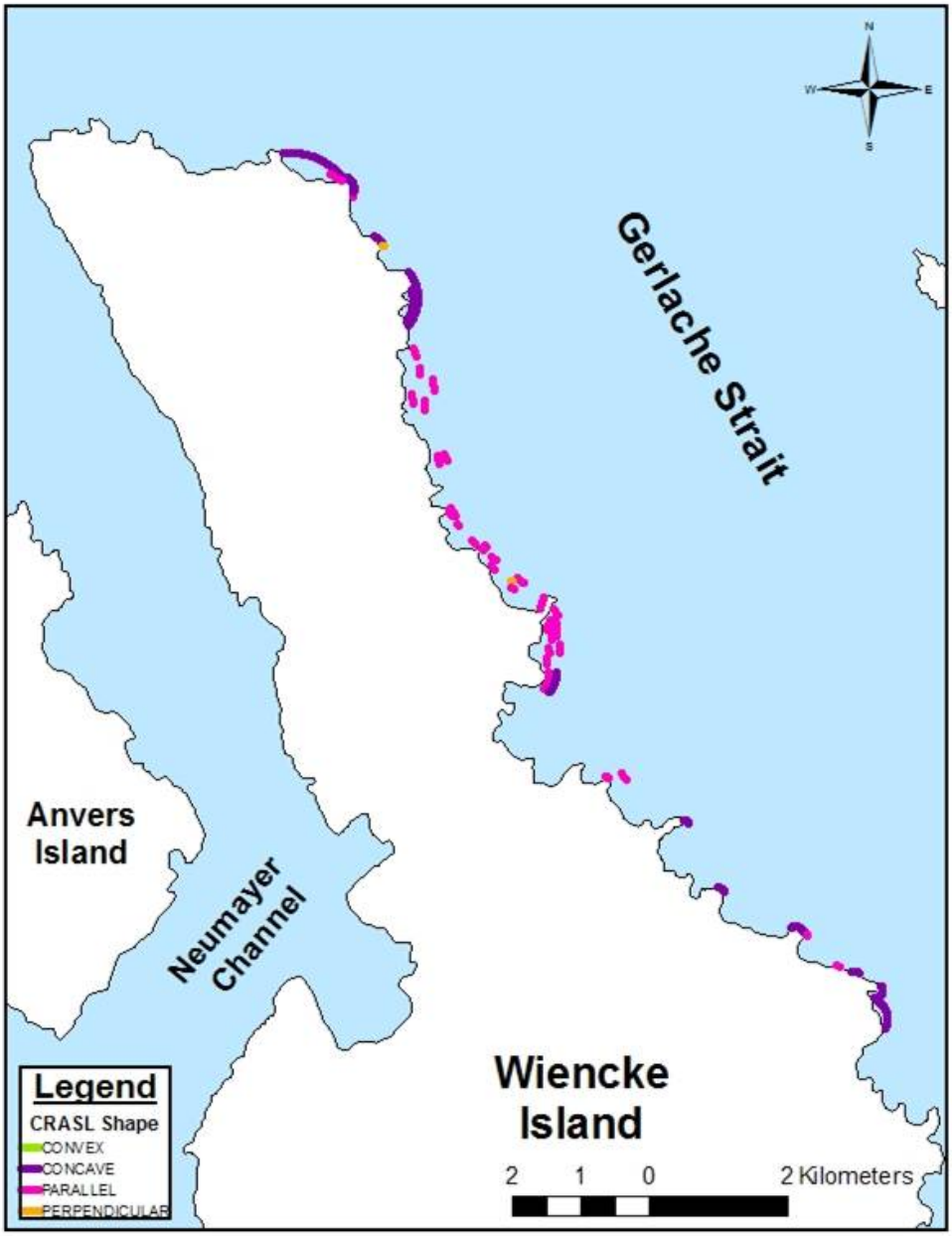

Figure 61 – Map showing the shape of CRASLs for Wiencke Island. See Figure 51 for map location.

E.

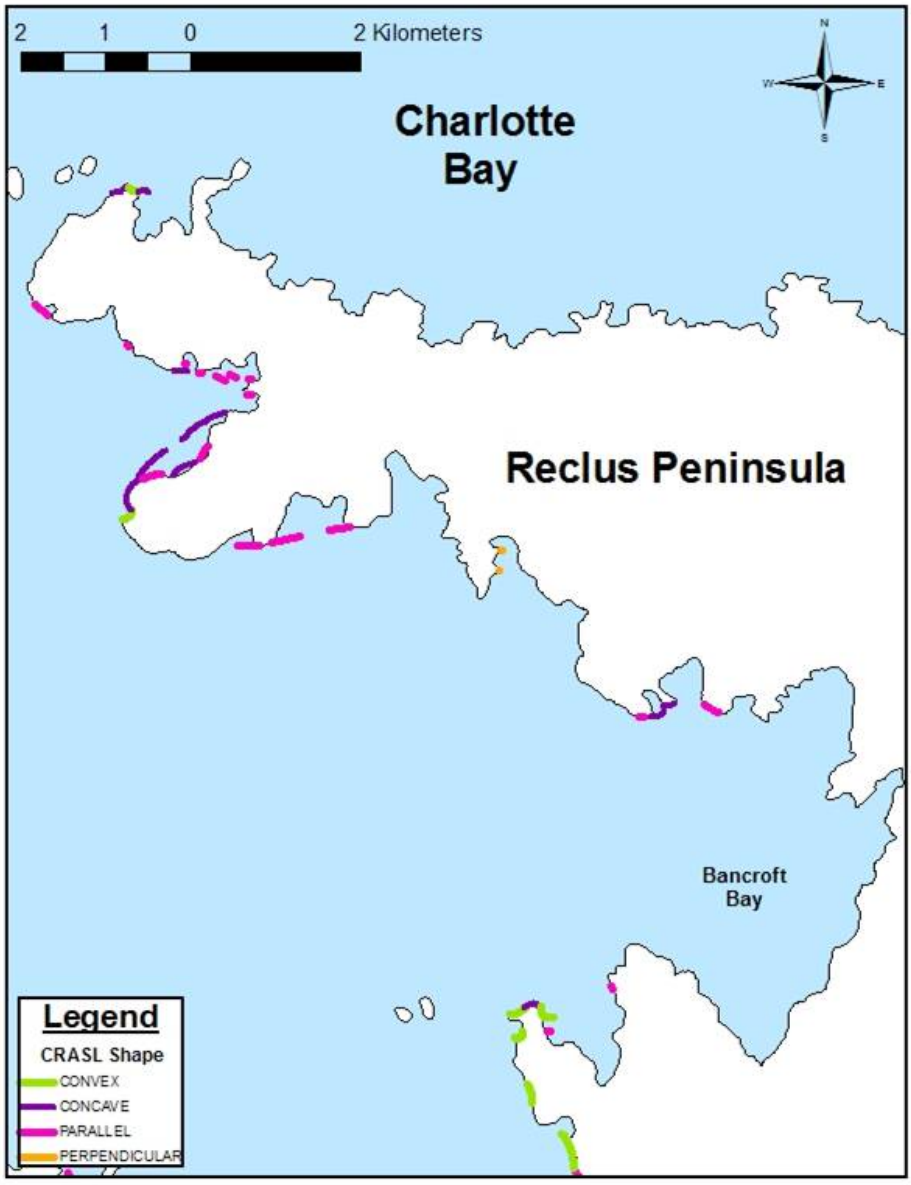

Figure 62 – Map showing the shape of CRASLs for Reclus Peninsula. See Figure 52 for map location.

F.

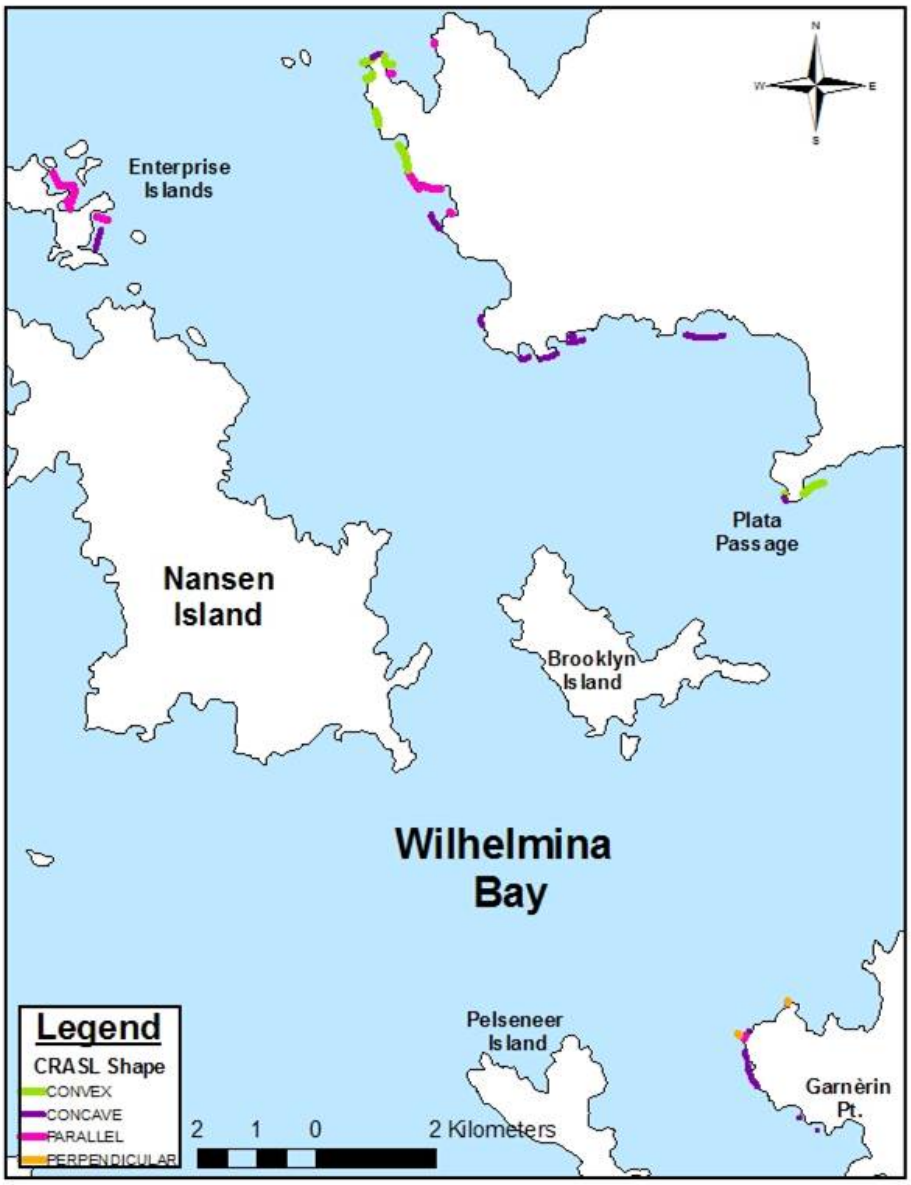

Figure 63 – Map showing the shape of CRASLs for Plata Passage. See Figure 52 for map location.

G.

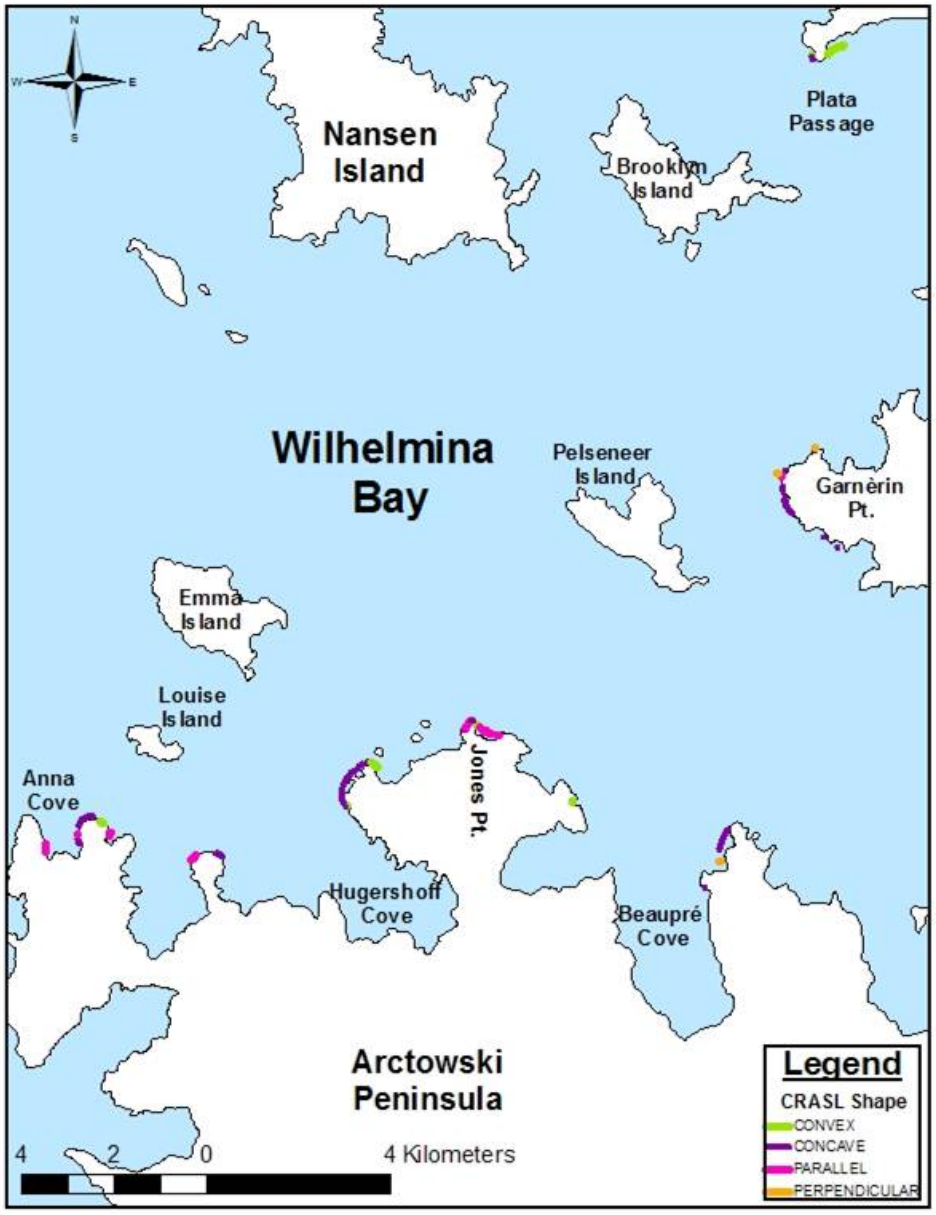

Figure 64 – Map showing the shape of CRASLs for Wilhelmina Bay. See Figure 52 for map location.

H.

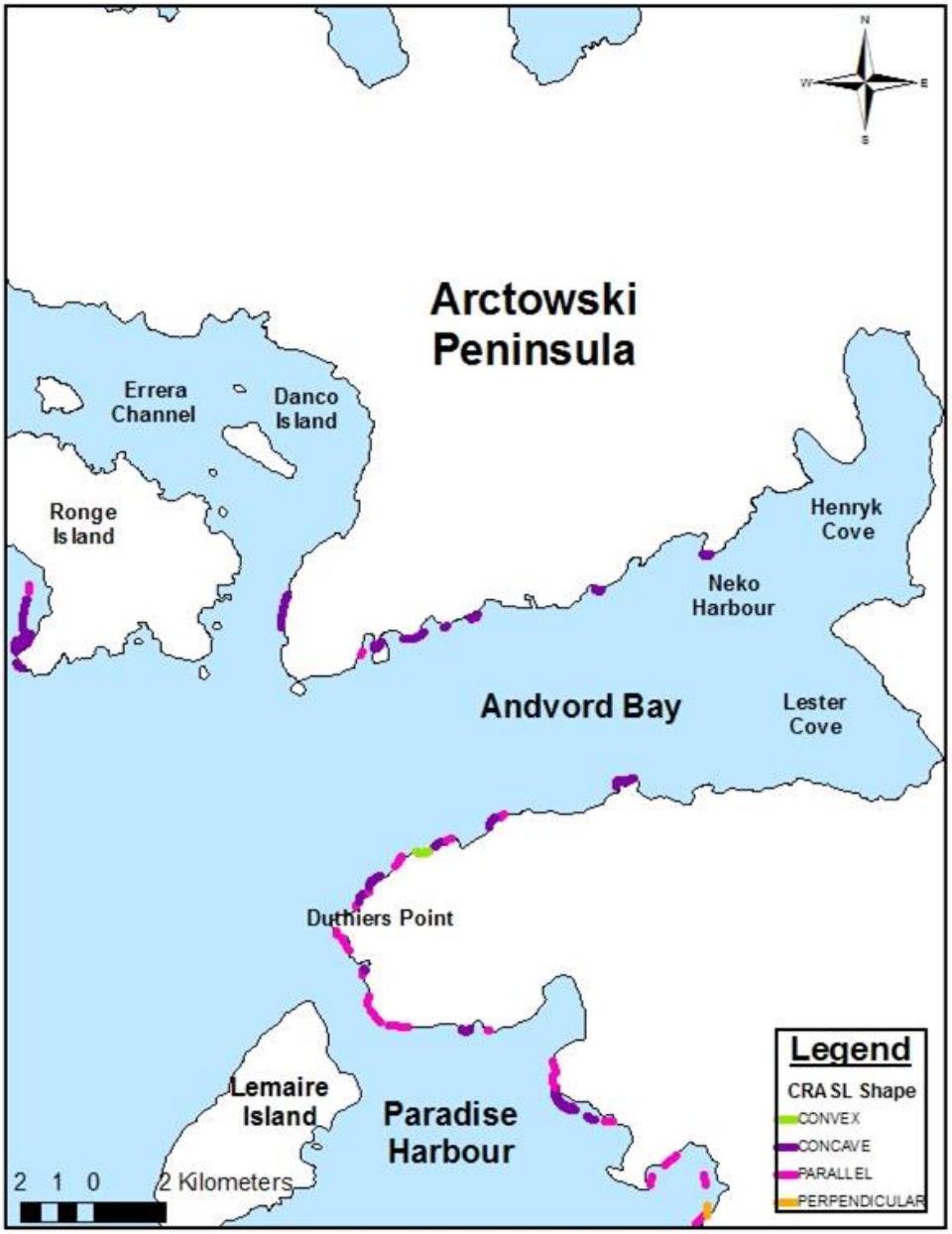

Figure 65 – Map showing the shape of CRASLs for Andvord Bay. See Figure 52 for map location.

I.

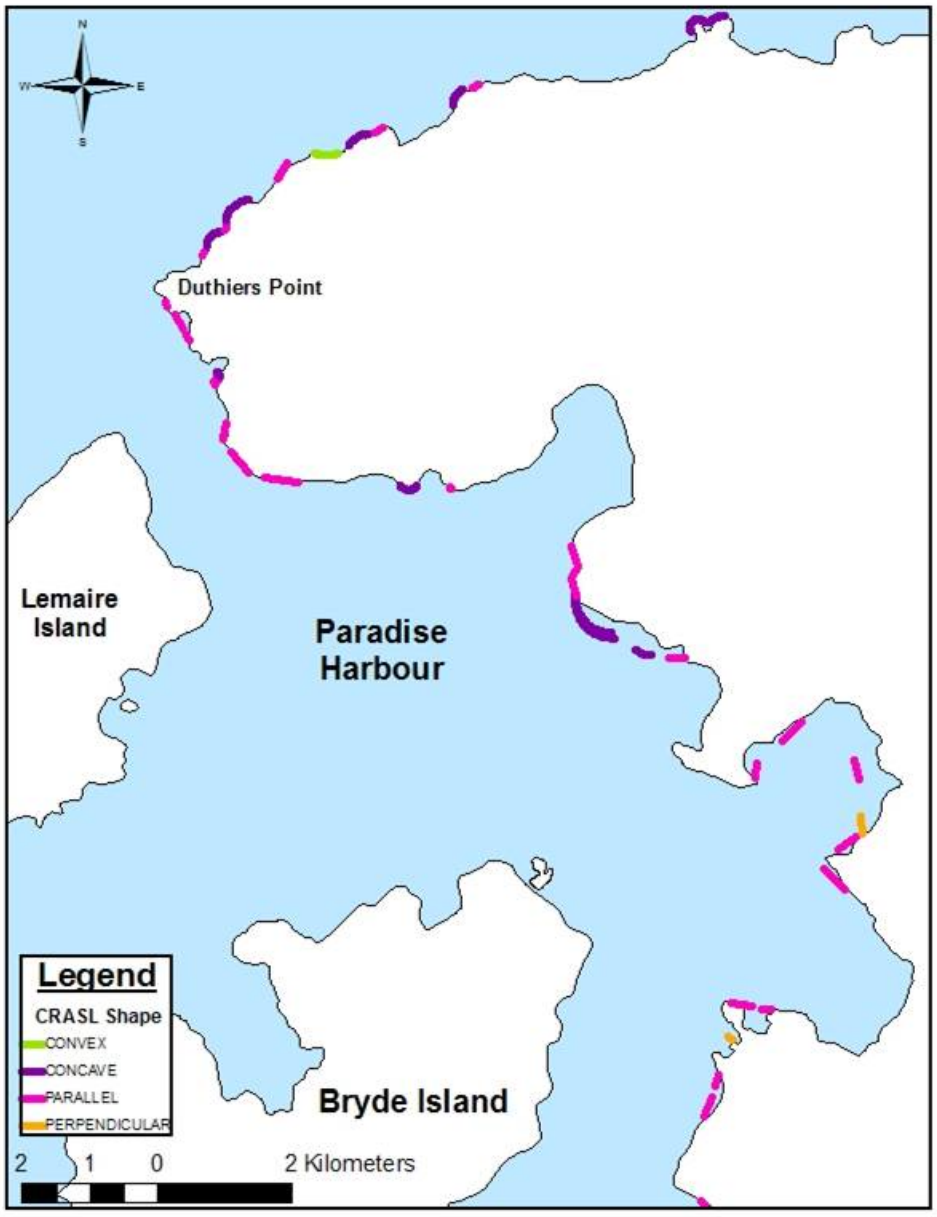

Figure 66 – Map showing the shape of CRASLs for Paradise Harbour. See Figure 53 for map location.

J.

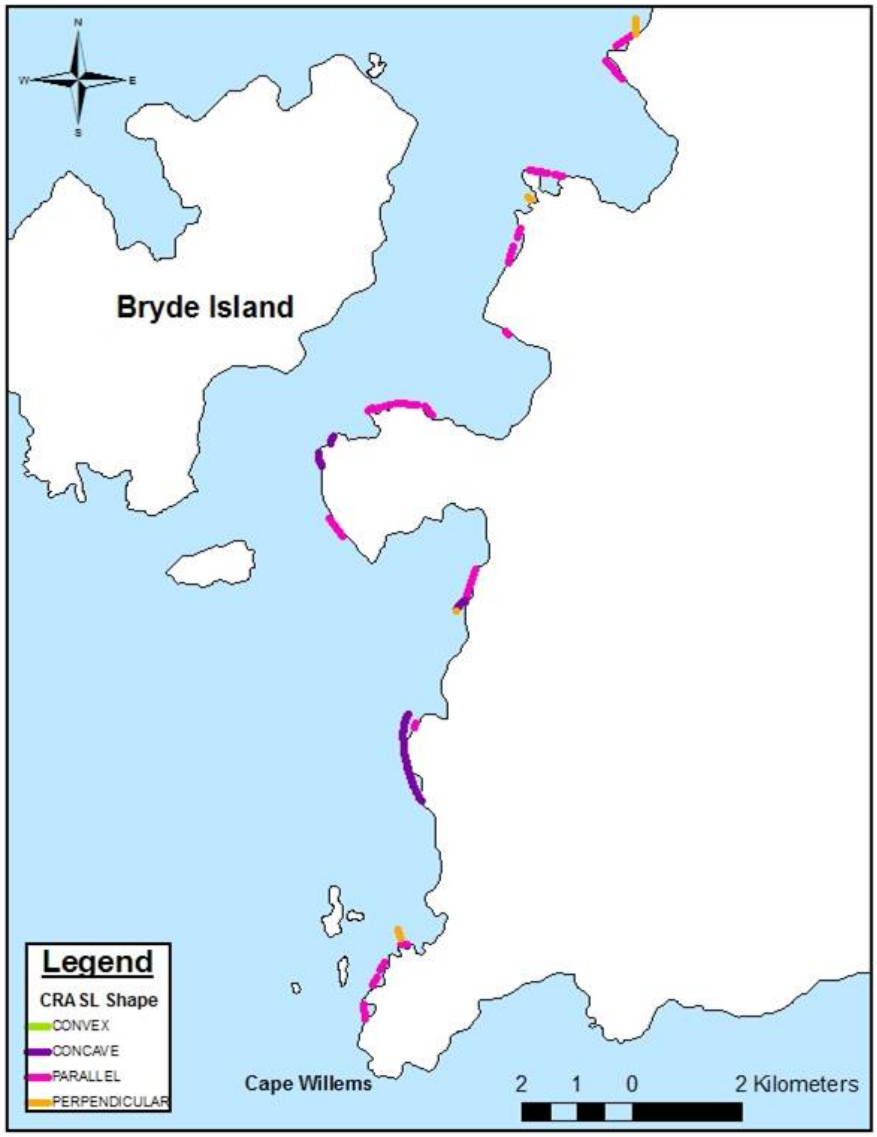

Figure 67 – Map showing the shape of CRASLs for Argentino Channel. See Figure 53 for map location.

K.

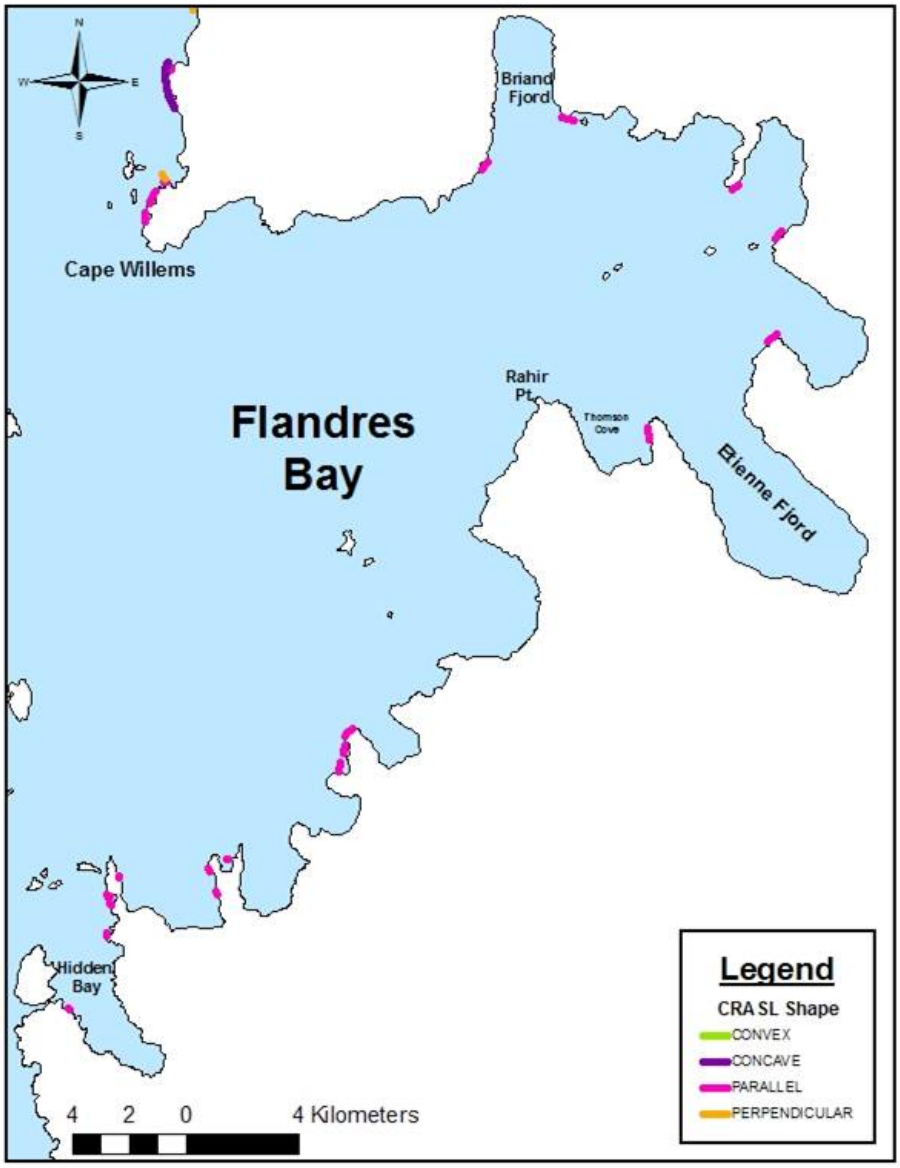

Figure 68 – Map showing shape of CRASLs for Flandres Bay. See Figure 53 for map location.

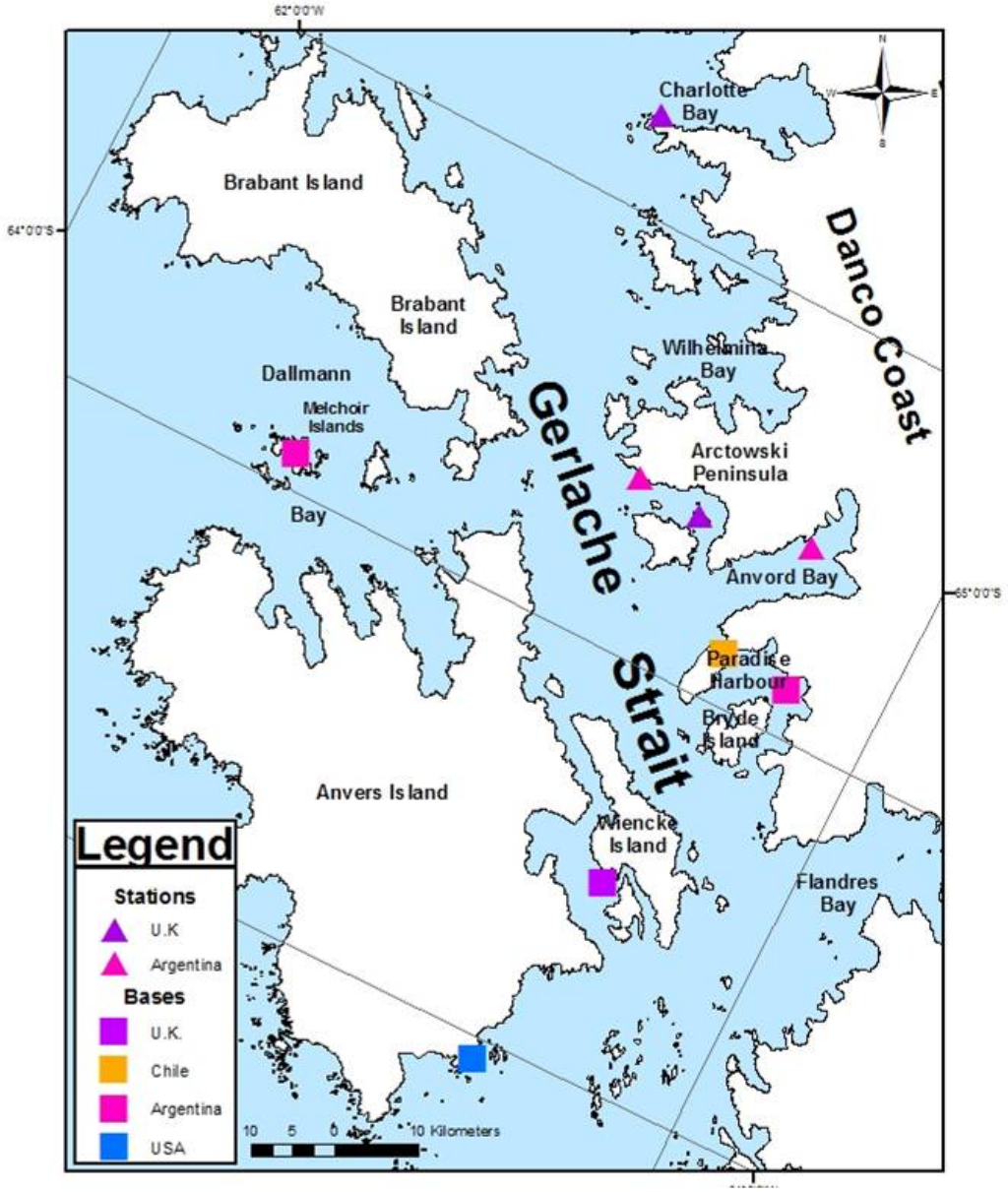

Figure 69 – Location of Bases (Squares) and Stations (Triangles) in the Gerlache Strait. Owned by either Argentina, Chile, United Kingdom (U.K.) or the United States of America (USA). A total of 5 bases and 5 stations were located in the study area.

claim to the Falkland Islands Dependencies (British Antarctic Survey website). Additionally, their presence would provide an opportunity for scientific research. The first British scientific station was established at Wiencke Island on February 11, 1944 (Fig. 69), making it the oldest government establishment in the Gerlache Strait. Table 22 lists the name or location descriptions, owner, operational date, structure type, and latitude and longitude of all known governmental structures in the Gerlache Strait.

Ten bases and/or stations, ten beacons and three structures, whose type is unknown, were identified in the study area (Fig. 70). An example of one of these structures, a Chilean base, built in 1951 in Paradise Harbour, is shown in Figure 71.

According to the BAS (British Antarctic Survey website), a few of these structures have been removed or dismantled and rebuilt in museums in the past ten years. Danco Island (Station O; Fig. 72) bears little to no trace of human activity. Station O on Danco Island had been abandoned since February 22nd, 1959, upon completion of research, and the majority of the site removed during March-April 2004. A hut at Portal Point was abandoned on April 25^{th,} 1958, dismantled on April 1st, 1997, and transported to the Falkland Islands Museum. Eventually it was re-erected as an exhibit in December 1998 at the Museum (British Antarctic Survey website).

Other bases and stations are still present throughout the study area such as the Argentinean Base Melchoir built in 1947 on the Melchoir Islands in Dallman Bay (Fig. 73), an Argentinean Station at Neko Harbour in Andvord Bay (Fig. 74), and the American owned Palmer Station (Fig. 75). At the beginning of this study, I hoped that some of these anthropogenic structures were built on CRASLs. However after further

TABLE 22. STRUCTURE IN GERLACHE STRAIT

Location Name	Owner	Opened/Closed	Type	Lat. (°S)	Long. (°W)
Arctowski Peninsula	Argentina		Station	-64°39’30”	-62°35’
Danco Island (Station “O”)	U.K.	Feb. 26, 1956 - Feb. 22, 1959	Station	-64°43’45”	-62°37’
Paradise Harbour (Waterboat Pt.)	Chile	1951	Base	-64°49’30”	-62°52’30”
Arctowkski Penin. (Neko Harbour)	Argentina	N.K.*	Station	-64°51’15”	-62°32’30”
Melchoir Islands	Argentina	1947	Base	-64°19’30”	-62°55’
Cape Reclus (Reclus Hut or Portal Pt.)	U.K.	Dec. 13, 1956 – Apr. 25, 1958	Station	-64°30’	-61°46’
Palmer Station	U.S.A.	Feb. 25, 1965	Base	-64°7’	-64°0’
Argentino Channel (Near Mascias Cove)	Argentina	N.K.*	Station	-64°55’30”	-62°59’
Argentino Channel (Near Skontorp Cove)	Argentina	N.K.*	Base	-64°54’	-62°53’
Weincke Island (Station “A”)	U.K.	N.K.*	Base	-64°49’10”	-63°31’
Weincke Island	Argentina	N.K.*	Not Specified	-64°48’50”	-63°31’30”
Gauthiers Pt.	Chile	N.K.*	Not Specified	-64°50’	-63°35’
Argentine Island (Near a Skua Island)	N.K.*	N.K.*	Not Specified	-65°14’45”	-64°16’30”
Arctowski Penin. (Near Cape Anna)	N.K.*	N.K.*	Beacon	-64°35’30”	-62°27’
Arctowski Penin. (B/T Spigot Peak and Hut)	N.K.*	N.K.*	Beacon	-64°38’30”	-62°34’45’’
Ronge Island (Near Ketley Pt.)	N.K.*	N.K.*	Beacon	-64°43’	-62°47’
Duthiers Pt. (On Danco Coast)	N.K.*	N.K.*	Beacon	-64°48’30”	-62°50’
Lemaire Island (Near Molina Pt.)	N.K.*	N.K.*	Beacon	-64°48’45”	-62°52’15”
Small Island West of Weincke Island	N.K.*	N.K.*	Beacon	-64°48’45”	-63°31’31”
Damoy Pt.	N.K.*	N.K.*	Beacon	-64°48’45”	-63°30’45”
Doumer Island	Chile	N.K.*	Beacon	-64°49’50”	-63°34’45”
Argentino Channel (Near Oscar Cove)	N.K.*	N.K.*	Beacon	-64°54’45”	-62°56’
Argentino Channel (Dallmayer Peak arm of Penin.)	N.K.*	N.K.*	Beacon	-64°52’30”	-62°50’30”

*N.K. = unknown.

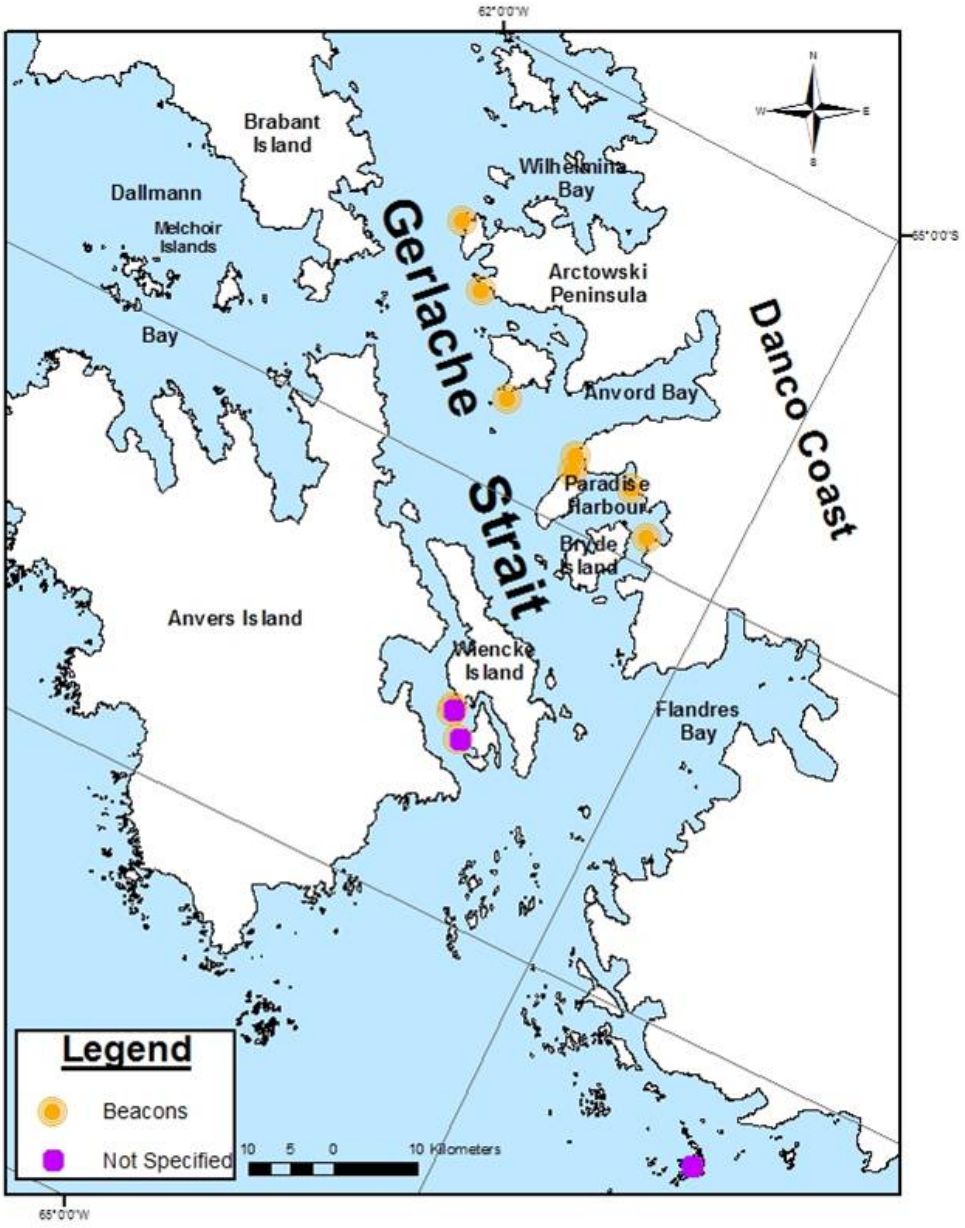

Figure 70 – Location of beacons and structures whose type (base, station, or beacon) is unknown (Not specified).

Figure 71 – Chilean Base opened in 1951 in Paradise Harbour. Photo taken during the NBP 0703 2007 cruise.

Figure 72 – Remains of Danco Islands Station “O” in the Errera Channel. Construction completed on February 26, 1956. Photo taken during the NBP 0703 2007 cruise.

Figure 73 – Argentinean Base, Melchoir, located in Dallman Bay on the Melchoir Islands. Photos taken during the NBP 0703 2007 cruise.

Figure 74 – Argentinean Station, Neko Harbour, located in Andvord Bay. Photo taken during the NBP 0703 2007 cruise.

Figure 75 – USA Base Palmer Station located on the southern tip of Anvers Island. Photo taken during NBP 0703 2007 cruise.

investigation, I found they were not. Thus, no age constrains can be placed on the features using the anthropogenic structures.

A shipwreck was observed on Enterprise Island off the northern coast of Nansen Island in Wilhelmina Bay in the 1980s DEEP FREEZE videos and during the 2007 cruise (Fig. 76). The ship was wrecked off the coast in 1916 (Werner, unknown). Upon further investigation of the video (1980s) and photos (2007) from the NBP 0703 cruise, the wrecked ship was located on a CRASL. The shipwreck occurred in 1916 indicating the CRASL formed prior to 1916.

Aerial Photos

Several aerial photos in the Gerlache Strait were obtained from the BAS. Six photos were taken 4.11 km above sea level during the 1956 -1957 Falkland Islands Dependencies Antarctic Service Expedition (FIDASE) throughout the study area. They include: Arctowski Peninsula (Jan., 1957), Danco Island (Dec., 1956), Paradise Harbour (Jan., 1957), Argentino Channel (Dec., 1956), Argentino Channel (Feb., 1957), and Cape Willems Point (Jan., 1957; Fig. 77). Two photos were also taken from the Arctowski Peninsula and the Errera Channel in 1981 by the Royal Navy. The final two photos were taken near Brabant Island by the BAS in February 2001. However, no aerial photos were available in Neko Harbour and Enterprise Islands. Therefore, video and photos taken during the NBP 0703 2007 were analyzed instead.

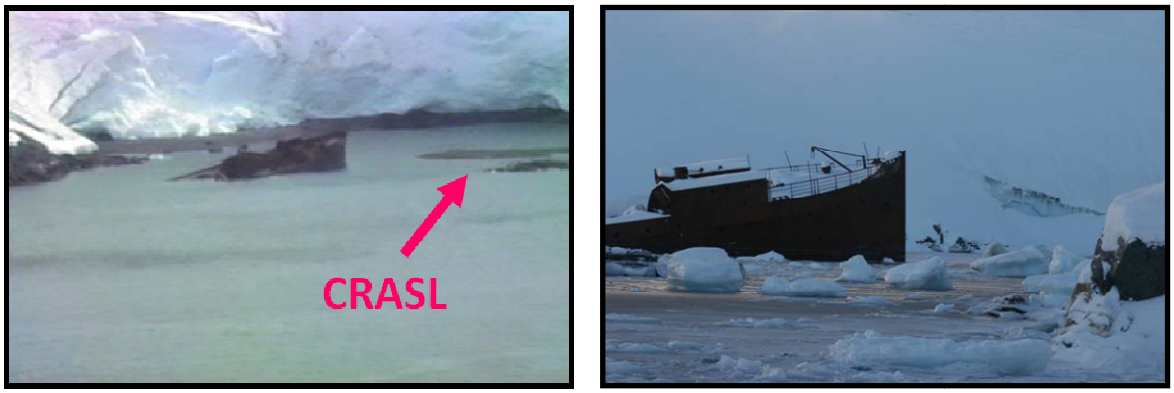

Figure 76 – Left: video of shipwreck on Enterprise Islands, taken during the 1980s DEEP FREEZE cruise. Right: Photo of same shipwreck, taken during the NBP 0703 2007 cruise.

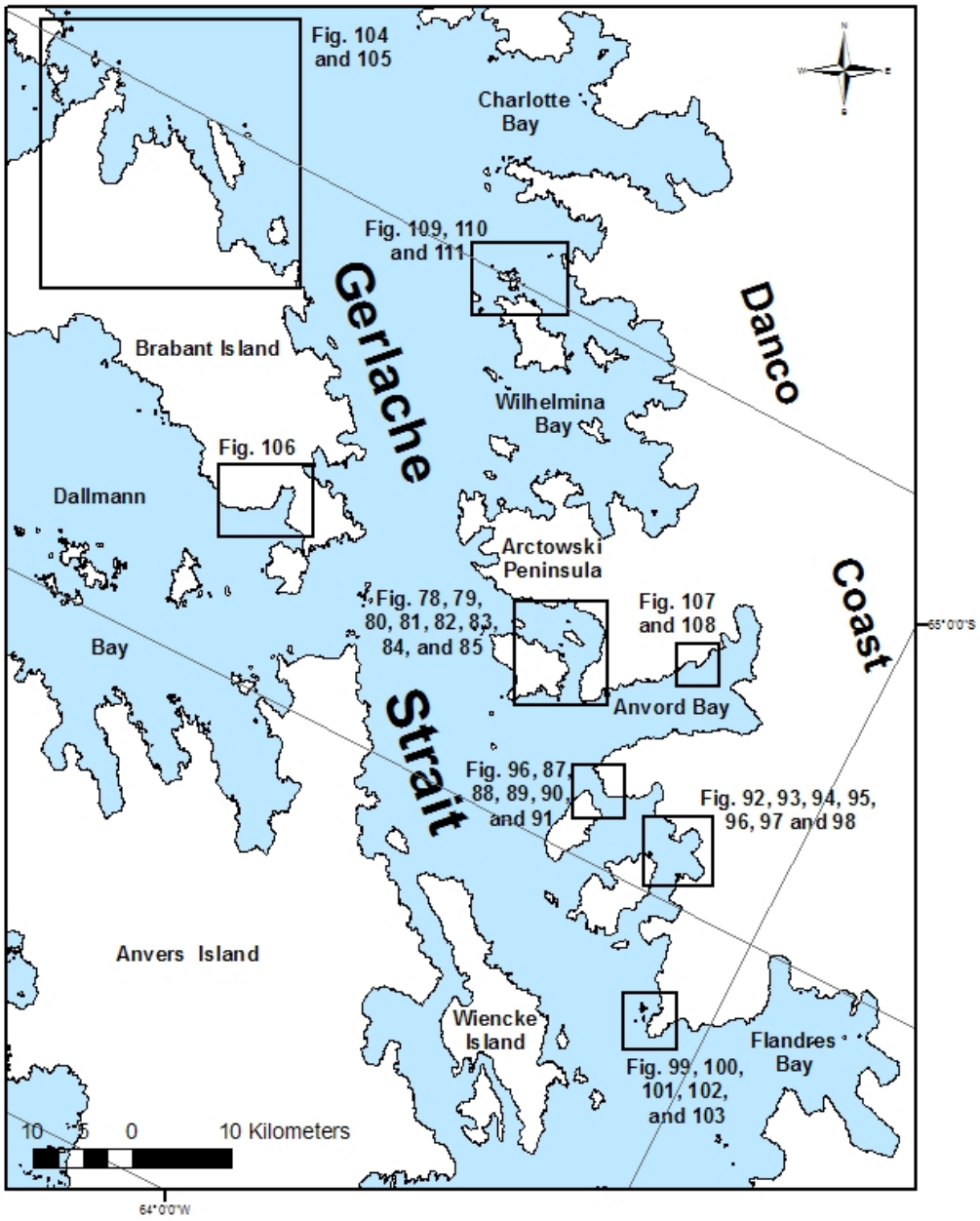

Figure 77 – Location of aerial photos, video images from 1980s DEEP FREEZE cruise, and photos from NBP 2007 cruise.

The similarities and differences between the aerial photos, the 1980s DEEP FREEZE cruise videos, and photos taken from the *Nathaniel B. Palmer* (NBP 0703) 2007 cruise, were examined in order to identify changes throughout the area over the last fifty years.

Errera Channel

The first aerial photos analyzed were located in the Errera Channel west of Arctowski Peninsula (Jan., 1957 and 1981; Figs. 78 and 79), Danco Island (Dec., 1956; Fig. 80), and Errera Channel (1981; Fig. 81). When comparing the Arctowski Peninsula aerial photos from 1956 to 1981, the same CRASL is observed (Figs 78 and 79). Between 1956 and 1981 the CRASL did not noticeably change. The CRASLs located along the Arctowski Peninsula appear to be of a smaller scale in 1981 than the one observed in the aerial photo in 1957and thus are not believed to be the same CRASL.

In the aerial photo of Danco Island (1956) three CRASLs were identified: one off the southeastern coast of Ronge Island and two off the coast of Arctowski Peninsula (Fig. 81). According to BAS data of Danco Island, Station O was built in February 1956 on the northern tip of the island; however Station O was not identified in either of the aerial photos of the island and thus the general area of its location is indicated by arrows in the photos (Fig. 80 and Fig. 81). However, the structure provides no constraint on the age of the features because it is not located on a CRASL and thus, its significance is limited.

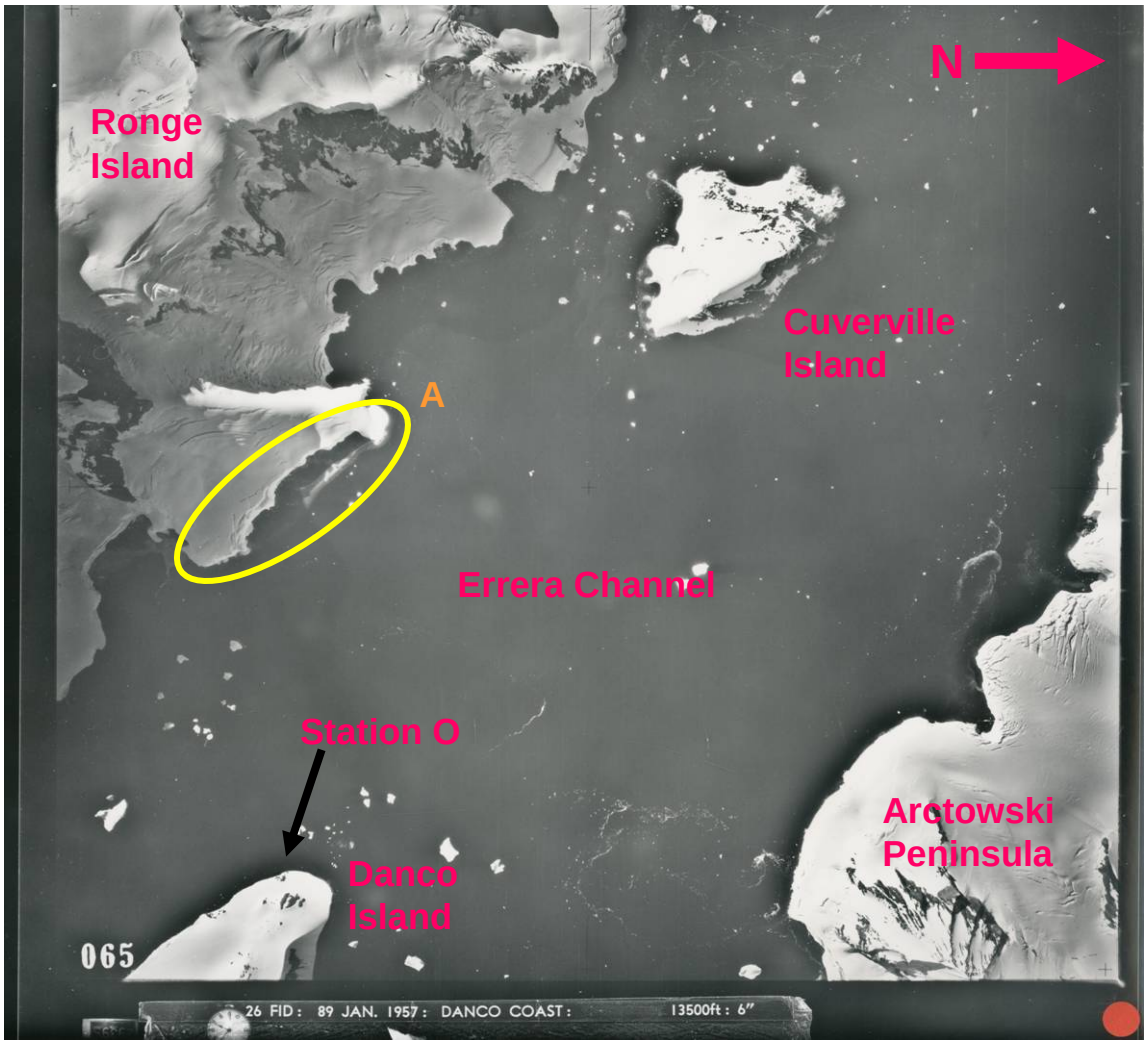

Figure 78 – Aerial photo taken west of the Arctowski Peninsula in January of 1957. The CRASL is indicated by the yellow oval. The general location of Station O is indicated by the arrow. (Courtesy BAS, 2008). See Figure 77 for location.

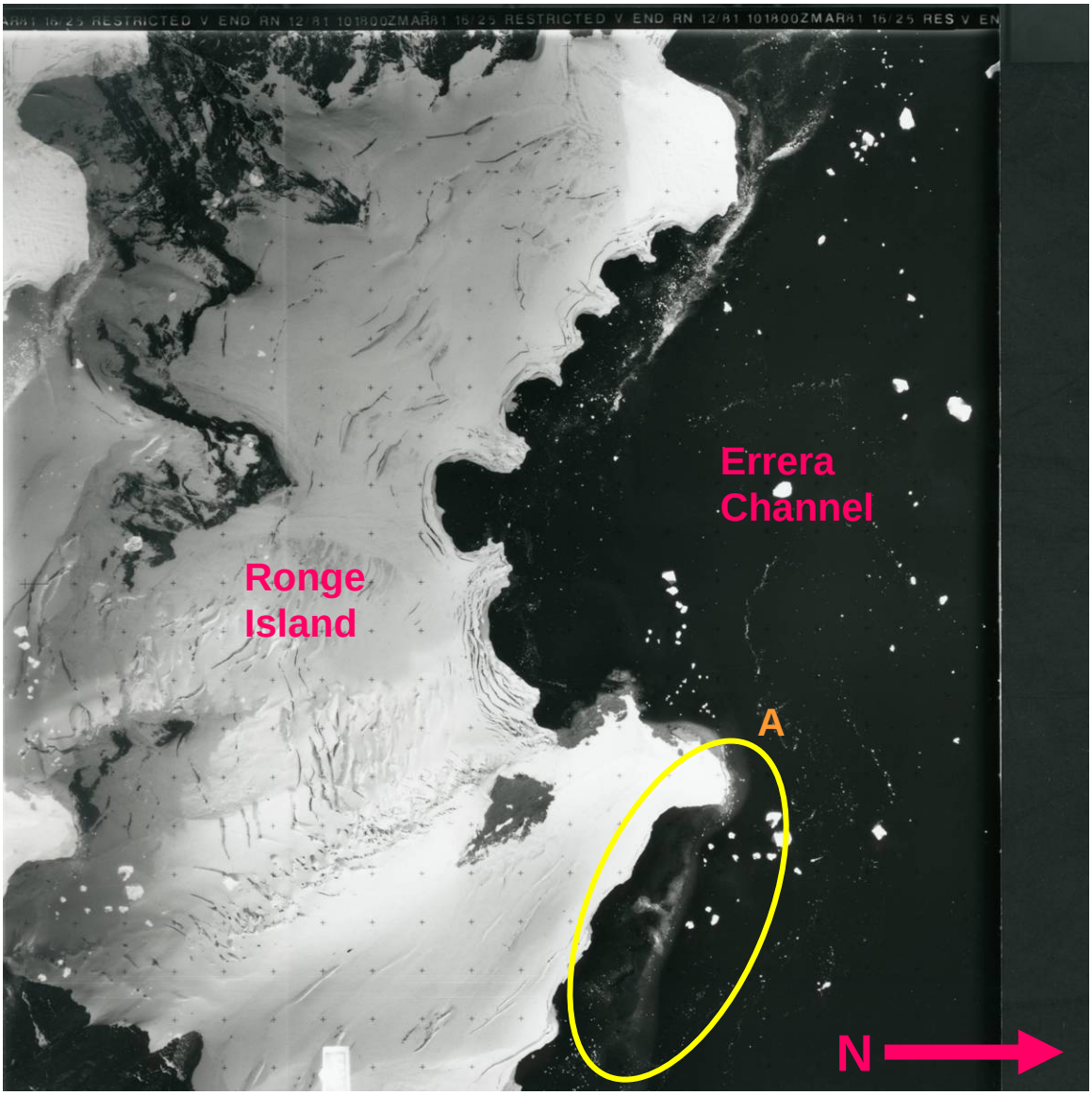

Figure 79 – Aerial photo taken off the coast of Ronge Island in 1981. The CRASLs is indicated by the yellow oval. (Courtesy BAS, 2008). Notice that it does not appear to have changed since 1957 (Fig. 78). See Figure 77 for location.

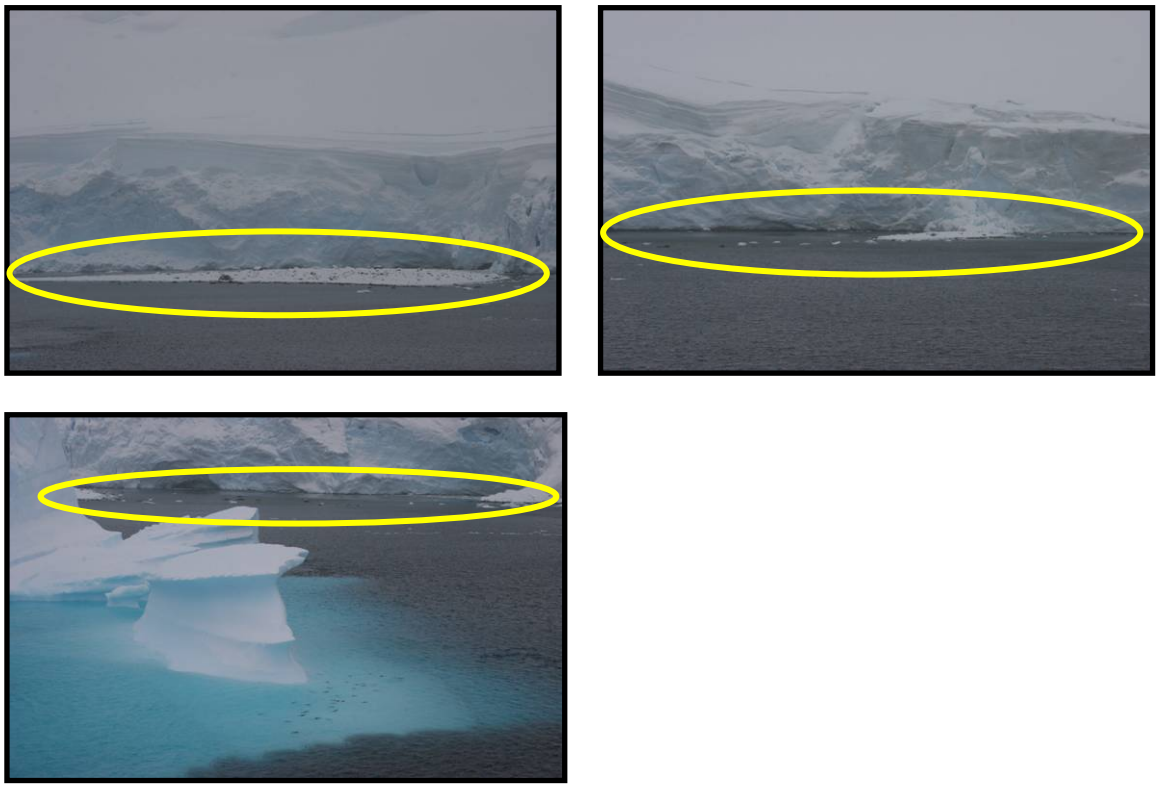

Figure 80 – Photos taken off the coast of Ronge Island during the NBP 0703 cruise. Exact location is not known. CRASLs were indicated by the yellow ovals. See Figure 77 for location.

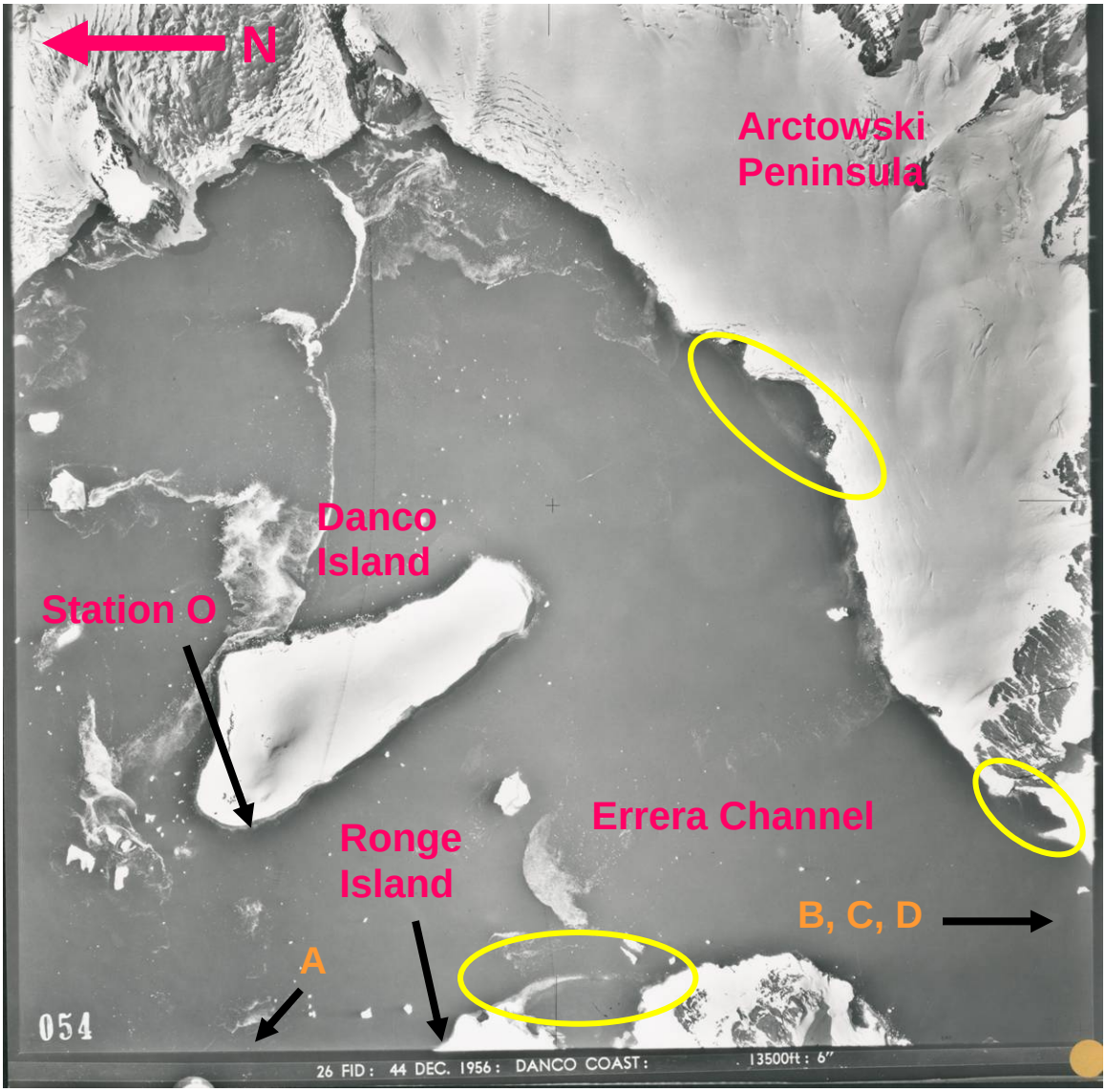

Figure 81 – Aerial photo taken off the Arctowski Peninsula during December of 1956. Three CRASLs were identified in this photo, indicated by the yellow ovals. The general location of Station O is indicated by the arrow. (Courtesy BAS, 2008). See Figure 77 for location.

Investigation of the Errera Channel (1981) aerial photo yields yet another CRASL off the coast of Arctowski Peninsula (Fig. 82). When comparing the Errera Channel (1981) photo with a photo taken from the NBP 0703 cruise in the area (Fig. 83) it is difficult to be sure that no changes have occurred in the area due to the different angles of the images and thus no conclusions can be drawn. Nearing the exit of the Errera Channel, near Andvord Bay, more CRASLs as well as a talus deposit and moraine were identified during the NBP 0703 cruise (Figs. 84 and 85). This is the location of some of the samples for the sedimentary characterization study.

Paradise Harbour

The second aerial photo analyzed was located near Paradise Harbour (Jan., 1957; Fig. 86). From this photo three CRASLs were identified: two east of Lemaire Island and another west of Danco Coast. Four areas within this photo were compared to video from the 1980s DEEP FREEZE cruise as well as photos from the NBP 0703 cruise. Comparing the aerial photo (1957) to the video images (1980s) of Duthiers Point (Fig. 87) reveals little to no change at the coastline. However, when the aerial photo (1957; Fig. 86) was compared to the video (1980s; Fig. 88) an additional CRASL was identified that was not seen in the aerial photo, suggesting that it formed sometime between 1957 and 1980.

In the 1957 aerial photo (Fig. 86) a small stretch of land above sea-level can be seen west of the Danco Coast. A Chilean Base is also observed west of Danco Island on a small stretch of land above sea level in the video (1980s; Fig. 89). According to the

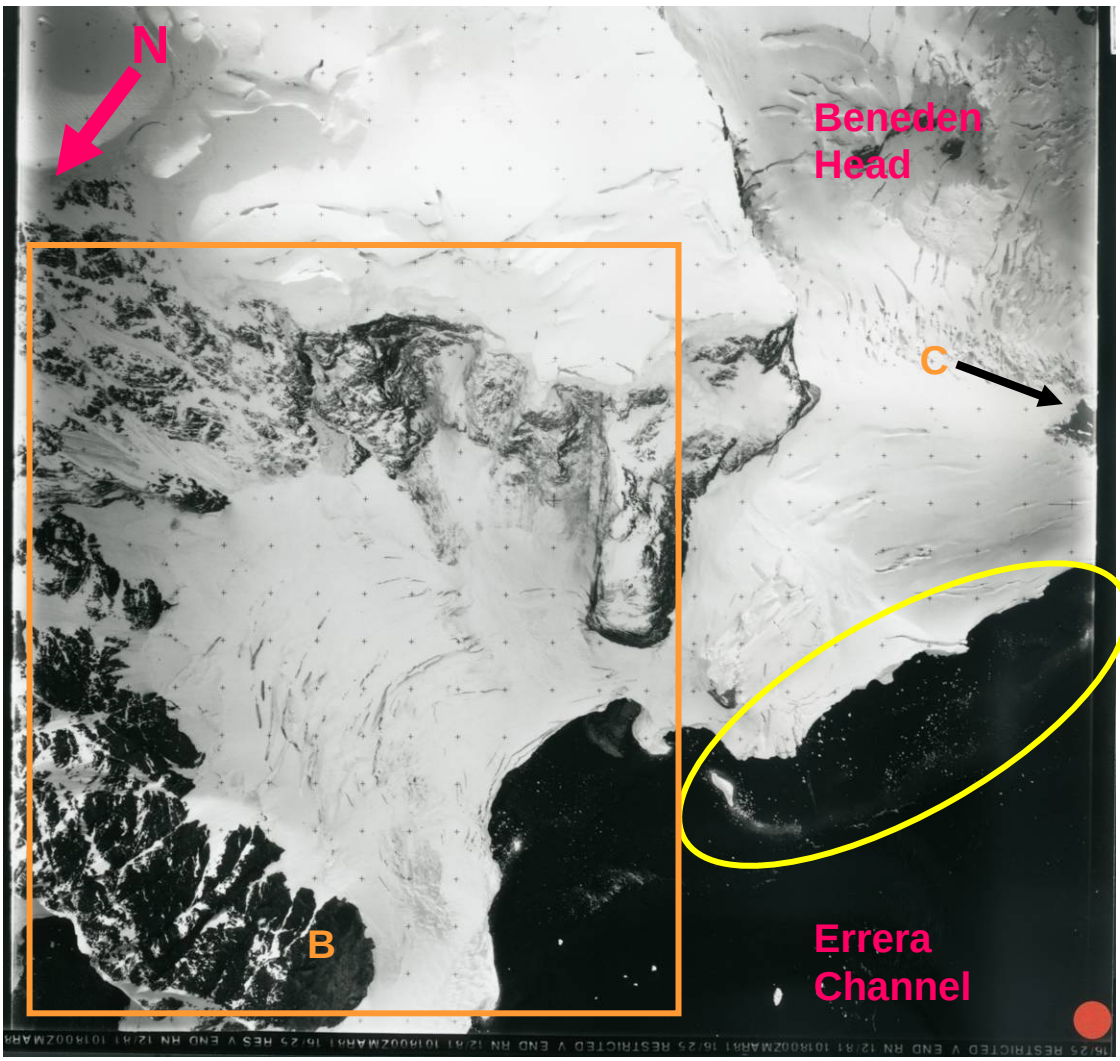

Figure 82 – Aerial photo taken off the coast of Arctowski Peninsula in 1981. The arrow labeled C indicates the general location of the C' photo. CRASL indicated by yellow oval. (Courtesy BAS, 2008). See Figure 77 for location.

Figure 83 – Photo taken during the NBP 0703 cruise in the Errera Channel. B corresponds to B', it is difficult to see if the coastline has changed due to the angle of this photo. See Figure 77 for location.

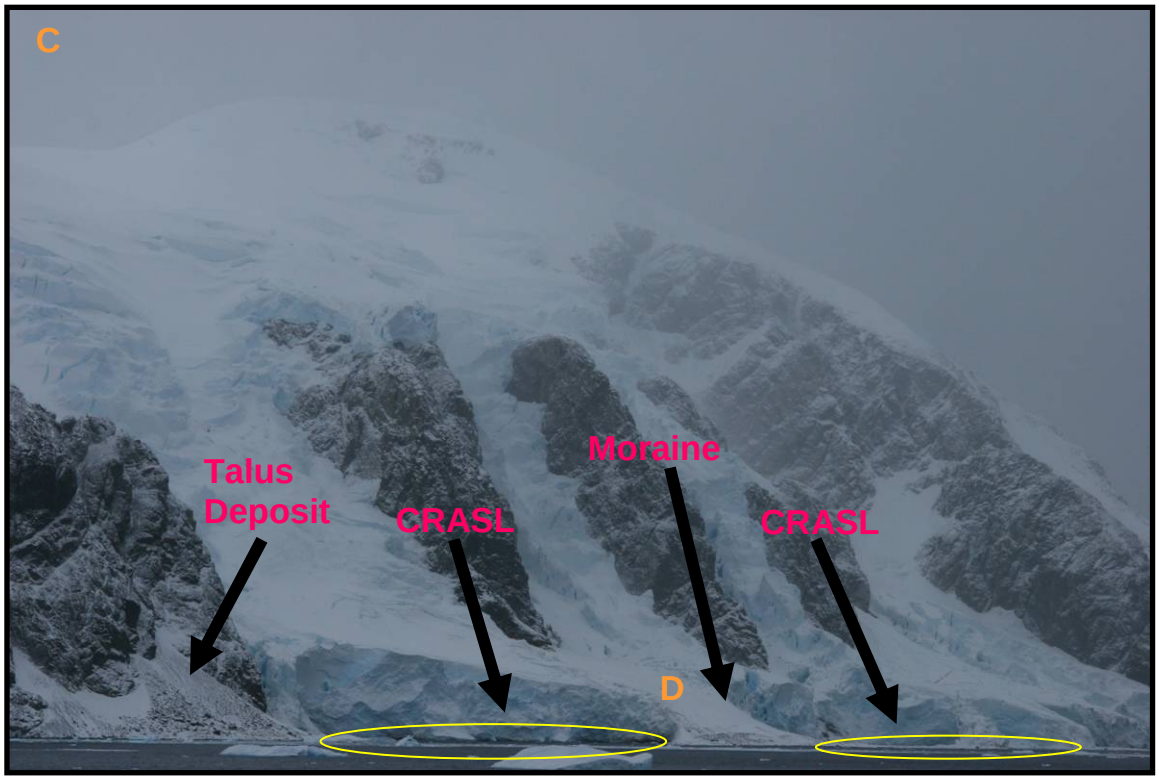

Figure 84 – Photo taken while nearing the exit of the Errera Channel during NBP 0703 cruise. The CRASLs are indicated by the yellow ovals. See Figure 77 for location.

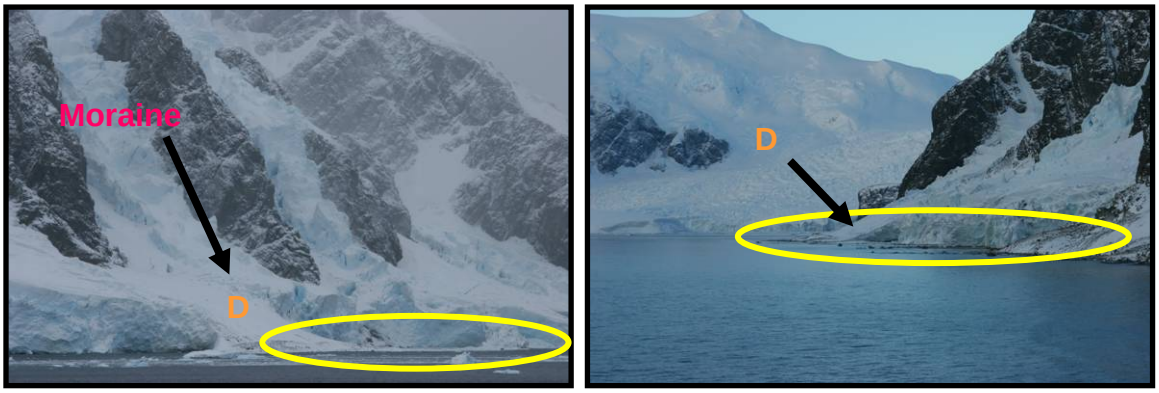

Figure 85 – Photos also taken near the exit of the Errera Channel. D indicates point of reference for the photos. CRASLs are indicated by yellow ovals. See Figure 77 for location.

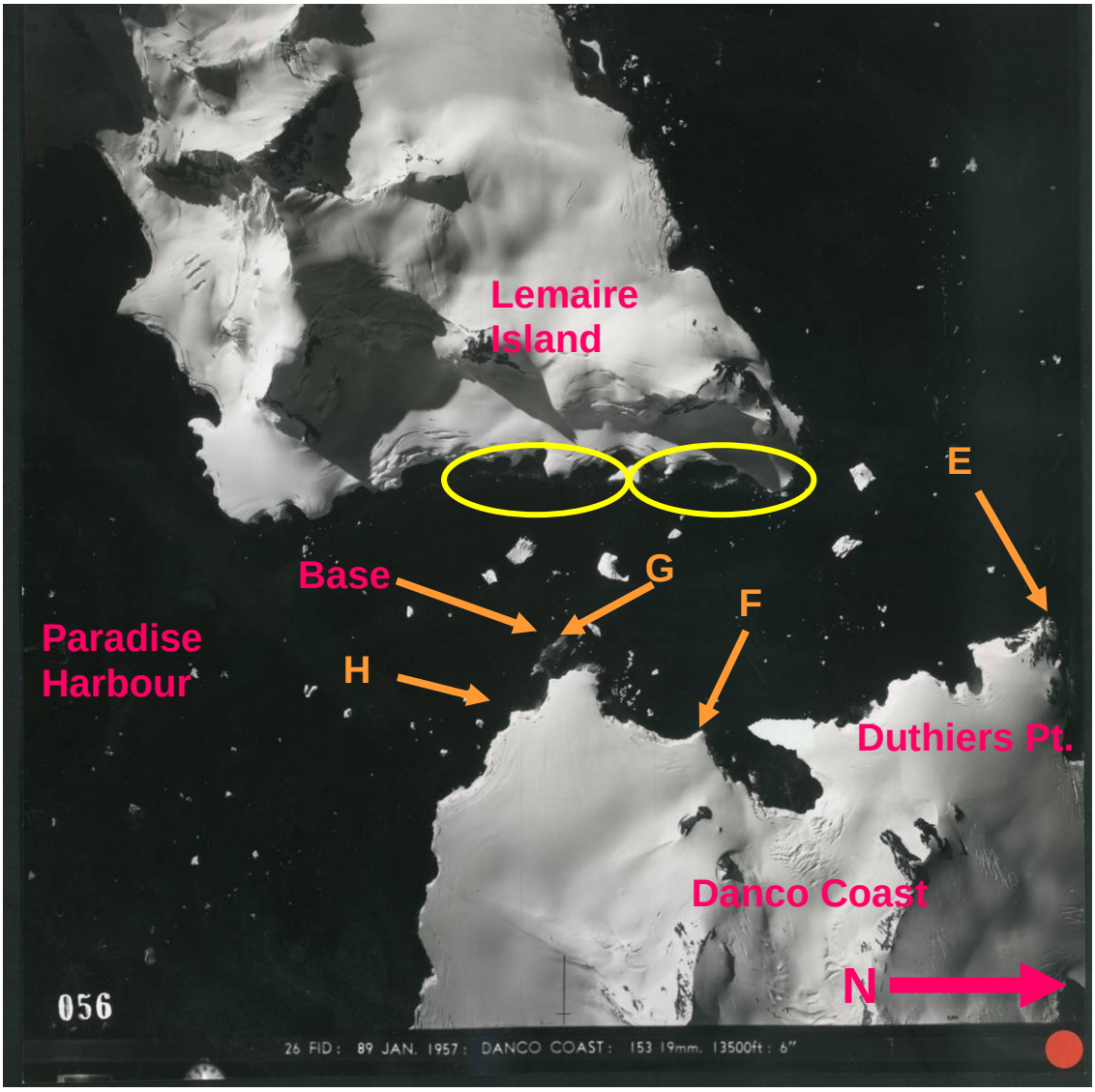

Figure 86 – Aerial photo near Paradise Harbour taken in January 1957. Two CRASLs can be identified off of Lemaire Island, indicated by the yellow ovals. Chilean Base station general location indicated by arrow. (Courtesy BAS, 2008). E, F, G, and H are points of references for other photos. See Figure 77 for location.

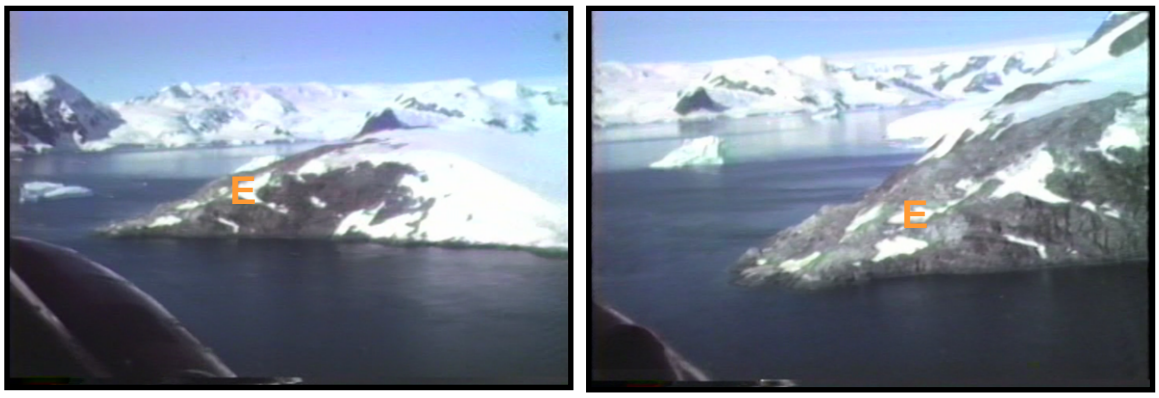

Figure 87 – Video images of Duthiers Point taken during the 1980s DEEP FREEZE cruise. Notice that by comparing this photo to the aerial photo (Fig. 86) little to no change has occurred. E indicates a point of reference. See Figure 77 for location.

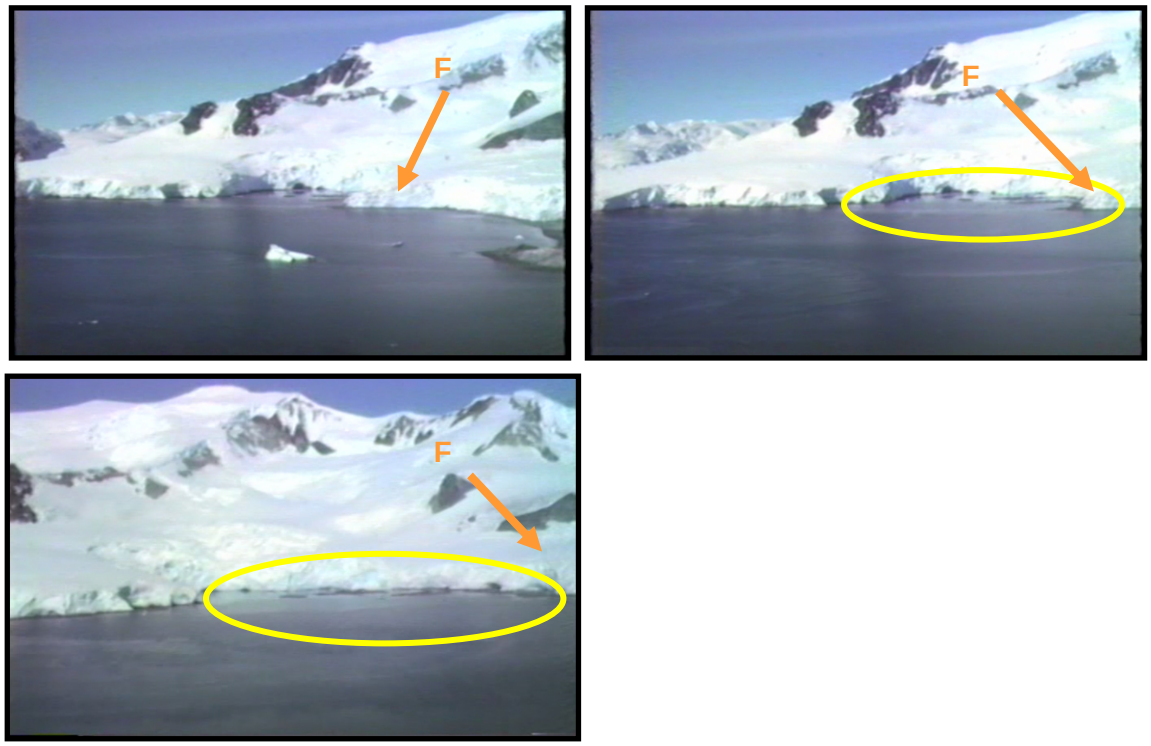

Figure 88 – Video images taken during the 1980s DEEP FREEZE cruise. F indicates a point of reference. Notice that in the aerial photo (Fig. 86) no CRASLs are present, however in these images the CRASLs can be identified. CRASLs are indicated by the yellow ovals. See Figs. 77 and 86 for location.

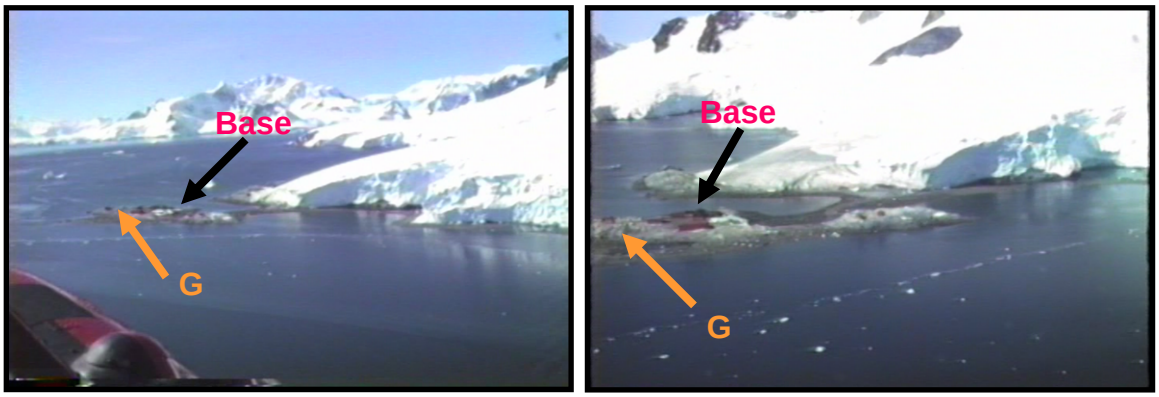

Figure 89 – Video images taken during the 1980s DEEP FREEZE cruise. G indicates a point of reference. See Figs. 77 and 86 for location.

Chileans, it was built in 1951. However, the base cannot be seen in the 1957 aerial photo and only the general location of the base is indicated in the aerial photo. The Chilean Base was also seen during the NBP 0703 cruise (Fig. 90). By comparing all three photos of the Chilean Base and its surrounding area little to no changes were observed along the coastline. The only exception is the appearance of a CRASL in the 1980s DEEP FREEZE video (Fig. 91) not present in the 1957 aerial photo, suggesting that the CRASL formed sometime between 1957 and the 1980s. However, it is important to note that it is possible the CRASL is not large enough to be seen in the aerial photo.

Argentino Channel

The third set of aerial photos analyzed were located near Skontorp Cove, Argentino Channel in December of 1956 (Fig. 92) and in the Argentino Channel in February of 1957 (Fig. 93). From these photos three areas of CRASLs were identified, one off the eastern tip of Bryde Island, and two off the Danco Coast. Four areas within these photos were compared to video from the 1980s DEEP FREEZE cruise as well as photos from the NBP 0703 cruise. By comparing the aerial photo from 1956 (Fig. 92) to the 1980s video (Fig. 93) several observations can be made. First, unlike the aerial photo, an Argentinean Base can be seen located just off Danco Coast in the 1980s video (Fig. 93). However, in both the 1957 aerial photo (Fig. 92) and the 1980s video (Fig. 93) CRASLs behind the base were identified. A well defined moraine just to the north of the tip of the coast was also identified. In the video (Fig. 93) it appears that the moraine back-stepped leaving two well defined ridges separated by water. The seaward

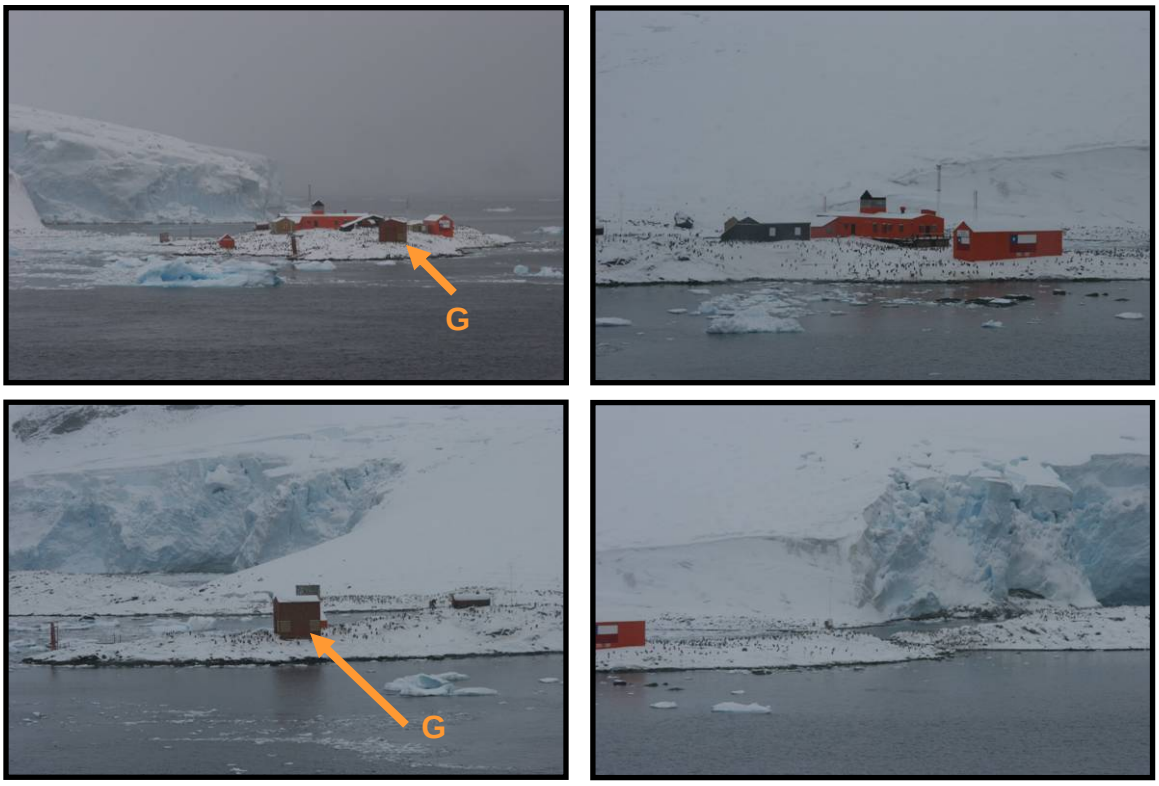

Figure 90 – Photos taken during the NBP 0703 cruise of the Chilean Base. Photos were taken while approaching the base. See Figs. 77 and 86 for location.

Figure 91 – Video taken during the 1980s DEEP FREEZE cruise. This CRASL is not seen in Figure 86 most likely because it is too small. See Figure 77 for location.

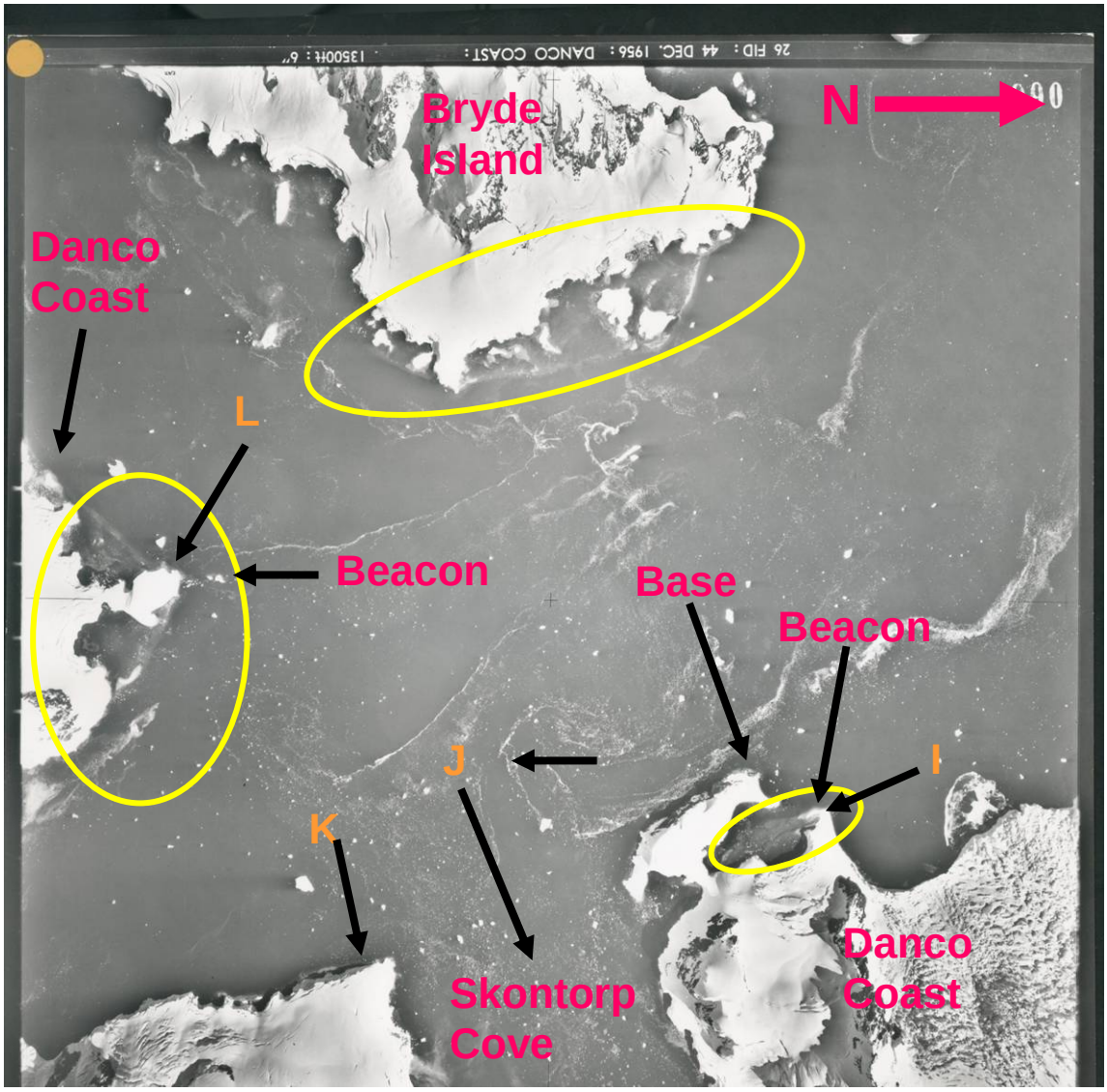

Figure 92 – Aerial photo in Argentino Channel taken in December 1956. Three CRASLs can be identified, one east of Bryde Island, and two west of Danco Coast, indicated by the yellow ovals. I, J, K, and L indicate points of reference. Argentinean Base station general location indicated by arrow. (Courtesy BAS, 2008). See Figure 77 for location.

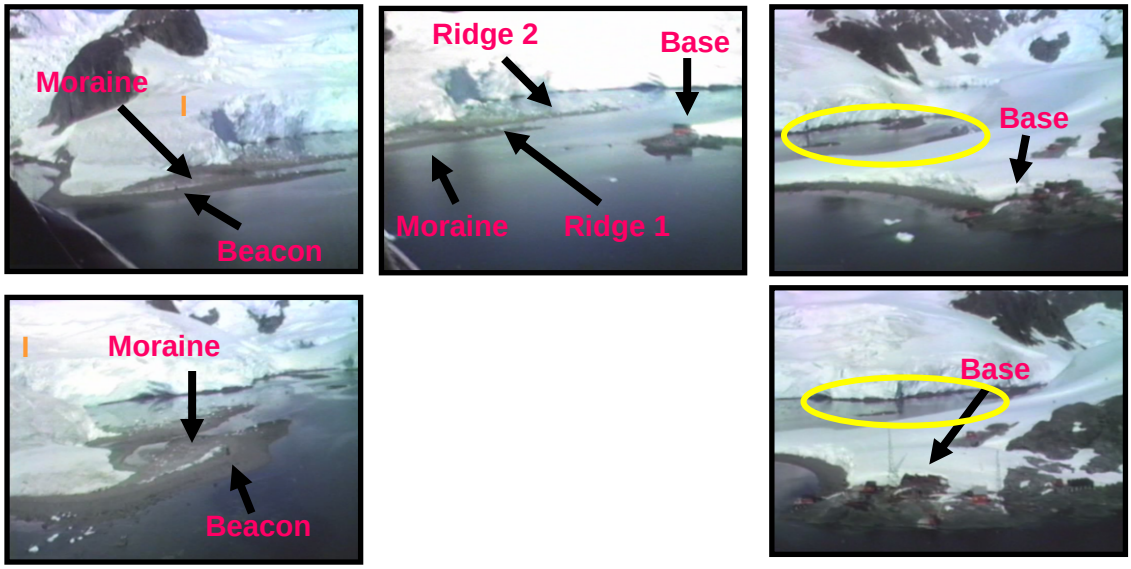

Figure 93 - Video of Argentino Channel taken during the 1980s. Notice the CRASLs, indicated by yellow ovals. See Figs. 77 and 92 for location.

ridge containing a beacon belonging to the Argentineans. Interestingly, the CRASLs appear very close to the moraines both in the aerial photo and the video. Also, in the aerial photo the CRASLs appear more prominent. When comparing the 1980s video images to photos taken during the NBP 0703 cruise (Fig. 94), the moraine does not appear to have changed. However the ice directly behind the moraine and the CRASLs does appear to have changed in height and length. However, this could not be quantified. Likewise the CRASLs do not appear to be as well defined as they are in both the aerial photo (1956) and the video (1980s) suggesting that in the last 26 years this area has undergone a reduction in the size of the CRASL deposits and ice cliffs. However, it is important to note that due to the different angles the images were taken and the lack of a scale, it is difficult to quantify these apparent changes.

A comparison between the 1957 aerial photo (Fig. 95) and 1980s video images (Fig. 96) also indicates some changes. In the 1957 aerial photo no obvious CRASLs can be seen in Skontorp Cove. However several CRASLs were observed in the 1980s videos (Fig. 96). This suggests that several CRASLs developed in Skontorp Cove between 1957 and the 1980s. However, the resolution of the photos and the scale of the features leave uncertainty in this interpretation.

On the western side of Skontorp Cove near the prominent tip, a well defined CRASL was observed in 1980s video images (Fig. 97). Unfortunately, due to the angles of both of the aerial photos (1956 and 1957; Figs. 92 and 95) the presence of a CRASL cannot be determined. In both the 1956 aerial photo (Fig. 92) and the 1980s video (Fig. 98) the CRASLs on the eastern and western side of the arrow-shaped point were very

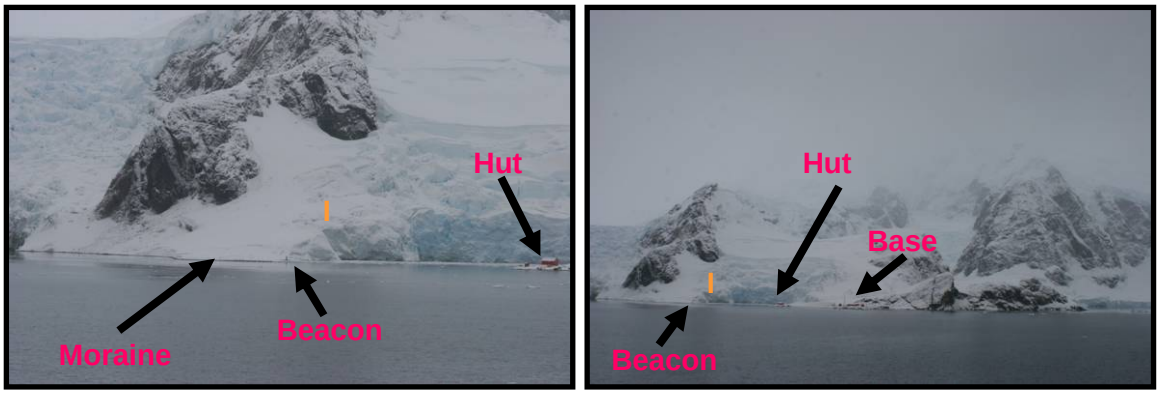

Figure 94 - Photos taken during NBP 0703 cruise 2007. See Figs. 77 and 92 for location.

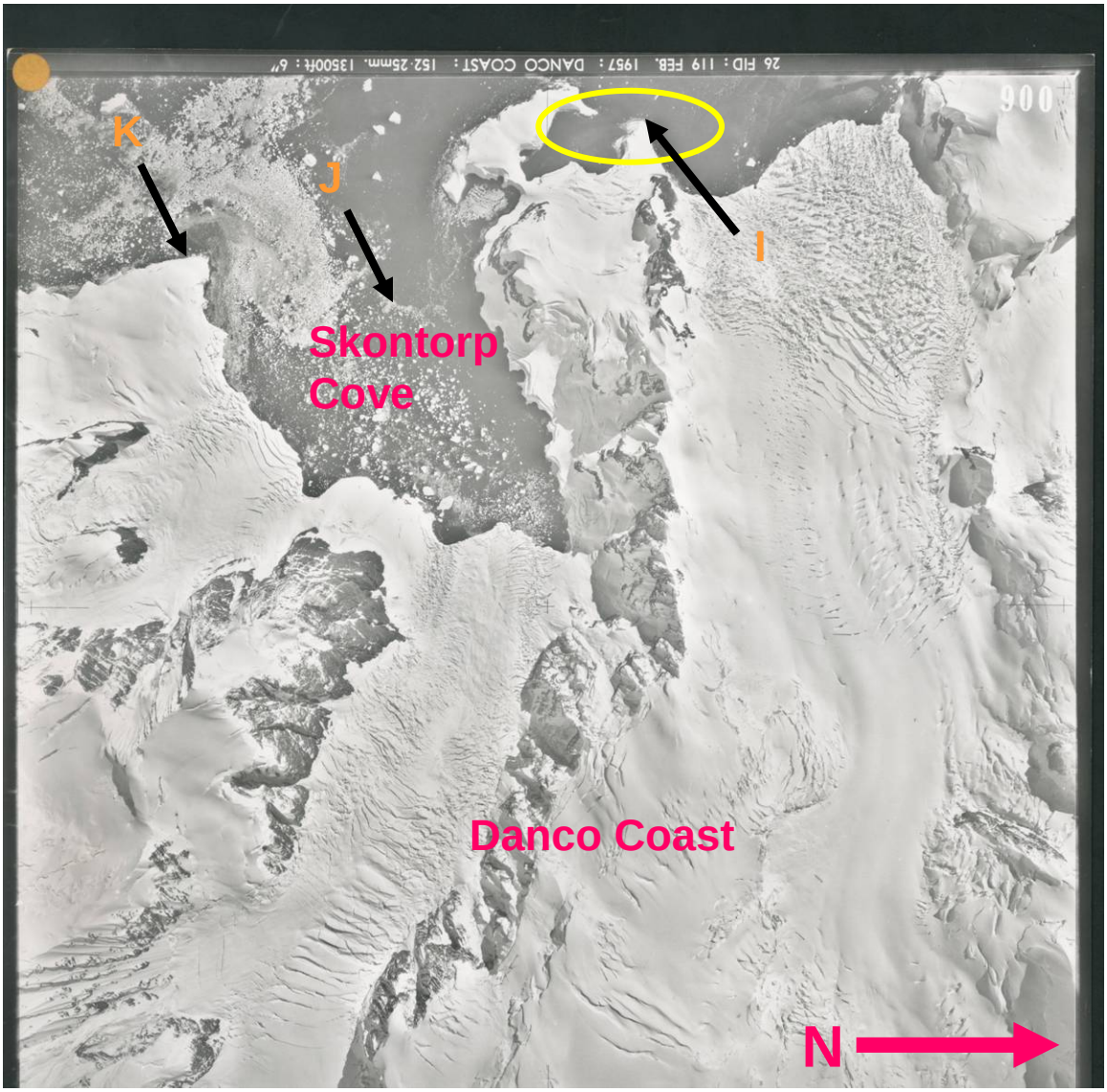

Figure 95 - Aerial photo of Argentino Channel taken during February 1957. The CRASLs near the Argentinean Base are indicated by the yellow oval. (Courtesy BAS, 2008). See Figure 77 for location.

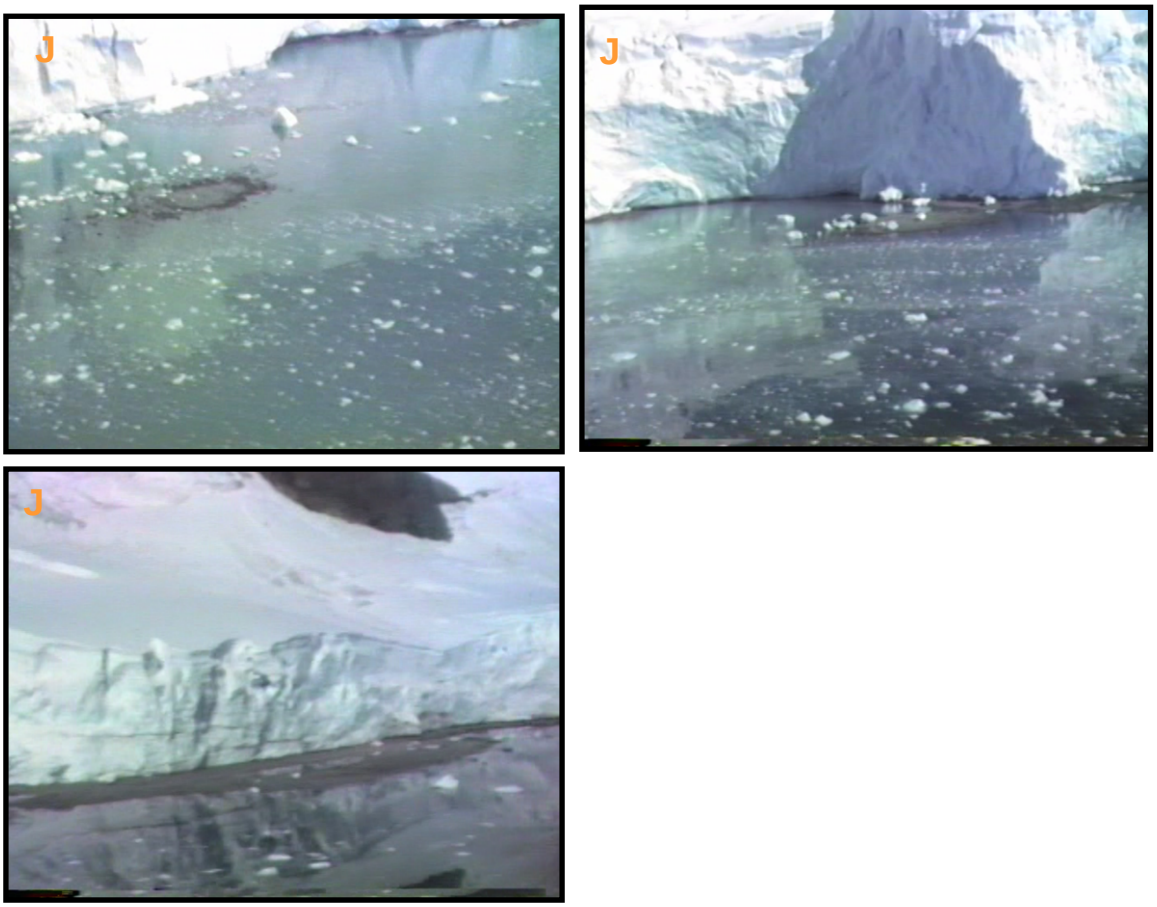

Figure 96 – Video of Skontorp Cove taken during the 1980s DEEP FREEZE cruise. In a three photos CRASLs are present. However, their exact location in Skontorp Cove is not known. See Figs. 77, 92 and 95 for location.

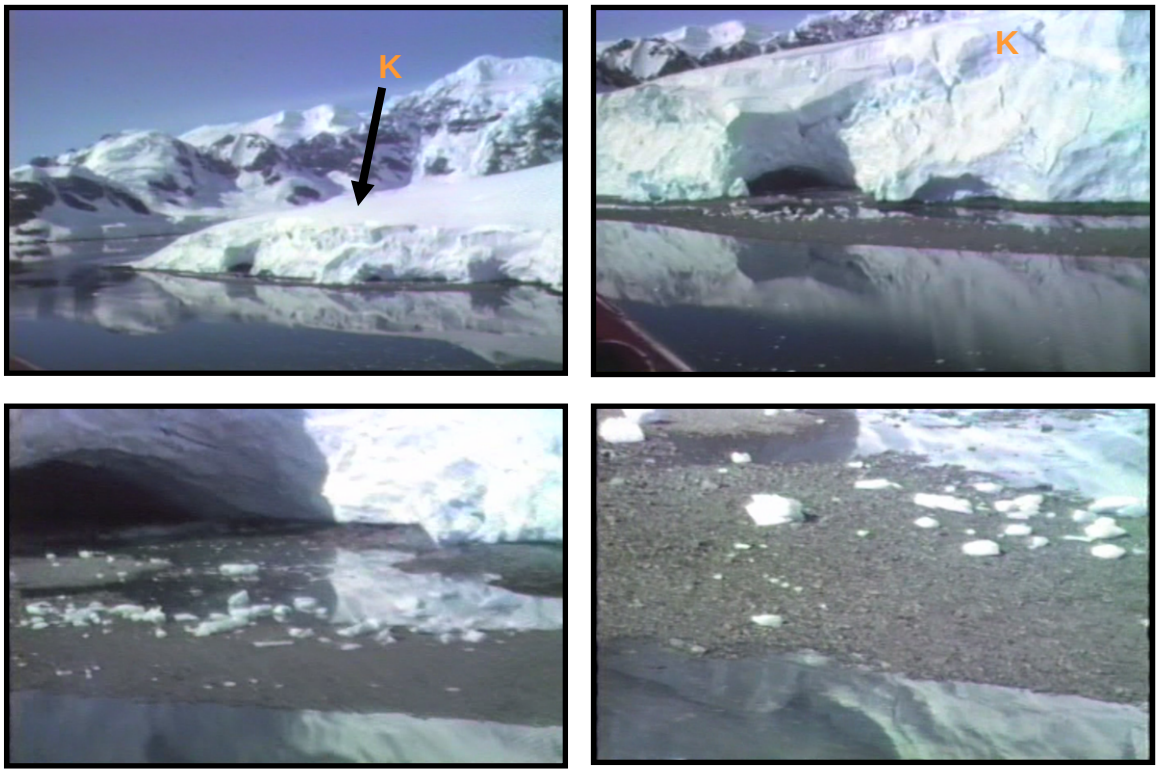

Figure 97 – Video of western Skontorp Cove taken during the 1980s DEEP FREEZE cruise. Note: the bottom two photos are closer views of the sediments of the top two photos. See Figures 77, 92 and 95 for location.

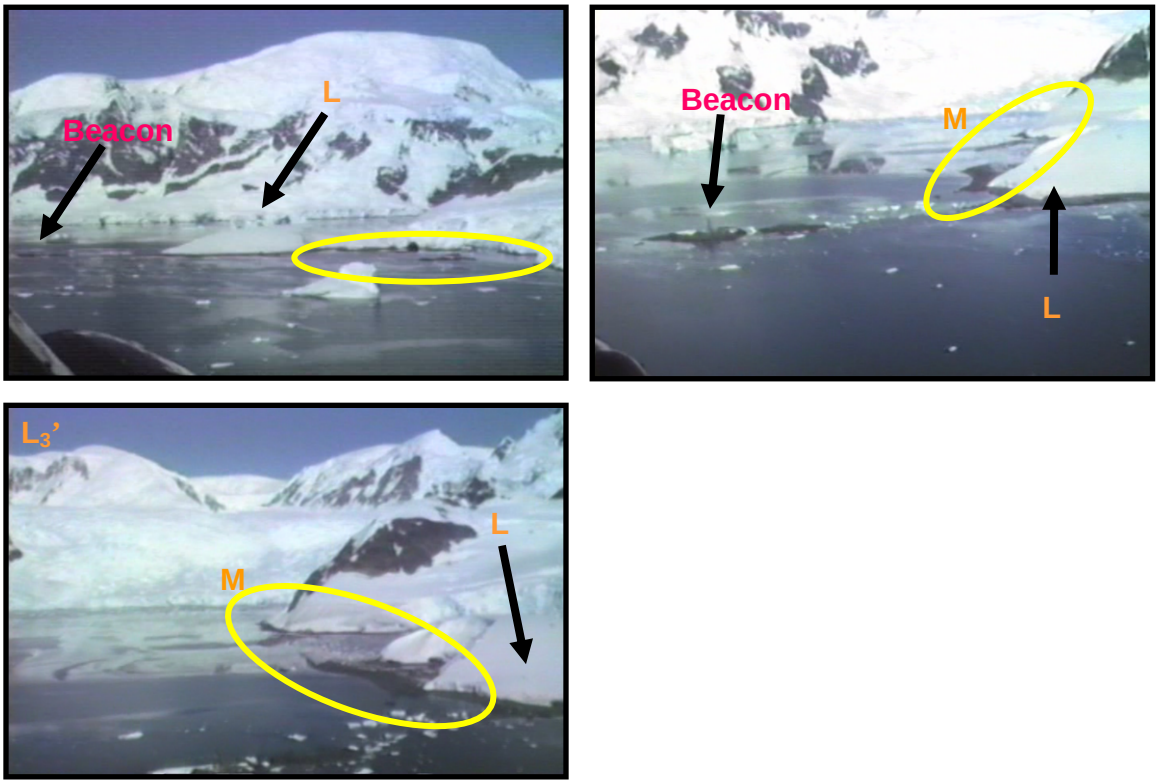

Figure 98 - Video of western Argentino Channel taken during the 1980s DEEP FREEZE cruise. The CRASLs are indicated in the images by the yellow ovals. Notice that the CRASL in circled and labeled M is the same as just at a different angle. See Figures 77, 92, and 95 for location.

prominent. Suggesting that little to no changes have occurred in this area from 1956 to the 1980s.

Cape Willems Point, Flandres Bay

The fourth set of aerial photos analyzed were located in Flandres Bay, Cape Willems Point taken in January of 1957 (Fig. 99). From these photos four CRASLs can be identified west of the Danco Coast. Two areas within these photos were compared to video from the 1980s DEEP FREEZE cruise and photos from the NBP 0703 cruise. By comparing the 1957 aerial photo (Fig. 99) to the 1980s video (Fig. 100) the area seems to have undergone little to no changes. In both, a very prominent CRASL is present, with similar orientation and shape, suggesting that the CRASL is the same and has not undergone changes. However, when comparing the 1957 aerial photo (Fig. 99) to the 1980s video of another CRASL in this area (Fig. 101) the results are different. This comparison yields a more developed CRASL in the 1980s videos (Fig. 101); suggesting that the CRASL did change between 1957 and the 1980s.

At the tip of Cape Willems Point another CRASL was identified in the video (1980s; Fig. 102) and in the NBP 0703 cruise (Fig. 103). Analysis of both photos indicates that the CRASL seems to be not as prominent in the NBP 0703 photo as it was in the 1980s videos, however this could be due to the angle or the tide at which the 2007 photo was taken. Likewise, the ice cliff behind the CRASL, at the tip of the cape, seems to have diminished in height and shape, suggesting that this area has undergone changes in the last 26 years.

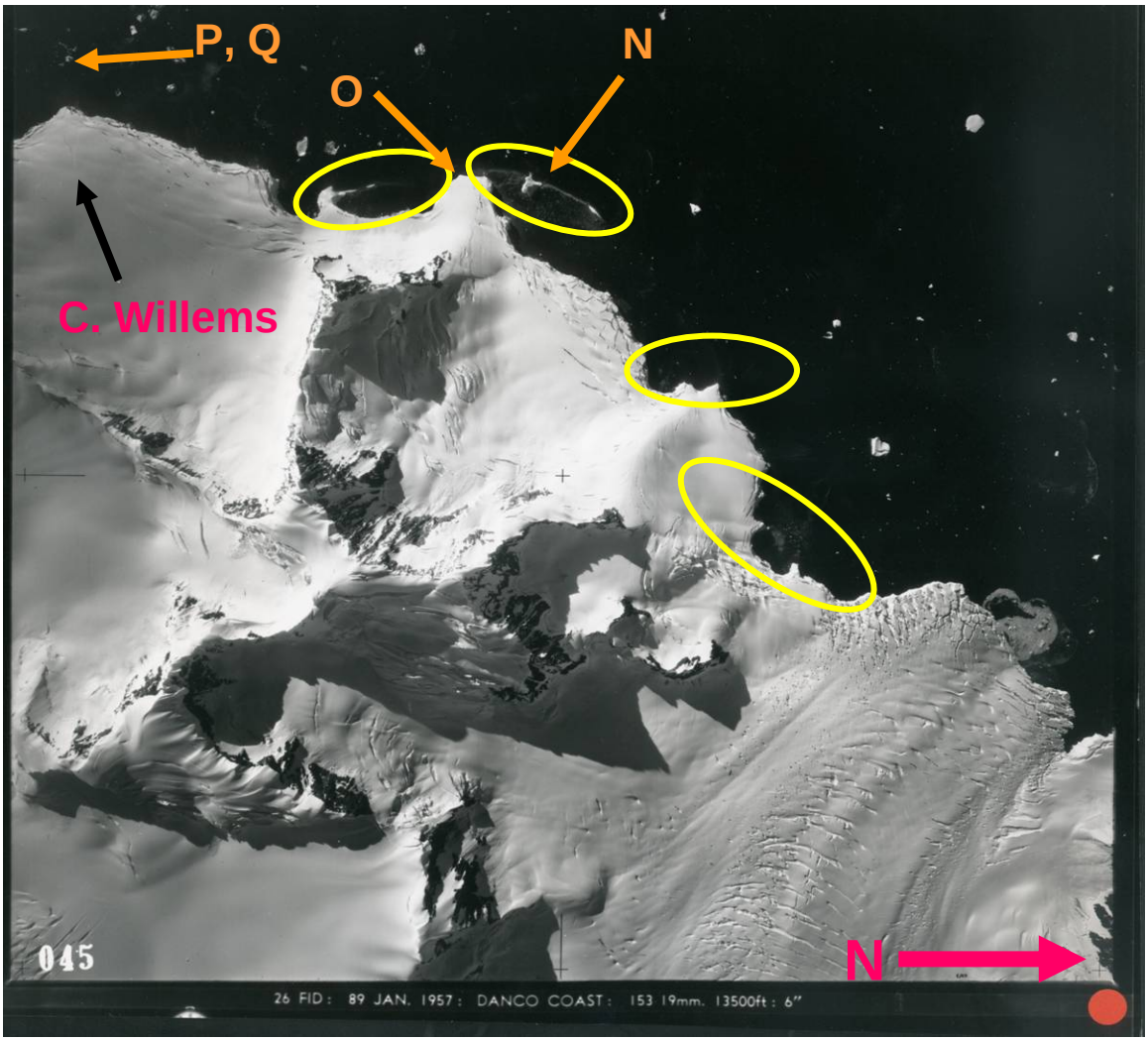

Figure 99 - Aerial photo of Cape Willems Point taken during January 1957. Four CRASLs are present in this photo, indicated by the yellow ovals. N, O and P are points of references. (Courtesy BAS, 2008). See Figure 77 for location.

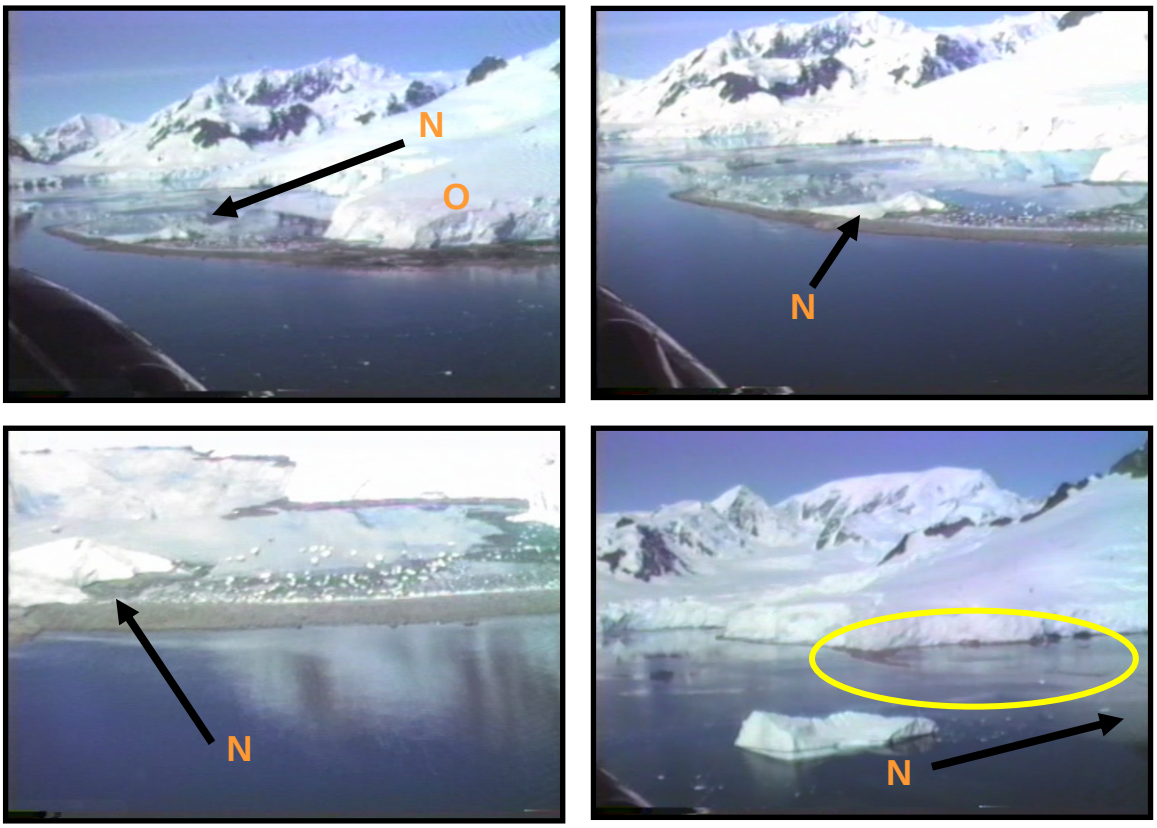

Figure 100 – Video of Cape Willems Point taken during the 1980s DEEP FREEZE cruise. See Figs. 77 and 99 for location.

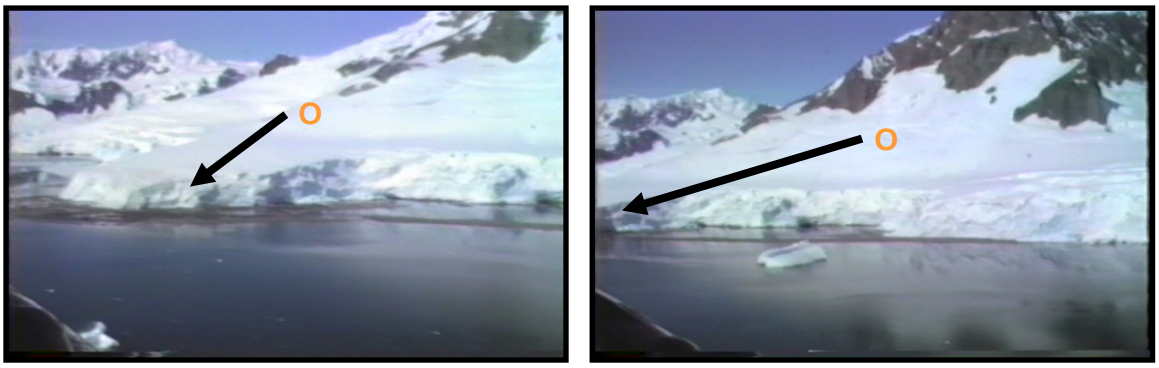

Figure 101 - Video of another CRASL just west of Cape Willems Point, taken during the 1980s DEEP FREEZE cruise. See Figure 77 and 99 for location.

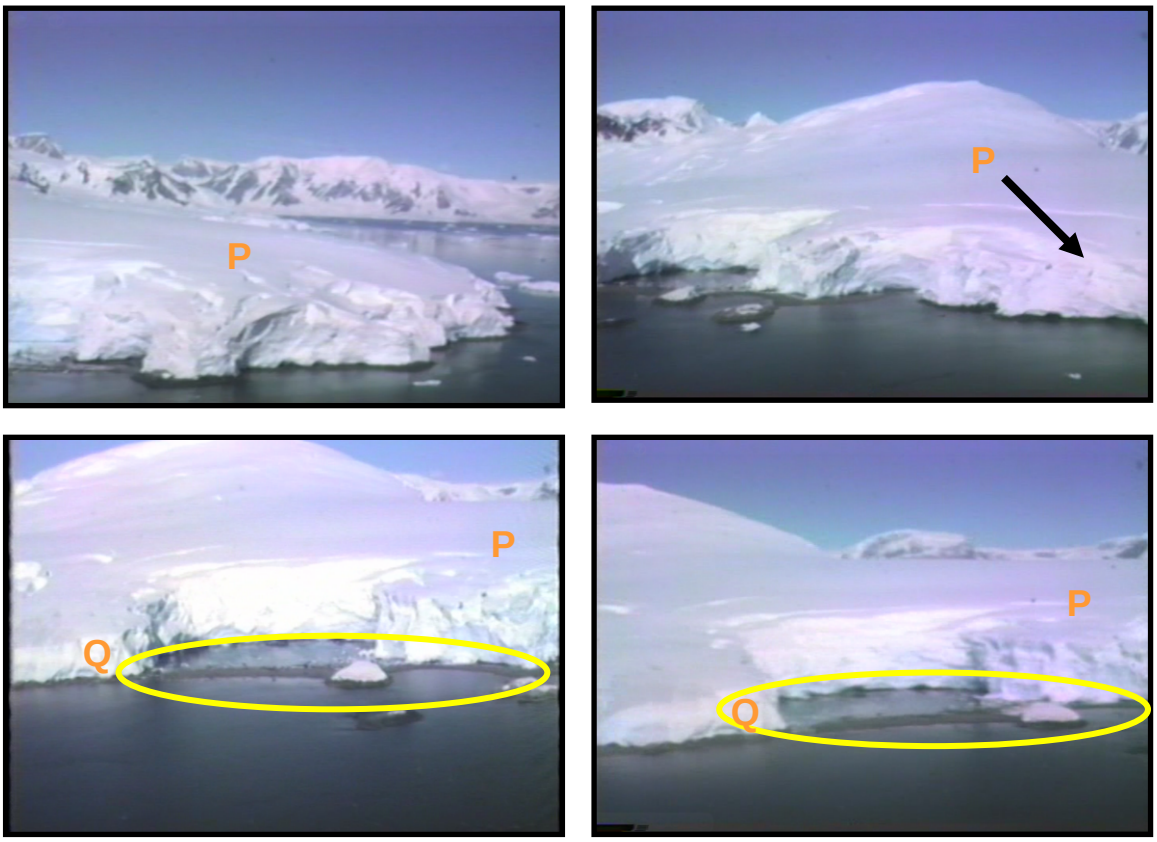

Figure 102 - Video of tip of Cape Willems Point taken during the 1980s DEEP FREEZE cruise. See Figure 77 and 99 for location.

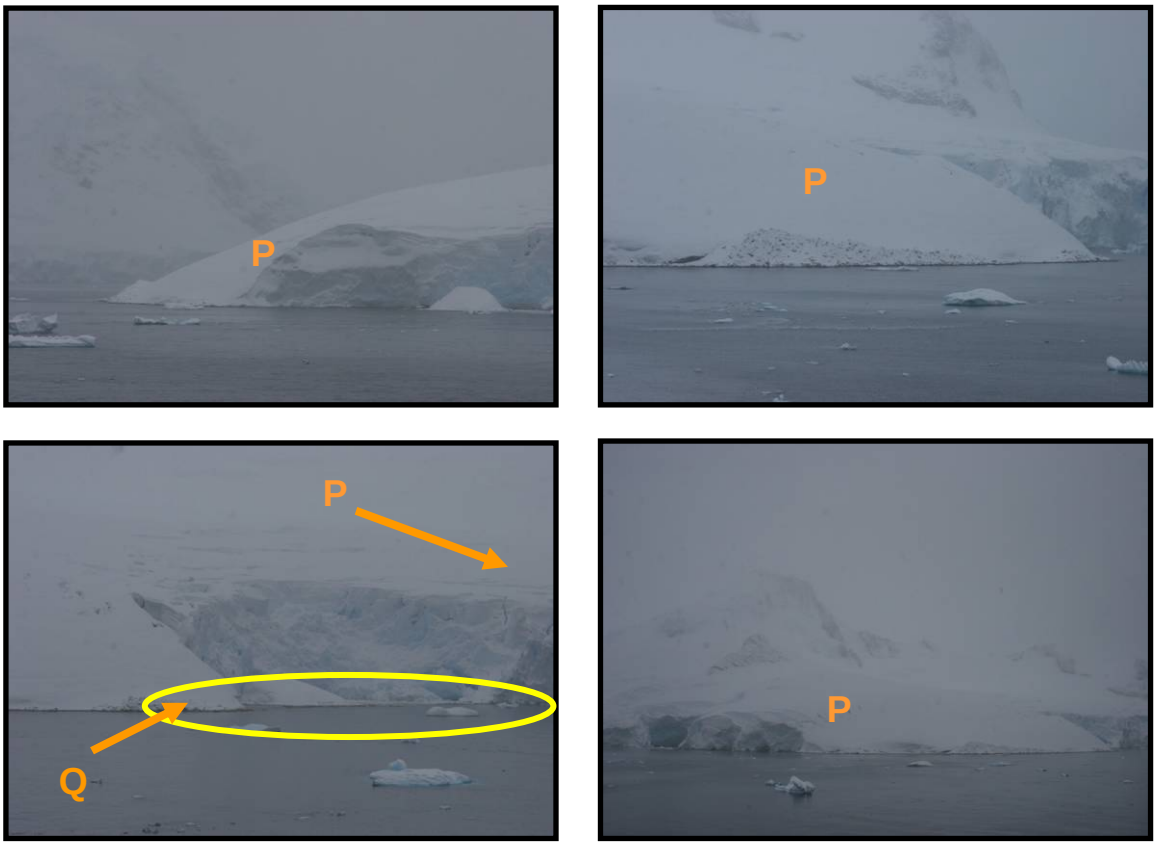

Figure 103 - Photos taken of Cape Willems Point tip during the NBP 0703 cruise in 2007. See Figure 77 and 99 for location.

Brabant Island

The final set of aerial photos analyzed was located east of the eastern coast of Brabant Island in 2001 (Figs. 104 and 105). Between the two photos eight CRASLs were identified. Unfortunately, there was no video (1980s) or photos (2007) available for this area. However, according to the BAS the CRASL located off of Pampa Island (Fig. 104) is in the same position as it was in 1956 (A. Cook; per. comm., 2008).

CRASLs were not only found on the northeastern side of Brabant Island, but also in other areas of the island. While analyzing the 1980s video a CRASL was identified along the southwestern tip of Brabant Island (Fig. 106). This CRASL was the most well developed CRASL, due to its size and shape, found throughout the area. The identification of this CRASL in the 1980s as well as other CRASLs in the videos and aerial photos (2001), suggests that these features form on both the eastern and southwestern portion of Brabant Island and have since at least the 1980s.

Neko Harbour

Although there were no aerial photos available for Neko Harbour in Andvord Bay, video taken from the 1980s DEEP FREEZE cruise (Fig. 107) and 2007 NBP 0703 cruise (Fig. 108) were available. By comparing the 2007 photos with the video little to no changes were observed.

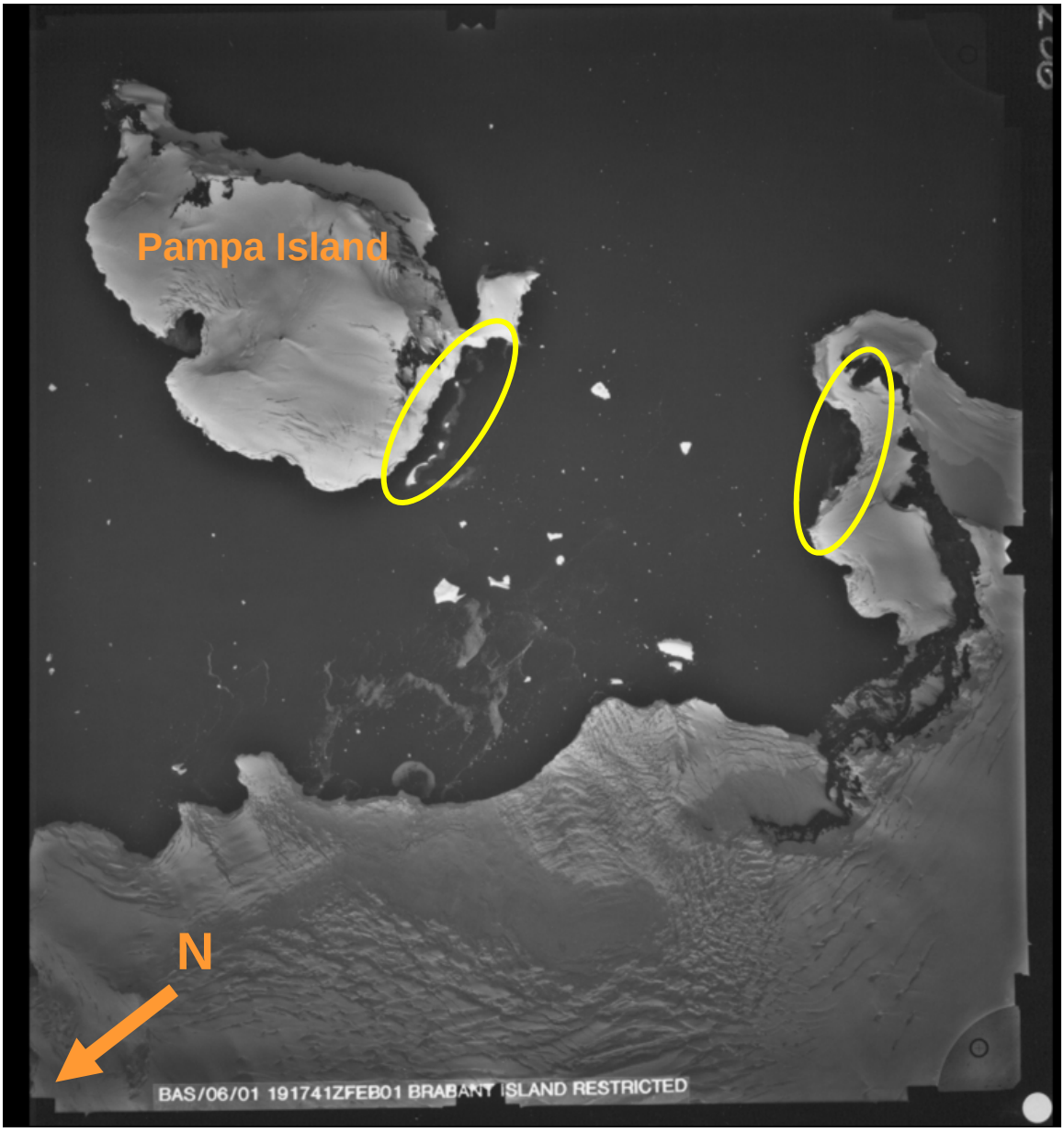

Figure 104 - Aerial photo of Brabant Island taken by the BAS in 2001. (Courtesy BAS, 2008). See Figure 77 for location.

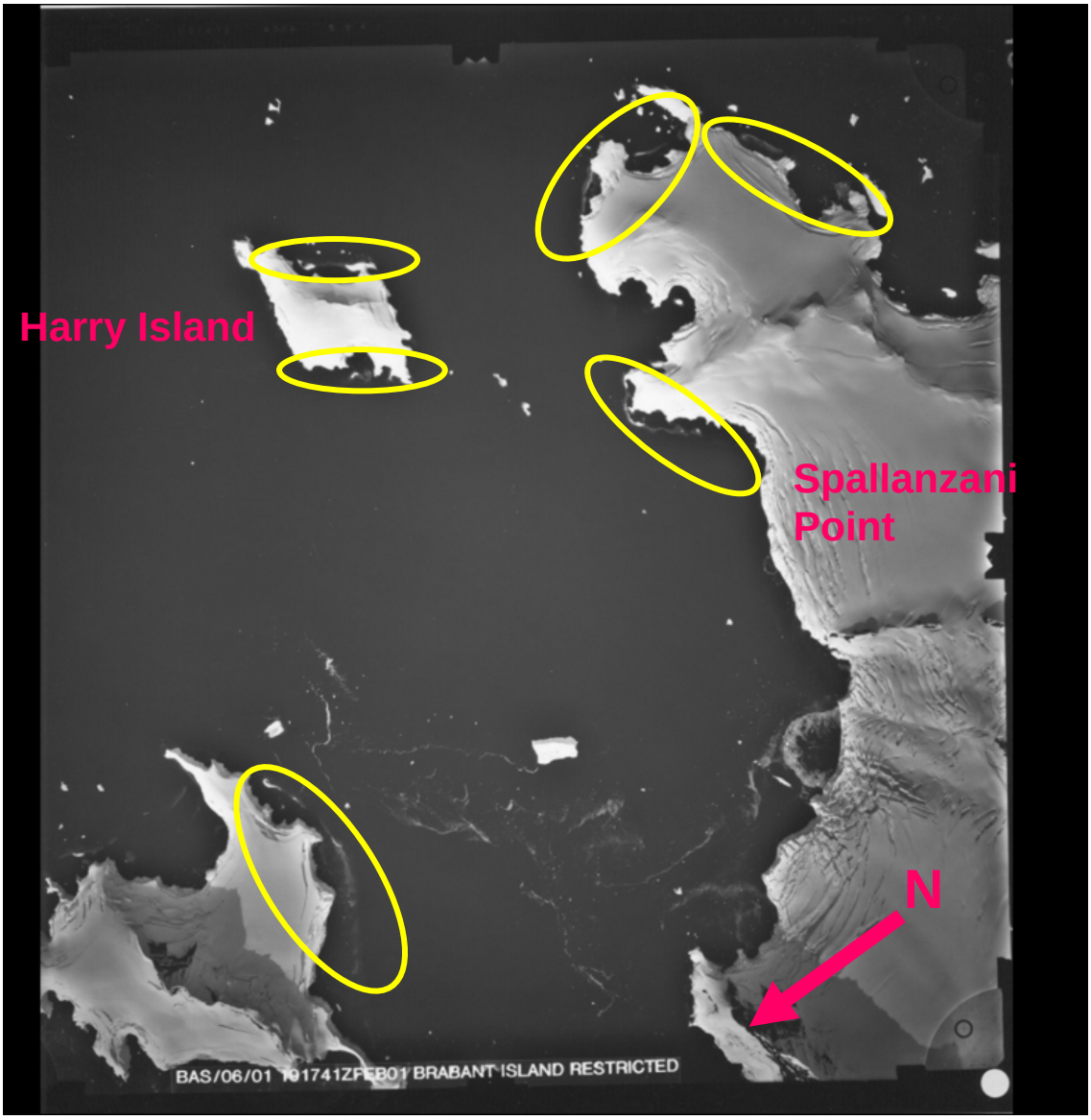

Figure 105 – Aerial photo of Brabant Island taken by the BAS in 2001. (Courtesy BAS, 2008). See Figure 77 for location.

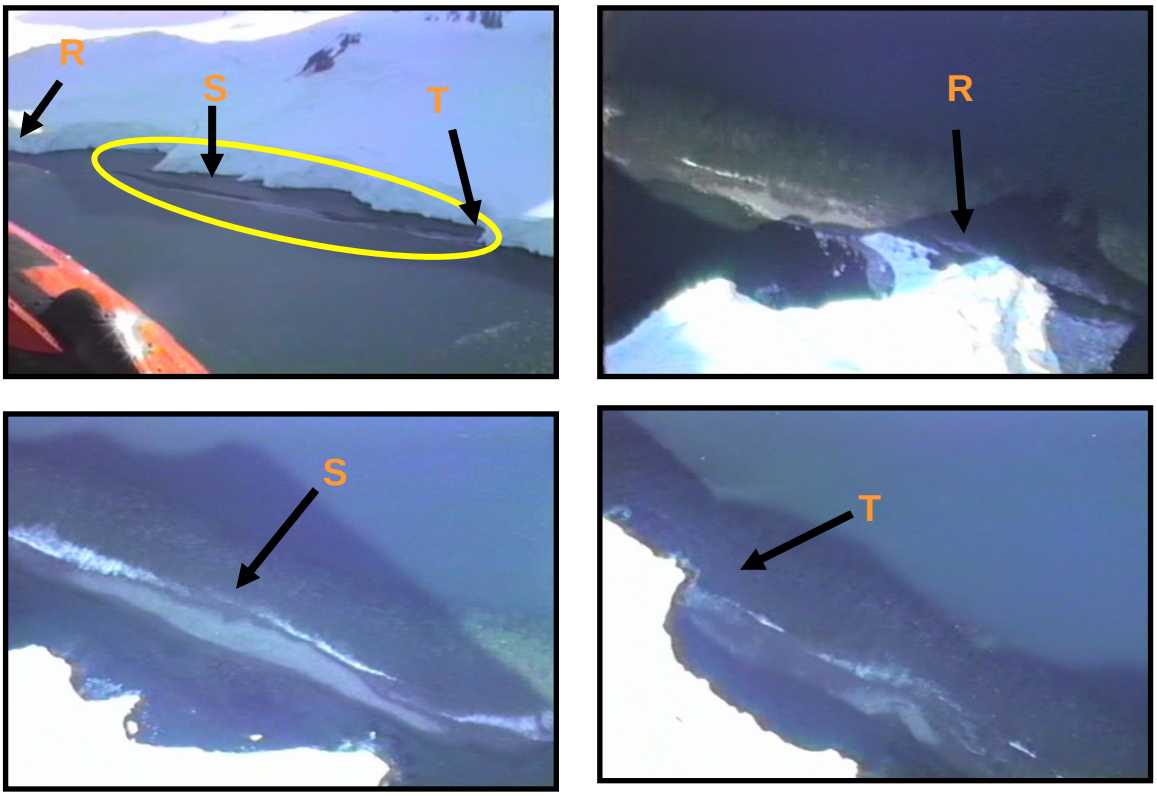

Figure 106 – Video of well developed CRASL of the southwestern point of Brabant Island during 1980s DEEP FREEZE cruise. See Figure 77 for location.

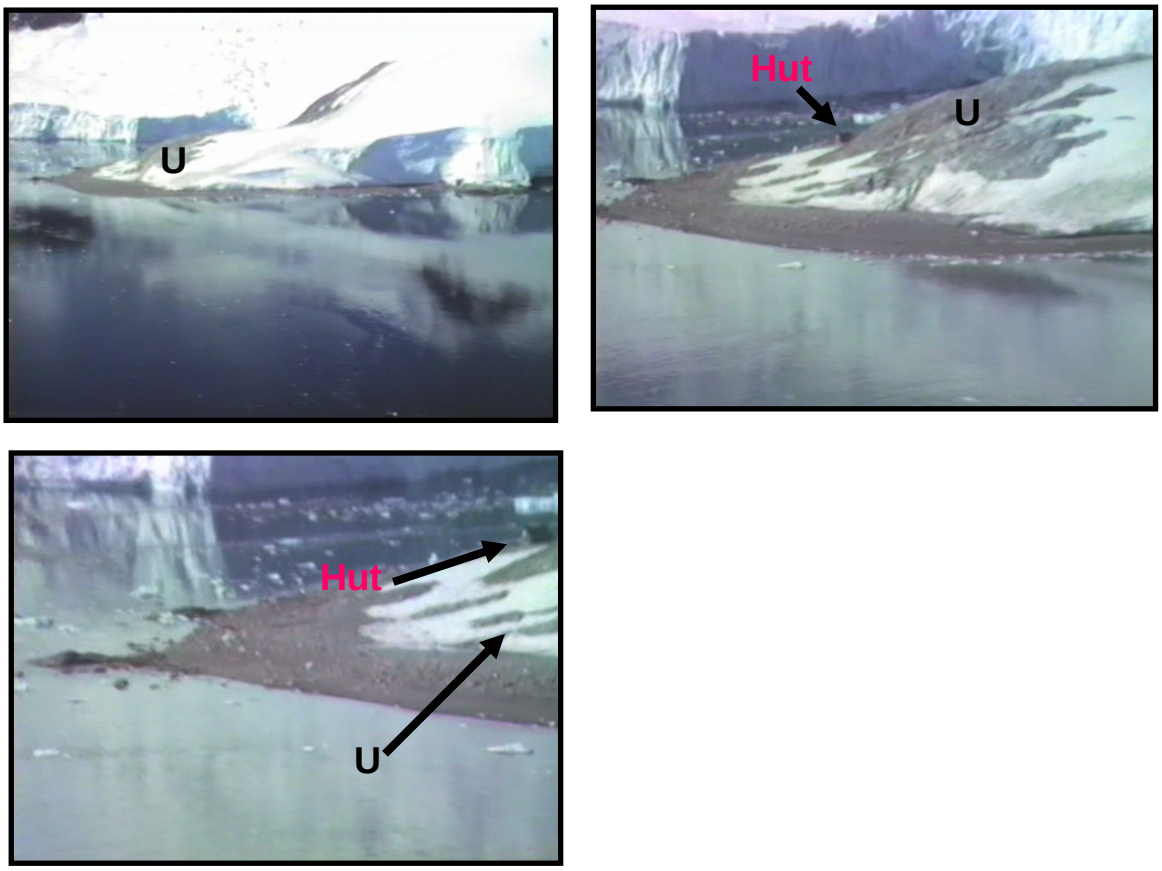

Figure 107 – Video of Neko Harbour taken during the 1980s DEEP FREEZE cruise. See Figure 77 for location.

Figure 108 - Photos of Neko Harbour, 2007. See Figure 77 for location.

Enterprise Islands

Another area where multiple CRASLs were located in the 1980s video was near the Enterprise Islands north of Nansen Island in Wilhelmina Bay (Figs. 109 and 110). Several well-developed CRASLs were observed in the video images. A shipwreck occurred in this area in 1916 on a CRASL (Fig. 109). Photos were also taken during the NBP 0703 cruise near the shipwreck (Fig. 111). A comparison of the water level on the side of the ship from the 1980s video (Fig. 110) and the 2007 photos (Fig. 111) gives a minimum estimate of the tidal range in the area, which is approximately 2 m. The CRASLs are visible in the 1980s video when the tide is out, indicated by the lower water line on the side of the ship. However, in photos taken in 2007 the CRASLs were not observed, and the water level is higher on the side of the ship indicating that the photo was taken closer to high tide. The CRASL next to the shipwreck was not observed in 2007 due to its submergence during a higher tide. Nevertheless, analysis of the photos suggests that CRASLs were present near the Enterprise Islands since 1916.

A summary of changes to the CRASLs discussed in this section is given in Figure 112.

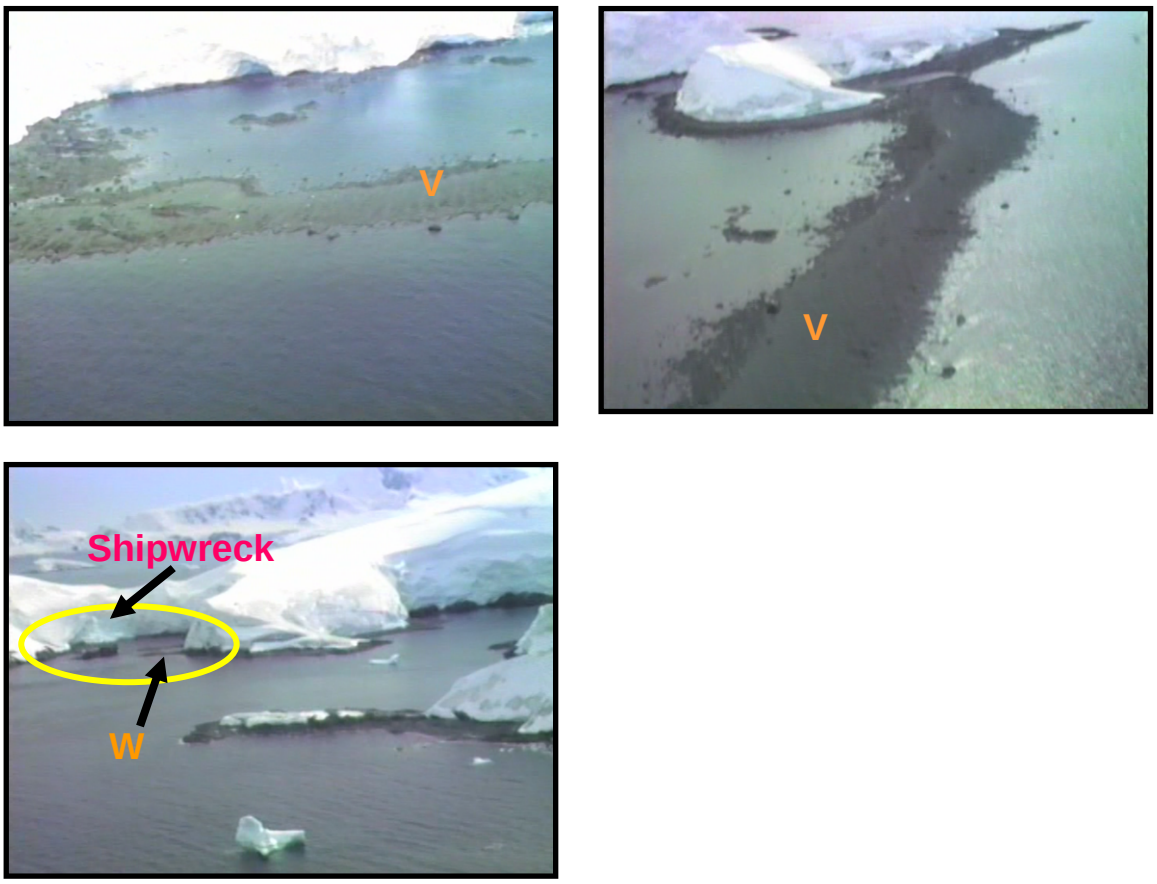

Figure 109 – Video near Enterprise Islands taken during 1980s DEEP FREEZE cruise. Notice the shipwreck circled. See Figure 77 for location.

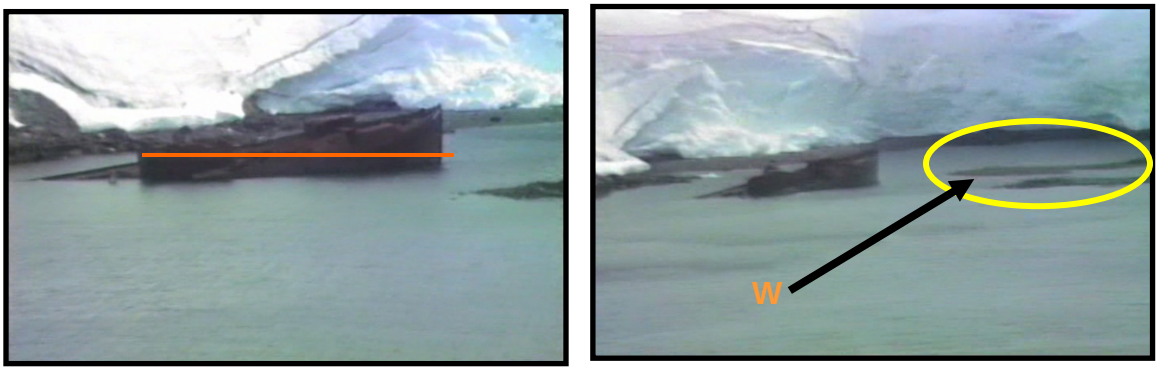

Figure 110 - Closer images of the 1916 shipwreck. Notice the proximity of the CRASLs to the shipwreck. Video was taken during the 1980s DEEP FREEZE cruise. The line indicates the 1980s high tide mark on the side of the ship. See Figure 77 for location.

Figure 111 - Photos of shipwreck on the Enterprise Islands north of Nansen Island in Wilhelmina Bay, taken during the NBP 0703 cruise in 2007. Notice the high tide water mark on the side of the ship. Comparing the high tide water marks on the sides of the ship (Fig. 110 and Fig. 111) gives a minimum estimate of the tidal range in the area (2 m). See Figure 77 for location.

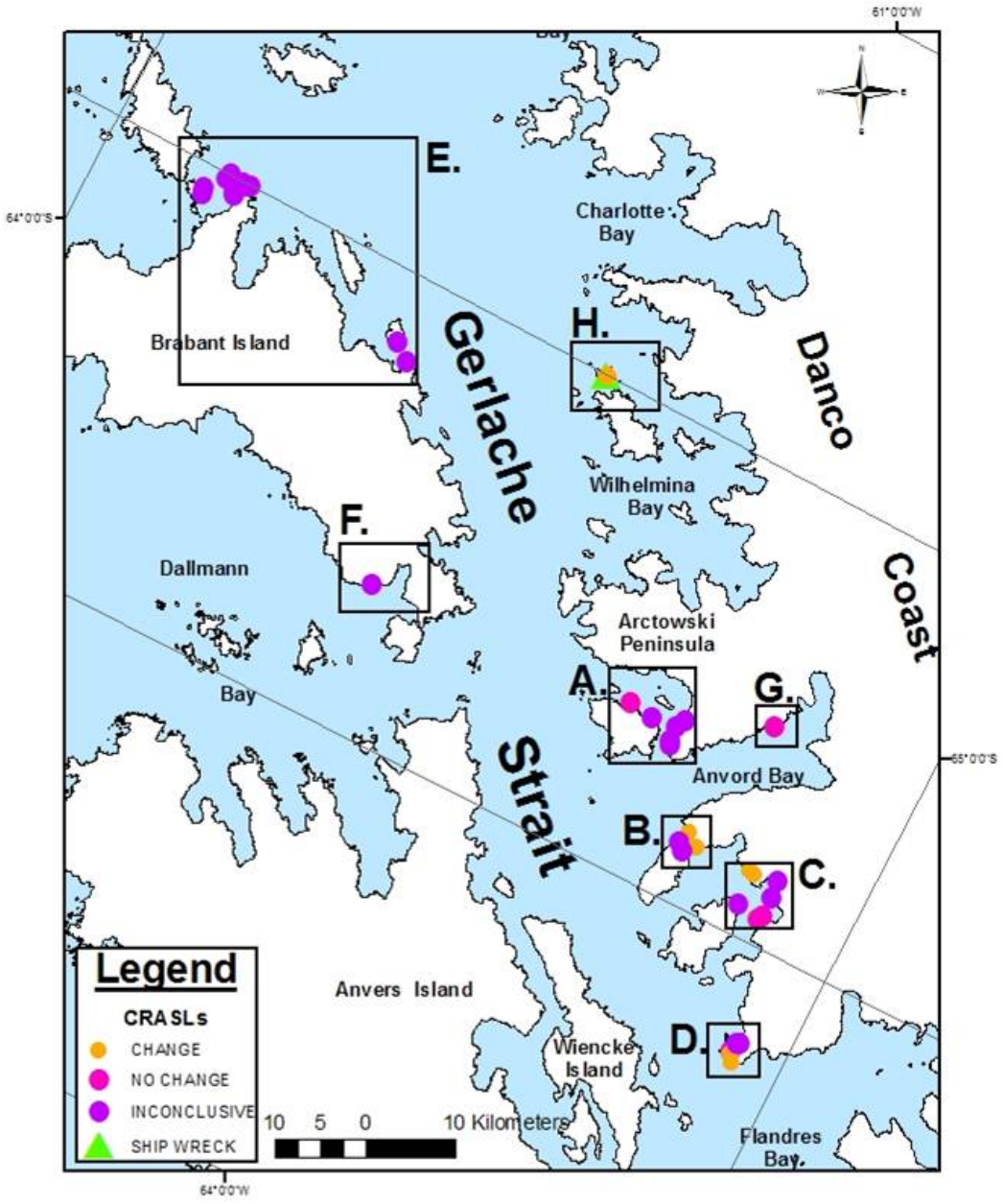

Figure 112 – Map indicating, CRASLs that changed and did not change throughout the study area. Three of the twenty-seven inconclusive CRASLs were not documented because their exact location was not known.

OSL Samples

Four samples were collected near Wiencke Island for OSL dating: PL01, PL02, PL03, and PL04 (Figs. 113 and 114). The cobbles were sampled from two different raised-beach ridges (Fig. 115). PL01, PL02, and PL03 were sampled from the 3 m beach ridge and PL04 was sampled from a 12-m beach ridge.

A total of 1055 aliquots were prepared and sampled. Of those, only 113 aliquots were found to have a signal. Twenty-five aliquots "passed" the four tests listed in Table 23.

Typical dose results tend to be distributed around an average value with some outliers ("Gaussian distribution"), depending on the conditions of resetting and deposition (Olley et al., 1998). Since the dose results obtained for PL02 had such a wide range (Fig. 116) an accurate Dose could not be calculated for PL02 and thus, an age for the sample could not be determined.

Sample PL02 was the largest cobble sampled from the first beach ridge. It also had the most material remaining after sample preparation and therefore the highest probability of yielding the minimum 16 "good" aliquots required for calculating a statistically sound average dose value, which is why it was analyzed first. PL01 and PL03 yielded considerably less quartz and we did not expect 16 "good" aliquots.

PL04 was believed to have been exposed to light during the sampling process in Antarctica, which was confirmed during the initial "dose" test. Thus, no further dose measurements were completed with samples PL01, PL03, and PL04.

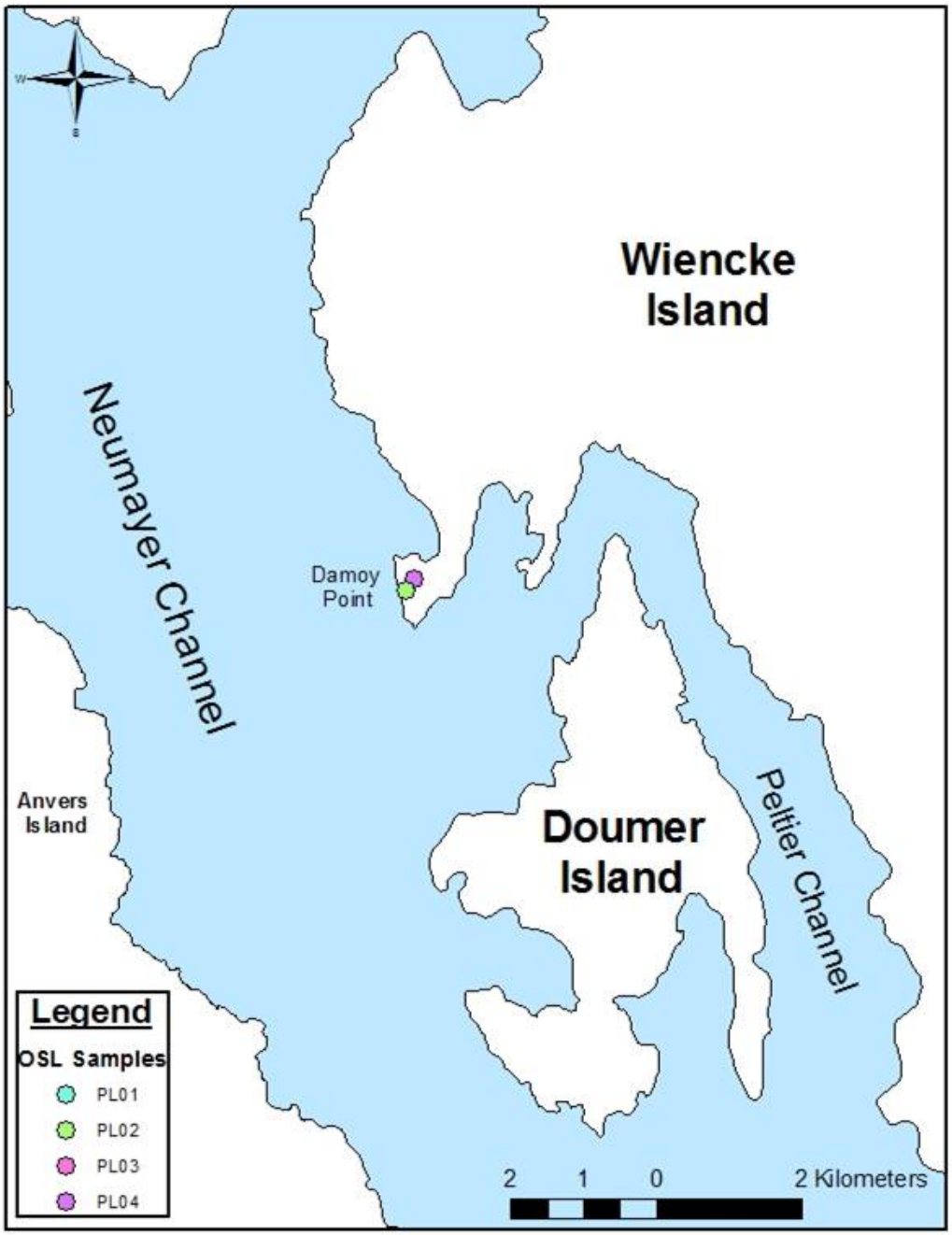

Figure 113 – Location map of OSL samples taken on Wiencke Island.

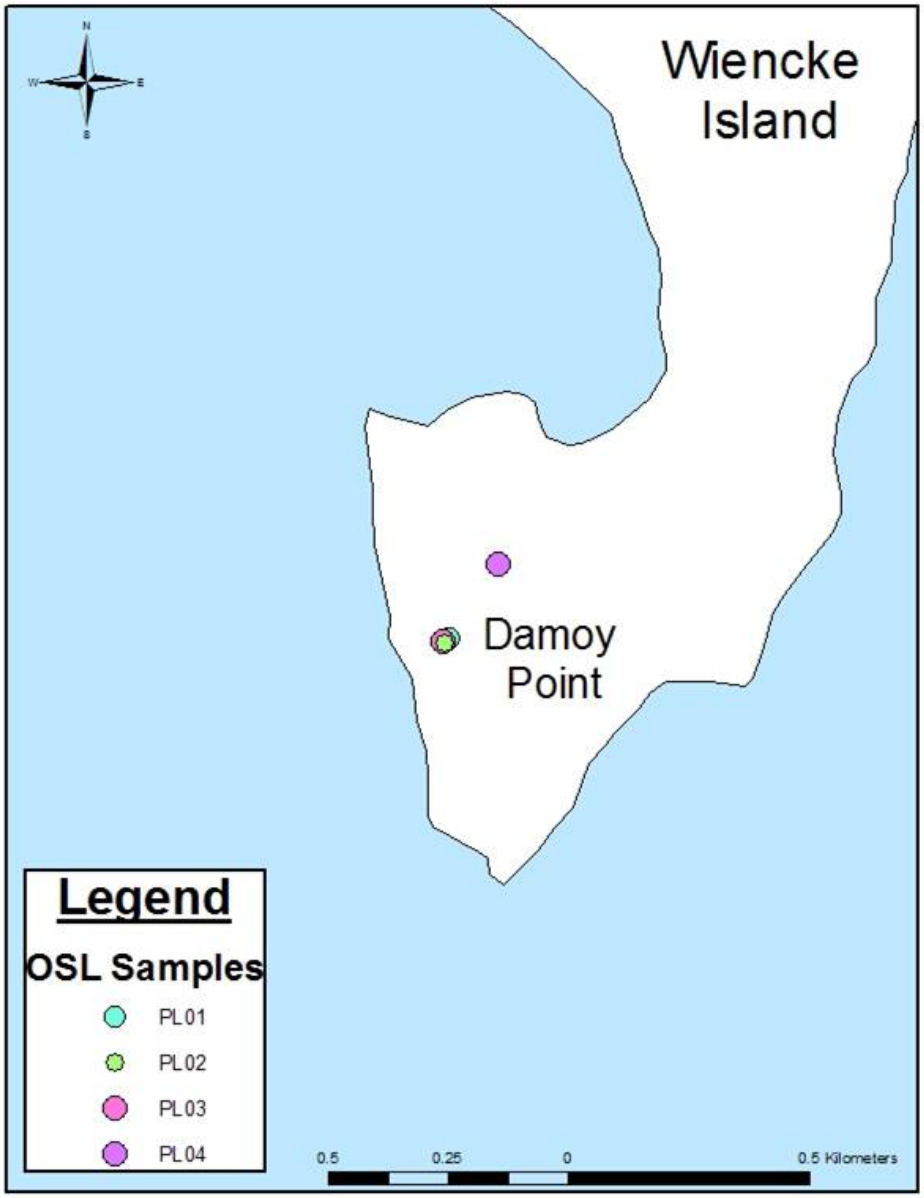

Figure 114 – Location of OSL samples.

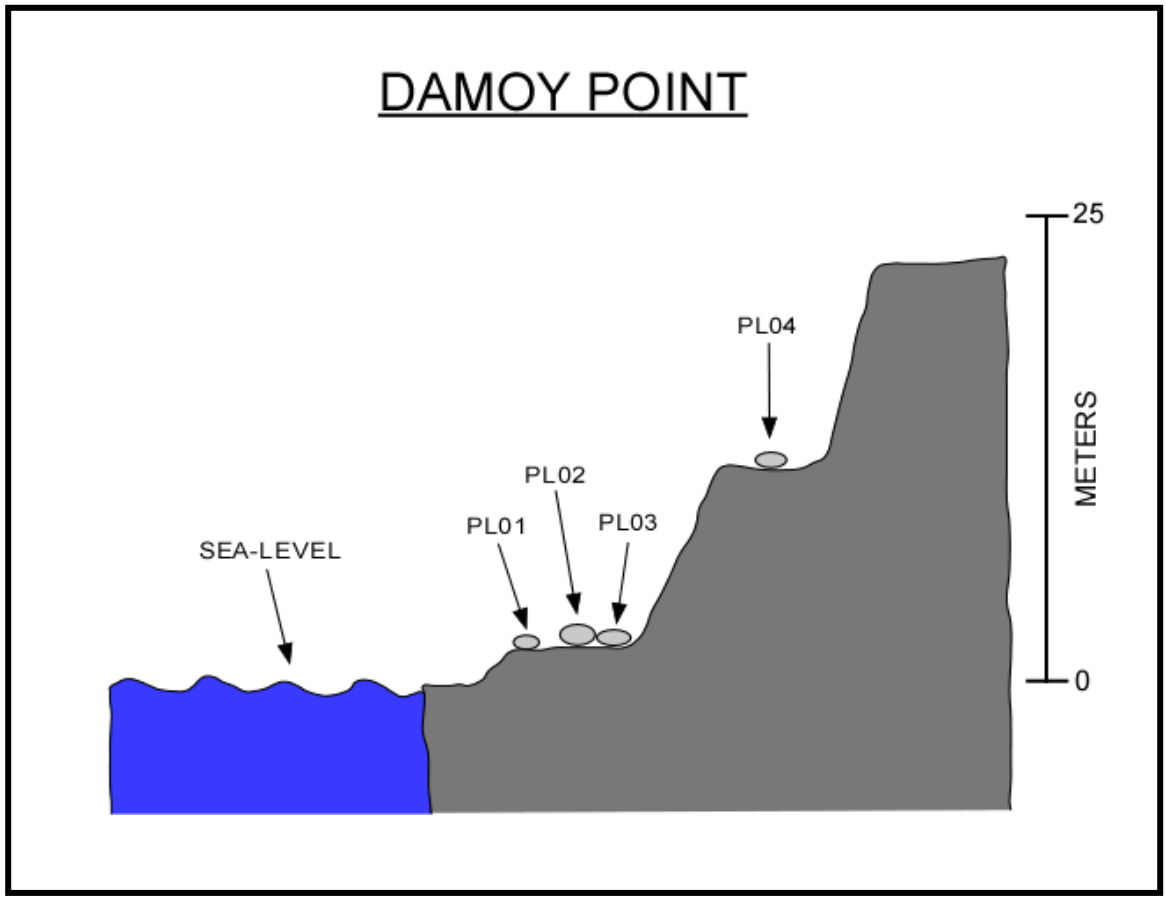

Figure 115 – Cross-sectional view of ridges at Damoy Point, where OSL samples were taken, on Wiencke Island.

TABLE 23. OSL RESULTS

Sample	Aliquot Position	Natural Dose (s)	Dose Error (s)	Dose Recovery	Recycling Ratio	Recuperation (%)	IR Test
PL02_1	1	23.09	4.35	-4.16	-2.99	0.16	0.94
PL02_1	7	66.81	28.49	-9.65	-320.35	10.85	1.00
PL02_1	25	262.45	84.17	-15.88	-1300.00	-12.85	0.76
PL02_1	31	749.53	59.78	-9.75	6.54	-4.48	0.93
PL02_2	5	1842.93	94.61	15.34	8.15	-0.70	0.68
PL02_2	7	319.48	22.63	10.72	-8.94	-0.91	0.61
PL02_2	11	151.01	11.06	-20.26	-14.82	2.88	0.91
PL02_2	19	130.66	6.77	4.44	-3.14	-2.54	0.56
PL02_16	7	75.43	6.54	-0.29	-6.94	N.A.*	0.39
PL02_16	11	30.23	6.75	1.39	9.90	2.62	0.73
PL02_16	15	246.83	27.68	-7.17	0.00	4.28	0.80
PL02_17	9	44.04	18.96	11.98	-16.90	-39.58	0.83
PL02_17	11	6.52	6.10	-0.36	-7.94	-43.84	0.92
PL02_17	33	54.46	11.45	-17.06	-47.07	-4.72	0.53
PL02_17	37	8.98	3.53	-16.71	-0.97	-7.41	0.99
PL02_17	39	87.40	13.49	-0.71	-37.66	-21.34	0.62
PL02_17	41	49.02	13.27	-2.20	-49.70	-13.15	0.50
PL02_24	7	249.21	41.70	7.77	17.45	-1.54	1.174
PL02_24	11	120.49	23.62	9.22	2.28	0.07	1.023
PL02_24	39	1701.32	151.52	-12.88	25.21	-1.10	1.252
PL02_24	43	91.38	15.93	0.23	17.38	-10.79	1.174
PL02_25	3	319.56	79.22	17.01	-12.22	-11.56	0.878
PL02_25	7	12.74	6.06	11.02	7.66	3.70	1.077
PL02_25	9	54.60	11.18	-27.54	-2.23	-50.00	0.978
PL02_25	27	7.94	3.26	8.91	7.28	-1.15	1.073

*N.A. = Not available

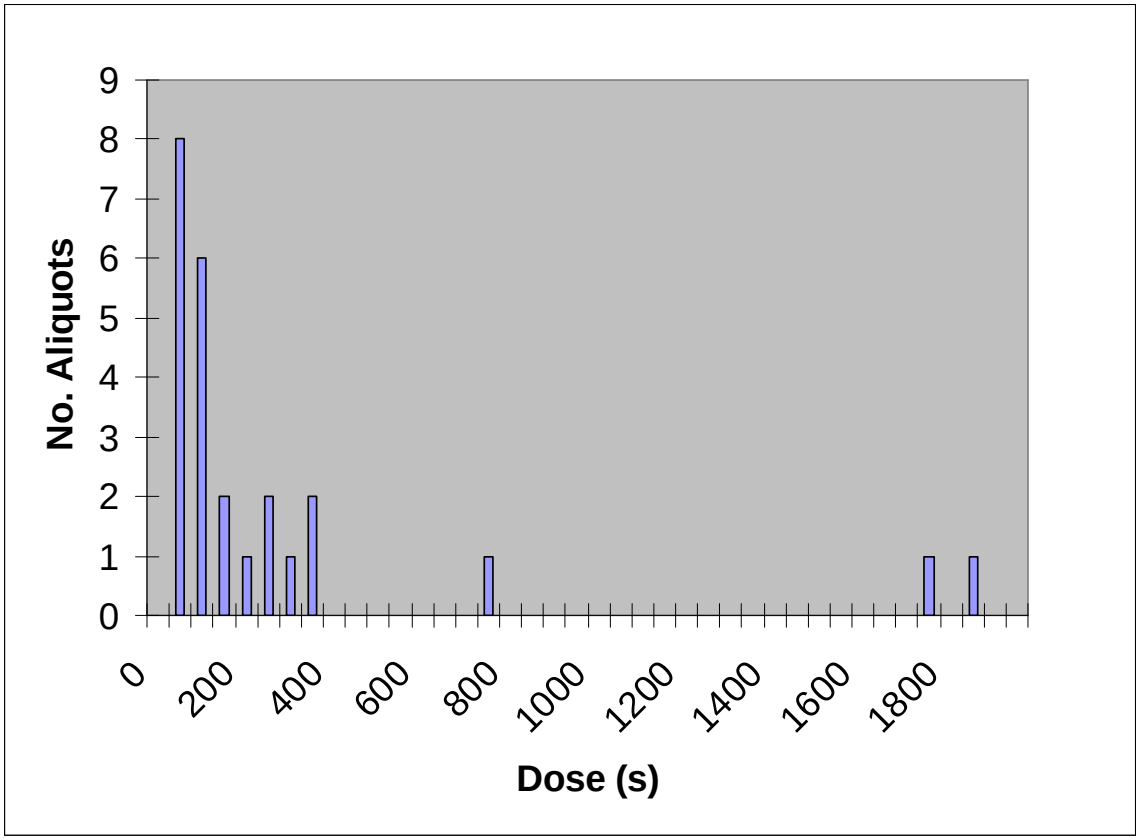

Figure 116 – Histogram of 25 aliquots that passed the aliquot test.

CHAPTER V

DISCUSSION

Sedimentary Characteristics

Sediments were most likely supplied to the CRASLs by recessional moraines. The distribution maps representing the orientation of the features (Figs. 48 - 57) indicate that they are oriented randomly. Therefore they are not likely to be formed solely by longshore currents, thus negating the spit model. Also, the majority of the CRASLs are found immediately seaward (Figs. 96, 97 and 106) of ice-cliff faces, therefore negating the pro-talus rampart model. The grain-size and angularity results (Figs. 35 - 38) indicate that the sedimentary texture of the CRASL deposits are between moraine and beach deposits.

Since local provenance can be the most dominate control on mineralogical variations, we first compare talus, moraine, beach, and CRASL deposits at the localities with the same provenance.

Grain-Size

A summary of grain-size parameters for the Errera Channel talus, moraine, and CRASL deposits are compared in Table 24. Neko Harbour beach and moraine deposits

are compared in Table 25. Finally, the Palmer Station moraine and surrounding island beach samples are compared in Table 26.

TABLE 24. GRAIN SIZE RESULTS FOR ERRERA CHANNEL SAMPLES

Features	Graphic Mean (M_Z)	Standard Deviation (σ_i)	Skewness (SK_i)
Talus	Cobble	Very poorly sorted	Near symmetrical
Moraine	Pebble	Poorly sorted	Strongly coarse skewed
CRASL1*	Pebble	Moderately sorted	Near symmetrical
CRASL2[@]	Pebble	Moderately sorted	Fine skewed
CRASL3[#]	Pebble	Moderately sorted	Fine skewed

*CRASL 1 – Same as ECC01 which was sampled from the back of the CRASL.
[@]CRASL 2 – Same as ECC02 which was sampled from the lower front portion of the CRASL.
[#]CRASL 3 – Same as ECC03 which was sampled from the upper front portion of the CRASL.

When comparing the graphic mean (M_Z), standard deviation (σ_i), and skewness (SK_i) from the Errera Channel deposits several observations can be made. First, the graphic mean of the moraine and CRASL deposits are both pebble, while the graphic mean for the talus deposits is cobble. This is to be expected as mass wasting processes are less efficient at breaking down material compared to glacial or moraine processes (Plummer and McGeary, 1996).

Secondly, the standard deviation of the talus implies a very poorly sorted deposit. The poor sorting is a result of the relatively short amount of time and distance the samples have been transported. Likewise, the standard deviation for the moraine also indicates a poorly sorted deposit. The poor sorting is a reflection of the way in which glaciers transport sediment. The sediment is not exposed to erosional processes once

collected by the advancing glaciers. Therefore, the sediment remains unsorted until deposition. The standard deviation of the CRASL deposits indicate moderate sorting. The difference in sorting of the CRASL deposit and the moraine is most likely due to the influence of wave action.

The skewness of the talus deposit is near symmetrical. This was to be expected because the deposit has not been reworked. However, the skewness of the moraine deposit is strongly coarse skewed. This was not expected, but is most likely the result of the way in which it was sampled. The samples collected for the moraine were not taken at random; rather the fine material and coarse material were selected for collection.

A marked difference is found between the skewness of the deposits from the front of the CRASL and the back of the CRASL. The deposits from the front of the CRASL are finely skewed, while those at the back of the CRASL are near symmetrical. The deposits from the back of the CRASL receive limited exposure to wave action, except for that created by calving ice. The skewness of the deposits from the front of the CRASL can not be explained at this point, but may be related to sea ice or other processes unique to polar settings. Thus, our results at Errera Channel support the idea that the CRASL is more closely related to the moraine and beach deposits, than the talus deposits.

TABLE 25. GRAIN SIZE RESULTS FOR NEKO HARBOUR SAMPLES

Features	Graphic Mean (M_Z)	Standard Deviation (σ_i)	Skewness (SK_i)
Beach1*	Granule	Very poorly sorted	Strongly coarse skewed
Beach2[@]	Pebble	Very poorly sorted	Strongly coarse skewed
Beach3[#]	Very coarse sand	Moderately well sorted	Strongly fine skewed
Moraine1	Granule	Very poorly sorted	Near symmetrical
Moraine2	Granule	Very poorly sorted	Near symmetrical

*Beach 1 – located on the middle portion of the beach.
[@]Beach 2 – located on the lower portion of the beach.
[#] Beach 3 – located on the upper portion of the beach.

When comparing the graphic mean (M_Z), standard deviation (σ_i), and skewness (SK_i) results for the Neko Harbour deposits several observations can be made. First, the graphic mean for the beach deposits varies from granule, to pebble, to very coarse sand depending on location within the beach. The graphic mean for the moraine deposits is a granule.

Second, the standard deviation for the beach deposits varies from very poorly sorted to moderately well-sorted. This is because the three different sample locations of the beach deposits vary with position from the shoreline, and because the sediments have not been transported very far from their source. However, the standard deviation of the moraine is very poorly sorted, which is to be expected considering the mode in which glaciers transport material. The sediment is not exposed to erosional processes once collected by the advancing glaciers. Therefore, the sediment remains unsorted until deposition.

Third, the skewness for the beach deposits ranges from strongly coarse skewed to strongly fine skewed. Strongly coarse skewed is what would be expected due to the high-

energy environment of the beach. The near symmetric distribution of the moraine deposits is also what would be expected due to the mode in which glaciers transport material.

TABLE 26. GRAIN SIZE RESULTS FOR PALMER STATION

Features	Graphic Mean (M_Z)	Standard Deviation (σ_i)	Skewness (SK_i)
NI01[*] Beach	Very coarse sand	Moderately well sorted	Near symmetrical
NI02[@] Beach	Cobble	Very poorly sorted	Fine skewed
TI01 Beach	Cobble	Moderately sorted	Coarse skewed
LI01 Beach	Pebble	Moderately well sorted	Fine skewed
HI01 Beach	Cobble	Well sorted	Fine Skewed
Moraine 1	Cobble	Poorly sorted	Near symmetrical
Moraine 2	Granule	Very poorly sorted	Strongly fine skewed

[*]NI01 Beach – is located in the intertidal zone.
[@]NI02 Beach – is located on the upper portion of the beach.

Comparing the graphic mean (M_Z), standard deviation (σ_i), and skewness (SK_i) from deposits collected at Palmer Station and the surrounding islands reveals several trends. First, the graphic mean varies within the beach deposits. This is most likely due to the setting of the different islands we sampled. Not all the beaches faced the same direction with respect to the prevailing waves nor are the rock types the same at every island. Likewise, the graphic mean of the moraine at Palmer Station ranges from granule to cobble and is overall finer than the local beaches. This suggests that either the waves are removing the finer material from the beach deposits or the material for the beach is derived from the local bedrock of the individual islands, not the moraine.

Second, the standard deviation of the beach deposits are mostly moderately sorted, which is expected of beach deposits. The only exception is NI02, which was sampled higher on the beach than NI01. NI01 was located in the intertidal zone, and undergoes more reworking by wave action than NI02. The standard deviation of the moraine deposits suggests the deposits are poorly sorted, as to be expected from a glacial deposit.

The skewness for the beach deposits varied significantly. For sample NI01 and TI01 the skewness values are in the expected range for beaches that are protected and have varying maturity. However, the other three beaches are finely skewed. One suggestions as to why the beaches are finely skewed could be that the sea ice is removing the larger clasts from the beach deposits. The skewness for the moraine deposits vary. The skewness for deposits from moraine 1 is what was expected. The skewness for deposits from moraine 2 was most likely due to the sampling technique, since the person who took the sample only sampled the fine material.

Overall, the textural characteristics of the CRASL deposits seem to be more closely related to the beach and moraine deposits than the talus deposits. This is particularly apparent in the graphic mean and skewness. The CRASL deposits appear to be more closely related to the beach deposits from the islands surrounding Palmer Station, more specifically Limitrophe Island, in regards to the graphic mean and skewness. Further, the grain-size analysis seems to indicate that the CRASL is more similar in textural characteristics to the beach deposits than either the moraine deposits or talus-slope deposits.

Angularity

The angularity results are summarized in Table 27 (refer to table 16 for complete angularity results.) Roundness measurements indicate that the talus and moraine deposits are characterized by angular clasts, CRASLs are characterized by subangular clasts, and beaches are characterized by subrounded clasts. This is to be expected as glacial

TABLE 27. SUMMARY OF ANGULARITY RESULTS

	Talus	Beach	Moraine	CRASL
Angularity	Angular	Subrounded	Angular	Subangular
Total # of clasts	135	715	260	332

(moraine) and rockfall (talus) processes are not very efficient at rounding clasts (Plummer and McGeary, 1996).

The results indicate that the angularity of the CRASL deposits is between that of moraine and beach deposits. This is consistent with a wave-reworked moraine. Of all the sedimentary characteristics analyzed, angularity best discriminates the depositional environments.

Sphericity

Deposits from talus slopes, beaches, moraines, and CRASLs are dominated by oblate clasts (refer to Table 17 for complete results). Thus, sphericity provides no assistance in environmental interpretation. Disc-shaped beach pebbles or oblate pebbles are believed to occur due to the selective transport of other shapes leaving behind

flattened or oblate pebbles as lag deposits (Kuenen, 1964) and by the flattening of the pebbles by waves (Dobkins and Folk, 1970). However, according to Boggs (1995) sphericity "*has not yet been demonstrated*" to be a "*reliable tool for interpreting depositional environments*". Thus, our results concur with Bogg's (1995) statement.

Petrology

A summary of the petrologic analysis of the Errera Channel talus, moraine, and CRASL deposits is given in Table 28. Neko Harbour beach and moraine deposits are summarized in Table 29. Finally, Palmer Station moraine and surrounding island beach samples are summarized in Table 30.

TABLE 28. ERRERA CHANNEL SAMPLES COUNTING RESULTS

	Talus	Moraine	CRASL 1*	CRASL 2[@]
Grain types	4	6	6	5

Note: - CRASL 3 (ECC03) was not represented because it did not have any grains at that sample size.
*CRASL 1 – Same as ECC01 sampled from the back of the CRASL.
[@]CRASL 2 – Same as ECC02 sampled from the lower front portion of the CRASL.

When comparing the number of mineral/rock fragment grain types among the Errera Channel deposits a few observations can be made. First, the talus deposits have the least amount of petrologic variability. The moraine and CRASL deposits have the same amount of petrologic variability. The moraine was created by a glacier which is

sourced by a larger area than the talus deposit. The variability in grain types of the CRASL deposit is more similar to the moraine than the talus deposits.

TABLE 29. NEKO HARBOUR SAMPLES COUNTING RESULTS

	Beach 1	Beach 2	Beach 3	Moraine 1	Moraine 2
Grain types	8	9	10	8	8

The variability in grain types of the beach deposits at Neko Harbour is greater than those of moraine deposits from Neko Harbour. This is to be expected as "exotic" grains are most likely to be added to the beach deposits from icebergs, where as the moraine deposits are only being sourced by a single glacier.

TABLE 30. PALMER STATION AND SURROUNING ISLANDS SAMPLES COUNTING RESULTS

	NI Beach 1	NI Beach 2	LI Beach	Moraine 1	Moraine 2
Grain types	6	6	5	6	7

Note: - Torgerson Island (TI01) and Humble Island (HI01) were not represented because they did not have grains of the sample size.

The moraine deposits from Palmer Station seem to have a similar number of grain types as the beach deposits from the surrounding islands. This could be because the beaches are on individual islands that are not connected. Therefore their only source would be the local island lithology as compared to the entire drainage of a glacier. For that reason, at Palmer Station and the surrounding islands the lithologic variability of the beach and moraine deposits is similar.

Maps

367 CRASLs were identified and mapped throughout the Gerlache Strait. Of those CRASLs, 319 were identified from the 1980s DEEP FREEZE video, 45 were identified during the *Nathaniel B. Palmer* (0703) cruise, and 3 were observed in both the video and during the cruise.

The features had a random distribution and are found on both sides of the strait. Also they have no specific orientation. Thus, they are not likely to have originated solely as spits created by longshore currents.

The features were further classified into 12 different categories based on their orientations (refer to Table 21). These 12 classifications were simplified into four broad types: Detached, Connected, Left, and Right. 138 of the CRASLs were classified as Detached; 80 were classified as Connected; 79 were classified as Left; and 70 were classified as Right. These features are predominately detached from the shoreline throughout the area (refer to Fig. 54). In regards to the 3 models presented, this would favor the recessional moraine-model or the pro-talus rampart model because the sediments are not attached to the shoreline but located immediately offshore. However, 98% of the features were found in front of an ice front, rather than a cliff face. This supports the recessional moraine-model over the pro-talus rampart model.

The features were also classified according to their shapes. Of the 367 CRASLs, 113 were classified as concave shaped, 18 as convex, 218 as parallel, and 18 as perpendicular (refer to Fig. 64). The parallel shape of the features supports both the spit model and recessional moraine model.

The distribution maps suggest that the most common type of CRASL is the detached type parallel to the coastline (refer to Fig. 54). The second most common features shape is concave (refer to Fig. 64). The reason for the number of concave and parallel shaped features in the area could be because the features are at different stages of wave reworking. Two moraines observed in the area at Neko Harbour and in the Errera Channel, are concave in shape.

A process known as coastal straightening is observed where irregular coastlines were present (Plummer and McGeary, 1996). According to Plummer and McGeary (1996) "*because wave refraction bends waves approaching such a coast until they are nearly parallel to shore, most of the waves' energy is concentrated on headlands, while the bays receive smaller, diverging waves.*" Assuming a microtidal coastline (tide range of 2 m) for this area, the irregular coast eventually is straightened by concentrated erosion on the headlands and deposition of the material eroded from the headlands into the bays (Plummer and MeGeary, 1996). Our observations seem to support this process for the reshaping of the concave shaped features into parallel shaped features.

Chronology

Age of Huts

Twenty-three anthropogenic structures were identified and located in the study area (refer to Table 22). Upon cataloging the structures, it appears that none were built on a CRASL. Thus, they do not constrain the age of the CRASLs. However, the shipwreck on Enterprise Island off the northern coast of Nansen Island in Wilhelmina Bay in 1916 suggests that CRASLs in the area could have formed as early as the

beginning of the 20th century. If so, this would indicate that the recession of these small glaciers occurred before the documented retreat of tidewater glaciers in the Antarctic Peninsula by Cook et al. (2005), and prior to 20th century warming.

Aerial Photos

Ten aerial photos taken between 1956 and 2001 in the study area were examined and compared to video from the 1980s DEEP FREEZE cruise and the *Nathaniel B. Palmer* (0703) cruise. A map of the results can be seen in Figure 118. A comparison between the video and photos suggest that 5 features have not noticeably changed over time, while 9 features have undergone a changes resulting in a decrease in the size of these features. The examination of an addition 27 features was found to be inconclusive.

OSL Samples

Four cobbles were taken from Wiencke Island in an attempt to obtain OSL dates. Only 25 aliquots from sample PL02 passed the aliquot test (refer to Table 23). The large dose distribution (refer to Fig. 122) did not allow for an age to be determined for PL02.

Three possible explanations exist as to why sample PL02 had such a wide distribution of dose values. First, mechanical stress has been found to reduce the luminescence in a thin surface layer of quartz grains (Takeuchi et al., 2006) and friction during sampling and slicing could have influenced the trapped charges. During sampling of the four cobbles a rock hammer was used to hit the exposed surface of the cobbles in order to dislodge them from the frozen ground, possibly causing enough friction to

reduce the luminescence. This sampling technique was not used in the South Shetland Islands where OSL results appear to be good (P. Kouremenos; per. comm., 2008). However, if this effect occurred in our samples, it is expected to be small and cannot explain the spread of doses over several orders of magnitude.

A second explanation is that the underside of the cobble had not been bleached, while the light-exposed surface was completely reset. During slicing, unbleached grains from the underside of the sample could have been mixed with bleached grains from the side of the sample. This would lead to a wide distribution similar to the one observed by Bateman et al., (2003) by mixing of the bleached grains with the unbleached grains, resulting in homogenous material. During sampling in Antarctica a reference line was drawn in order to delineate the exposed surface from the unexposed surface in the lab. Everything under the reference line was sliced and chemically treated. Therefore if the sides of the cobble at some point were exposed to sunlight and combined with slices from the underside of the cobble that was not exposed, it is possible that those exposed slices could be the source of the wide dose distribution observed.

A third explanation of the large dose distribution is that the underside of the cobble was only partially bleached during light exposure (Olley et al., 1998). However, a cobble from a modern beach was sampled in the South Shetland Islands and its luminescence signal revealed that its underside was completely bleached during transport (Kouremenous, per. comm.; 2008).

None of the OSL dates provided constraints on the sea-level history. If dating of the raised beaches would have been successful, these dates would have put constraints on CRASL formation since features at sea level are younger than the raised beaches. It

would have also helped eliminate the pro-talus rampart-model for CRASL formation, since this model requires a sea-level rise. However, two observations can still be used to rule out the pro-talus rampart model. First, beach ridges younger than the deglaciation of the Gerlache Strait (8 ka) were found in the area suggesting that sea-level is falling in relation to land. However, without an age, a fall followed by a recent rise can not be ruled out. Second, GPS studies indicated that the land is rising at a rate greater than global sea levels; thus, relative sea level is falling in this area (Dietrich et al., 2004).

Interpretation: Evolution Model

Our data most favors the interpretation that the moraines are being reworked into beach deposits by wave action (Fig. 117). The following model for CRASL evolution is suggested. First the glacier advances, forming a terminal moraine composed of till (A-A'; Fig. 117 and 118). Eventually, the glacier begins to retreat, leaving a recessional moraine (B-B'; Fig. 117 and 118). Over time, waves begin to remove the sediment and rework the deposits, transforming them into spit deposits (C-C'; Fig. 117 and 118). Eventually, waves most likely erode all of the sediment carrying it seaward and the features are no longer present (D-D'; Fig. 117 and 118).

Modern beaches tend to be parallel in nature, while sediments deposited by moraines are concave shaped (Easterbrook, 1999). The concavity of moraines varies, so that the farthest extent of the moraine would be eroded more quickly by wave processes than the sides of the moraine. Over time this process probably reshapes the concave-shaped features into parallel-shaped features (C-C'; Fig. 117 and 118).

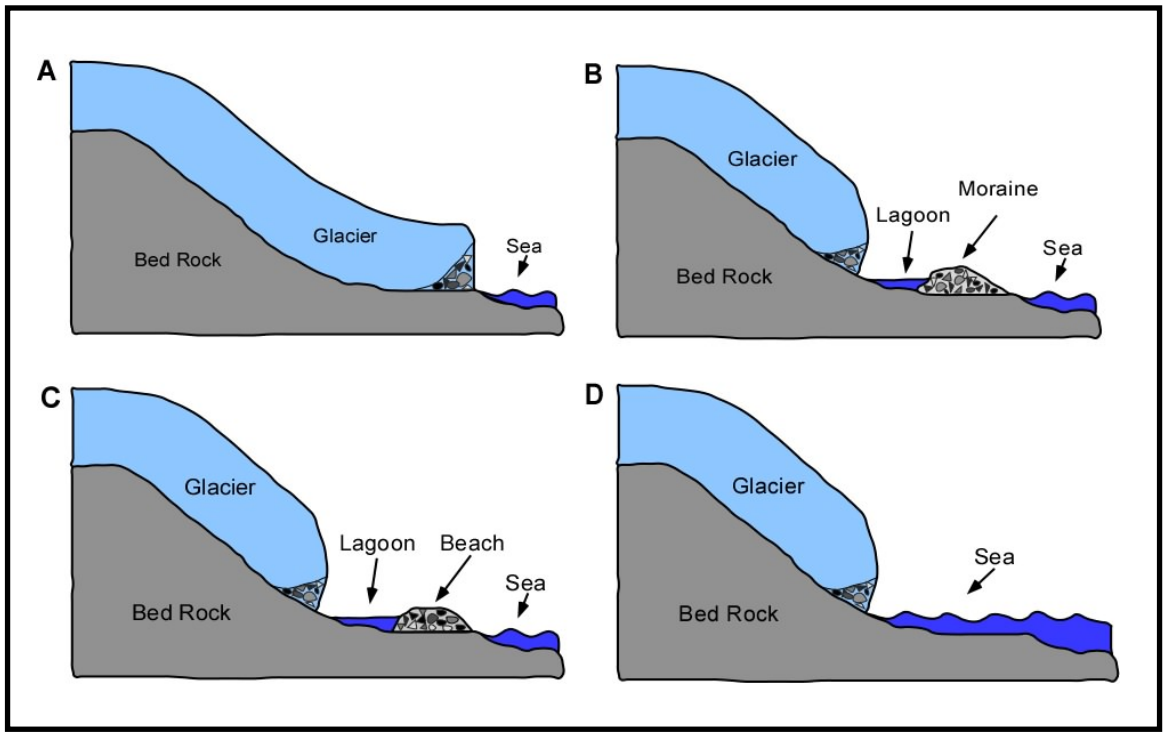

Figure 117 – Schematics of coastline cross-sectional view. A – Glacier with a grounding line in the water. B - The retreat of the glacier left a recessional moraine exposed to wave action. C- The moraine has been reworked into a beach due to erosion. D – The beach is completely gone due to erosion. The different stages correspond to those in Figure 118.

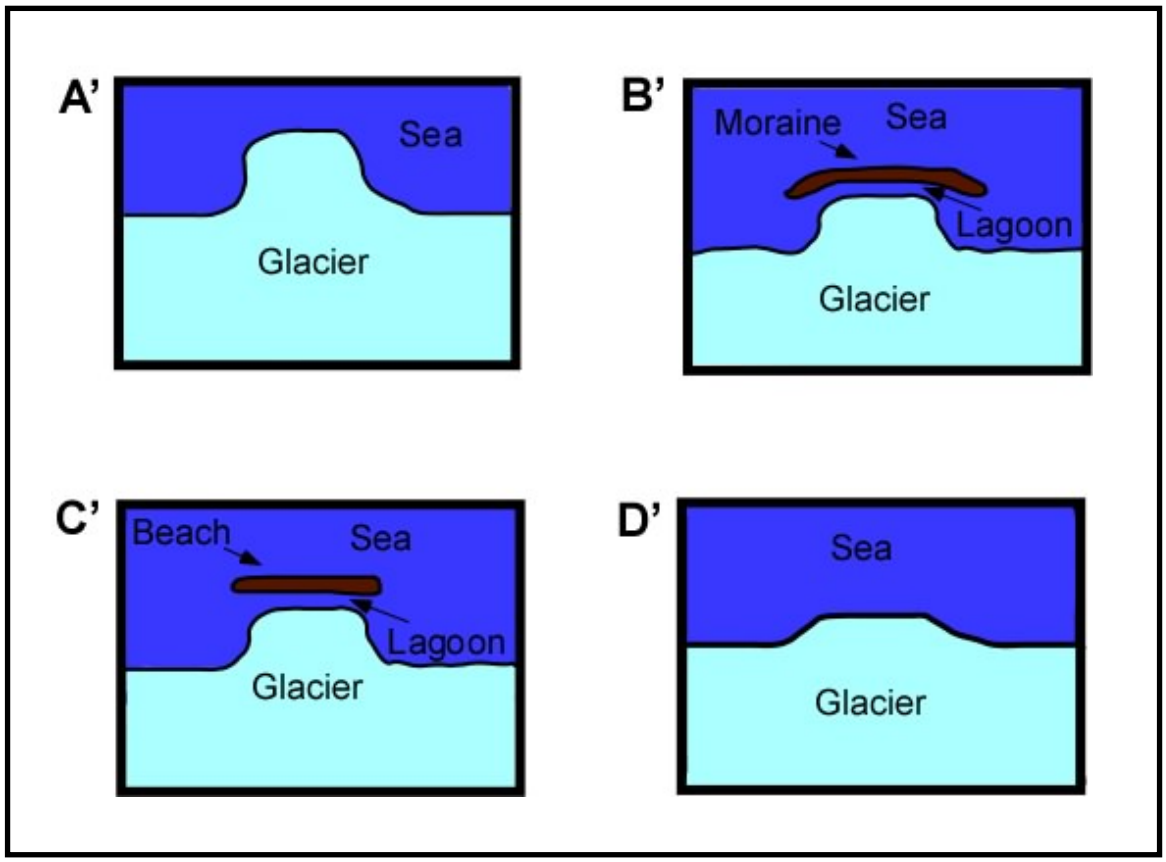

Figure 118 – Schematics of coastline from aerial view. A' – Glacier with a grounding line in the water. B'- The retreat of the glacier, left a moraine that is exposed to wave s. C'- The moraine has been reworked into a beach due to wave action. D' – The beach is completely removed by wave processes. The different stages correspond to those in Figure 117.

In order to determine the relationship between wave-action and feature shape (concave, convex, parallel, and perpendicular) the average fetch was calculated for each CRASL (Table 31). This was done by measuring the distance between the feature and the nearest coastline in the direction of the prevailing wind directions, north (S. Stammerjohn; per. comm.,

2008).

TABLE 31. FEATURES AVERAGE FETCH

Feature shape	Average Fetch (m)
Convex	4,362
Concave	6,566
Parallel	6,136
Perpendicular	11,075

Based on the average fetch the perpendicular-shaped features are subjected to the most intense erosional processes, followed by the concave-shaped features, the parallel-shaped features, and lastly the convex-shaped features. The data in Table 35 does not support the interpretation that the concave features were reshaped into parallel features probably because the features are of differing ages and thus, at varying stages between the recessional moraine and beach deposit endmembers of CRASL formation.

However, while measuring the fetch, I noticed in areas within an overall greater fetch, such as Wiencke Island (Fig. 2), there were more parallel features than in areas that were protected from a large fetch, such as Andvord Bay (Fig. 2). For example, 70% of

the features near Wiencke Island were parallel in shape, 26% were concave in shape and 4% were perpendicular in shape. In contrast, 32% of CRASLs in Andvord Bay are parallel, 64% were concave, and 4% were convex in shape. This supports the idea that fetch is a significant factor in determining the shape and evolution of these features.

CHAPTER VI

CONCLUSION

While searching for raised marine features in the Gerlache Strait, during the NBP 2007 cruise, small arc-shaped ridges in the intertidal zone were observed. It became clear that their origin could be due to a number of processes, so they were given a temporary name of conspicuous ridges at sea-level (CRASL). Because CRASLs are very common in the Gerlache Strait, it became critical to identify these ridges and determine how they form.

Three possible hypotheses for the formation of the CRASLs were tested in this study: 1) spit-model, 2) recessional-moraine model, 3) pro-talus rampart model. In order to test these hypotheses, samples were taken from three known geomorphic features, talus deposits, moraine deposits, and beach deposits, and from the unknown geomorphic feature, a CRASL. A total of eighteen samples were obtained: one sample from a talus slope, three samples from a CRASL, five samples from three moraines, and nine samples from six beaches.

Analysis of the sedimentary characteristics, which included grain size, angularity, roundness, and petrology, suggest that the CRASL deposits are more closely related to the moraine and beach deposits than the talus-slope deposits. Maps were also created in order to determine the distribution of the features. Over 350 features were identified and

classified based on orientation and shape throughout the Gerlache Strait. The features were located randomly and on both sides of the strait, arguing against the spit-model. Furthermore the most prevalent orientation of the features was found to be detached from the shoreline and the most prevalent shape was found to be parallel to the shoreline; therefore supporting both the talus slope-model and the recessional moraine-model.

Analysis of anthropogenic structures, aerial photos and OSL dated beach ridges were used to attempt to constrain the age of these features. Unfortunately, no anthropogenic structures were built on the CRASLs and thus provided little constraint on the age of the CRASLs. Finally, OSL did not work for the samples I prepared.

Neither the talus-slope model nor the exclusively spit-origin model can explain the evolution of the CRASLs. My best interpretation for the evolution of these features is that they represent recessional moraines that are being reworked into beach deposits. Additionally I suggest that the majority of the features observed were in varying stages between recessional moraine deposits and beach deposits. Furthermore, the prevalence of these features indicates changes in the study area since the beginning of the 20th century and further work to determine their age of formation is needed.

REFERENCES

Alarcón, B., Ambros, J., Olcay, L., Vieira, C., 1976, Geológia del Estrecho de Gerlache entre los parallelos 64° y 65° lat. Sur, Antártida Chilena, Ser. Cient., Inst. Antárt. Chil., 4, p. 7-51.

Anderson, J.B., Shipp, S.S., Lowe, A.L., Wellner, J.S., Mosola, A.B. 2002. The Antarctic Ice Sheet during the Last Glacial Maximum and its subsequent retreat history: a review. Quaternary Science Reviews, Vol. 21. p. 49-70.

Baroni, C. and Hall, B. 2004, A new Holocene relative sea-level curve for Terra Nova Bay, Victoria Land, Antarctica. Journal of Science, Vol. 19, p. 377-396.

Bateman, M.D., Frederick, C.D., Jaiswal, M.K. and Singhvi, A.K. 2003. Investigations into the potential effects of pedoturbation on luminescence dating. Quaternary Science Reviews. 22. p. 1169-1176.

Behre Jr., C.H., 1933, Talus behavior above Timber in the Rocky Mountains. *Journ. of Geol.*, Vol. 41. p. 622-635.

Bentley, M.J., and Anderson, J.B., 1998, Glacial and marine geological evidence for the ice sheet configuration in the Weddell Sea-Antarctic Peninsula region during the Last Glacial Maximum: Antarctic Science, v. 10, no. 3, p. 309-325.

Bentley, M.J., Hodgson, D.A., Smith, J.A. and Cox, N.J. 2005. Relative sea level curves for the South Shetland Islands and Marguerite Bay, Antarctic Peninsula. Quaternary Science Reviews. v. 24. p. 1203-1216.

Birkenmajer, K. 1995. Geology of Gerlache Strait, West Antarctica. I. Arctowski Peninsula, Pol. Polar Res., v. 16. p. 47-60.

Birkenmajer, K. 1998. Geology of Gerlache Strait, West Antarctic. II. Wiencke Island to Brabant Island, Bulletin of the Polish Academy of Science Earth Science., v. 46. p. 167-190.

Blatt, H., G.V. Middleton, and R. Murray, 1980, Origin of sedimentary rocks, 2nd ed.: Prentice-Hall, Englewood Cliffs, N.J., 782 p.

Boggs Jr., S., 1995, Principles of Sedimentology and Stratigraphy, 2nd ed.: Prentice-Hall, Englewood Cliffs, N.J., 774 p.

Bøtter-Jensen, L., McKeever, S.W.S., Wintle, A.G., 2003. Optically Stimulated Luminescence Dosimetry. Elsevier Science, Amsterdam.

British Antarctic Survey: British Research Stations and Refuges – History. http://www.antarctica.ac.uk/about_bas/our_history/stations_and_refuges/index.php.

Bryan, K., 1934, Geomorphic processes at high altitudes. Geographical Review: 4, p. 655-656.

Cook, A.J., Fox, A.J., Vaughan, D.G. and Ferrigno, J.G. 2005. Retreating Glacier Fronts on the Antarctic Peninsula over the Past Half-Century. Science 308: 541-543.

DeConto, R.M. and Pollard, D. 2003. Rapid Cenozoic glaciation of Antarctica induced by declining atmospheric CO_2. Nature. Vol. 421. p. 245-249.

Denton, G.H., Prentice, M.L., and Burckle, L.H., 1991, Cainozoic history or the Antarctic Ice Sheet, in Tingey, R.J., ed., The geology of Antarctica: Oxford, Claredon Press, p. 365-433.

Dietrich, R., Rülke, A., Ihde, J., Lindner, K., Miller, H., Niemeier, W., Schenke, H., Seeber, G., 2004, Plate kinematics and deformation status of the Antarctic Peninsula based on GPS. Global and Planetary Change. v. 42. p. 313-321.

Dobkins, J.E., and R.L. Folk, 1970, Shape development on Tahati-Nui: Jour. Sed. Petrology, v. 40, p. 1167-1203.

Domack, E.W., Leventer, A., Dunbar, R., Taylor, F., Brachfeld, S., and Sjunneskog, C., and ODP leg 178 Scientific Party, 2001, Chronology of the Plamer Deep site, Antarctic Peninsula: A Holocene palaeoenvironmental reference for the circum-Antarctic: The Holocene, v. 11(1), p. 1-9.

Easterbrook, D.J. 1999, Surface processes and landforms, 2nd ed.: Prentice Hall: Upper Saddle River, N.J. 546 p.

Evans, J., Dowdeswell, J. A., and Ó Cofaigh, C. 2004. Late Quarternary submarine bedforms and ice-sheet flow in Gerlache Strait and on the adjacent continental shelf, Antarctic Peninsula. J. Quaternary *Sci.,* **Vol. 19** p 397-407. ISSN 0267-8179.

Fleming, E.A., Thomson, J.W., 1979, British Antarctic Territory, Geological Map 1:500,000. Ser. BAS 500G, sheet 2, ed. 1

Florindo, F., Cooper, A.K., O'Brien, P.E. 2003. Introduction to 'Antarctic Cenozoic palaeoenvironements: geolgic record and models'. Palaeogeography, Palaeoclimatology, Palaeoecology. 198. p. 1-9.

Folk, R.L. and W.C. Ward. 1957. Brazos River bar: a study in the significance of grain size parameters. Journal of Sediment Petrology 27, 514-529.

Folk, R.L., 1974, Petrology of sedimentary rocks: Hemphill, Austin, Tex., 182 p.

Forman, S.L. 2000. Luminescence Geochronology. Quaternary Geochronology: Methods and Applications: p. 157-176.

French, H.M., 1976: The periglacial environment. Longman, London. 309 p.

Hall, B.L. and Denton, D.H. 1999. New relative sea-level curves for the southern Scott Coast, Antarctica: evidence for Holocene deglaciation of the western Ross Sea. Journal of Quaternary Science. v. 14. p. 641-650.

Hall, B.L. and Perry, E.R. 2004. Variations in ice rafted detritus and beaches in the South Shetland Islands: a possible climate proxy. Antarctic Science. vol. 16. p. 339-344.

Hansom, J.D., 1983. Ice-formed intertidal boulder pavements in the sub-Antarctic. *Journal of Sedimentary Petrology*, **53**, 135-145.

Harden, S.L., DeMaster, D.J., Nittrouer, C.A., 1992. Developing sediment geochronologies for high-latitude continental shelf deposits: a radiochemical approach. Marine Geology 103, 69-97.

Heroy, D.C., and Anderson, J.B. 2005. Ice-sheet extent of the Antarctic Peninsula region during the Last Glacial Maximum (LGM) – Insights from glacial geomorphology. *GSA Bulletin;* v. 117. No. 11/12; p. 1-16.

Hooper, P.R. 1966. The dykes of Anvers Island and adjacent islands. *Br. Antarct. Surv. Bull.*, No. 9., p. 75-85.

Kouremenous, Peter; personal communications. 2008.

Krumbein, W.C., and Pettijohn, F.J., 1938, Manual of sedimentary petrography: Appleton-Century-Crofts, New York, 549 p.

Kuenen, Ph. H., 1964, Experimental abrasion, pt. 6: Surf action: Sedimentology, v. 3, p. 29-43.

Lian, O.B. and Roberts, R.G. 2006. Dating the Quaternary: progress in luminescence dating of sediments. Quaternary Science Reviews. v. 25. p. 2449-246.

Meistrell, F.J. 1996. The Spit-Platform Concept: Laboratory observation of spit development. Bulletin of Canadian Petroleum Geology. Vol. 16, No. 2, p. 212-213.

Murray, A.S., Wintle, A.G., 2000. Luminescence dating of quartz using an improved single-aliquot regenerative-dose protocol. Radiat. Meas. 32, 57-73.

Murray, A.S., Wintle, A.G., Wallinga, J., 2002. Dose estimation using quartz OSL in the non-linear region of the growth curve. Radiat. Prot. Dosim. 101, 371-374.

Murray, A.S., Wintle, A.G., 2003. The single aliquot regenerative dose protocol: potential for improvements in reliability. Radiat. Meas. 37, 377-381.

Nichols, R.L. (1961). Characteristics of beaches formed in polar climates. *Am. J. Sci.* **259**, 694-708.

Olley, J., Caitcheon, G., Murray, A., 1998. The distribution of apparent dose as determined by optically stimulated luminescence in small aliquots of fluvial quartz: implication for dating young sediments. Quaternary Science Reviews, Vol. 17, p. 1033-1040.

Ono, Y. and Wantanabe, T., 1986: A protalus rampart related to alpine debris flows in the Kuranosuke Cirque, Northern Japanese Alps. *Geogr. Ann.* 68 A (3): 213-223.

Parada, M.A., Orsini, J.-B., Ardila, R., 1992. Transverse variations in the Gerlache Strait plutonic rocks: effects of the Aluk ridge-trench collision in the northern Antarctic Peninsula, in: Recent Progress in Antarctic Earth Science, ed.: Yoshida, Y., Kaminuma, K., Shiraishi, K., Terra Sci. Publ. Co., Tokyo, p. 477-482.

Plummer, C.C. and McGeary, D., 1996, Physical Geology, 7th ed.: Times Mirror Higher Education Group, Inc., 539 p.

Pudsey, C.J., Barker, P.F., and Larter, R.D., 1994, Ice sheets retreat from the Antarctic Peninsula shelf: Continental Shelf Research, Vol. 14, no. 15, p. 1647-1675, doi: 10.1016/0278-4343(94)90041-8.

Ringe, M.J., 1991, Volcanism on Brabant Island, Antarctica, in: Geological Evolution of Antarctica, ed.: Thomson, M.R.A., Crame, J.A., Thomson, J.W., Cambridge Univ. Press. p. 515-519.

Risø DTU, 2008. Guide to "The Risø TL/OSL Reader". Denmark.

Scott, K.M., 1965, Geology of the southern Gerlache Strait region, Antarctica. *Journ. of Geol.*, Vol. 73. p. 518-527.

Sekine, K. 1973. Mechanism of the formation of a protalus rampart at the bottom of the so-called Kuranosuke Glacial Cirque, Japanese Alps. Geographical Review of Japan. v. 46., p. 273-274.

Stammerjohn, Sharon; personal communications. 2008.

Takeuchi, A., Nagahama, H., Hashimoto, T., 2006. Surface resetting of thermoluminescence in milled quartz grains. Radiat. Meas. 41, 826-830.

Tricart, J. and Cailleux, A., 1962: Le Modelé Glaciaire et Nival. SEDES, Paris. 508 p.

Vaughan, A.P.M., and Storey, B.C., 2000, The eastern Palmer Land shear zone: a new terrane accretion model for the Mesozoic development of the Antarctic Peninsula magmatic arc: Geological Society of London, Journal, v. 157, p. 1243-1256.

Wagner, G.A. 1998. Age Determination of Young Rocks and Artifacts: Physical and Chemical Clocks in Quaternary Geology and Archaeology. Springer-Verlag Berlin Heidelberg, Germany. 466 p.

Werner, A.D.B. Antarctica: Guío de Navegacion Gouvemoreu (Navigation Guide). ISBN N° 956-291-671-5.

Willan, R.C.R. 2003. Provenance of Triassic-Cretaceous sandstones in the Antarctic Peninsula: Implication for Terrane Models during Gondwana Breakup. Journal of Sedimentary Research, Vol. 73, No. 6, November, 2003, p. 1062-1077.

Wintle, A.G., Murray, A.S., 2006. A review of quartz optically stimulated luminescence characteristics and their relevance in single-aliquot regeneration dating protocols. Radiat. Meas. 41, 369-391.

Zingg, Th., 1935, Beiträge zur Schotteranalyse: Schweiz. Mineralog. Petrog. Mitt., v. 15, p. 39-140.

.

APPENDICES

Appendix A – Angularity

The picture below is an example of how the clasts were classified according to their angularity in the field.

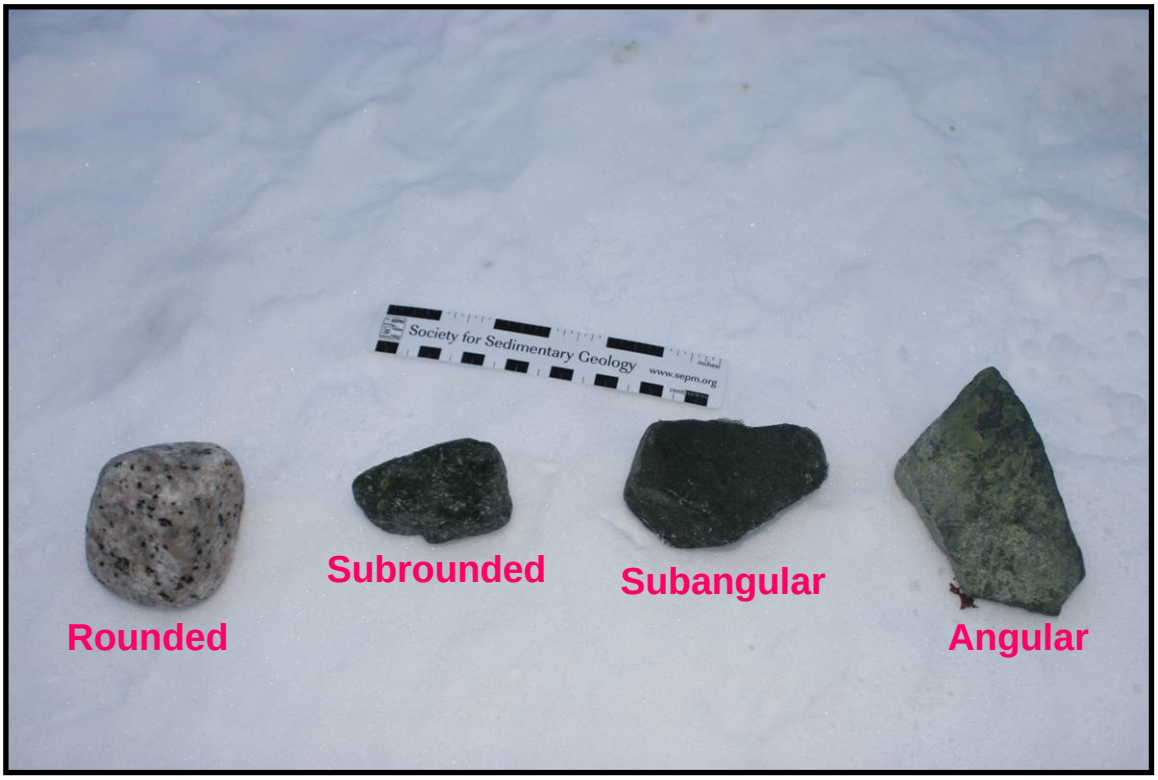

Appendix B -OSL Riso software conversion to Excel instructions.

In order to be converted to a text document the follow commands had to be performed. Upon opening of the file needed, the *Lumin. Type* and *Num. Points* buttons were selected in the *Displayed Information* window. Upon the display of those categories in the spreadsheet columns, the *Records* tab was selected. Then the *Unselect all* button, followed by the *Records of type* buttons were selected. Once the *Unselect Records* window was available the *Lumin Type, =*, and *IRSL* were selected. Followed by the reopening of the *Unselected Records* window in order to select the *Num pts., =, 40*. Once the previous task was completed the *Lumin. Type* and *Num. Points* buttons in the *Displayed Information* window were unselected. Next, *Integral 1* and *Integral 2* were selected in the *Displayed Information* window. Upon view of the *Set Integration Limits* window the follow commands were executed: for *Integral 1* the *Lower integration limit* was set to *1* and the *Upper integration limit* was set to *2*; for *Integral 2* the *Lower integration limit* was set to *91* and the *Upper integration limit* was set to 100. Finally, to export the data the *Export* tab and *Current data display* were selected. Upon view of the *Export Data window* the selected *Records* and *TAB* were selected. The document was then saved and ready to be opened in Microsoft Excel.

VITA

Ann Marie Drewry

Candidate for the Degree of

Master of Science

Thesis: COASTAL GEOLOGY OF THE GERLACHE STRAIT, ANTARCTICA

Major Field: Geology

Biographical:

Personal Data: Born in Columbus, Ohio, on January 9, 1984, the daughter of Wayne and Rebecca Drewry.

Education: Graduated from Sequoyah High School, Claremore, Oklahoma in May 2002; received an Associates of Science degree in Chemistry from Rogers State University, Claremore, Oklahoma in August 2004; received a Bachelor of Science degree in Geology from Oklahoma State University, Stillwater, Oklahoma in December 2006. Completed the requirements for the Master of Science in Geology at Oklahoma State University, Stillwater, Oklahoma in May, 2009.

Experience: Employed by Oklahoma State University, Geology Department as an undergraduate; employed by Devon Energy Corporation as an intern; employed by Oklahoma State University, Geology Department as a teaching assistant, 2007 to present.

Professional Memberships: Geological Society of America, American Association of Petroleum Geologists, Oklahoma State University Geological Society, Secretary 2007, American Association of Petroleum Geologist Student Chapter.

Name: Ann Marie Drewry Date of Degree: May, 2009

Institution: Oklahoma State University Location: Stillwater, Oklahoma

Title of Study: COASTAL GEOLOGY OF THE GERLACHE STRAIT, ANTARCTICA

Pages in Study: 212 Candidate for the Degree of Master of Science

Major Field: Geology

Scope and Method of Study: While mapping the coastal deposits in the Gerlache Strait of the Antarctic Peninsula, we observed several "conspicuous ridges at sea level" (CRASL). Usually, located directly in front of a glacier, these features were only observed in the intertidal zone. Three hypotheses for their origin are considered: 1) recessional moraines, 2) detached spits, and 3) partially submerged pro-talus ramparts. In order to determine which of these hypotheses best explains their origin, we compared the grain size, angularity, sphericity, and petrology of the CRASL deposits with surface samples taken from modern moraine, beach, and talus-slope deposits in the area. In addition to documenting their sedimentological characteristics, their distribution was mapped according to their orientation and shape, throughout the Gerlache Strait. Aerial photos from 1956/1957, 1981, and 2001 were examined for CRASLs. Finally, samples were obtained from raised beach ridges in the study area in an attempt to date using Optically Stimulated Luminescence (OSL).

Findings and Conclusions: Data from grain size, angularity, sphericity, and petrology suggest that the CRASL deposits are supplied by recessional moraines and are reworked into beach deposits. A model for how the transition occurs was proposed. The distribution maps created indicated that the CRASLs vary in size, occur on both sides of the strait, and have no specific orientation. Furthermore, it was found that the most common type of CRASL is one that is detached and parallel in relation to the coastline. Aerial photos indicated that CRASLs were present in 1956/1957, 1981, and 2001. In addition, it was determined that OSL dating of the beach ridges did not work on the samples obtained. Finally, the prevalence of these features indicates changes in the study area since the beginning of the 20th century and further work to determine their age of formation is needed.

ADVISER'S APPROVAL: Dr. Alexander Simms